A Novel Mooring Tether for Highly Dynamic Offshore Applications

Submitted by David Nigel Parish to the University of Exeter

as a thesis for the degree of

Doctor of Philosophy in Renewable Energy

In September 2015

I certify that all material in this thesis which is not my own work has been identified and that no material has previously been submitted and approved for the award of a degree by this or any other University.

Signature: ……..

Abstract

The mooring of vessels and other floating bodies at sea, such as offshore platforms has necessitated the development of specialised moorings technology. The marine renewable energy (MRE) sector is now at a stage in its development whereby floating devices are adding new challenges to the moorings industries. Floating MRE devices are smaller than, for instance offshore platforms, and are usually targeted for deployment in highly energetic environments. The extreme conditions and the highly dynamic response of an MRE device present challenges in terms of peak loading within the mooring system itself and load transfer to the floating body.

Compliant mooring systems provide advantages by reducing the peak loads and fibre ropes are an important asset in achieving such compliance. However, the extent to which existing fibre ropes can safely extend axially to provide compliance is insufficient and is strongly associated to the minimum breaking load (MBL) of the rope.

A novel fibre rope mooring tether is presented here that provides advantages over existing ropes. The tether employs a hollow fibre rope containing an elastomeric core, this mechanism de-coupling the extension properties from the strength of the line. The load path is carried through the polyester rope which is terminated conventionally by eye splices, thus minimising any new risks to reliability.

Very low axial stiffness is achieved and is shown to be selectable within limits. For comparison, the prototype tether's MBL of 222 kN is assigned to polyester and Nylon reference ropes. The axial stiifness of these ropes are 590 kN and 463 kN respectively when measured by a secant between the origin and 30% MBL; the novel tether displays an axial stiffness of 72 kN by the same method. This enables the novel tether to achieve more than two and a half times the extension of a comparable Nylon rope in its working range. Numerical modelling of a moored installation demonstrates a threefold reduction in peak load magnitude compared to the existing Nylon rope solution.

The tether exhibits two distinct stages of extension, the first having very low axial stiffness. It is demonstrated that the extent of this soft phase can be

selected by design and that this might add another useful element of control to moorings design work.

Acknowledgements

I would like to gratefully acknowledge the cooperation of Lankhorst Euronete Ropes in the manufacture of the hollow ropes which made prototyping of the Exeter Tether possible. Similarly important to this part of the work was the proof of concept funding which was accessed through the Open Innovation Platform, supported by the Higher Education Council for England.

I am also very grateful to Lars Johanning and Ian Ashton for their support and guidance as supervisors to my PhD work and to Tessa Gordelier who assisted me so generously with much of the tether test work.

I would also like to remember the Late George Smith who encouraged me to undertake this work and supported me in the early stages.

Contents

Abstract 3

Acknowledgements 5

List of Figures 12

List of Tables 17

Abbreviations 19

Chapter 1 Introduction 21

1.1 Background 21

1.1.1 Design Factors of Safety 23

1.2 Motivation for This Work 24

1.3 The Aim of this Work 27

1.4 The Research Methodology 28

1.5 Scope 29

1.6 Contributions to Knowledge 29

Chapter 2 Literature Review 31

2.1 An Introduction to Mooring Systems 31

2.1.1 Ship Anchoring 31

2.1.2 Industrial Mooring Systems 33

2.1.3 Mooring Lines 34

2.1.4 Mooring Loads 35

2.2 Mooring Systems for Highly Dynamic Bodies such as Marine Energy Converters 36

2.2.1 WEC Mooring Requirements 36

2.2.2 WEC Mooring System and Line Architecture 38

2.3 Fibre Ropes: Their use as Mooring Tethers for Highly Dynamic Floating Bodies such as Marine Energy Converters 44

2.3.1 Offshore Standards 44

2.3.2 Axial Stiffness 45
2.3.3 Material and Construction Choices 46
2.4 Novel MEC Mooring Tethers having Advantageous Extension Properties 49
2.5 Conclusions and Further Discussion 56
2.6 Summary of the Literature Review 56

Chapter 3 Inventions and Critical Design Considerations 58
3.1 Hydraulic Tether 58
3.1.1 Hollow Rope 59
3.1.2 Applications 60
3.1.2.1 Tide Height Compensation 60
3.1.2.2 Peak Load Mitigation 61
3.1.2.3 Latching 61
3.2 Solid Core Tether 61
3.2.1 The Core Material 63
3.2.2 Applications 64
3.3 Summary of Tether Inventions and Potential Applications 64

Chapter 4 Initial Assessments and Tether Selection 66
4.1 Limitations and Experimental Equipment 66
4.1 Hydraulic Tether Benchtop Prototype 67
4.2 Solid Core Tether Benchtop Prototypes 68
4.3 Test Methods 69
4.3.1 Hydraulic Tether Test 69
4.3.2 Solid Core Tether Pressure Test 70
4.3.3 Solid Core Tether Performance Test 71
4.4 Test Results 73
4.4.1 Hydraulic Tether Test 73

4.4.2 Solid Core Tether Pressure 73
4.4.3 Solid Core Tether Performance 76
4.5 Calculation of Theoretical Core Pressure 77
4.5.1 Calculation of Hydraulic Pressure 79
4.5.2 Calculation of Solid Core Pressure 79
4.6 Outcomes 80
4.7 Design Failure Mode and Effect Analysis 81
4.7.1 Hydraulic Tether FMEA 82
4.7.2 Solid Core Tether FMEA 82
4.8 Discussions and Decision 82

Chapter 5 The Proof of Concept Prototypes 86
5.1 Industrial Collaboration 86
5.2 Hollow Rope Design 86
5.2.1 Scaling the Rope Design 87
5.3 Polymer Core Designs 91
5.3.1 Pressure Considerations 91
5.3.2 Core Architecture and Component Design 94
5.3.2.1 Hexagonal Pack Core 95
5.3.2.2 Articulated Core 97
5.4 Helically Wound Tape 98
5.5 The P1 Prototype General Specifications 98
5.6 Manufacture of the P1 Prototypes 100
5.6.1 The Cores 100
5.6.2 The Hollow Rope 101
5.6.3 The Rope Terminations 103

Chapter 6 The Proof of Concept Test Work 107
6.1 The DMaC Test Facility 107

6.1.1 Adaptations for This Work 108
6.1.2 Calibration of the Tailstock Load Cell 109
6.2 Test Considerations 112
6.2.1 The Mullins Effect 112
6.2.2 Lubrication and Cooling 114
6.2.3 Test Cycles 115
6.3 Test Methods 117
6.3.1 Performance Tests Referenced to a Tension Load Datum 118
6.3.2 Eye Splice Extension Tests 119
6.3.3 Breaking Load Test 120
6.3.4 Testing the Effect of Load Cycle Frequency 120
6.3.5 Performance Tests Referenced to a Displacement Datum 121
6.3.6 Durometer Hardness Tests 122
6.3.7 Poisson's Ratio and Young's Modulus Tests 122
6.4 Test Results 124
6.4.1 Durometer Hardness Tests 124
6.4.2 Eye Splice Extension Tests 124
6.4.3 Breaking Load Test 126
6.4.4 Performance Tests Referenced to a Tension Load Datum 127
6.4.5 The Effect of Load Cycle Frequency 129
6.4.6 Performance Tests Referenced to a Displacement Datum 131
6.4.7 Poisson's Ratio and Young's Modulus Tests 134
6.4.8 Hysteretic Damping 137

Chapter 7 Modelling the Tether in Operation 141
7.1 Methodology for the Numerical Study 141
7.2 The SWMTF 142
7.2.1 The SWMTF Mooring System 142

7.2.2 The SWMTF Instrumentation and SCADA Unit 144
7.2.3 The SWMTF Buoy 146
7.3 Measured Data from the SWMTF 148
7.3.1 Wave Data 149
7.3.2 Mooring Line Tension and Buoy Excursion 152
7.3.3 Wind Data 152
7.3.4 Current Data 153
7.4 Orcaflex 154
7.4.1 6D Buoys 154
7.4.2 Waves 154
7.4.3 Lines 155
7.4.4 Integration Methods 155
7.5 The SWMTF Model and Model Validation 156
7.5.1 The SWMTF Model 156
7.5.2 Model Validation 158
7.6 The Tether Performance Simulations 162
7.6.1 Explicit Integration Simulations 162
7.6.1.1 Reduced MBL Tether 164
7.6.1.2 Reduced Chain Mass 164
7.6.2 Implicit Integration Simulations 166
7.6.3 Implicit Simulations with Increased Surface Current 168
7.6.4 Summary of Simulation Outcomes 171
7.7 Mooring System Stiffness 172
7.8 Limitations and Assumptions 176
7.9 Summary of Operational Tether Modelling and Outcomes 177

Chapter 8 Discussions 179
8.1 The Tether Design and Mechanisms 179

8.1.1 The Hollow Rope 179
8.1.2 The Eye Splice 180
8.1.3 The Core Architecture 181
8.1.4 The Core Material 182
8.1.5 1st Phase Tether Extension 183
8.1.6 2nd Phase Tether Extension 184
8.1.7 Radial Core Pressure 185
8.2 The Tether Test Work 186
8.2.1 Wet Testing 186
8.2.2 Tension Data Accuracy 186
8.2.3 Extension Data Accuracy 187
8.2.4 Dynamic Zero Load Length 188
8.3 The Modelling Outcomes and Interpretation 189
8.4 Hydrodynamic Line Damping 190
8.5 An Alternative View of MEC Moorings Design 191

Chapter 9 Conclusions and Further Work 193
9.1 Research Questions 193
9.2 Further Work 195

Appendices 198
Appendix A – UK Patent Application GB 2467345 A 198
Appendix B – UK Patent Application GB 2476986 A 199
Appendix C – FMEA Guidance 200
Appendix D – Male double hemisphere drawing 202
Appendix E – Female double hemisphere drawing 203
Appendix F – Male double hemisphere (cropped) drawing 204
Appendix G – Tether Scaling Guide 205
References 206

List of Figures

Figure 1.1 Wave power frequency at FaBTest 22
Figure 1.2 Wave height / period scatter plot for FaBTest 23
Figure 1.3 The SWMTF design spiral 25
Figure 1.4 Simplified schematic diagram of the SWMTF mooring system. 25
Figure 1.5 Extension properties for Bridon's polyester Braidline rope 27
Figure 2.1 Schematic diagram of a ship's catenary anchor line 32
Figure 2.2 A catenary mooring spread applied to a semi-submersible platform 33
Figure 2.3 Breakdown of the types of compliant reaction systems for WECs . 38
Figure 2.4 Schematic diagram of the CALM (upper) and SALM (lower) WEC moorings 40
Figure 2.5 Force vs displacement and mooring stiffness curves for the two mooring systems at 30 m water depth 40
Figure 2.6 Limb compositions 42
Figure 2.7 Possible mooring configurations for a single MEC 43
Figure 2.8 Examples of single filament tensile properties for fibre rope 45
Figure 2.9 Comparison of axial stiffness for Nylon and polyester rope 47
Figure 2.10 Fatigue endurance results for Nylon rope, polyester rope, steel wire rope and steel chain 48
Figure 2.11 The GLOBEC Crest mooring as deployed at Georges Bank 50
Figure 2.12 Comparison of predicted tension with and without the snubber ... 51
Figure 2.13 Superflex units with 100 strands 52
Figure 2.14 Graph showing extension (mm) vs tension (kN) for a single strand of Superflex having a 200mm original length 52
Figure 2.15 The Seaflex strand construction 53
Figure 2.16 Seaflex extension and recovery curve 54
Figure 2.17 Novel mooring tether utilising tension of an elastomeric element and compression of a thermoplastic element 55
Figure 2.18 Novel mooring tether utilising tension of an elastomeric element and compression of a thermoplastic element - as tested 55
Figure 3.1 Double braid rope 60
Figure 3.2 Schematic diagram of bundled core cross section 62
Figure 3.3 Schematic diagram of multi element core arranged axially 62

Figure 4.1 Hollow rope used in benchtop prototype 67
Figure 4.2 Solid core bundle wrapped in PVC tape..... 68
Figure 4.3 Pressure sensitive film positioned within core bundle 70
Figure 4.4 Benchtop prototype ready for test in the DMaC test facility..... 72
Figure 4.5 Displacement driven test script used..... 72
Figure 4.6 Prescale film pieces after disassembly of the tether..... 74
Figure 4.7 Prescale film colour reading charts (continuous pressure), as read. 75
Figure 4.8 Displacement test results for prototype solid core tether..... 76
Figure 4.9 Comparison of tether with plain hollow rope..... 77
Figure 4.10 Schematic diagram of hollow rope cut axially and laid flat 78
Figure 5.1 Hexagonal pack core structure..... 94
Figure 5.2 Articulated core components assembled and exploded 94
Figure 5.3 Cross section of tether with hexagonal pack core 95
Figure 5.4 Calculating equivalent circumference..... 96
Figure 5.5 Winding Dacron sail tape onto an articulated core assembly..... 98
Figure 5.6 The P1 prototype assembly drawing 99
Figure 5.7 The empty hollow rope with a moulded core piece introduced..... 102
Figure 5.8 P1-12 core being fed into the back of the machine and P1-12 tether emerging from the machine..... 103
Figure 5.9 Tuck through splice in 12 strand hollow braid 104
Figure 5.10 Unravelled strands re-made into two 3 strand laid ropes 106
Figure 5.11 An example of a 'short splice' (LH) and applied to the tether with the aramid sleeve in place 106
Figure 5.12 The completed tether eye splice..... 106
Figure 6.1 The DMaC test machine..... 108
Figure 6.2 Specially designed DMaC extension and pre-tension adjuster (LH) and a tether fitted within the DMaC test bed..... 109
Figure 6.3 Initial calibration graph showing an error in gain, represented by the equation given 111
Figure 6.4 Partially corrected calibration graph with an improved calibration of gain but showing a positive offset..... 111
Figure 6.5 Result of the completed calibration 112
Figure 6.6 The idealised Mullins mechanical behaviour 112

Figure 6.7 An example of uniaxial cyclic response with an increase of maximum strain every 5 cycles 113
Figure 6.8 5th cycle loops for P1-1 in the dry and wet conditions..... 115
Figure 6.9 4th and 5th cycle loops for P1-1 in the wet condition 116
Figure 6.10 The displacement drive data for test ETT_08..... 119
Figure 6.11 Linear transducer recording eye splice extension 120
Figure 6.12 A submerged tether awaiting testing 121
Figure 6.13 Schematic diagram of the Poisson's ratio / Young's modulus test equipment..... 123
Figure 6.14 P1-3 eye splice extension during test ETT_08 125
Figure 6.15 The final cycle load up data and best fit straight line..... 125
Figure 6.16 Tension vs displacement plot showing failure at 222 kN..... 126
Figure 6.17 Images showing the failure of tether P1-17 127
Figure 6.18 P1 series tether extension properties at > 20% extension 128
Figure 6.19 Data from Figure 6.18 clipped to achieve r2 = 0.9995 linear regressions..... 128
Figure 6.20 Tension vs displacement plots for tests 1 - 5 130
Figure 6.21 Tension vs displacement plots for tests 6 – 10 (reverse sequence)..... 130
Figure 6.22 Full ETT_19 test data for P1-2 131
Figure 6.23 Pre-tension data used to obtain the 'dynamic zero load' length . 132
Figure 6.24 Comparison of tether extension properties with a double braid polyester reference rope 133
Figure 6.25 Further comparison of tether extension properties with conventional highly compliant fibre rope 133
Figure 6.26 Poisson's ratio of the EPDM cord materials 135
Figure 6.27 Young's modulus of the EPDM cord materials 136
Figure 6.28 Hysteresis loops for the hexagonal pack core tethers..... 138
Figure 6.29 Hysteresis loops for the articulated core tethers..... 139
Figure 6.30 The hysteresis loop split into load up and unload components for integration (P1-2) 139
Figure 7.1 The SWMTF buoy in calm water (LH) and its position in Falmouth Bay 142
Figure 7.2 Plan view diagram of the SWMTF mooring spread and ADCP position..... 143

Figure 7.3 The welded steel column assembly that provides the SWMTF buoy structure 147
Figure 7.4 Outline dimensions of the float including the buoy draft at mid tide 148
Figure 7.5 The SWMTF buoy during a southerly gale 149
Figure 7.6 The maximum offsets between an ADCP beam and the instantaneous buoy position 150
Figure 7.7 Directional spectrum output from WaveView for the 17.07 minute peak load wave burst 151
Figure 7.8 Time series plots (s) of surface elevation (m) for beam 1 (top left), beam 2 (top right), beam 3 (bottom left) and beam 4 (bottom right) – given for comparison 151
Figure 7.9 Limb 3 tension (upper) and buoy excursion to the west (lower) time series plots for the 240 second data 152
Figure 7.10 Current profiles eastward (LH) and northward (RH) during the peak event 153
Figure 7.11 The modelled SWMTF buoy 156
Figure 7.12 The Bridon stiffness curves for Nylon Superline rope (LH) and the digitised version imported to the model (RH). 158
Figure 7.13 The full 1200 second surface elevation time series from beam 1 with the 240 second simulation period identified 159
Figure 7.14 Spectral density plots for each ADCP beam time series computed by Orcaflex. Beam 1 top left, beam 2 top right, beam 3 bottom left, beam 4 bottom right 160
Figure 7.15 Simulation outcomes for limb 3 tension, beams 1 – 4, overlaid onto the real data for comparison 161
Figure 7.16 Simulated limb 3 tension for Superline rope and the P1-6 tether 163
Figure 7.17 Simulated buoy excursion for Superline rope and the P1-6 tether 163
Figure 7.18 Simulated limb 3 tension for Superline rope and the P1-6 146 kN MBL tether 164
Figure 7.19 Simulated limb 3 tension for Superline rope (24mm chain) and the P1-6 146 kN MBL tether (19mm chain) 165
Figure 7.20 Simulated limb 3 tension for Superline rope by explicit and implicit integration simulations 166

Figure 7.21 Simulated buoy excursion for Superline rope by explicit and implicit integration simulations 167
Figure 7.22 Simulated outcome for limb 3 tension with increased current, overlaid onto the real data for comparison 169
Figure 7.23 Simulated excursion time series for the first implicit simulation base case and that of increased current velocity 169
Figure 7.24 Limb 3 peak tensions through the three series of simulations and limb design iterations 172
Figure 7.25 Quazi-static mooring system stiffness curves for the implicit simulation series mooring designs 173
Figure 7.26 Mooring system stiffness curves reproduced from Figure 7.25 shown with corresponding peak tension from the dynamic simulation 173
Figure 7.27 Mooring stiffness tangent modulus vs simulated dynamic peak tension (all simulations) 175
Figure 7.28 Mooring stiffness tangent modulus vs simulated dynamic peak tension by simulation series 175
Figure 7.29 Hysteresis loops evident in the SWMTF peak load data 176
Figure 7.30 The peak hysteresis loop showing the straight line bridge used to close the gap 177
Figure 8.1 An articulated core tether demonstrating advantageous bending stiffness 182
Figure 8.2 Tether P1-2 at zero extension having a rounded hexagon form (LH) and at 30% extension with a fully round form (RH) 183
Figure 8.3 The tension error band limits applied to P1-6 performance data .. 187
Figure 8.4 The combined extension and tension error band applied to P1-6 performance data 188

List of Tables

Table 1.1 Partial safety factors for ULS 24
Table 2.1 Extension for worked polyester and Nylon ropes 48
Table 3.1 Properties of EPDM and FFKM 64
Table 3.2 Tether inventions and their potential applications. 65
Table 4.1 Prescale film pressure ranges 70
Table 4.2 Hydraulic tether test results 73
Table 4.3 Extension and load data during solid core pressure test 73
Table 4.4 Parameter values and derivations used to calculate hydraulic pressure 79
Table 4.5 Parameter values and derivations used to calculate radial pressure 80
Table 4.6 FMEA - Major risks associated with the hydraulic tether 84
Table 5.1 Scaled rope dimensions, solidity and scaling factor 89
Table 5.2 Derivation of diameter and braid pitch factors. 92
Table 5.3 Parameter values and derivations used to calculate P1 radial pressure 93
Table 5.4 Planned P1 series prototypes 100
Table 6.1 DMaC Z ram load cell calibrations 110
Table 6.2 Force mode conditioning test descriptions 118
Table 6.3 The sequence and description of the load cycle frequency tests . 121
Table 6.4 Durometer hardness test results 124
Table 6.5 Results of the eye splice extension tests 126
Table 6.6 Tabulated results of the linear regressions shown in Figure 6.18.. 129
Table 6.7 Comparison of axial stiffness outcomes by secant method. 134
Table 6.8 Poisson's ratio and Young's modulus of the EPDM cords measured between 30% and 40% extension 136
Table 6.9 The calculation of tension load carried by the hexagonal pack core bundles 137
Table 6.10 Hysteretic losses during ETT_08 5th cycle 140
Table 7.1 The component parts and effective length of the mooring limbs ... 143
Table 7.2 A summary of the primary SWMTF instrumentation 145
Table 7.3 Mass properties of the SWMTF buoy 148
Table 7.4 Non-directional wave parameters 09.18 – 09.35 09/10/2010 150

Table 7.5 Wind parameters recorded by the SWMTF buoy during the time window under consideration 153
Table 7.6 Modelled buoy dimensions 156
Table 7.7 Hydrodynamic coefficients assigned to the modelled buoy 157
Table 7.8 Environmental inputs and peak load results for the validation simulations 158
Table 7.9 Summary of the validation simulations using time history wave data 162
Table 7.10 A summary of the iteration steps and simulated outcomes from the explicit integration simulations 165
Table 7.11 Simulated outcomes for comparison of explicit and implicit integration 167
Table 7.12 A summary of the iteration steps and simulated outcomes from the implicit integration simulations 168
Table 7.13 Simulated outcomes for comparison of the first implicit integration simulation and that of increased current velocity 170
Table 7.14 A summary of the iteration steps and simulated outcomes from the implicit integration simulations with increased current velocity 170
Table 7.15 Summary of the outcomes of the simulations and mooring limb design iterations 171
Table 7.16 Mooring stiffness tangent moduli at dynamic simulation peak tensions 174

Abbreviations

ADCP	acoustic Doppler current profiler
API	American Petroleum Institute
BV	Bureau Veritas
CALM	catenary anchor leg mooring
DECC	Department of Energy and Climate Change
DGPS	differential global positioning system
DMAC	Dynamic Marine Component test facility
DNV	Det Norske Veritas
DOF	degrees of freedom
EPDM	ethylene propylene diene monomer
FEA	finite element analysis
FFKM	perfluoro elastomer
FFT	fast Fourier transform
FLS	fatigue limit state
FMEA	failure mode and effect analysis
FOS	factor of safety
GPS	global positioning system
HMPE	high modulus polyethylene
IEC	International Electrotechnical Commission
IPCC	Intergovernmental Panel on Climate Change
LCAP	liquid crystal aromatic polyester
LCICG	Low Carbon Innovation Co-ordination Group
LCOE	levelised cost of energy
MBL	minimum breaking load
MEC	marine energy converter
MRE	marine renewable energy
OCIMF	Oil Companies International Forum
PCD	pitch circle diameter
PET	polyester
PTO	power take off
PVC	polyvinyl chloride
RPN	risk priority number

RTK	real time kinematic
SALM	single anchor leg mooring
SCADA	supervisory control and data acquisition
SPM	single point mooring
SWMTF	South West Moorings Test Facility
TINA	Technology Innovation Needs Assessment
ULS	Ultimate limit state
UOE	University of Exeter
UTC	coordinated universal time
WEC	wave energy converter

Chapter 1 Introduction

This thesis describes research work to innovate, design, develop, prove and numerically model a novel fibre rope mooring tether. The mooring tether is conceived for wave energy converter (WEC) applications and other floating marine renewable energy devices. However, it is equally applicable to other highly dynamic floating bodies such as large oceanographic and research buoys. The tether exhibits greater axial extension than conventional fibre ropes and thereby affords greater compliance to the mooring system. Mooring line compliance is described in this work by the term axial stiffness, whereby a low axial stiffness represents a high level of compliance.

1.1 Background

The mitigation of climate change is of critical importance. The Intergovernmental Panel on Climate Change (IPCC) urges us to decarbonise our energy supply and to reduce our energy use (Pachauri and Meyer, 2014). The UK is well placed to utilise carbon free renewable energy having excellent resources in wind, wave and tidal energy. A study commissioned by the Carbon Trust estimates that the total UK wave energy resource is 230 TWh per year and that of this, 70 TWh per year is practical resource (Boud, 2012). For comparison, the final consumption of electricity in the UK for 2013 was reported as 317 TWh (DECC, 2014) with just 15% of the UK generation being renewable energy.

Before the tremendous potential for wave energy can be realised in the UK and worldwide, there remain certain technical barriers that need to be addressed. One area that is identified as requiring novel solutions is moorings and foundations (MacGillivray et al., 2013). This view is supported by the findings of The Technology Innovation Needs Assessment (TINA) for Marine Energy. The TINA study by the Low Carbon Innovation Co-ordination Group (LCICG) finds that foundations and moorings require targeted R&D noting that there is a need for improved station keeping technologies (LCICG, 2012).

The mooring system is an important sub-system of any floating marine energy converter (MEC). Project developers will aim to deploy devices in areas of high energy resource so that the financial return is maximised and hence the

levelised cost of energy (LCOE) is minimised. Deployment of a floating device in highly energetic wave conditions or tidal currents, will inevitably subject the device and the mooring system to correspondingly high magnitude loads. In extreme conditions these loads will be very much greater than those loads experienced ordinarily. These loads, termed extreme loads, drive the engineering design of both the mooring system and the structural elements of the floater. Whilst it is technically feasible to cater for these elevated loads within the mooring design, the cost of components increases in proportion to their rated minimum breaking load (MBL) (Harris et al., 2004). This creates a disparity between the cost of the system and the financial returns during operation. Gordelier et al. (2014) note that "the capital cost of the mooring system is driven by extreme (peak load) conditions, whilst the revenue is generated under normal operating conditions". To illustrate this, the difference between typical conditions and extreme conditions at the FaBTest MEC test site is shown in Figures 1.1 and 1.2 (van Nieuwkoop et al., 2013). Figure 1.1 shows the cumulative frequency of wave power density from a validated 23 year hindcast model and Figure 1.2 shows the corresponding wave height / period scatter plot. It is clear that the extreme power density (50 kW/m) accounts for less than 1% of the time whilst the power density is less than 10 kW/m for nearly 90% of the time. Similarly the peak wave height (H_{m0} = 3.5 to 4.0 m) is shown to have an occurrence of just 0.2%.

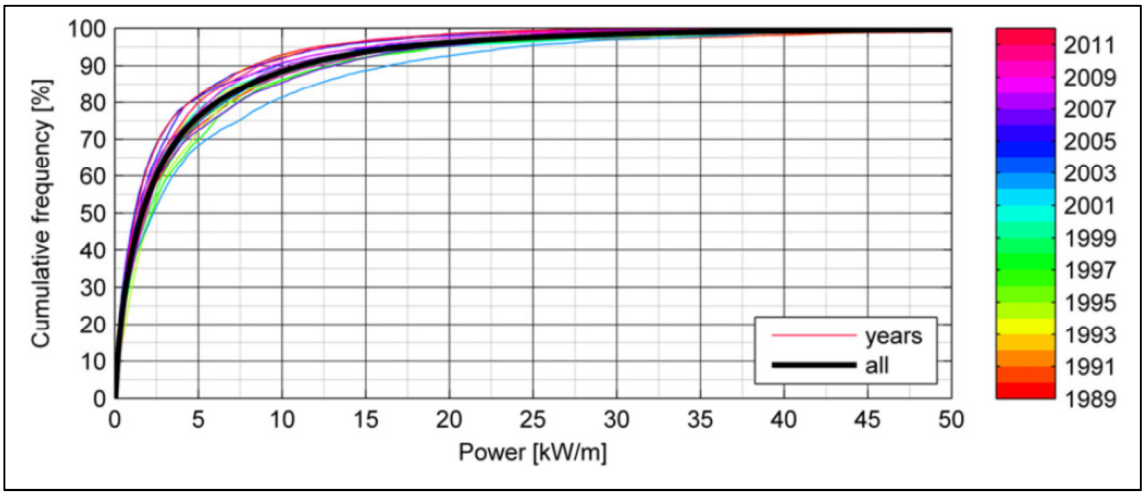

Figure 1.1 Wave power frequency at FaBTest

(van Nieuwkoop et al., 2013)

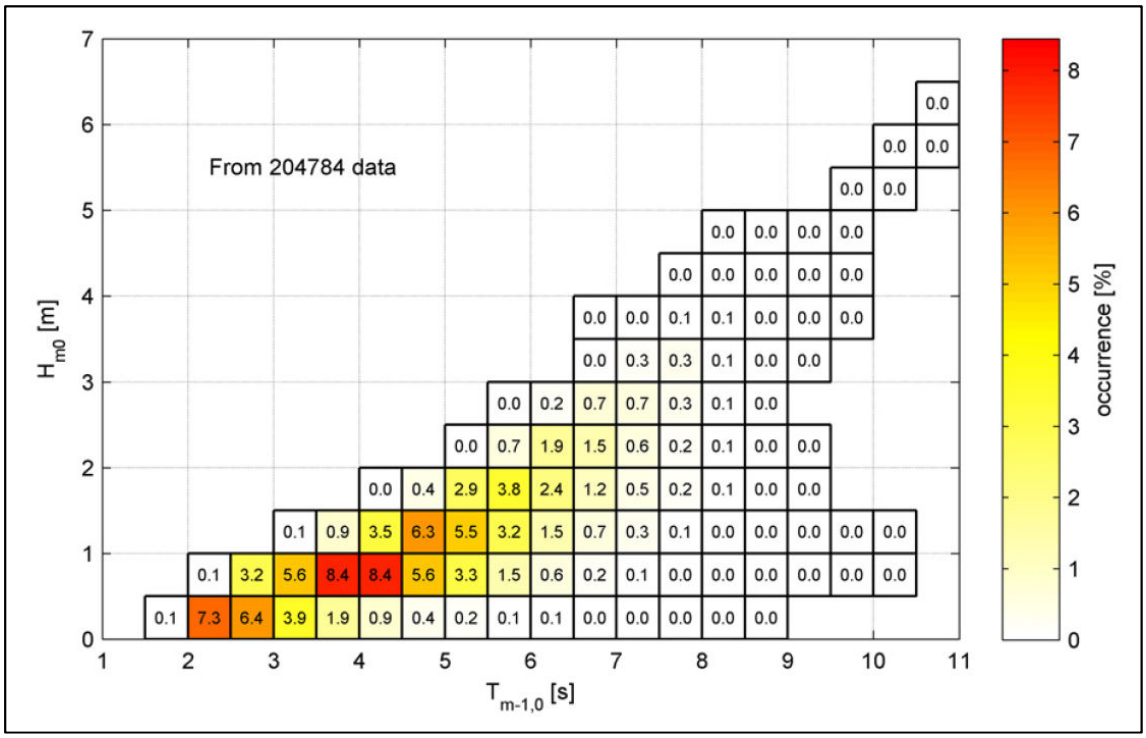

Figure 1.2 Wave height / period scatter plot for FaBTest

(van Nieuwkoop et al., 2013)

1.1.1 Design Factors of Safety

In the mechanical engineering design process for a component or system, the forces that will act are predicted by means of calculation and modelling. The loading regimes, including both peak loads and fatigue loads, then constitute the load cases for the design. It is essential that a factor of safety (FOS) is applied to load cases to allow a margin between the predicted load magnitudes and the predicted loading capability of the design. This margin is necessary to allow for:

1. Negative deviations from the predicted material properties.
2. Uncertainties resulting from the operating environment.
3. Uncertainties resulting from the calculation / modelling of forces.

The FOS that is applied to a design might be selected by the design authority or it might be specified by a code or standard that is applicable. In the case of MEC mooring systems, offshore standard DNV-OS-E301 (Position Mooring) is applicable. This standard addresses peak loads as the *Ultimate limit state* (ULS) and fatigue loads as the *Fatigue limit state* (FLS), these states being

further defined. The standard specifies safety factors according to the risks (consequence class) and the methods used to determine the load case. The safety factors applicable to chain, steel wire rope and synthetic fibre rope are given in Table 1.1 (DNV, 2013a).

Table 1.1 Partial safety factors for ULS

Consequence class	Type of analysis of wave frequency tension	Partial safety factor on mean tension	Partial safety factor on dynamic tension
1	Dynamic	1.10	1.50
2	Dynamic	1.40	2.10
1	Quasi-static	1.70	
2	Quasi-static	2.50	

Whilst it is wholly necessary to apply a FOS, the consequence is that the disparity between the loads predicted during normal operating conditions and those that define the engineering design, is magnified (load case x FOS). The result of this is to further hinder the financial viability of the technology by raising the LCOE.

1.2 Motivation for This Work

The motivation for this work originates from the author's detailed design, construction and commissioning of the South West Moorings Test Facility (SWMTF). The SWMTF is an advanced facility comprising a highly instrumented data buoy, seabed mounted acoustic Doppler current profiler (ADCP), compliant mooring system and communications link (Johanning et al., 2008).

During the design work it became increasingly clear that the level of compliance provided by a mooring system greatly affects the peak loads that arise within the system. This outcome is well recognised and was previously reported by Johanning et al. (2007) and others.

The initial design for the SWMTF resulted in the buoy having a diameter of 2.6 m and a mass of 2000 kg. However, through resolving design conflicts the final design of the SWMTF buoy called for a diameter of 2.9 m and a mass of 3243 kg. These design conflicts arose in terms of axial line loads, line breaking

strength, axial stiffness, structural integrity, structural mass, factor of safety, static vertical mooring pre-tension and reserve buoyancy.

The iterative design process that led to these changes followed the classic design spiral which is illustrated by Smith (1988). This illustration is modified (Figure 1.3) to reflect the SWMTF design criteria.

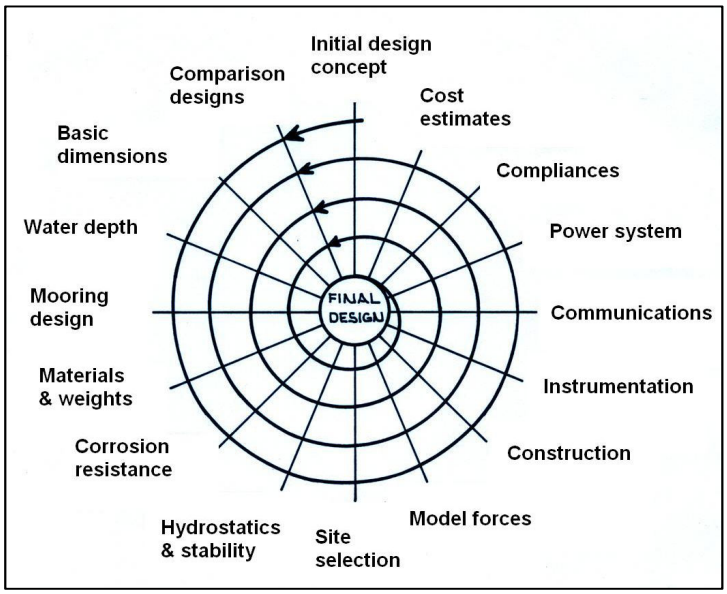

Figure 1.3 The SWMTF design spiral

The SWMTF design employs a three limbed catenary mooring system. Each limb comprises 41 m of steel chain (bottom end) and 20 m of fibre rope (top end). This layout is illustrated in the schematic diagram given as Figure 1.4.

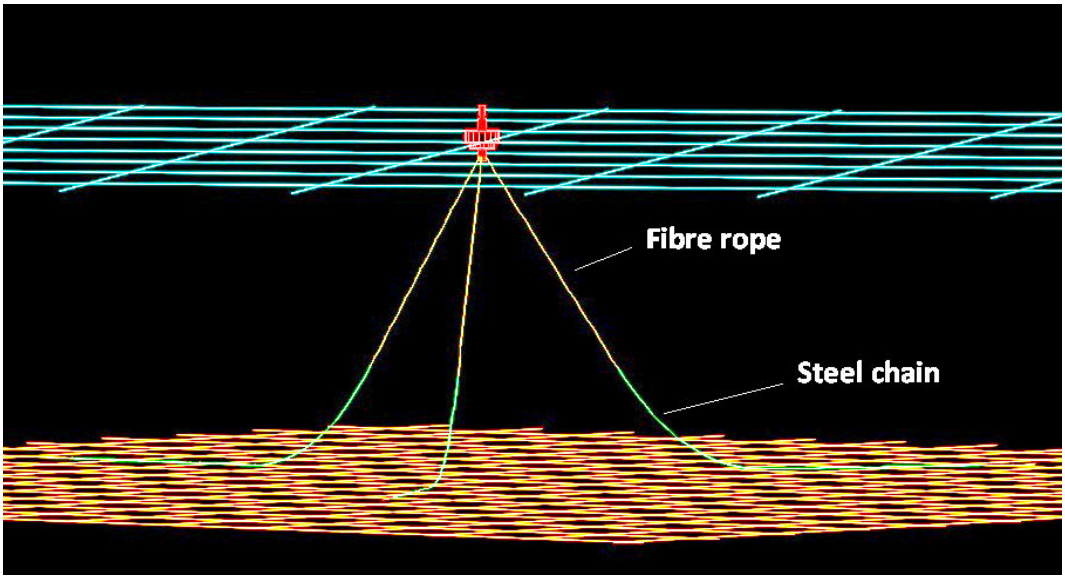

Figure 1.4 Simplified schematic diagram of the SWMTF mooring system.

The iteration process prompted an increase in the chain catenary mass to alleviate snatch loads within the mooring system. The 19 mm chain originally specified was increased to 24 mm. This increased the vertical loading on the buoy which called for greater reserve buoyancy. Additional buoyancy was achieved by increasing the buoy diameter and this elevated the hydrodynamic loads which were passed into the mooring system. The increased mooring line loads then called for higher strength fibre ropes so that the required FOS was maintained. An increase to the minimum breaking load (MBL) of the rope was accompanied by increased axial stiffness; this change once again elevated the load case. Each time the load case was elevated, the structural strength of the floating body also required review and the mass increased incrementally through the design iteration process. As the mass of the buoy increased, so did the predicted deceleration loads.

The design iteration had spiralled in a way which had increased masses, loads and cost before arriving at an elevated solution level. It was recognised that several coupled factors had driven this escalation, these were:

1. Catenary action – Catenary mass
2. Catenary mass – Vertical load on buoy
3. Vertical load on buoy – Buoyancy required of buoy
4. Buoyancy of buoy (diameter) – Hydrodynamic loading
5. Load case – Mass of buoy (structural elements)
6. Mass of buoy – Deceleration loads
7. Required fibre rope MBL – Axial stiffness
8. Axial stiffness – Force reaction / load generation

Many of these couples result from fundamental relationships and cannot be de-coupled. However, couples 1 and 2 can be affected by variations to the pre-tension that is set in the catenary. Couple no. 5 can be affected by specifying an alternative structural material, for instance aluminium instead of steel. Couple no. 7 can be affected by specifying an alternative material and / or construction for the fibre rope. Critically though, the axial stiffness for a fibre rope of a given material and construction is coupled to its MBL. This relationship is demonstrated in Figure 1.5 which shows the axial load plotted against the axial extension (%) for a specific rope in the ‘new’ and ‘worked’

condition (Bridon, 2007). The load data has been normalised against the MBL to produce generic curves for all sizes of this double braid, polyester rope, manufactured by Bridon.

From the SWMTF design process, it was evident that a significant advantage could be gained if a rope's axial stiffness could be de-coupled from its MBL. This would allow the axial stiffness to be selected independently of the required strength, thus breaking the spiral of load escalation described above and allowing a lower order solution level to be achieved.

If possible, the resulting mooring line technology would have the potential to make a significant contribution to the progress of the wave energy sector and other floating MECs.

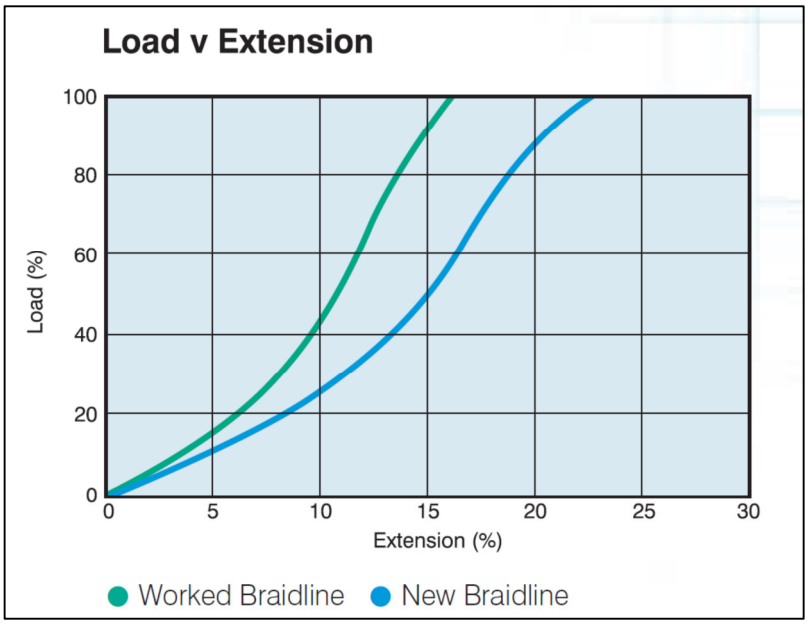

Figure 1.5 Extension properties for Bridon's polyester Braidline rope (Bridon, 2007).

1.3 The Aim of this Work

The aim of this work is to conceive, develop and prove a novel mooring tether having preferential extension properties over conventional ropes. Importantly, the tether will still use fibre rope as the load carrier. This will provide an uncompromised load path along the tether and through conventional terminations and connections.

Through this process, the following research questions will be addressed:

Q1. Is it possible to develop a novel, fibre rope mooring tether whereby the axial stiffness is decoupled from the MBL of the rope?

Q2. Can the novel tether provide more favourable axial extension properties for MEC mooring lines than conventional fibre ropes?

Q3. Can the novel tether facilitate the selection of axial stiffness, for a given MBL, at the tether design stage?

Q4. Does the novel tether have the capability to significantly reduce peak mooring loads for highly dynamic MEC devices?

1.4 The Research Methodology

The following methodology is used to answer the research questions. For each stage, the chapter or chapters where the work is presented is identified:

a) Review the existing literature, identify the state of the art and validate the need for novel tether solutions. This work is presented in ***Chapter 2***.

b) Conceive two fibre rope mooring tether inventions. Assess the two concepts using small scale prototypes, conduct failure mode analysis and select a single design to take forward. This work is presented in ***Chapters 3 and 4***.

c) Develop the proof of concept prototype design, up-scaling from the small scale prototype. Manufacture a range of prototypes in collaboration with an industrial partner. The prototypes have varying material properties and constructions so that the mechanisms are best identified and understood. This work is presented in ***Chapter 5***.

d) Plan and conduct test work on the tether and the materials. This includes the modification and preparation of the Dynamic Marine Component Test Facility (DMaC) to facilitate highly compliant tether testing. Analyse the tether performance, characterise the extension properties and relate this to the material properties. This work is presented in ***Chapter 6***.

e) Investigate the ability of the tether to significantly reduce peak loads using numerical modelling of the SWMTF buoy and mooring system. A validated numerical model is modified to substitute the existing lines for tethers with axial properties derived from the test work. This work is presented in ***Chapter 7***.

f) Discuss the outcomes from the tether design, test work and modelling. This is presented in ***Chapter 8***.

g) Draw conclusions and outline the further work. This is presented in ***Chapter 9***.

Referencing these method stages to the research questions:

Q1 – Q3 are addressed by stages (b) – (d).

Q4 is addressed by stage (e).

1.5 Scope

This work is limited to the development and analysis of the tether functionality, taking the tether through the proof of concept stage. The work does not explore or significantly address the durability of the tether which is the subject of separate research work.

1.6 Contributions to Knowledge

The contributions to existing knowledge made by this work are broadly as follows:

1. The innovation of the elastomeric tether described within this work. This tether utilises a hollow braided rope and the primary load carrier which is entirely new in the burgeoning technology sector of elastomeric mooring tethers.
2. The work defines a methodology for fully wet extension testing of such an elastomeric tether, where no previous standard or practice is recorded. The methodology includes the evolution of a ‘dynamic zero load length’ which represents the ‘in cycle’ free length of the tether which exhibits a time dependant recovery from axial extension.

3. The modelling work numerates the advantage provided by the elastomeric tether using a numerical simulation that has the base case validated by real sea testing. This represents a step forward from the existing numerical studies of elastomeric tethers that use cross validated or un-validated numerical simulations. This analysis of mooring load reduction includes the downward iteration of axial stiffness and catenary mass in the mooring design which is not previously numerated.

Chapter 2 Literature Review

In this chapter arguments are developed that support the innovation and development of the novel tether. The literature demonstrates that there is a clear need for compliance in, for instance, WEC mooring systems and that currently the practicable level of compliance is limited by the axial stiffness of fibre ropes. The axial stiffness of fibre ropes is maintained at an elevated level (low compliance) by the load case itself and the FOS that is applied.

This review is conducted in three sections:

- Mooring Systems for Highly Dynamic Floating Bodies such as marine energy converters (MECs).
- Fibre Ropes; their use as Mooring Tethers for Highly Dynamic Floating Bodies such as MECs.
- Novel MEC Mooring Tethers having Advantageous Extension Properties.

An introduction to mooring systems is included at the beginning of this chapter to provide a background to the principles discussed.

2.1 An Introduction to Mooring Systems

Floating bodies that are required to hold station typically do so by means of a mooring system. The alternative method, termed dynamic positioning, utilises motorised thrusters to achieve station keeping and is not discussed here.

2.1.1 Ship Anchoring

In its most simple form a mooring system can comprise a single mooring line and a seabed fixing. Such a system is used commonly for boats and ships of all sizes with the seabed fixing being a drag embedment anchor and the mooring line being attached to the bow of the vessel.

It is useful to consider the ship's simple anchoring system as it embodies many of the solutions and limitations that are dealt with by more complex mooring systems. Figure 2.1, provided by an anchor manufacturer, shows a small ship anchored with an embedment anchor, using steel chain for the anchor line. For low and moderate conditions (shown as A and B), the heavy chain adopts a curved form, termed a catenary. When subjected to oscillating loads

(emanating from waves and wind gusts) the catenary extends and recovers, allowing controlled excursions and minimising the line tension by avoiding snatch loads during the peak events. However, in extreme conditions (shown as C), the catenary might straighten completely giving rise to unacceptably high tension loads in the line.

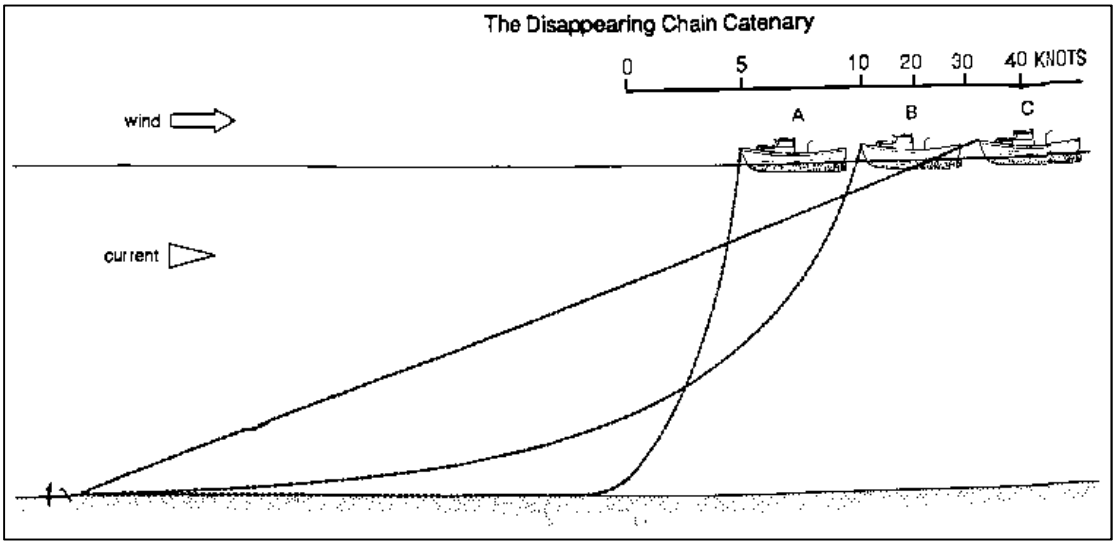

Figure 2.1 Schematic diagram of a ship's catenary anchor line (Dulmison, 2016).

A secondary problem for the system depicted in C is that the drag embedment anchor is likely to break free from the seabed if it is subjected to vertical loading. Other than this observation, anchors are not dealt with in this work.

To avoid the unacceptable condition demonstated by case C, the length of the chain is increased, as is the weight per metre of the chain. This inevitably increases the maximum distance between the ship and the anchor and increases the pre-tension of the line acting on the ship. Smaller vessels such as yachts might reduce the weight of the catenary by replacing the upper portion of the chain with fibre rope. If this rope is correctly specified, its ability to stretch can replace or exceed the energy absorption achieved by the mass of chain catenary that is removed.

The ship's single anchor line allows it to swing through 360° around the anchor and in so doing it will automatically offer the least resistance possible to the prevailing conditions. However, by weathervaning in this manner the ship's station keeping is relatively poor.

2.1.2 Industrial Mooring Systems

More complex mooring systems have evolved through the late 20th century to satisfy the requirements of the offshore oil and gas industries. These systems can be split into two main categories; those that prioritise horizontal station keeping, such as catenary mooring systems and those aimed at minimising vertical motions, such as vertical tension leg mooring systems. The latter of these two systems is utilised for tension leg platforms (TLP) which use the mooring pre-tension to hold a buoyant structure at a deeper position in the water than its weight alone would achieve (Faltinsen, 1990). The TLP system must utilise mooring lines that are stiff enough so that the vertical dynamics of the system have a high natural frequency with respect to the input forces (Barltrop, 1998). Therefore mooring lines with low axial stiffness are not appropriate to TLP systems and these mooring systems are not discussed further here.

Industrial catenary mooring systems often employ multiple mooring limbs spread radially around the moored body, hence these are sometimes referred to as a mooring spread. In so doing these systems seek the advantages of the catenary whilst significantly improving the station keeping over the single catenary line of a ship at anchor. Figure 2.2 shows a diagram of this arrangement applied to a semi-submersible platform.

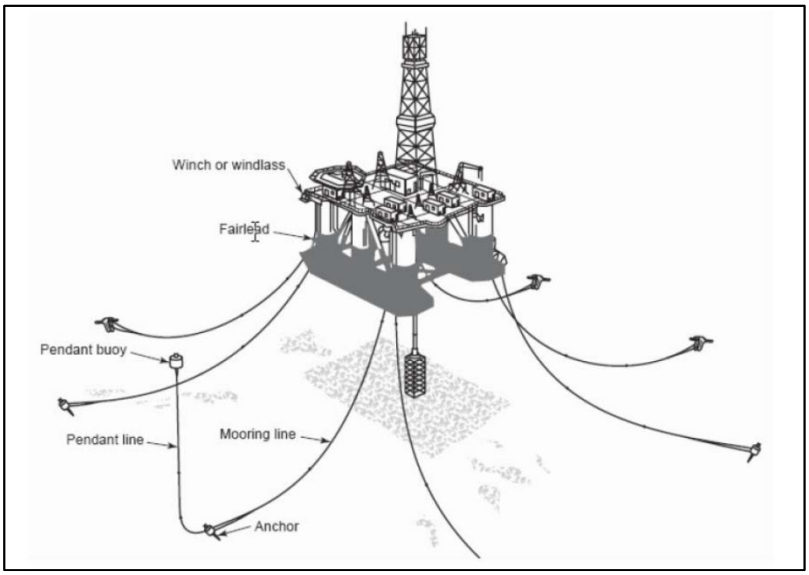

Figure 2.2 A catenary mooring spread applied to a semi-submersible platform (Chakrabarti, 2005).

The box like shape of the platform shown in Figure 2.2 would not achieve the same advantage by aligning with the environmental forces (weathervaning) that a ship would. Therefore the improvement in station keeping is achieved with little negative impact in terms of loading. When a ship requires improved station keeping whilst maintaining its ability to swing freely, a rotating turret mounted towards the bow of the vessel provides the attachment point for a mooring spread.

2.1.3 Mooring Lines

Disregarding the seabed anchors, mooring systems comprise lines and connectors. More complex line architecture might also call for sub-surface floats and clump weights whereby applying uplift and weight respectively, the mooring line is deformed into a zig-zag or wave form.

Mooring line types fall into three broad categories as follows:

1. Steel chain. This can be studless or studded chain where studded chain has an additional strut across the middle of the link, perpendicular to the chain axis. This additional member was introduced for ease of handling and to prevent kinking (Barltrop, 1998). The breaking strength, sometimes termed the catalogue break strength, varies for different grades of chain that are available, these being identified as grades 1, 2, 3 and 4. Chain provides weight to a mooring line hence achieving the catenary form. It also tolerates seabed contact better than other line types due to its robust nature.
2. Wire rope. There are several types of construction for wire rope, these achieving differences in bending and axial stiffness for a given strength. In all cases the wire rope displays greater elasticity than chain of a corresponding strength and is significantly lower in cost (Barltrop, 1998). The greater elasticity of wire rope might be used to provide axial compliance at the top of a mooring limb, perhaps with a chain catenary beneath it. For deep water moorings, wire rope might be favoured over chain to reduce the vertical mooring load acting on the floating body, although chain will still be used for the touchdown to the seabed.
3. Fibre rope. Similarly to wire rope, fibre rope is made in several types of construction and this affects the mechanical properties of the rope. For

fibre rope there is also a polymer choice according to the properties required. The use of fibre ropes in mooring limbs can provide even greater axial compliance than wire rope. Further discussion of fibre ropes is provided in 2.3.

2.1.4 Mooring Loads

The mooring pre-tension will result from the static equilibrium of the floating body and mooring system with no environmental forces acting (wave, wind and current). There will be a total vertical pre-tension which is reacted by the buoyancy of the floating body. This tension might result from the weight of the mooring lines for a catenary system or the tension in the lines for a TLP system for instance. Individual lines might exert opposing horizontal load components which have a horizontal vector sum of zero.

The static loading of a mooring system represents the sum of the steady wind loads, steady current loads and steady wave drift loads. These loads result from the fluid flow around and through the structures comprising the floating body and the mooring system itself.

The dynamic loading of a mooring system is more complex and requires a coupled analysis of the mooring forces and the floating body dynamics. Barltrop (1998) states that a set of equations of motion must be solved which are in the form:

$$M\frac{d^2x}{dt^2} + C\frac{dx}{dt} + Kx = F_{static} + F_{wavefreq} + F_{slowdrift} + F_{mooring}$$

where,

M, C and K are matrices of hydrodynamic mass, damping and stiffness respectively.

x is the displacement vector.

F is the load vector having four primary components.

Software applications such as Orcaflex, used within this work, are able to perform the required coupled analysis.

2.2 Mooring Systems for Highly Dynamic Bodies such as Marine Energy Converters

Whilst this novel tether development work aims to be inclusive of non MEC applications, it is the MEC arena where a significant amount of the literature exists. Specifically, wave energy converters (WECs) are often the subject matter due to the requirement for optimal dynamic response and siting within high energy environments.

2.2.1 WEC Mooring Requirements

Harris et al. (2004) state that there are two major requirements for a WEC mooring system, these are:

1) To withstand the forces at play to effect adequate station keeping.
2) To be cost effective so as not to make the project financially unviable.

This is a simple overview of the mooring systems function; it is further argued that the mooring should be considered to be an integral part of the WEC system, contributing to its performance and not simply treated as an added cost (Harris et al., 2004).

With regard to requirement (2) identified by Harris et al, It is important to consider that the costs relating to a mooring system will not simply be the capital costs. There will inevitably be costs arising from the deployment and decommissioning of WEC mooring systems and possibly from operations e.g. maintenance.

A more detailed breakdown of the mooring system requirements and considerations is given (Harris et al., 2004)

a) Station keeping within limits during operational and storm conditions.
b) Limit excursion induced tension in power transmission cable.
c) Maintain clearance between devices in array configurations.
d) Be sufficiently compliant to minimise the forces acting on the system.
e) Have adequate strength, fatigue strength and environmental durability.
f) Provide redundancy where possible.
g) Have a system life ≥ 30 years with individual component life ≥ 5 years.
h) Accommodate the tidal height range.

i) Allow single WEC removal from an array or cluster.
j) Allow mooring line removal for inspection and maintenance.
k) Be sufficiently stiff to facilitate berthing for maintenance and inspection.
l) Prevent contact between mooring lines.
m) Should not impair the operational efficiency of the device.

Relating to point (m), Paredes et al. (2013) note that some WECs deliberately aim to achieve a resonant response to waves to amplify the wave induced motions. This contrasts with good practise in standard offshore moorings design where it is required that the system does not resonate with the environmental load regime. Paredes et al add that such high amplitude resonance will result in higher magnitude dynamic loads and an increased rate of fatigue damage compared to other floating platforms.

Combining the requirements stated by Harris et al and Paredes et al, we see some interesting conflicts arising with regard to station keeping, compliance, strength, durability and dynamics. This theme of conflicts within the performance requirements for mooring systems is discussed by Fitzgerald and Bergdahl (2007). They note that the mooring system must react the steady and low frequency loads arising from wind, current and wave drift whilst also accepting higher frequency wave induced dynamics. Agreeing with Paredes et al, they add that the wave induced dynamics have the potential to impart unacceptably high loads which must be mitigated.

In their work towards ranking risk and reliability of WEC systems, Hamedni et al. (2014) remind us of the role that WEC moorings systems play in providing reaction to the power take off (PTO) system. They divide the WEC reaction systems into two categories, compliant and rigid, where rigid implies a form of rigid structure. Figure 2.3 shows the different forms of compliant reaction systems.

The reaction of PTO forces might add a further conflict to the already complex situation. There is a clear difference between station keeping within defined limits and reacting the PTO forces. However, both of these functions are achieved by the same mooring system in many instances of WEC design.

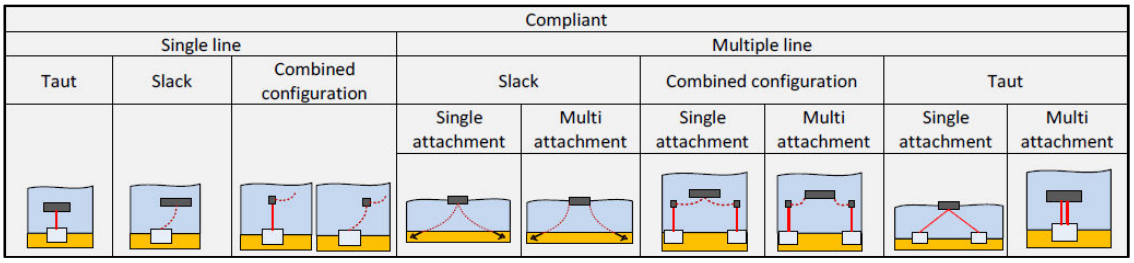

Figure 2.3 Breakdown of the types of compliant reaction systems for WECs (Hamedni et al., 2014)

To this point, the argument presented applies to single WEC devices; a financially viable WEC project will necessitate an array of devices. This adds another conflicting requirement to any moorings design, that of minimal moorings footprint. Karimirad et al. (2014) suggest that the separation distance between MRE devices in an array may be as little as tens of metres in some cases. They add that mooring system compliance will need careful attention to ensure that surge and sway device motions do not result in clashes and that mooring lines must be kept apart.

The picture that is being built up of an effective WEC mooring system is that of a careful balance between restraint and freedom or 'resist' and 'yield' according to the exact needs of a device. This balance must be met whilst providing adequate strength and durability according to the required FOS and whilst not occupying an excessive area of consented seabed. A sub-optimal system is likely to impair the financial viability of a project by elevating the loads and costs whilst having a negative impact on energy yield. This view is supported by Paredes et al. (2013) who suggest that careful optimisation of the mooring system for a WEC project will have a significant effect on the cost of the electricity generated.

The careful balance argued above implies a high level of design control over the mooring system compliance. Such design control is possible via mooring system architecture and the axial stiffness of the lines.

2.2.2 WEC Mooring System and Line Architecture

A simple form of a compliant mooring limb is provided by a chain catenary as explained in 2.1.1. The chain hangs in a catenary form from the floating body and usually makes contact with the seabed at a distance from the anchor point.

Mc Evoy (2012) explains that the weight of the chain catenary provides the restoring force when the floating body undertakes an excursion.

A single limb catenary mooring will allow a moored object to weathervane around the anchor point according to wave, wind and current forces, thus occupying a large area. A two, three or four limbed catenary mooring system might be considered but concerns are also raised with this approach.

Harris et al. (2004) suggest that free hanging chain catenary systems may not allow sufficient extension without introducing excessive loads where the tidal range is high. They add that the restraining stiffness of such a system could impair the required motions of the device. In this case it might be necessary to soften the mooring system to allow the required dynamic response. This can be achieved by reducing the catenary weight. However, Johanning and Smith (2008) note that simply reducing the number of catenary lines or reducing catenary weight will increase the risk of line lifting towards the anchor point and hence the generation of elevated peak loads.

The implication here is that the balance between restraint and freedom discussed earlier will be difficult to achieve with a simple catenary system without incurring snatch loads as the catenary fully straightens.

One solution that might allow a catenary system to have minimal impact on the WEC dynamics, whilst having sufficient catenary weight, is to tether the WEC to a catenary anchor leg mooring (CALM) buoy. A study by Pecher et al. (2014) compares the performance of a CALM buoy system with a single anchor leg mooring system (SALM) in respect of WECs. The CALM buoy utilises a three limbed chain catenary with the WEC being horizontally tethered to the CALM buoy by wire rope. The SALM system utilises a single tension limb of wire rope from the seabed to a sub-surface buoy to which the WEC is tethered by wire rope. Figure 2.4 shows these two configurations in schematic form.

A quasi-static analysis is performed with a horizontal reference load of 3000 kN. The resulting horizontal excursions and mooring system stiffness are compared for the two systems. Figure 2.5 shows the outcomes for a 30 metre water depth.

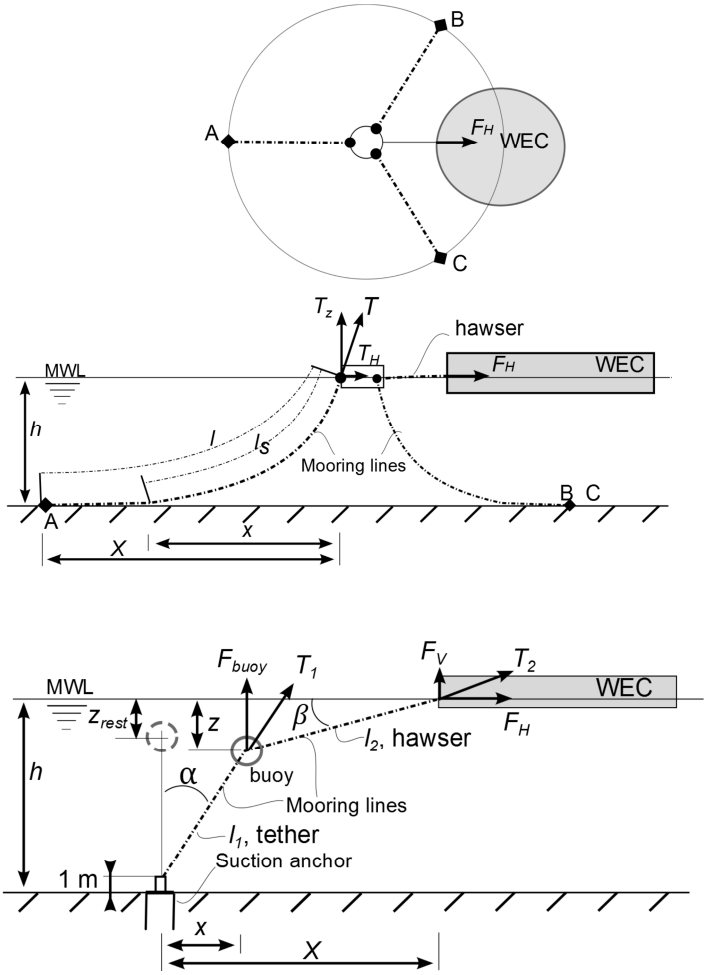

Figure 2.4 Schematic diagram of the CALM (upper) and SALM (lower) WEC moorings (Pecher et al., 2014)

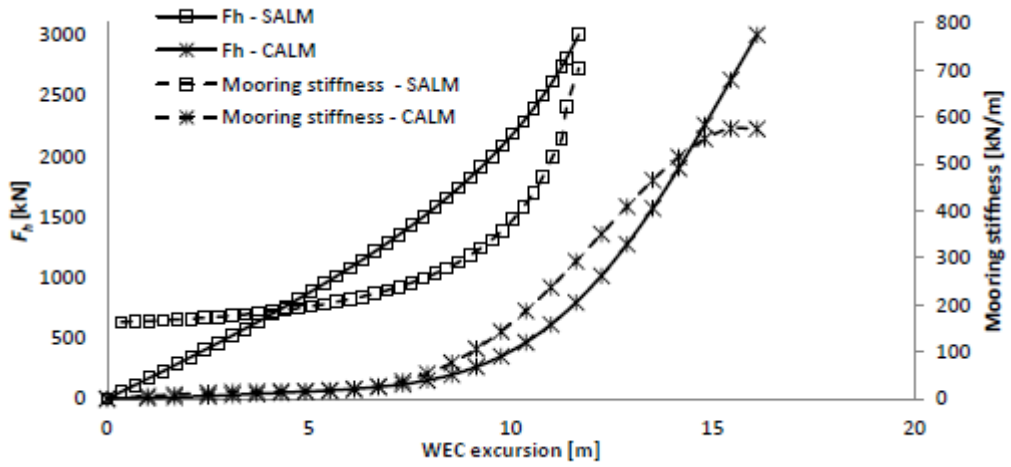

Figure 2.5 Force vs displacement and mooring stiffness curves for the two mooring systems at 30 m water depth (Pecher et al., 2014).

Pecher et al. (2014) conclude that the mooring system stiffness increases with excursion very differently for the two systems. The CALM mooring system has a very low stiffness until approximately 50% excursion after which it increases steeply. The SALM displays a more progressive increase to mooring stiffness until a level of around 80% excursion and then it increases steeply. They suggest that the operational working range of the SALM system exceeds that of the CALM system. Pecher et al. (2014) add that "this will have a very strong influence on the dynamic behaviour of the system and the resulting mooring loads".

Earlier work by Fitzgerald and Bergdahl (2007) concludes more strongly that simple catenary mooring systems are not an effective solution for WECs. They argue that in a catenary system it is the inertia and damping properties of the cable that react the wave induced dynamic forces. They suggest that to minimise the associated loadings and allow the dynamics, a mooring limb utilising elastic or hydrostatic characteristics might be advantageous. In their study Fitzgerald and Bergdahl assess five different limb compositions: (1) simple chain catenary, (2) chain catenary with surface buoy and synthetic rope, (3) chain catenary with clump weight, steel rope, buoy and synthetic rope, (4) vertically loaded anchor with steel rope, buoy and clump weight, (5) vertically loaded anchor with steel rope and compliant nylon rope. These limb compositions are illustrated in Figure 2.6.

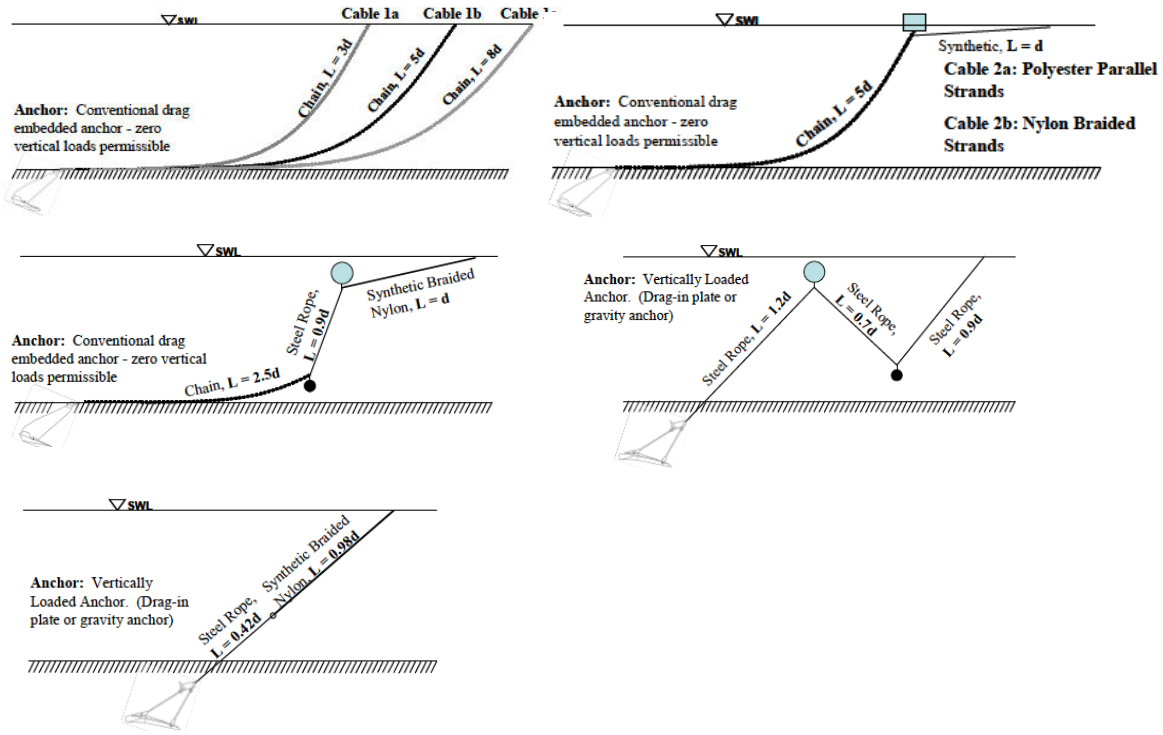

Figure 2.6 Limb compositions; simple chain catenary (top left), chain catenary with surface buoy and synthetic rope (top right), chain catenary with clump weight, steel rope, buoy and synthetic rope (middle left), vertically loaded anchor with steel rope, buoy and clump weight (middle right) and vertically loaded anchor with steel rope and compliant nylon rope (bottom) (Fitzgerald and Bergdahl, 2007).

From their analysis Fitzgerald and Bergdahl (2007) conclude that:

1. Simple catenary moorings are not an efficient solution for WECs.
2. Hydrostatic stiffness from buoys can reduce line weight and induced loads as well as allowing better motion response of the device.
3. The use of compliant synthetic line shows an even greater advantage than that found with hydrostatic configurations. This is particularly so if the axial stiffness of the line is low.
4. Anchors that can react vertical loads bring benefit to array moorings.
5. The combination of low axial stiffness lines and vertical anchors provides the potential for very efficient WEC mooring solutions. Further research should concentrate in this area.

This view is strengthened further by Johanning and Smith (2008) who use experimental and modelled data to study the relationship between axial line load and floater excursion for three different line types; catenary chain, catenary

chain with fibre rope top section and a fibre rope line in an S shape with float and weight. They concur with Fitzgerald and Bergdahl (2007) that hybrid (chain – rope) and S shape configurations can provide advantages in terms of reduced peak loading and un-impaired floater dynamics. These advantages are associated with the lower stiffness which also allows an increased excursion.

More recently Karimirad et al. (2014) agree that it is possible to add compliance and reduce peak loads by using a combination of synthetic ropes and chains. Figure 2.7 illustrates the use of synthetic rope in five configurations, three of these employing both rope and chain components.

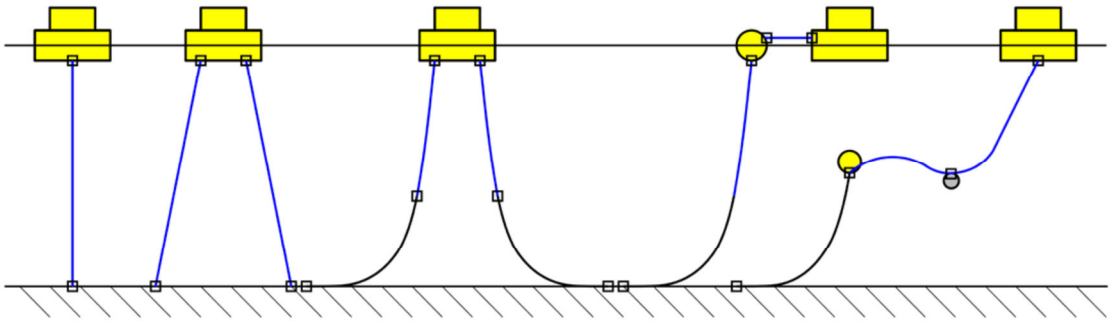

Figure 2.7 Possible mooring configurations for a single MEC: (from left) taught single line (rope), taught multiple lines (rope), basic catenary (rope and chain), catenary with surface buoy (rope and chain) and lazy wave (rope and chain) (Karimirad et al., 2014).

Taut moorings such as the two illustrated in Figure 2.7 provide a stiffer system than is achieved with slack systems. In these cases the compliance offered by the system depends on the axial properties of the mooring lines (Karimirad et al., 2014).

In summary, the literature takes us towards a view that simple catenary mooring systems will not achieve the resolution of the conflicts discussed in 2.2.1. More complex architecture moves us closer to an effective solution but highly compliant mooring lines might provide the best solutions, perhaps in a hybrid arrangement.

2.3 Fibre Ropes: Their use as Mooring Tethers for Highly Dynamic Floating Bodies such as Marine Energy Converters

The literature described in 2.2 demonstrates that mooring systems for highly dynamic floating bodies, such as WECs, can benefit from lines having low axial stiffness. Fibre ropes, particularly Nylon ropes, offer low axial stiffness relative to other mooring lines and are therefore considered for such applications.

2.3.1 Offshore Standards

Before any argument can be made towards the use of fibre ropes or novel fibre rope tethers, it is necessary to consider the situation regarding certification.

It is important that any mooring solution conceived for MECs can be validated against an applicable standard. This ensures that sufficient rigour is applied to the process to achieve a predictable performance. Certification also underpins critical financial activities such as insurance and investment thus allowing a sound financial basis to a project.

Offshore standard DNV-OS-E303, Offshore Fibre Ropes, specifies the technical requirements for fibre ropes and tethers in accordance with DNV-GL certification of a MEC utilising fibre ropes within the mooring system. The standard allows for the use of aramid, polyester, high modulus polyethylene (HMPE), liquid crystal aromatic polyester (LCAP) or polyamide materials for the load-bearing yarns. Applications include taut mooring systems, semi-taut mooring systems and catenary mooring systems where only a portion of the system contains fibre line (DNV, 2013b).

Alternative standards pertinent to fibre ropes in offshore moorings are drawn up by the American Petroleum Institute (API, 2005), Bureau Veritas (BV, 2007) and others. The marine renewables industry is currently awaiting a specific standard for floating MEC moorings which will be published by the International Electrotechnical Commission (IEC) (Johanning, 2015).

2.3.2 Axial Stiffness

It is useful to further explain this term and how it is affected in fibre rope by material and construction choices.

The level of compliance that a rope provides by extending axially when it is subjected to a tension load is defined by its axial stiffness. The Handbook for fibre rope technology states that the axial stiffness of a rope can be quantified at any load by the slope of the load / strain curve, giving axial stiffness the unit of newtons (N). However, it is common practise to normalise the load against the MBL and express strain as a percentage extension. Axial stiffness can be determined as a tangent or secant modulus (McKenna et al., 2004).

For a conventional fibre rope of a given strength, the axial stiffness is determined by the material selection and the rope structure; the load history will also have an effect (Weller et al., 2015a) as will wetting (McKenna et al., 2004).

In a recent review paper Davies et al. (2014) present a useful guide to the relative extension properties of synthetic rope fibres according to the applied stress. In this case the stress is given in terms of N/tex, tex being a measure of linear density applied to fibres; 1 tex equals 1 gm per 1000 metres. The graphical comparison is given as Figure 2.8 and clearly demonstrates the low axial stiffness of Nylon in particular and polyester (PET) in comparison to other materials.

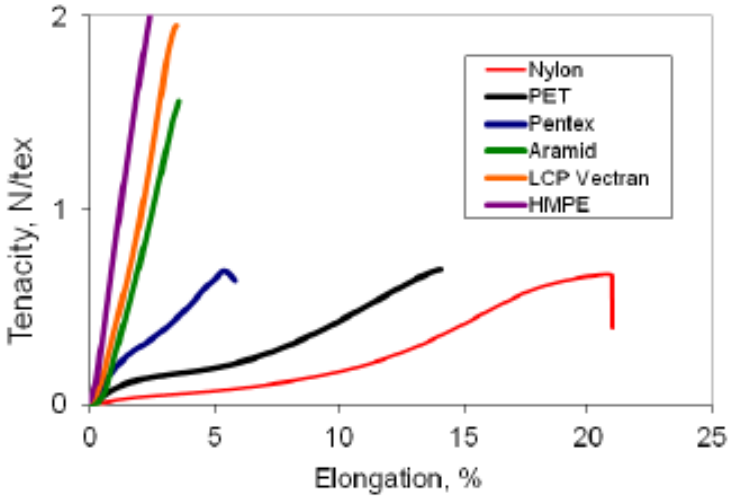

Figure 2.8 Examples of single filament tensile properties for fibre rope materials (Davies et al., 2014)

The effect that the rope construction has on the axial stiffness is evident in the technical sales literature e.g. (Bridon, 2007). The difference in extension properties reflects the route of the load path along the rope. The stiffest construction offered by Bridon has the load carrying sub-ropes running parallel to the rope axis (parallel lay).

2.3.3 Material and Construction Choices

Early studies of the properties and suitability of fibre ropes for offshore moorings were conducted during the late 1970s and 1980s. This work focused on the use of fibre rope hawsers to tether tankers to single point moorings (SPMs) and led to the publication of the SPM Hawser Guidelines by the Oil Companies International Marine Forum (OCIMF) (Ridge et al., 2010).

Hawsers used at this time were typically Nylon or polyester and had breaking strengths in the region of 2500 – 4500 MN. One study discovered that the breaking strengths of individual ropes were often lower than those published in the specifications. Another finding was that the strength of wet Nylon rope deteriorated significantly during tension cycling due to internal abrasion (Flory, 2000). This result for Nylon rope contrasts with the findings for polyester rope which can have a fatigue life greater than 50 times that of steel wire rope (Weller et al., 2015b).

Unfortunately the hierarchy between Nylon and polyester rope is reversed when considering axial stiffness where a low axial stiffness is desirable. This is demonstrated by the technical sales literature for fibre ropes. Bridon (2007) characterise the axial stiffness of their ropes in graphical form; Nylon Superline rope achieving 12.5% extension at 40% of breaking load and polyester Superline rope achieving 6% by comparison. A similar result is shown by Ridge et al. (2010), their result for this comparison is shown in Figure 2.9.

The conflict between excellent fatigue life in polyester rope but superior axial stiffness in Nylon rope, prompted Ridge et al. (2010) to further investigate the fatigue properties of Nylon ropes for WEC applications. Their work seeks to identify and characterise the best case Nylon rope in this respect.

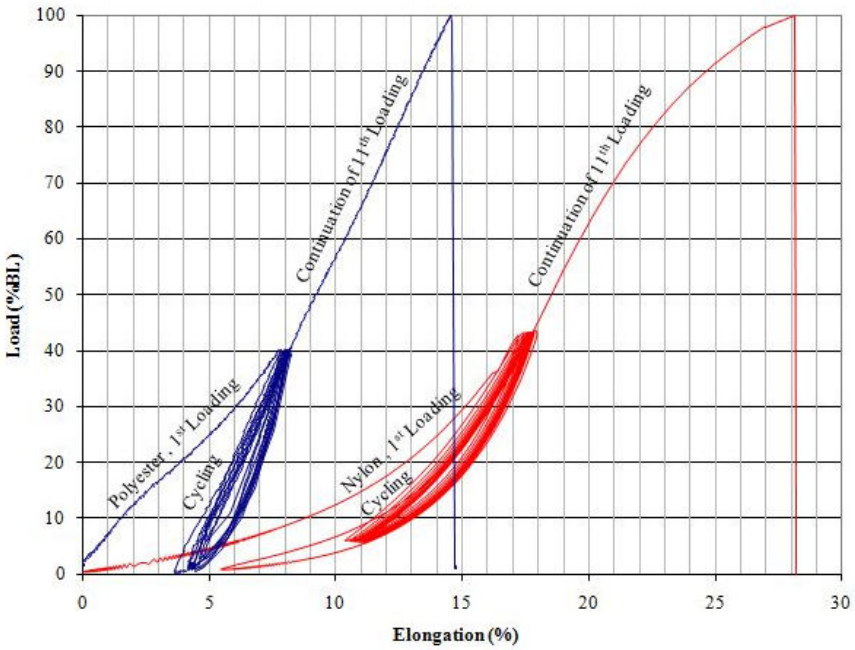

Figure 2.9 Comparison of axial stiffness for Nylon and polyester rope (Ridge et al., 2010)

Ridge et al. (2010) reject the double braid and 8 strand rope constructions commonly used for polyester ropes as these types have too many strand crossovers. The crossovers cause damage to Nylon ropes giving them a correspondingly poor cyclic fatigue performance. Instead they favour the parallel lay rope construction (Superline) for Nylon rope, whereby the sub-ropes are arranged axially within the outer jacket. The sub-ropes are laid ropes with a long lay length i.e. a slow helix. The test work is performed on sub-ropes rather than the full rope construction. Their results are summarised in Figure 2.10 and show a much improved fatigue resistance for the long lay Nylon sub-rope compared to the double braid or 8 strand Nylon ropes.

The findings of the study suggest that Nylon Superline ropes, in a WEC mooring system will give a service life according to fatigue, in excess of 2000 years. They add that this is comparable or superior to the performance of chain or wire rope. By the same test and prediction methodology, conventional Nylon double braid and 8 strand rope would be expected to have a service life of around 3 months (Ridge et al., 2010)

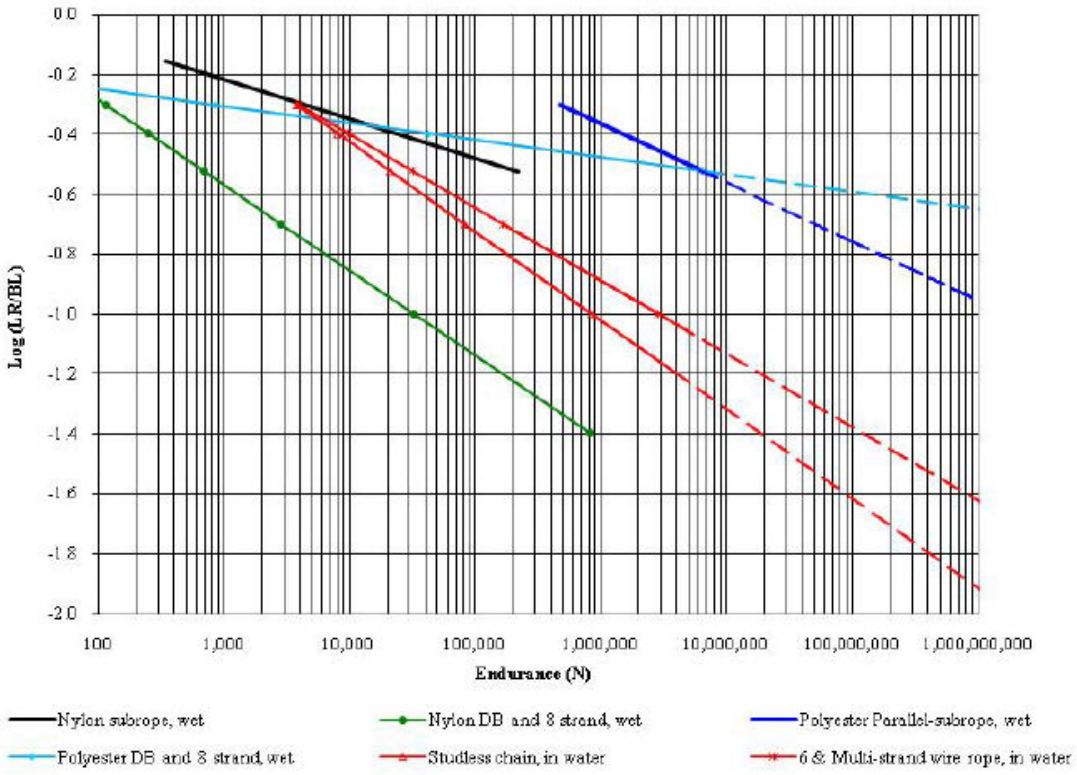

Note: The dashes indicate an extrapolation of the trend line (i.e. there are no actual data points available at such high numbers of cycles).

Figure 2.10 Fatigue endurance results for Nylon rope, polyester rope, steel wire rope and steel chain (Ridge et al., 2010). Log (load cycle range / breaking load) plotted against the number of cycles at failure.

This is an encouraging outcome which progresses the use of Nylon ropes in MEC moorings. However, it is important to focus on the objective of this work which is to achieve low axial stiffness. Referring to the technical sales literature (Bridon, 2007) and reading the extension at 40% MBL from the curves provided for worked rope, Table 2.1 is constructed.

Table 2.1 Extension for worked polyester and Nylon ropes subjected to 40% MBL (Bridon, 2007)

Extension at 40% MBL	Polyester	Nylon
Worked double braid construction	**9.5%**	**18%**
Worked parallel lay construction	**6%**	**13%**

Whilst the 13% extension achievable with the Nylon Superline rope is helpful in terms of compliance, it is not a large step forward from the 9.5% achievable with double braid polyester which has superior fatigue strength (Figure 2.10). It is argued here that a much more significant improvement to axial stiffness is required to reduce WEC mooring loads and hence achieve the target cost reductions (LCICG, 2012). It is further argued that a better ability for moorings designers to select axial stiffness would be advantageous in achieving the optimal resolution of the conflicts previously discussed. Both of these highly desirable outcomes are only possible if the axial stiffness of the fibre rope can be de-coupled from the MBL.

2.4 Novel MEC Mooring Tethers having Advantageous Extension Properties

There are only a few examples of novel mooring tethers of a scale suitable for MECs and consequently little literature in this area. This reflects the very early stage that this strand of research and development work is at. Due to the scarcity of scientific literature, some review of technology status is also included. Although of a different scale, there is a parallel with the elastomeric moorings for oceanographic data buoys and seabed observatories; some literature from this area is included to inform the argument.

Irish and Kery (1996) recognised that the data buoy mooring systems of the day, successfully used in deep water, often failed prematurely in shallow coastal deployments. They attributed this to the reduced length of the Nylon rope that provided adequate compliance in deep water but not in shallow coastal waters. The solution that they propose replaces the Nylon rope with an elastic tether, achieving a higher level of compliance.

The trial of the system used a 900 kg displacement data buoy, having 1400 kg of reserve buoyancy, moored at the Georges Bank, Gulf of Maine. The site is located in 40 metres water depth, tidal currents are typically 1.5 m/s and wave heights of up to 15 metres are experienced. The conventional mooring system utilised chain, which would lift from the seabed to add compliance to the system. However, in these extreme conditions the chain would be lifted fully leaving little or no compliance and the buoy would be overtopped by waves, causing damage (Irish and Kery, 1996). The elastic element trialled at this site

comprised six 1” diameter rubber cords in a parallel array and is shown in Figure 2.11.

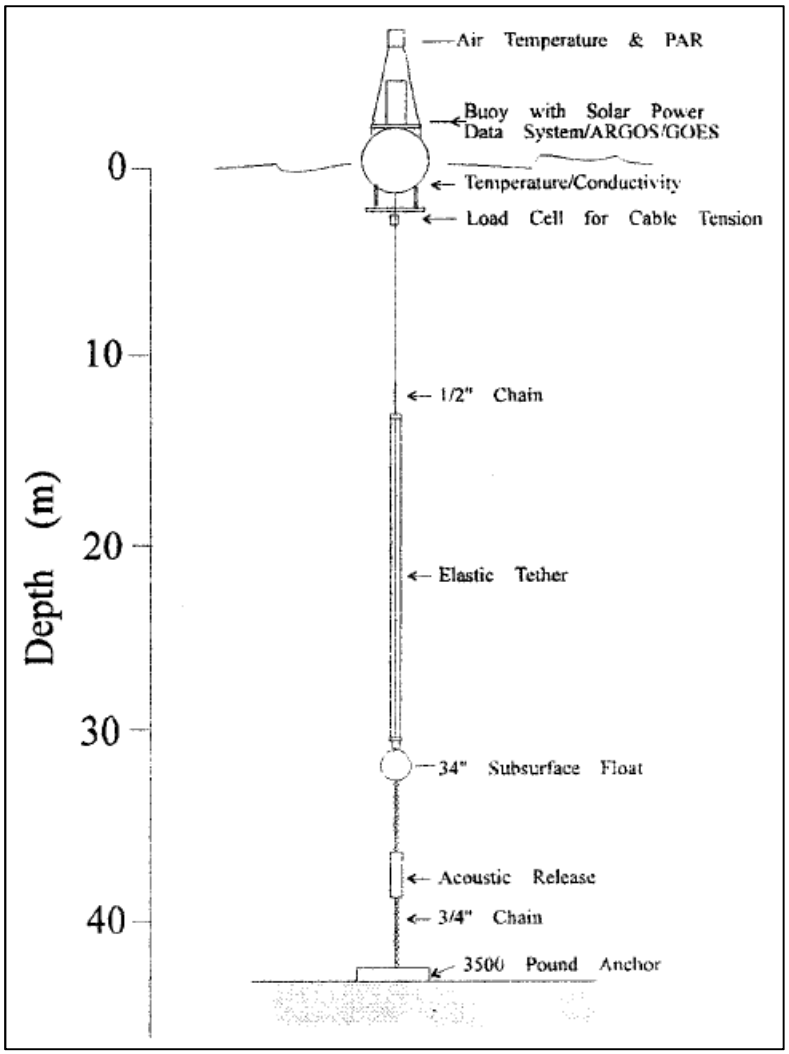

Figure 2.11 The GLOBEC Crest mooring as deployed at Georges Bank (Irish and Kery, 1996)

The data buoy was on station for one year during which time the measured mooring tension remained between 50 – 600 kgf. This gave a FOS in excess of 4 and the mooring system remained operational without damage (Irish and Kery, 1996).

This demonstrates a clear advantage from a relatively simple elastomeric mooring system. The solution of a simple round section rubber cord in tension mode, is also used by Datawell BV for their Waverider directional wave buoys (Datawell, 2015).

The success of an elastomeric tether is replicated by Paul et al. (2005) who discuss a variant to the rubber cord, a rubber tube. Seabed observatories that are connected to surface buoys for communications and power, present another problem, that of electrical cable strain. They suggest it is possible to route a cable along an inverted catenary limb but that this mooring will not provide sufficient compliance and will result in very high peak mooring loads and corresponding damage. The solution is a hollow rubber tube termed a snubber, within which a helically formed electrical cable (akin to a telephone handset cable) is routed. Paul et al. (2005) model the performance of the snubber for a particular site in a 25 year storm. A graphical output of these results is provided in Figure 2.12.

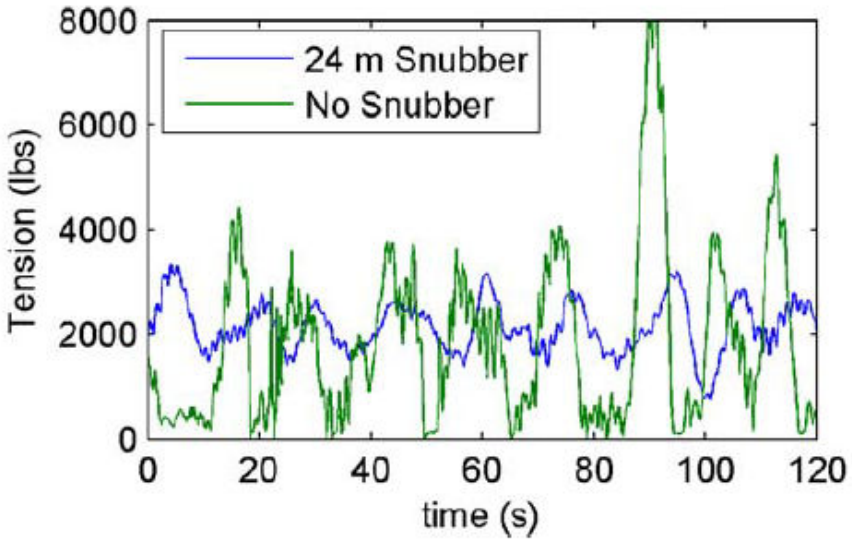

Figure 2.12 Comparison of predicted tension with and without the snubber (Paul et al., 2005)

The results of this modelling show a much steadier modulation of mooring tension with the snubber and a reduction in the peak loading of approximately 60%.

Two commercial manufacturers of mooring systems take the principle of a round section rubber cord in tension and apply it to larger floating bodies.

Marketed by Supflex Pontoon Mooring Systems Inc. in the U.S.A., the Superflex system employs multiple 26 mm diameter rubber cords terminated at each end to a steel chassis via threaded fasteners. The rubber cord is a composite of rubber, carbon fibre and Kevlar fibre in repeating concentric layers and can

achieve 120% extension (Huang, 2005). A version of the Superflex with 100 strands is shown in Figure 2.13. Figure 2.14 shows a graph of extension (mm) vs tension (kN) for a single 26 mm cord of 200 mm original length. The cord fails at just less than 100% extension (Supflex, 2014). The Superflex system is available with as many as 600 strands providing a MBL of 18.9 MN (Bowie, 2012).

Figure 2.13 Superflex units with 100 strands (Supflex, 2015).

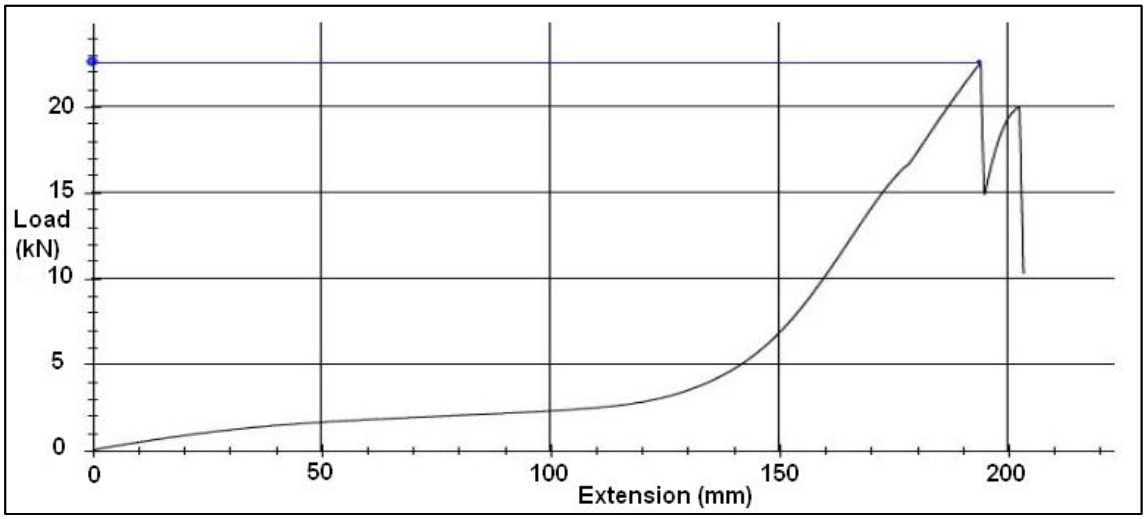

Figure 2.14 Graph showing extension (mm) vs tension (kN) for a single strand of Superflex having a 200mm original length (Supflex, 2014).

There are two important points to note here:

1. The maximum extension of ~ 100% for this composite of elastomer and stiff fibre (carbon / Kevlar) is markedly less than for the homogenous rubber cords used by Datawell and others. These rubber cords can accept an extension in excess of 500% (Datawell, 2015).

2. The internal structure of the stiff fibre appears to limit the extension in a manner that results in two stages of axial stiffness during extension.

No literature detailing the use or trial of the Superflex unit for MEC mooring is found however (Wang et al., in review) propose the system for the Eagle II WEC. Eagle II has a semi-submersible barge platform measuring 22 metres x 18 metres x 13 metres (including PTO). Predicted peak loads within the mooring limbs are reduced from 2982 kN (mooring plan 20) to 845 kN (mooring plan 41) by the replacement of a section of chain with the Superflex system (Wang et al., in review). This prediction equates to a 72% reduction in the peak loads.

Seaflex AB markets a similar system to the Superflex but with a different rubber strand construction. As with the Superflex, the Seaflex system was originally conceived for pontoon mooring applications. The Seaflex rubber strand has a tubular, braided textile cord embedded immediately beneath the outer surface of the strand. Upon extension of the rubber strand, this cord applies compressive radial force onto the rubber core as shown in Figure 2.15. A single rubber strand has a MBL in excess of 10 kN and can achieve greater than 100% extension (Bengtsson and Ekström).

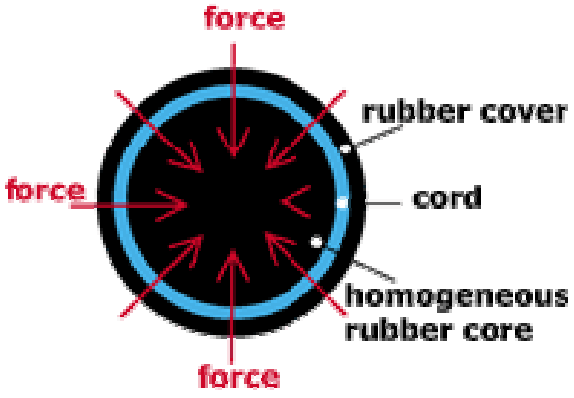

Figure 2.15 The Seaflex strand construction (Bengtsson and Ekström).

The Seaflex elastomer strands attach to end chassis pieces in a similar manner to the Superflex unit. However a recent invention by Seaflex removes threaded fasteners from this assembly in an effort to eliminate crevice corrosion of the stainless steel which threatens to cause failures (Segerljung, 2013). Segerljung adds that an alternative action might be to replace stainless steel with titanium alloy but that the cost of this would be significant.

The Seaflex mooring technology is assessed with regard to the Pelamis P2 WEC by the GeoWAVE project. Scaled test work in a wave basin suggests that a taut mooring system utilising Seaflex units can provide a 70% reduction in the magnitude of peak tension compared to a simple chain catenary system (Casaubieilh et al., 2014). They add that the magnitude of surge motions is also reduced, giving potential advantages in terms of array spacing.

Casaubieilh et al. (2014) note that the Seaflex strand also provides hysteretic damping and they imply a potential advantage from this property. Figure 2.16 demonstrates the two stage extension properties of the Seaflex strand and the hysteretic damping. Hysteretic damping is further explained in 6.4.8.

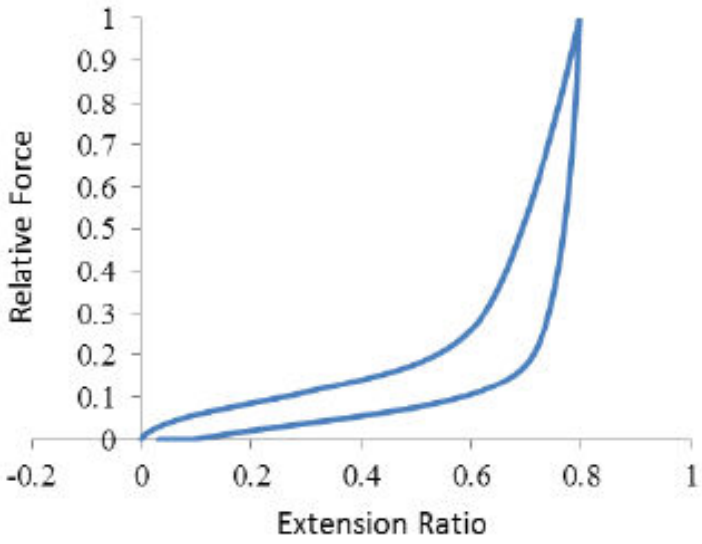

Figure 2.16 Seaflex extension and recovery curve showing two stages of axial stiffness and significant hysteretic damping (Casaubieilh et al., 2014).

Another elastomeric mooring tether is proposed and designed specifically for the floating MEC sector. The designer aims to achieve a two stage extension, similar to that shown in Figures 2.14 and 2.16, using tension of an elastomeric element and subsequent compression of a thermoplastic element (Mc Evoy, 2012). Figures 2.17 and 2.18 show configurations of this concept provided by (Mc Evoy, 2012) and (Thies et al., 2014) respectively.

Figure 2.17 Novel mooring tether utilising tension of an elastomeric element and compression of a thermoplastic element (Mc Evoy, 2012).

Numerical modelling of a two limbed mooring system and floating body is used to compare the performance of the tether against a simple catenary system and a catenary system that includes two surface buoys. Mc Evoy (2012) reports a reduction of the peak mooring line tension by 80 – 90% when simulating the elastomeric tether; mean tension and standard deviation are also significantly reduced.

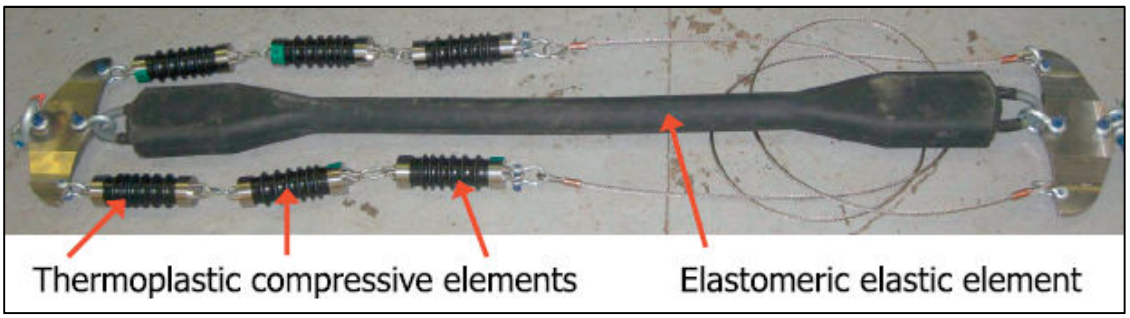

Figure 2.18 Novel mooring tether utilising tension of an elastomeric element and compression of a thermoplastic element - as tested (Thies et al., 2014).

2.5 Conclusions and Further Discussion

To conclude the argument that is being developed; there is general agreement within the literature that elastomeric mooring tethers can provide significant advantages to moorings for highly dynamic bodies. The findings that are reported suggest that the peak axial tension generated within a mooring line can be reduced by between 60% and 90% when elastomeric tethers are substituted for chain or conventional rope in a system.

However, the argument is extended here to suggest that the reliability of the existing elastomeric tethers is relatively uncertain. The current systems are often available with a 'safety' or 'by-pass' line which is designed to prevent extension beyond a prescribed limit (Bowie, 2012). Datawell (2015) state that "for reasons of buoy survival it is possible to attach a safety line parallel to the rubber cord". The terminations of the elastomer strands for the Supflex and Seaflex units are of steel or stainless steel and are consequently vulnerable to corrosion mechanisms as discussed by Segerljung (2013). Additionally there is an inherent risk associated with new technology; in their review of integrity issues relating to permanent mooring systems, Ma et al. (2013) remark that "unknown or new failure mechanisms are troubling because, since they are unanticipated, they cannot be easily detected or prevented".

This uncertainty in terms of reliability can be contrasted with the well-developed understanding of fibre ropes which are known to have existed for 5000 years, synthetic materials being utilised since around 1950 (McKenna et al., 2004). Fibre rope terminations via eye splicing are also well developed. McKenna et al. (2004) confirm that eye splices are widely used and that they present the most efficient fibre rope terminations, adding that they should be used wherever possible. Polyester rope in particular has superior cyclic tension fatigue properties and is now commonly used for deep water offshore platform moorings (Ridge et al., 2010).

2.6 Summary of the Literature Review

Summarising the arguments that are presented above: It is evident that significant advantage will be gained if the axial stiffness demonstrated by elastomeric tethers can be replicated with well proven and reliable synthetic fibre rope e.g. polyester. This rope should form the primary load carrier and be

external to the tether allowing the use of conventional eye splices to effect a secure and reliable termination. This is in contrast to the Seaflex unit, for instance, which uses an internal braided textile element to control extension but relies on the rubber element for significant axial load carrying and termination.

The desired design solution will result in reduced mooring loads without the introduction of additional and perhaps unknown reliability risks into mooring systems. The novel tether development work described incrementally within chapters 3, 4 and 5 aims to satisfy this requirement.

Chapter 3 Inventions and Critical Design Considerations

This section describes two fibre rope tether inventions, the hydraulic tether and the solid core tether. The two major elements of these concepts are discussed, these being the hollow rope and the core; generic solutions for both are proposed. Applications for the two types of tether are also presented.

3.1 Hydraulic Tether

The hydraulic tether was the initial invention and is described within UK Patent Application GB 2467345 A, (Parish, 2010). The cover sheet of this publication is given as Appendix A in this thesis.

It was noted that when a conventional rope extended under axial load, the diameter of the rope reduced. This is an intuitive result due to the helical or near helical structure of the strands / sub-ropes that carry the load. As a load is applied, the helices extend axially and contract diametrally. This diametral contraction acts to compact the structure and eliminate the free space between strands. As the extension progresses, the pressure within the rope structure increases thus providing resistance to any further diametral contraction. This simplistic model ignores the complications of irregularities in the fibres and the extension properties of the material itself but served to realise the opportunities that existed in resisting the diametral contraction.

The first inventive step was to propose that if a hollow rope was employed as the load carrier, a separate core might be inserted that would act to resist diametral contraction and thus resist axial extension. This core would play little or no part in carrying the axial load, so its specification could be tailored wholly to providing quantitative diametral resistance. Importantly, if the resistance to diametral contraction was controllable or selectable, then the axial extension would be controllable or selectable.

The second inventive step was to propose that the resistive core be a liquid held within an impervious sleeve inside the hollow rope. Axial load applied to the hollow rope would cause a circumferential tension, or hoop load, around the

hollow rope which would pressurise the liquid. Relieving the hydraulic pressure would allow diametral contraction and axial extension.

The liquid within the flooded chamber might be either:

a) Seawater - exchanging directly with the surrounding seawater via pressure / flow control valves and one way flow valves.

b) Hydraulic fluid - contained within an enclosed system utilising a hydraulic accumulator to receive and dispense the fluid according to the pressure within the tether chamber and the pressure control system.

System (a) requires a restoring mechanism within the tether. This mechanism must be capable of re-expanding the diameter of the hydraulic chamber when the axial loading on the tether is decreasing. In so doing, this mechanism will draw seawater back in, via a one way flow valve. Discharge of seawater to allow the tether to extend will be via fixed orifice or pressure relief valve.

System (b) requires a hydraulic connection between the tether chamber and the hydraulic accumulator which might be seabed mounted or accommodated on the floating device.

In both cases it is possible to create a tether of very low axial stiffness by offering low resistance to diametral contraction.

3.1.1 Hollow Rope

Low axial stiffness is also conditional upon the nature of the hollow rope construction, which must allow the rope to extend with ease. Figure 3.1 shows a typical double braid rope. The core has a long braid pitch (shallow helix angle) to provide high strength and low extension. Conversely, the cover has a short braid pitch (steep helix angle) to allow it to extend and close tightly onto the cover (McKenna et al., 2004).

It is clear that a hollow braided rope with a short braid pitch has the ability to extend considerably and whilst doing so, the braid angle will decrease and the diameter will reduce. This construction is well suited to the tether invention for these reasons.

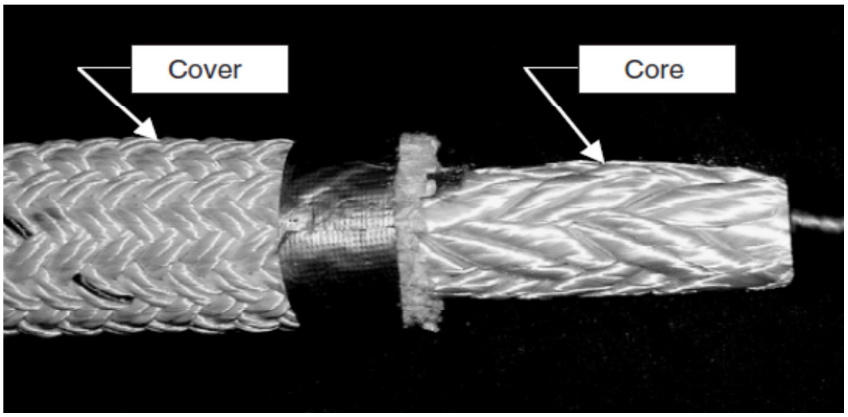

Figure 3.1 Double braid rope

(**McKenna et al., 2004)**

3.1.2 Applications

The following sections describe potential applications for the hydraulic mooring tether within floating WECs and other MECs.

3.1.2.1 Tide Height Compensation

Mooring systems for floating MECs must accommodate the change in tide height at the installation site. In UK waters this change in still water depth might be significant. For example, the tidal range at the Wave Hub test site in Cornwall is 7.3 metres (Daruvala, 2009). The depth in the shallowest test berth is approximately 50 metres, the tidal range adding 15% to this still water depth. Changes in atmospheric pressure and surge effects can further increase the range of the water depth.

The effect of a change in still water depth is to vary the static pre-tension of the mooring system. The change in pre-tension might result from lifting a catenary, axially extending a line or stretching out a lazy s type system. In any case, the change in pre-tension due to tide height will consume part of the compliance of the system that would otherwise be available for dynamic load mitigation.

The hydraulic tether would have the potential to slowly extend by bleeding hydraulic fluid, thus allowing a constant still water pre-tension in the mooring system as the depth of water increased. The reverse process would see the tether slowly contracting in length as the depth decreased, either relying on the restoring mechanism or the accumulator pressure to drive this action.

3.1.2.2 Peak Load Mitigation

As already discussed in 2.2.1 compliance in the mooring system can be used to reduce the magnitude of extreme loads; such compliance in the system can be provided by an axially compliant line. Both systems (a) and (b) described in 3.1 can provide low axial stiffness via a low hydraulic pressure threshold within the tether chamber.

3.1.2.3 Latching

Latching is a floating WEC control measure that might be accomplished by the PTO or an active mooring system. It is suited to point absorber devices that rely on heave motion to convert energy. The principle was examined by Budal and Falnes (1980). The motion of a device is stalled when its velocity is zero and the device is released to achieve a particular phase difference between the wave and the device response. The phase difference is optimised to achieve maximum energy conversion (Drew et al., 2009).

Latching is commonly discussed with regard to hydraulic PTO systems e.g. by (Drew et al., 2009). A hydraulic latch affords the advantage of a high load resistance and a rapid release, thereby achieving the enhanced dynamics sought. The same advantages might be presented by the hydraulic tether in a suitable configuration. The inherent stretch of the rope fibre might need to be limited by material choice and the rapid release would call for adequately sized valves. Clearly in this case a latch could only be achieved at the bottom of the devices vertical cycle.

3.2 Solid Core Tether

The solid core tether is a follow up invention and is described within UK Patent Application GB 2476986 A, (Parish, 2011). The cover sheet of this publication is given as Appendix B in this thesis.

This tether was conceived as a simplification of the hydraulic version, presenting less technical risk particularly in terms of reliability. In this version the resistance to diametral contraction of the hollow rope is provided by a solid core which is compressible and resilient. The core might be a single element running continuously along the length of the tether or it might be multiple lengths in a bundle as depicted by Figure 3.2 (Parish, 2011). A further option of

core architecture is a multi-element core whereby the separate elements are organised axially along the tether as shown in Figure 3.3 (Parish, 2011).

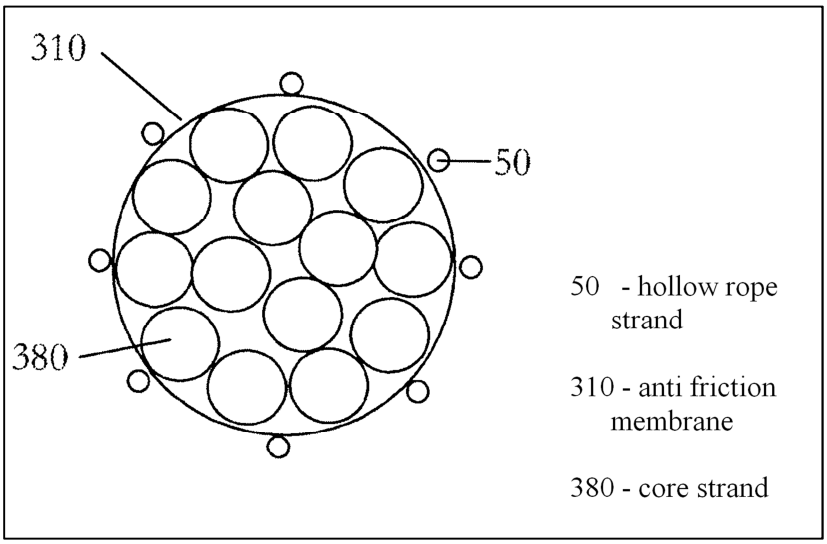

Figure 3.2 Schematic diagram of bundled core cross section

(Parish, 2011)

To reduce abrasion effects within the tether, an anti-friction membrane is included between the core and the hollow rope. Where a multi-element core is employed, the anti-friction membrane also acts to contain the individual core elements during the subsequent manufacturing operations.

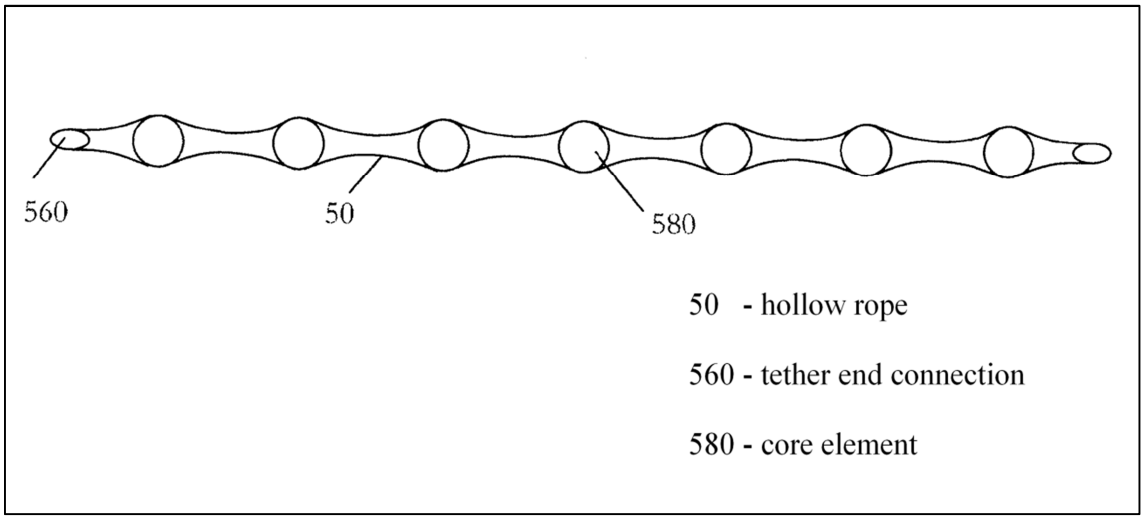

Figure 3.3 Schematic diagram of multi element core arranged axially

(Parish, 2011)

In the case of tether variants that employ full length core elements such as that described by Figure 3.2, it is likely that some tensile load is taken by the core structure. Patent application GB 2476986 A specifically addresses this issue by specifying limits to the Young's modulus for the core material if it contributes to tensile load carrying. The reason for such a limit is to maintain > 95% of the tensile load within the hollow rope and thus to prevent the tether from simply mimicking a rubber bungee with a spring-like response.

3.2.1 The Core Material

The core material must satisfy the following requirements:

1. It must provide resilient resistance to diametral contraction.
2. It should have a low Young's modulus such that < 5% tensile load is carried by the core (in the case of continuous cores).
3. It must survive the marine environment without degrading.
4. It must resist abrasion and tearing.
5. It must have an adequate life in air without degrading.

Some consideration was given to cork as a resilient material but rubber-like elastomers best satisfy the requirements. A non-technical requirement for the material at this stage was that suitably sized cord should be available from stock to avoid tooling and setup charges during prototyping.

Elastomer behaviour and elastomer selection is a complex material science which is not thoroughly explored within this work. In this case generic elastomer materials guidance was obtained. In a book on technical elastomers, Rinnbauer (2007) provides two tables describing 16 elastomer types by:

1. Tolerance to different media and temperature ranges.
2. General properties and typical applications.

Of the 16 elastomers only two, ethylene-propylene-diene rubber (EPDM) and perfluouro-elastomer (FFKM), are credited with excellent resistance to both water and air. The general properties and typical applications of these two elastomers are given in Table 3.1.

Table 3.1 Properties of EPDM and FFKM

(Rinnbauer, 2007)

Abbreviation	Chemical nomenclature	Properties	Trade name	Application
EPDM	Ethylene-propylene-diene rubber (ethylene-propylene copolymer)	• Very good heat and weathering behavior • High ozone resistance • Very good abrasion and wear resistance • Very good low-temperature performance • High hot water and steam resistance • Not oil resistant	Dutral®, Nordel®, Buna EP®, Keltan®, Vistalon®	O-rings, molded parts, bearing elements in the food and beverage industry, also used to seal brake fluids in automobiles
FFKM	Perfluoro-elastomer	• Excellent chemical resistance • Extreme heat and weathering resistance • Special types resistant to –20°C	Kalrez®, Simriz®	Radial shaft seals, O-rings, diaphragms, molded parts, high-precision parts for chemical and process engineering, aerospace applications, also used to seal against aggressive media and steam

Table 3.1 suggests that EPDM has superior abrasion and wear resistance. It is also clear that FFKM is a specialist elastomer that is used in chemical and aerospace applications. EPDM cord is readily available from UK stock at low cost whereas FFKM cord is only available to order.

3.2.2 Applications

The solid core version is aimed primarily at peak load and fatigue load mitigation. This is achieved by affording mooring designers better control over the axial stiffness and extension range of the mooring lines specified within a system. This allows for the selection of lower axial stiffness and hence a more compliant mooring system.

3.3 Summary of Tether Inventions and Potential Applications

The inventions and their potential applications are summarised in Table 3.2.

Table 3.2 Tether inventions and their potential applications.

	Hydraulic Tether	Solid Core Tether
UK patent application	GB 2467345 A	GB 2476986 A
Axial load carrier	Hollow braided fibre rope	Hollow braided fibre rope
Means of tether extension control	Hydraulic pressure (seawater or closed system hydraulics)	Elastomeric compression (EPDM)
Potential applications	Tide height compensation Peak load mitigation Latching control	Peak load mitigation

Chapter 4 Initial Assessments and Tether Selection

It was necessary to make limited initial assessments of the two inventions in order that one could be identified for continued development according to the research methodology described in 1.4. It was also useful at this early stage to gain an understanding of the pressure generated within the tethers and to validate a numerical method for predicting this. The process to achieve the preliminary assessments, inform the decision and to inform the contingent design work comprised three components:

1. Construct small scale 'benchtop' prototypes, referred to later as the P0 prototypes, and conduct simple evaluation tests. These tests provide confirmation and improved understanding of the mechanisms at play and aid the decision making.
2. Determine and validate a method to evaluate the internal pressure of the tethers.
3. Conduct a design failure mode and effects analysis (FMEA) for each tether version and hence expose any inherent design weaknesses.

4.1 Limitations and Experimental Equipment

The work described within this chapter precedes the formal proof of concept work detailed in chapters five and six. Facilities within the undergraduate teaching laboratory were used together with improvised test apparatus as appropriate. During this stage of the tether development work, the Dynamic Marine Component test facility (DMaC) was commissioned and became available. This test facility was then incorporated into the early stage test work where appropriate.

DMaC is a large horizontal tensile test machine with added functionality designed to replicate ocean induced motions and forces. It has a hydraulic actuator providing tension or compression of up to 441 kN. The required load or displacement test cycle is achieved via a numerical script and the hydraulic system utilises full feedback control. DMaC is fully described in section 6.1.

4.1 Hydraulic Tether Benchtop Prototype

A benchtop prototype was constructed for initial analysis. A hollow braided rope was sourced from a local chandlery. The rope is Polyester, has 40 strands and is a 2 x 2 braided construction. This construction is achieved using 20 carriers on the braiding machine (10 in each direction), each carrier laying two strands adjacent to each other. This rope is shown in Figure 4.1. Because the rope was purchased 'off the shelf', the technical specifications are not fully known but measurement in a relaxed condition provides the following approximations:

- Inside diameter 19 mm
- Strand diameter 1.7 mm
- Outside diameter 26 mm
- Braid angle 45°

Figure 4.1 Hollow rope used in benchtop prototype

The rope was selected because it has a relatively loose construction and a relatively high braid angle of 45° (measured from the rope's axis). Applying axial tension to the rope results in easy extension causing the braid angle and diameter to decrease.

A 500 mm length of rubber tubing cut from a bicycle tyre inner tube (700 x 22) was inserted into an 800 mm length of the hollow rope to form an impervious liner. Completion of the prototype was as follows:

1. Align one end of the liner with the end of the rope (end A).

2. Fold rope and liner back at end A to form an eye and bind tightly with whipping twine to seal the liner.
3. Work the rope back by hand to expose the open end of the rubber liner.
4. Fill the liner with water, insert 6 mm nylon tubing into mouth of liner and bind liner around the tubing to achieve a seal.
5. Restore the rope back to its original length and open the braid to pull the Nylon tube through the rope's wall.
6. Use the 300 mm of free rope length to tie a bowline knot to form a second eye, ensuring that the knot is tight against the end of the sealed rubber liner.
7. Fit a bleed valve to the exposed end of the Nylon tube, top up with water and expel all of the air from the hydraulic chamber.

4.2 Solid Core Tether Benchtop Prototypes

Two benchtop prototypes, (a) and (b), were constructed using the rope described in 4.1. Cores were constructed from 7 strands of round section EPDM rubber cord as follows:

- Cord diameter 6.35 mm
- Length of core bundle (a) 450 mm (b) 300 mm
- EPDM durometer hardness 70 Shore A

The 7 core strands were arranged in a hexagonal close pack structure and bound together with an adhesive PVC tape which was applied helically. Figure 4.2 shows the core bundle construction.

Figure 4.2 Solid core bundle wrapped in PVC tape

The core assembly was inserted into the hollow rope. Tight bindings were made around the rope at the ends of the core so that the core would extend with the rope. The concern was that the rope braid might slip off at the ends of the core if this binding was not in place. Eyes were formed at each end of the tether by folding the rope back on itself and binding it firmly. A half hitch knot was added to strengthen the terminations. The final lengths of the tethers were:

- Working length (a) 450 mm (b) 300 mm
- Eye to eye length (a) 650 mm (b) 500 mm

A further test piece was prepared in the same manner but with no core inserted into the hollow rope. This provides a basis for comparison.

4.3 Test Methods

The following describe the methods used during the benchtop prototype tests.

4.3.1 Hydraulic Tether Test

A simple test was performed to confirm the predicted characteristics of the hydraulic tether and to determine the hydraulic pressure produced for a given axial load and braid angle. The water filled tether adopted a catenary form if mounted horizontally making test work at low loads difficult. For this reason and for electrical safety, the hydraulic tether was tested in a vertical orientation using a structure and a mass rather than dedicated test equipment.

The test was conducted as follows:

1. A 200 bar pressure transducer (serial no. 25654) was introduced into the water filled chamber. The signal lead exited the tether via the tightly folded and bound end and connected to a voltmeter (serial no. F2895).
2. The prototype tether was hung vertically by end B from a structural frame.
3. A marker pen was used to mark two circumferential lines around the tether at a distance of 300 mm apart (by rule). These marks defined the gauge length at load = zero (self-weight only).
4. The transducer voltage output was recorded for zero load.
5. The outer diameter of the tether was measured using a Vernier calliper gauge.

6. A readily available steel mass of 48 kg was attached to the lower eye by means of cord and the load was gradually applied to the tether.
7. The transducer voltage output was recorded.
8. The outer diameter of the tether was measured using a Vernier calliper gauge.
9. The gauge length was measured between the marks using a steel rule.
10. Water was bled from the tether in three increments until empty with measurements (7, 8 and 9) repeated at each stage.

4.3.2 Solid Core Tether Pressure Test

The benchtop prototype (b) described in 4.2 was fitted with pressure sensitive film inserted between the strands as shown in Figure 4.3.

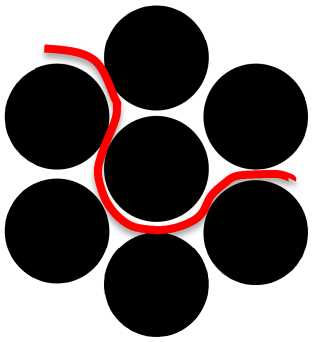

Figure 4.3 Pressure sensitive film positioned within core bundle

The Prescale pressure sensitive film is manufactured by Fujifilm. The Micro-encapsulated colour-forming material reacts with a colour developing material to produce a red hue according to the maximum pressure encountered (Fujifilm, 2007). Six different grades of Prescale film cover a pressure range as follows:

Table 4.1 Prescale film pressure ranges (Fujifilm, 2007)

Prescale pressure sensitive film	
Kinds of films	Pressure range: [MPa] 0.2 0.5 0.6 2.5 10 50 130 300
Ultra super low pressure (LLLW)	
Super low pressure (LLW)	
Low pressure (LW)	
Medium pressure (MS)	
High pressure (HS)	
Super High pressure (HHS)	

A 20 mm wide strip of each of the six Prescale film grades was inserted into the core bundle before covering with the PVC tape. These grades span the pressure range of 0.2 MPa - 300 MPa (2 bar – 3000 bar).

A gauge length of 100 mm was marked in the middle of the tether with pen before mounting it in a Hounsfield 20 kN W-Series horizontal tensile test machine. The tether was subjected to three consecutive extension tests, achieving target peak loads of 2500 N, 4000 N and 5800 N. During each test the machine's travelling cross beam was stopped at the target peak load and measurements were taken of the gauge length and the outer diameter before returning to the relaxed condition. The rate of extension displacement was 50 mm/min and the cross beam was reversed at the same speed.

4.3.3 Solid Core Tether Performance Test

Performance tests were undertaken on tether (a) at the Dynamic Marine Components test facility. The objectives of the tests were to:

1. Characterise the potential benefits of the solid core version.
2. Compare extension and hysteretic damping characteristics of the prototype to the base case of the hollow rope.

The tests were conducted with the prototype tether in the dry condition. DMaC is designed for larger test pieces and it was necessary to use 1.5 metres of steel chain to couple each end of the tether to the test bed. A 50 kN in-line load cell was added between the chain and the tether at one end. Data from this load cell was used in preference to DMaCs built in 444 kN load cell to improve the resolution and accuracy of the load data. Details are as follows:

- Load cell – Tension link type, serial number 2005 – 507
- Chain – stainless steel, 2 x 1.5 m length, open link, 10 mm bar diameter.

Figure 4.4 shows the benchtop prototype in place ready for test.

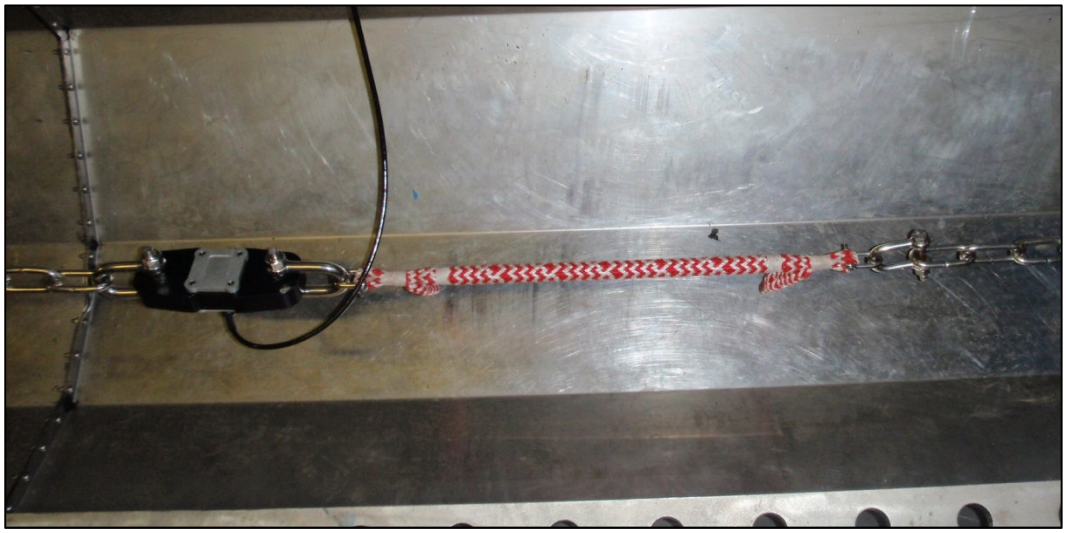

Figure 4.4 Benchtop prototype ready for test in the DMaC test facility

DMaC can either run tests according to a force driven test script or a displacement driven test script. In this case a displacement driven test script was used with a linear ramp up and down as shown in Figure 4.5.

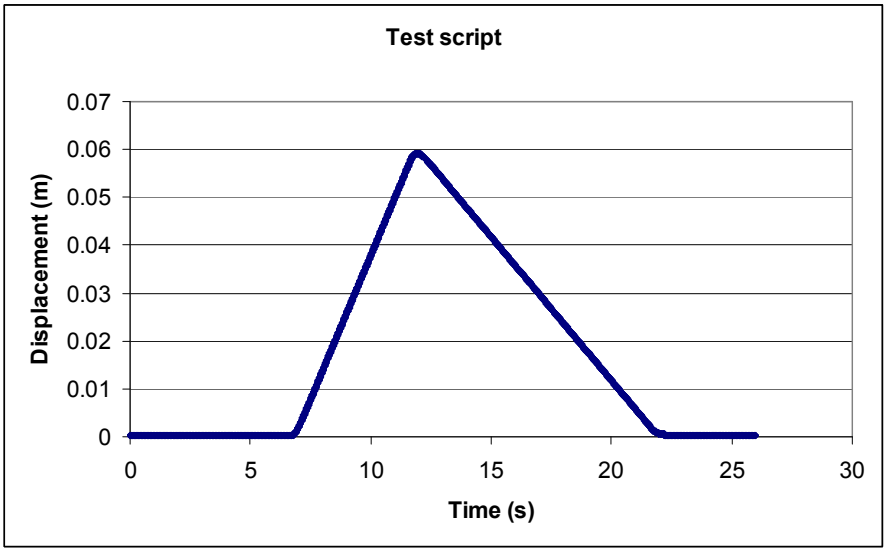

Figure 4.5 Displacement driven test script used

Variations of the script provided for 30 mm, 60 mm, 90 mm, 120 mm and 150 mm displacements at the same rate of travel.

The 30 mm test was run 5 times to bed in the tether and its terminations before running the 5 different displacement tests in sequence.

The empty rope test piece was mounted within DMaC in the same manner as the tether. Due to the increased axial stiffness of the empty rope, the displacement applied to bed in this test piece and for the extension test was reduced. A 20 mm displacement test was conducted 5 times to bed in the rope and terminations before conducting a 25 mm displacement test.

4.4 Test Results

The following sections provide the results of the three tests conducted.

4.4.1 Hydraulic Tether Test

The pressure transducer output recorded in mVDC is converted to pressure by scaling linearly according to the calibration, 200 bar = 1000 mV. The results are given in Table 4.2.

Table 4.2 Hydraulic tether test results

Load (N)	mV	Pressure (bar)	Gauge length (mm)	Extension	Outer diameter (mm)
0	0	0	300	0	26
471	29	5.8	395	32%	20
471	19.2	3.8	410	37%	18.5
471	9.2	1.8	421	40%	17
471	0	0	433	44%	15.5

4.4.2 Solid Core Tether Pressure

The loads achieved for each stage of the test are given in Table 4.3 together with the extension to the gauge length and the outer diameter.

Table 4.3 Extension and load data during solid core pressure test

Test no.	Gauge length extension	Outer diameter	Maximum load
1	19.6 %	23.1 mm	2500 (N)
2	22.4 %	22.5 mm	4000 (N)
3	23.0 %	22.3 mm	5800 (N)

Figure 4.6 shows the Prescale film having been removed from the tether after the test. The film displays the colour change that corresponds to 5800 N axial loading on the tether prototype. The highest three pressure grades remain un-coloured whereas the lowest two are densely coloured red. The LW film grade is selected for colour reading according to the manufacturer's instructions described below.

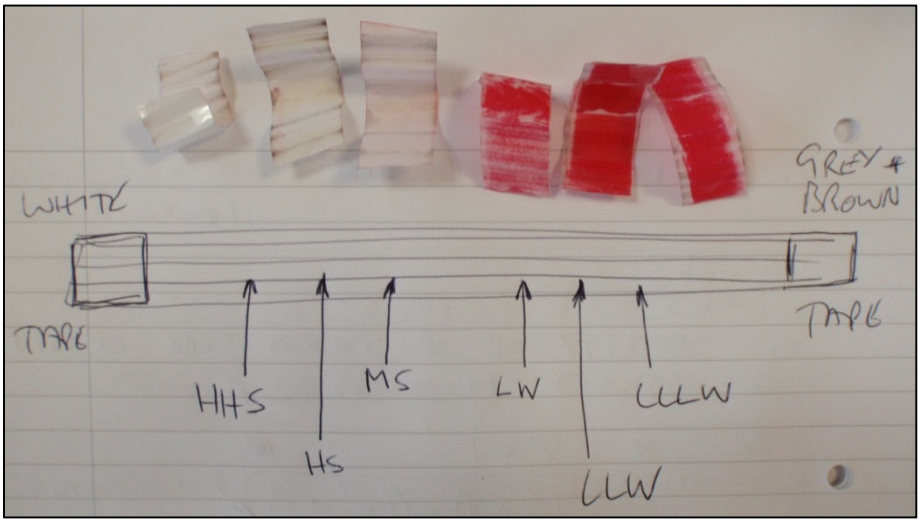

Figure 4.6 Prescale film pieces after disassembly of the tether

The affected Prescale film is read in three stages as shown in Figure 4.7 taking care to discriminate between the pressure charts for momentary and continuous application of pressure. In this case the chart for continuous pressure is valid.

1. Applying the ambient temperature in the laboratory (22.5° C) and the relative humidity (70%), zone B is identified by the crossover.
2. Matching the colour density of the film to the colour chart, colour factor 0.7 is identified.
3. Using the pressure chart, reading across from colour factor 0.7 to line B and downwards, the pressure is indicated to be 5.2 MPa (52 bar).

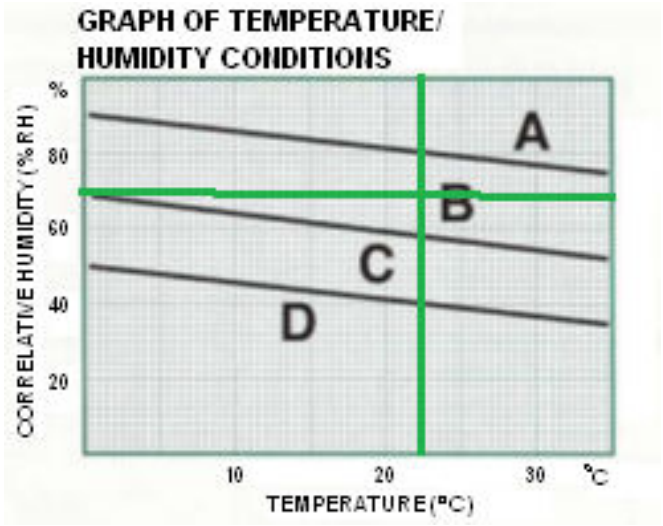

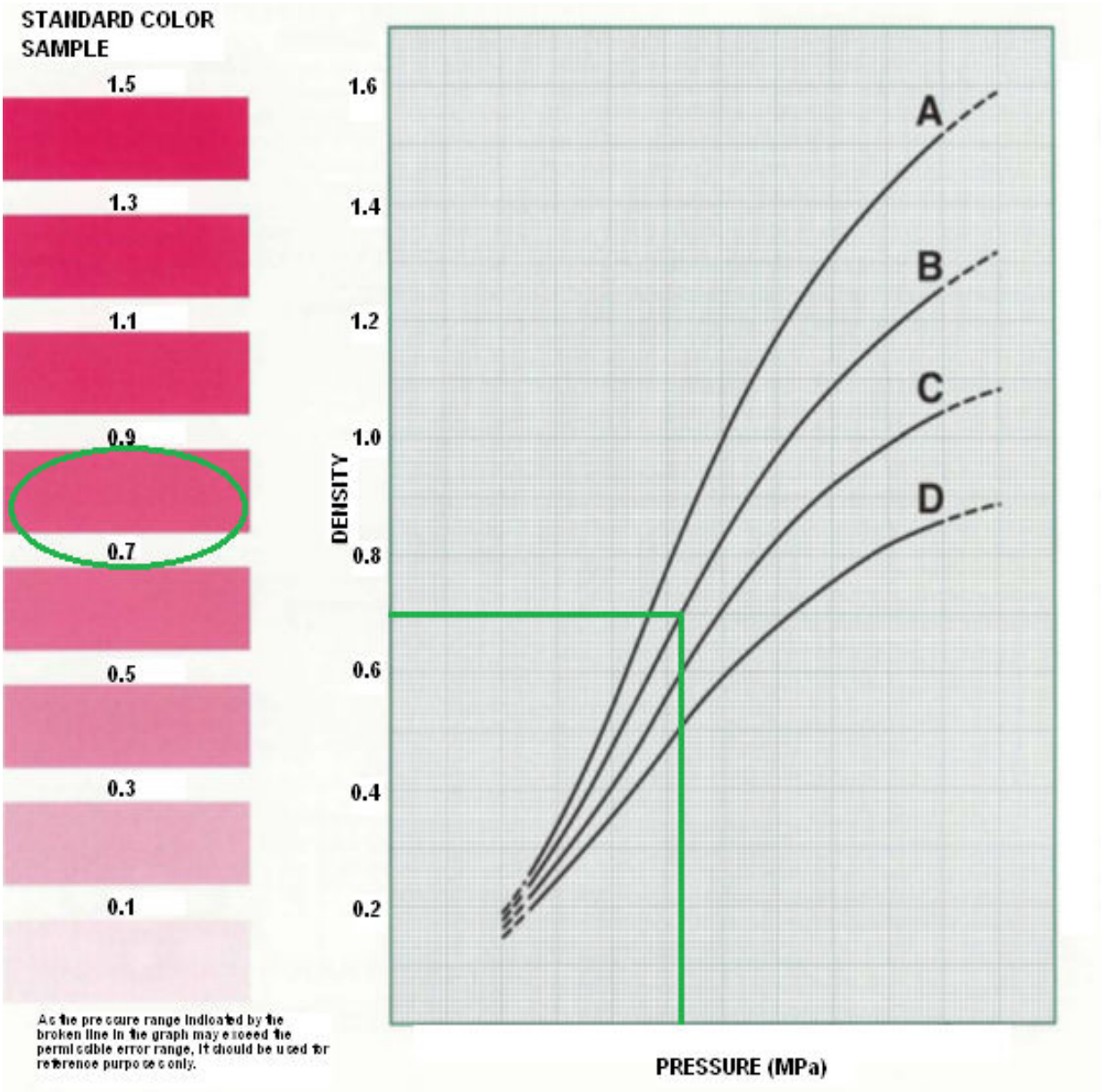

Figure 4.7 Prescale film colour reading charts (continuous pressure), as read. (Fujifilm, 2007).

4.4.3 Solid Core Tether Performance

The results are presented in the form of tension / displacement graphs. Due to hysteresis, energy is dissipated by the tether which results in a different plot line when the load is reducing to that produced when the load is rising. For each hysteresis loop, the higher line (greater force) represents the increasing load. Hysteresis is further explained in 6.4.8.

Figure 4.8 shows the results of the 5 sequential displacement tests for the prototype tether. It is evident that during the 90 mm, 120 mm and 150 mm tests, slippage occurred at the eye terminations. However it is clear that before slippage occurred, the tether achieved approximately 0.12 m extension during the final test. This represents 27% extension.

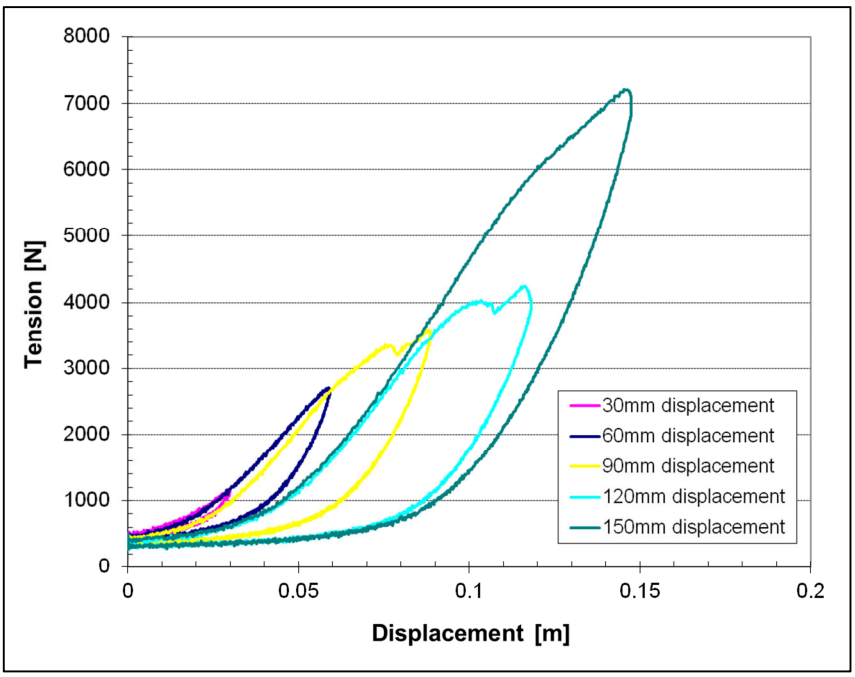

Figure 4.8 Displacement test results for prototype solid core tether.

Figure 4.9 shows a comparison between the behaviour of the prototype tether and the empty hollow rope. Both display an approximation to linear behaviour at higher loads as the load increases. The shallower gradient of the tether 'load-up' line signifies a lower axial stiffness than the hollow rope. The tether exhibits considerably more hysteretic damping than the hollow rope, as represented by the area enclosed by the loop formed by the load-up and recovery lines.

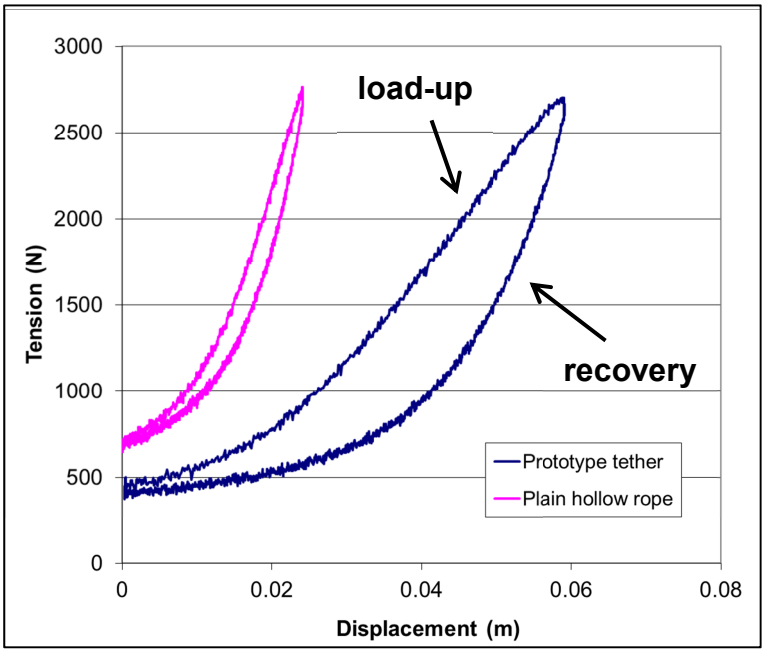

Figure 4.9 Comparison of tether with plain hollow rope

4.5 Calculation of Theoretical Core Pressure

Calculation of the radial pressure within the tether is made by using the thin walled cylinder theory. This theory is more usually applied to pressure vessels whereby the hoop force in the cylinder walls is reacting the force created by the internal pressure. In this instance it is reversed, the pressure is reacting the hoop force but the principle is the same.

The theory states that $\sigma_{hoop} = \frac{PD}{2t}$ where:

σ_{hoop} = hoop stress, P = pressure, D = diameter, t = thickness

and since for a cylinder wall $\sigma_{hoop} = \frac{F_{hoop}}{tl}$ where:

F_{hoop} = hoop force, t = thickness of wall, l = length of wall

then $\frac{F_{hoop}}{tl} = \frac{PD}{2t}$ or $\frac{F_{hoop}}{l} = \frac{PD}{2}$

re-arranging for P gives:

$$P = \frac{2F_{hoop}}{Dl} \tag{3.1}$$

In pressure vessel calculations the outside diameter of the thin walled cylinder is used which gives the worst case outcome for stress. Here, where the interest is in the pressure outcome rather than the maximum stress, the mid-section diameter is used as it better represents the mean effort applied by the rope strands.

For convenience, rather than considering the full length of the tether for the length term, the length of the braid pitch is used. This length corresponds to each of the rope strands completing one helix turn. The force term is normalised against this pitch length.

Referring to Figure 4.10; if the hollow rope is cut along its axis as shown and laid flat, the braid angle is given by α, the pitch length is represented by dimension B and the mid-section circumference by dimension C.

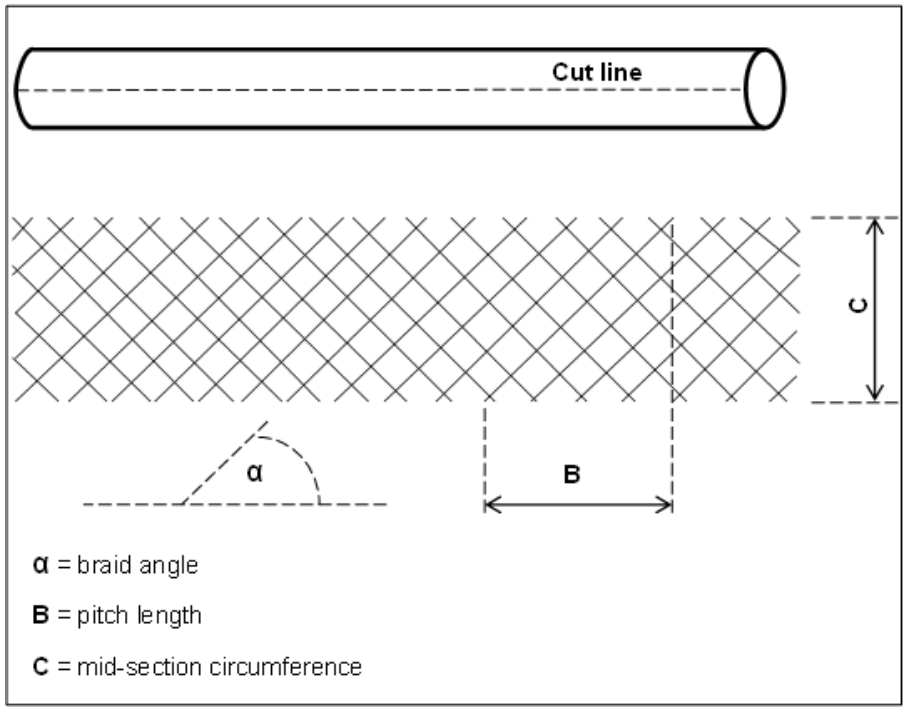

Figure 4.10 Schematic diagram of hollow rope cut axially and laid flat.

4.5.1 Calculation of Hydraulic Pressure

The hydraulic pressure is calculated according to the test conditions presented for the hydraulic tether test in Table 4.2 and the rope specifications given in 4.1. The initial steps of this calculation are given in Table 4.4.

Table 4.4 Parameter values and derivations used to calculate hydraulic pressure.

Parameter	Derivation	Value
Original mid-section diameter	26.0 mm – 2 x 1.7 mm	22.6 mm
Original mid-section circumference	π x 22.6 mm	71.0 mm
Original braid angle	measured	45°
Original braid pitch length	71.0 mm / tan 45°	71.0 mm
Axial load applied	48 kg x 9.81	471 N
Extension	(395 – 300) / 300	31.7%
New braid pitch length (l)	71.0 mm x 1.317	93.5 mm
New mid-section diameter (D)	20.0 mm – 2 x 1.7 mm	16.6 mm
New mid-section circumference	π x 16.6 mm	52.2 mm
New braid angle	$\tan^{-1}$ (52.2 / 93.5)	29.2°
F_{hoop} per strand per pitch length	tan 29.2° x (471 / 40)	6.581 N
F_{hoop} per pitch length	40 x 6.581 N	263.2 N

Applying equation (3.1)

$$P = \frac{2 \times 263.2\ N}{0.0166\ m \times 0.0935\ m}$$

therefore $P = 339153\ Pa$

or $P = 3.4\ bar$

4.5.2 Calculation of Solid Core Pressure

The radial pressure is calculated according to the test conditions presented for the solid core tether (version b) test in Table 4.3 and the rope specifications given in 4.1. The initial steps of this calculation are given in Table 4.5.

Table 4.5 Parameter values and derivations used to calculate radial pressure.

Parameter	Derivation	Value
Original mid-section diameter	26.0 mm – 2 x 1.7 mm	22.6 mm
Original mid-section circumference	π x 22.6 mm	71.0 mm
Original braid angle	measured	45°
Original braid pitch length	71.0 mm / tan 45°	71.0 mm
Axial load applied	measured	5800 N
Extension	measured	23%
New braid pitch length (l)	71.0 mm x 1.23	87.3 mm
New mid-section diameter (D)	22.3 mm – 2 x 1.7 mm	18.9 mm
New mid-section circumference	π x 18.9 mm	59.4 mm
New braid angle	$\tan^{-1}$ (59.4 / 87.3)	34.2°
F_{hoop} per strand per pitch length	tan 34.2° x (5800 / 40)	98.5 N
F_{hoop} per pitch length	40 x 98.5 N	3940 N

Applying equation (3.1)

$$P = \frac{2 \times 3940\ N}{0.0189\ m\ \times 0.0873\ m}$$

therefore $P = 4775844\ Pa$

or $P = 48\ bar$

4.6 Outcomes

The outcomes of initial testing of the two tether types are as follows:

1. The solid core tether is capable of achieving at least 27% extension when starting from a 45° braid angle.
2. The solid core tether demonstrates significantly lower axial stiffness than the ‘parent’ rope.
3. The solid core tether exhibits considerably more hysteretic damping than the ‘parent’ rope.
4. The Hydraulic tether exhibits very low axial stiffness, extending by 32% at low load.

5. After initial loading and tether response, the hydraulic tether became relatively stiff and the tether length was controlled hydraulically.

6. The calculated value for hydraulic pressure of 3.4 bar is a reduction of 41% from the measured value of 5.8 bar.

7. The calculated value for radial pressure in the solid core tether of 48 bar gives a good agreement with the measured value of 52 bar.

4.7 Design Failure Mode and Effect Analysis

A design FMEA was performed on both tethers to consider potential risks associated with the concepts. FMEAs are routinely used within manufacturing industry as a tool to consider and numerate technical risk in both design and process. Three factors (severity, occurrence and detection) are each scored between 1 and 10 depending on their contribution to risk, 10 being a high risk score. These three scores are then multiplied (severity x occurrence x detection) to produce a risk priority number (RPN). The RPN guides the design team to those risks that require control measures to be put in place and those that require re-design to alleviate the risk. When these measures are defined, the FMEA is repeated and this process continues until the risks are deemed to be acceptable.

Within this work the term detection is not used. When dealing with potential failures of offshore components, it is arguably more appropriate to consider routine replacement than detection and rectification. Therefore the term detection is replaced with prevention to allow recognition that a realistic maintenance regime might avert failure without any detection phase. The three factors utilised here are described as follows:

Severity of effect – The score is allocated according to the most severe outcome that might realistically result from the failure.

Likelihood of occurrence – The score is allocated from experience of the marine environment, the dynamics of floating MEC devices and history within the sector.

Likelihood of prevention – The score reflects the possibility that the condition can be prevented by operational measures e.g. inspection, maintenance and component exchange.

Further guidance in scoring these factors is taken from McDermott et al. (2009). The guidance is provided in table form in this thesis as Appendix C.

When conducting a design FMEA, particularly in areas of new technology, it is sometimes necessary to make certain assumptions to qualify the analysis. In this case assumptions are made as follows:

1. The tethers are to be retired from service and replaced with new tethers every 5 years.
2. Anti-biofouling layers are included within the design and these are very effective but do not provide total exclusion of marine growth within the tether structure.
3. Anti-friction layers are included within the design and these are very effective but do not eliminate internal fretting.
4. All of the available design enhancements aimed at minimising the noted risks have been actioned in the designs as analysed.

4.7.1 Hydraulic Tether FMEA

The hydraulic tether FMEA identified several remaining risks inherent within the design. The major risks are summarised in Table 4.6.

4.7.2 Solid Core Tether FMEA

Of those major risks exposed for the hydraulic tether only one remains for the solid core tether, that being ‘failure of the load carrying rope via fretting fatigue’.

4.8 Discussions and Decision

An axial load of 471 N resulted in the considerable extension of 32% for the hydraulic tether on initial loading. This is surprising because the hydraulic pressure was ‘locked’ during the test and the high bulk modulus of water should result in little or no extension of the tether. It is likely that the extension is attributable the following factors:

a) Inflation of the hydraulic liner within the tether to eliminate the free space at the ends of the tether.

b) Tightening of the previously loose rope strands around the core.

c) Compression of a small amount of air remaining within the system.

Factors (a) and (b) suggest that the hydraulic tether would require a 'pre-pressure' during operation to avoid these effects. This implies the use of a hydraulic accumulator described as system (b) in 3.1. Once the hydraulic tether was pressurised and the slack was taken up, it behaved as expected allowing extension via hydraulic bleed.

The solid core tether performed well during the test work demonstrating a much reduced axial stiffness compared to the hollow rope and a capability to extend significantly. It was possible to fit the hollow rope more tightly around the solid core thus minimising the take up of slack evident with the hydraulic version. There remains one major risk to reliability with the solid core version, that being fretting of the load carrying rope, leading to premature failure. This failure mode produced a RPN of 350 during the FMEA and requires attention in later design work to alleviate the risk.

The wider applications that are envisaged for the hydraulic tether suggest that this version is potentially of greater significance to the marine renewables sector. However it is equally evident that the greater functionality comes with considerably higher technical risk, in respect of reliability. The hydraulic version shares the risk of fibre fretting but also returned six further RPN results in excess of 350, all associated with failures of the hydraulic system.

The application of thin cylinder theory to the pressure calculations was validated by the results for the solid core but not by the hydraulic version. Some inaccuracy in the hydraulic result might be attributable to the low pressure achieved which represents just 3% of full scale deflection for the pressure transducer. The mechanism by which the rope generates the internal pressure is the same in both tether types. It is therefore assumed that the 52 bar pressure measured in the solid core tether is representative of the working pressure for the hydraulic tether. This is a very considerable hydraulic pressure to contain within the impervious liner and it clearly adds risk to the reliability.

Table 4.6 FMEA - Major risks associated with the hydraulic tether.

Failure mode	Effect of failure	Severity of effect	Cause of failure	Liklihood of occurrence	Liklihood of prevention	Risk priority number
Tear to impervious liner	Spill of hydraulic fluid to ocean	9	Fretting fatigue	7	7	**441**
	(system b only)	9	Laceration by trapped marine growth	7	7	**441**
		9	Material decay	3	3	**81**
	Full / permanent extension of tether	9	Fretting fatigue	7	7	**441**
		9	Laceration by trapped marine growth	7	7	**441**
		9	Material decay	3	3	**81**
Rupture of connection to accumulator	Spill of hydraulic fluid to ocean	9	Failure of strain relief	4	5	**180**
(system b only)		9	Material decay	3	3	**81**
	Full / permanent extension of tether	9	Failure of strain relief	4	5	**180**
		9	Material decay	3	3	**81**
Failure of discharge valve (system a only)	Tether fails to extend drowning device	8	Marine growth	8	8	**512**
Failure of refill valve (system a only)	Full / permanent extension of tether	9	Marine growth	8	8	**576**
Failure of load carrying rope	Mooring failure	10	Fretting fatigue	3	7	350

The consequence of the perceived risks associated with the hydraulic tether is to discourage further development work at this stage. This raises the question; can the solid core tether address the research questions defined earlier in 1.3? Taking these questions in turn:

Q1. *Is it possible to develop a novel, fibre rope mooring tether whereby the axial stiffness is decoupled from the breaking strength (MBL) of the rope?*

The solid core tether appears to satisfy this requirement at this early stage.

Q2. *Can the novel tether provide MEC moorings with more favourable axial extension properties than conventional fibre ropes?*

It is too early to know at this stage but the 27% extension achieved is encouraging.

Q3. *Can the novel tether facilitate the selection of axial stiffness, for a given MBL, at the tether design stage?*

Axial stiffness has certainly been changed by the implementation of a compressible core. Logic suggests that changes to the mechanical properties of the core will affect axial stiffness independently of the MBL.

Q4. *Does the novel tether have the capability to significantly reduce peak mooring loads for highly dynamic MEC devices?*

It is too early to assume this at this stage but the axial properties are moving in the right direction to achieve this.

The decision is therefore made that no further development of the hydraulic tether is included within this work; the solid core tether only is progressed through the proof of concept stage.

Chapter 5 The Proof of Concept Prototypes

Following the research methodology laid out in 1.4 it was necessary to design and manufacture a range of solid core tether prototypes for detailed test and analysis. These prototypes are referred to as the P1 series.

5.1 Industrial Collaboration

The P0 prototypes were successfully assembled by inserting a core assembly into the expanded hollow rope. However, it was evident that this technique would not be plausible when working with larger diameter rope of a significant length. It would be necessary to braid the hollow rope directly onto the core assembly in the same manner that the outer braid is laid onto the inner core of a double braid rope as shown in Figure 3.1. This would require a bespoke production set up and manufacturing run in one of Europe's major rope manufacturing plant.

To facilitate such a bespoke production, a collaboration agreement was sought with one of Europe's offshore rope manufacturers. Three companies were identified as having the capability to manufacture to the required specification these being:

- Bridon Ropes – based in the UK.
- Lankhorst Ropes - based in the Netherlands having plant in Portugal.
- Bexco – based in Belgium.

Meetings were held with Bridon Ropes and Lankhorst Ropes before reaching an agreement with Lankhorst to collaborate in the proof of concept study. Production of the P1 rope would be at Lankhorst's manufacturing plant in Maia, Portugal.

5.2 Hollow Rope Design

The tethers required for the proof of concept work needed to be of a realistic scale with reference to the DMaC test facility (described fully in 6.1).

The P0 prototypes performed well. The P1 rope was scaled up from the P0 rope whilst maintaining the same geometric proportions as far as possible. The braid angle was increased slightly to allow a greater extension limit of the tether.

In summary the outline design requirements were:

1. Material: polyester
2. Strength: 200 kN < MBL < 300 kN
3. Construction: hollow braid
4. Braid angle: 50° < angle < 55°
5. Geometry: similar proportions to benchtop prototype

5.2.1 Scaling the Rope Design

The linear density (weight per unit length) was used as the primary scaling parameter in the P1 rope design. There is a close relationship between linear density and strength for any given rope as detailed below. It was important to achieve a significant up-scaling whilst ensuring that the tether could be subjected to sufficient force to achieve tensile failure in DMaC. It was also critical that the hollow rope maintained its ability to extend which meant maintaining geometric proportions whilst increasing the linear density.

The weight per unit length of the hollow rope can be determined in relation to the required strength by applying generic guidance. A strength to weight ratio of 26.4 x 10^3 kgf per kg/m can be assumed for polyester 12 strand single braid rope at the required scale (McKenna et al., 2004). Converting this to newtons gives 259 kN per kg/m. Whilst the 12 strand rope doesn't exactly match the hollow rope of the tether, it is the closest construction that is listed in the guidance and is broadly similar.

The breaking strength of a specific fibre rope (MN) is the product of linear density (kg/m), tenacity (N/tex) and the strength conversion efficiency factor. The conversion factor addresses the efficacy of the load path and hence the conversion of material strength to rope strength (McKenna et al., 2004). Strength conversion factors typically vary between 50% and 85% (McKenna et al., 2004). In this case a factor of 80% is assumed for the 12 strand single braid rope which has a slow helix angle providing a reasonably direct and efficient load path. A factor of 70% is assumed for the tether rope representing a greater braid angle and hence a less direct load path which elevates the axial load within each strand. Therefore to achieve the mid target MBL of 250 kN for the tether rope, the weight per metre in air is given by:

$$\frac{250\ kN}{259\ kN\ kg^{-1}\ m^{-1} \times \frac{1}{0.8}\ \times 0.7} = 1.1\ \text{kg/m} \qquad (5.1)$$

The P0 hollow rope was assessed to find the weight per metre in air. A length of the hollow rope was eased onto a 19 mm diameter, 1.5 m long mandrel and was then 'milked' along its length to tighten it onto the mandrel. In this condition the hollow rope adopted the dimensions described in 4.1 which are representative of the rope with a working core fitted. A one metre length was marked on the rope; it was removed from the mandrel and cut to the marked length. This one metre sample length was weighed using a microbalance which recorded 106.1 gm.

Therefore the scale factor for weight that satisfies the target MBL of 250 kN is given by:

$$linear\ density\ factor = \frac{P1\ density}{P0\ density}$$

therefore

$$linear\ density\ factor = \frac{1.1\ kg/m}{0.1061\ kg/m} \qquad (5.2)$$

$$linear\ density\ factor = 10.4\ (1\ dp)$$

To determine the dimensions of the P1 hollow rope, a spreadsheet was created with the primary inputs for the rope design and the key outcomes. Table 5.1 shows the dimensions, cross sectional solidity and the scaling factor for a series of incremental increases in diameter from the P0 rope. The P0 rope is shown at the top with a scale factor of one. This rope had 40 strands; the machine at the Lankhorst factory in Maia has 48 carriers and therefore must produce a 1 x 1 braid rope with 48 strands or a 2 x 2 with 96. The option of a 2 x 2 braid having 96 strands would mean departing significantly from the geometry intended, therefore a 1 x 1 braid is adopted. The maximum strand diameter achievable at this plant is 4.5 mm. These points are factored into the scaling process.

Table 5.1 Scaled rope dimensions, solidity and scaling factor.

A	B	C	D	E	F	G	H	I	J
Inside diameter (mm)	Strand diameter (mm)	Braid angle (°)	No. strands	Outside diameter (mm)	Annulus area (mm^2)	Strand elipse area (mm^2)	Rope strand area (mm^2)	Solidity (%)	Linear density scale factor
	A/0.089 capped			A + 4.B	π.E^2/4 - π.A^2/4	(π.B.B/cosC) /4	D.G	H/Fx100	H/128.4
19	1.7	45	40	25.8	239	3.2	128.4	54	1.0
20	1.8	52.5	48	27.2	265	4.1	198	75	1.5
25	2.2	52.5	48	33.9	414	6.5	310	75	2.4
30	2.7	52.5	48	40.7	597	9.3	446	75	3.5
35	3.1	52.5	48	47.5	812	12.7	607	75	4.7
40	3.6	52.5	48	54.3	1060	16.5	793	75	6.2
45	4.0	52.5	48	61.1	1342	20.9	1004	75	7.8
50	4.5	52.5	48	67.9	1657	25.8	1239	75	9.7
55	4.5	52.5	48	73.0	1810	26.1	1254	69	9.8
60	4.5	52.5	48	78.0	1951	26.1	1254	64	9.8
65	4.5	52.5	48	83.0	2092	26.1	1254	60	9.8
70	4.5	52.5	48	88.0	2234	26.1	1254	56	9.8
75	4.5	52.5	48	93.0	2375	26.1	1254	53	9.8
80	4.5	52.5	48	98.0	2516	26.1	1254	50	9.8
85	4.5	52.5	48	103.0	2658	26.1	1254	47	9.8

Details of Table 5.1 are as follows by column identifier:

A. Inside diameter: Commencing with the P0 diameter at 19 mm and then incrementing upwards. This dimension is driving the up-scaling in logical increments.

B. Strand diameter: This parameter is driven by the requirement to maintain the proportions of the P0 rope where strand diameter / inside diameter = 0.089. The strand diameter is then capped at 4.5 mm according to the maximum strand diameter accepted by the Lankhorst manufacturing plant.

C. Braid angle: 45° for the P0 rope and then fixed at 52.5° thereafter according to the outline design for the P1 prototypes.

D. No. strands: 40 for the P0 rope and 48 thereafter according to the requirements of the Lankhorst manufacturing plant.

E. Outside diameter: This parameter is derived from the inside diameter and the strand diameter. Outside diameter = inside diameter + 4 x strand diameter. This is an approximation that ignores flattening of the strands.

F. Annulus area: Simple cross section area derived from the outside and inside diameters.

G. Strand ellipse area: Considers the cross section area of a single strand that is cut normally to the rope's axis to expose an ellipse. The ellipse is derived from the braid angle and the strand diameter.

H. Rope strand area: A driven parameter equal to the strand ellipse area x no. of strands. It approximates to the cross section of load carrying material.

I. Solidity: A target parameter that is derived as the proportion (%) of the annulus area that is occupied by load carrying material.

J. Linear density scaling factor: A target parameter derived as the ratio of the rope strand area to that of the P0 rope.

The result of the scaling exercise is that a hollow rope with an inside diameter of 75 mm and strand diameter of 4.5 mm is achievable at the Lankhorst plant and will have a linear density scaling factor of 9.8 in relation to the P0 rope. This is very close to the target scaling factor of 10.4. This rope will have a cross sectional solidity of 53% which is very close to that of the P0 rope at 54%.

Referring to equation 5.2; rearranging for P1 linear density and applying the scale factor of 9.8 gives:

$$P1\ linear\ density = 0.1061\ kg/m \times 9.8$$

$$P1\ linear\ density = 1.04\ kg/m$$

Referring to equation 5.1; rearranging for the predicted P1 rope MBL and substituting the revised linear density gives:

$$MBL\ (kN)\ = 1.04\ kg\ m^{-1} \times 259\ kN\ kg^{-1}\ m^{-1} \times \frac{1}{0.8} \times 0.7$$

therefore $P1\ MBL = 236\ kN$

In summary, the P1 hollow rope design parameters that were supplied to Lankhorst Ropes are:

- Material — polyester
- Construction — 1 x 1, 48 strand hollow braid
- Inside diameter — 75 mm
- Strand diameter — 4.5 mm
- Braid angle — 52.5°
- Braid pitch length — 202.5 mm
- MBL — approximately 236 kN

5.3 Polymer Core Designs

Whilst only one hollow rope design is used for the proof of concept work, a range of elastomeric cores providing differing properties to the tether were designed and constructed. The intention was to achieve a similar effect with the core as that demonstrated by the P0 tether and to explore both stiffer and softer properties as well as alternative constructions.

5.3.1 Pressure Considerations

The pressure created by the P1 hollow rope is considered here with regard to the pressure value calculated for P0 as given in 4.5.2. A simple comparison is initially made according to the following assumptions:

1. The axial force applied is increased by a factor of 9.8 in line with the increase to linear density.
2. The same extension of 23% is achieved.
3. The braid angle is 45° (as for P0).

Referring back to equation 3.1

$$P = \frac{2F_{hoop}}{Dl}$$

It can be predicted that the pressure created by P1 will be reduced relative to P0 by a factor derived as follows:

$$Pressure\ factor\ = \frac{force\ factor}{diameter\ factor\ x\ braid\ pitch\ factor} \qquad (5.3)$$

The diameter factor and the helix pitch factor are ratios based on the mid-section diameter as used in 4.5.2 and shown in Table 5.2.

Table 5.2 Derivation of diameter and braid pitch factors.

	Outside Ø (mm)	Strand Ø (mm)	Mid-section Ø (mm)	Mid-section braid pitch (mm)
P-0	25.8	1.7	22.4	70.4
P-1	93	4.5	84	263.9
Ratio			3.75	3.75

therefore

$$Pressure\ factor\ = \frac{9.8}{3.75\ x\ 3.75} = 0.70\ (2dp)$$

This indicates that the radial pressure generated within the P1 tether, for a particular core that allows 23% extension at 57.4 kN load, will be:

$$0.7 \times 48\ bar = 34\ bar$$

However, the increase in braid angle from 45° to 52.5° for the P1 tethers will result in an increased braid angle at the point of 23% extension considered here. The significance of this is that the mechanical advantage acting to create radial pressure will be higher for this increased braid angle.

This being the case, it is likely that increased radial pressure will allow greater extension of the tether due to compression of the core. However, to allow a representative assessment of the pressure within the P1 tether the same extension of 23% is assumed; the initial steps of the calculation are given in Table 5.3.

Table 5.3 Parameter values and derivations used to calculate P1 radial pressure.

Parameter	Derivation	Value
Original mid-section diameter	93.0 mm – 2 x 4.5 mm	84.0 mm
Original mid-section circumference	π x 84.0 mm	263.9 mm
Original braid angle	specified	52.5°
Original braid pitch length	263.9 mm / tan 52.5°	202.5 mm
Axial load applied	5800 N x 9.8	56840 N
Extension	specified	23%
New braid pitch length (l)	202.5 mm x 1.23	249.1 mm
Original axial strand length per pitch	202.5 mm / cos 52.5°	332.6 mm
New mid-section circumference	$(332.6^2 - 249.1^2)^{0.5}$	219.5 mm
New mid-section diameter (D)	219.5 mm / π	69.9 mm
New braid angle	$\tan^{-1}$ (219.5 / 249.9)	41.3°
F_{hoop} per strand per pitch length	tan 41.3° x (56840 / 48)	1040.3 N
F_{hoop} per pitch length	48 x 1040.3 N	49934 N

Applying equation (3.1)

$$P = \frac{2 \times 49934\ N}{0.0699\ m\ \times 0.2491\ m}$$

therefore $P = 5735555\ Pa$

or $P = 57\ bar$

These two assumed cases act to provide an important understanding of pressures within the tether. It is clear from equation 5.3 that the internal pressure of the tether results from the relative magnitudes of axial load, diameter and braid pitch length (or braid angle). Maintaining geometric similarity with the P0 prototype rope as described in 5.2.1 will therefore provide similar relative compression of a core bundle comprising 7 strands of EPDM 70 Shore A and hence similar normalised extension properties.

5.3.2 Core Architecture and Component Design

Two forms of core architecture are investigated within this work, these are:

1. Seven round section rubber cords, continuous in length and assembled in a hexagonal pack as shown in Figure 5.1. This configuration matches that of the P0 prototype.

2. Articulated full diameter core comprising two moulded components that repeat in an alternating linear pattern as shown in Figure 5.2.

In both cases the elastomer core components are bound together within a helically wound tape.

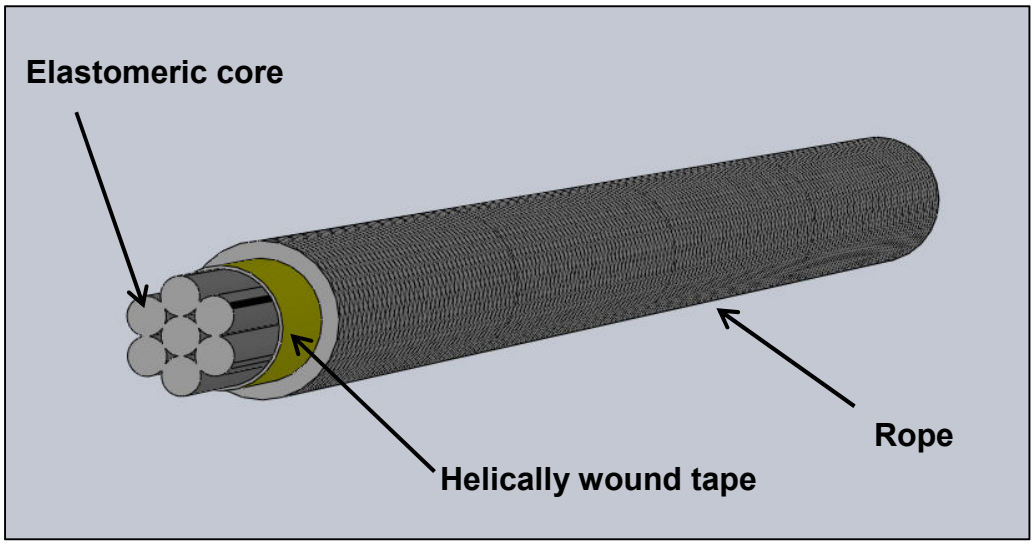

Figure 5.1 Hexagonal pack core structure

Figure 5.2 Articulated core components assembled (upper) and exploded

The aim with both core structures is to leave a small percentage of the rope's cross sectional area unfilled. The intension here is to achieve two stages of tether extension which display different axial stiffness characteristics. During stage one the elastomer components are deformed in compression so as to eliminate the free space. This compression will provide a lower resistance to the rope's diametral reduction and will therefore result in lower axial stiffness. During stage two the solid cross section of elastomer is compressed, relying on axial extension to facilitate diametral compression. This compression will provide a higher resistance to diametral reduction of the rope and hence a higher axial stiffness.

A tether that provides two distinct phases of extension as described above is a preference stated by Dr Borna Hamedni, representing OPT Ltd, in discussions regarding the tether development 7 November 2012 (Hamedni, 2012).

5.3.2.1 Hexagonal Pack Core

The inside diameter of the hollow rope derived in 5.2.1 is 75 mm. This is a useful result in that several rubber extrusion companies hold dies to produce cord of 25 mm diameter. Using seven strands of Ø 25 mm will give a dimension of 75 mm 'across corners' of the bundle but the 'across flats' dimension will be less, the perimeter of the cross section being a rounded hexagon as shown in Figure 5.3.

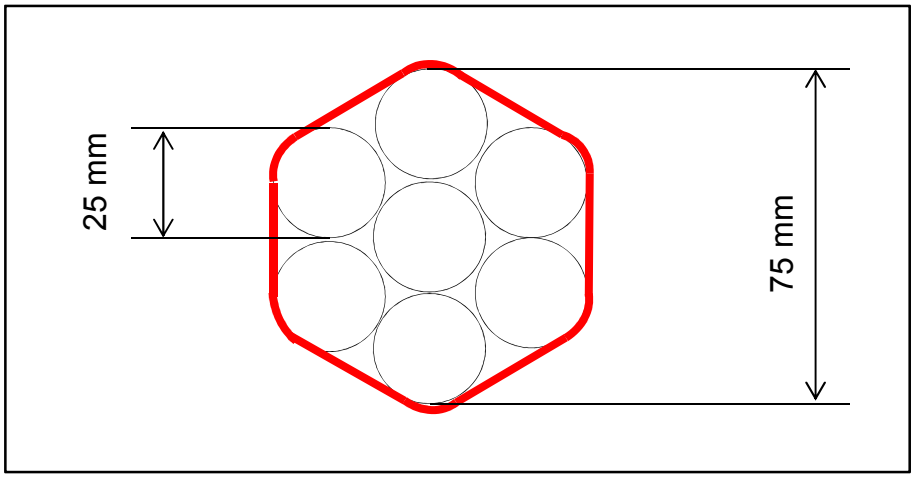

Figure 5.3 Cross section of tether with hexagonal pack core

Referring to Figure 5.4, the effective circumference of the hexagonal pack core is given by:

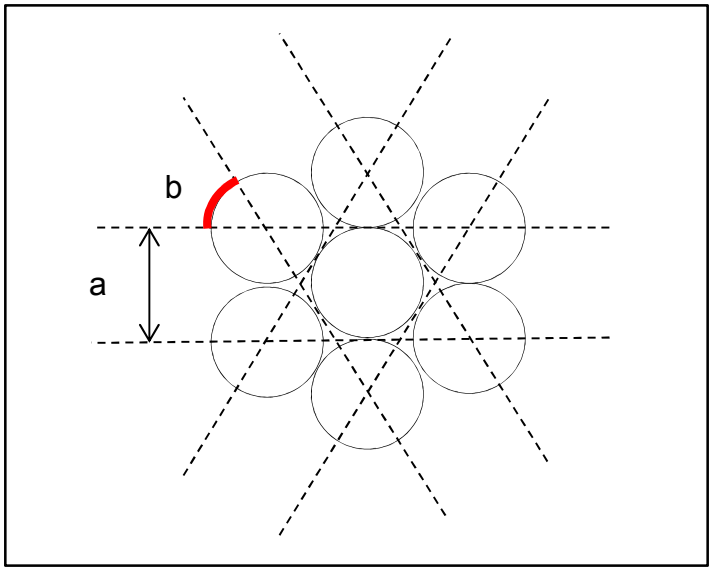

Figure 5.4 Calculating equivalent circumference

$$effective\ circumference = 6\ (a + arc\ length\ b\ )$$

$$effective\ circumference = 6\left(25\ mm + 2\pi \times \frac{12.5\ mm}{6}\right)$$

$$effective\ circumference = 228.54\ mm\ (2\ dp)$$

and

$$effective\ diameter = \frac{228.54\ mm}{\pi}$$

$$effective\ diameter = 72.75\ mm$$

The cross sectional area enclosed by the hollow rope around this rounded hexagon is found to be 3990 mm^2 using Solidworks design software. The cross sectional solidity of the tether is therefore:

$$solidity = \frac{(\pi \times \emptyset^2 \times 7)/4}{3990}$$

$$solidity = 0.86\ or\ 86\%$$

5.3.2.2 Articulated Core

The articulated core has two moulded rubber components; the Male double hemisphere and the Female double hemisphere. Engineering drawings for these two parts are provided as Appendices D and E. These parts are designed to nest into one another axially along the tether to form a round section core. The intention is to produce tethers with reduced bending stiffness in comparison to the tethers having hexagonal pack cores. Additionally the articulated core will not take any axial load and therefore it is anticipated that tethers with articulated cores will exhibit lower axial stiffness than corresponding tethers with hexagonal pack cores.

The Female double hemisphere has draft applied to its diameter in order to achieve release from the mould tool. The 1° draft reduces the diameter from a nominal 74.0 mm to 72.25 mm over 50 mm in each direction from the mould split line. The Male double hemisphere has an outer diameter of 72.25 and requires very little draft over the 10 mm length. Therefore the mean diameter along the 110 mm length of one pair of core mouldings is given by:

$$mean\ diameter = \frac{100 \times \frac{74.0 + 72.25}{2} + 10 \times 72.25}{110}$$

$$mean\ diameter = 73.0\ mm\ (1\ dp)$$

The free space described in 5.3.2 is provided by the Ø 30.0 mm hole that runs axially through both parts. Therefore the cross sectional solidity of the articulated core tethers is given by:

$$solidity = 1 - \frac{\pi \times 30.0^2/4}{\pi \times 73.0^2/4}$$

$$solidity = 0.83\ or\ 83\%$$

5.4 Helically Wound Tape

The hexagonal pack core and the articulated core both require containment as an assembly prior to over-braiding the hollow rope. To achieve this each assembled core was bound together with a continuous length of tape wound helically along the length of the core. The tape serves a secondary purpose by presenting a lower surface friction than the EPDM rubber. This allows the rope strands to move more freely across the surface of the core.

Two tape materials were specified for the P1 tethers for comparison:

1. PVC adhesive tape, 50 mm width x 0.13 mm thickness.
2. Dacron sailcloth tape, 50 mm width x 0.20 mm thickness.

In both cases the tape was wound by hand with a helix angle of approximately 80° to achieve around 1/3rd width overlap per rotation. Figure 5.5 shows this operation in process applying the sailcloth tape to an articulated core assembly.

Figure 5.5 Winding Dacron sail tape onto an articulated core assembly.

5.5 The P1 Prototype General Specifications

Figure 5.6 shows the general assembly arrangement for the P1 prototype tethers. It was important to maximize the length of the working part of the tether whilst remaining within the length limitation imposed by the test work at the DMaC facility.

Figure 5.6 The P1 prototype assembly drawing.

A range of prototypes were planned in order that several facets of tether behaviour could be assessed, these are:

a) The effect of core material hardness on tether axial stiffness.
b) The relative merits of hexagonal pack and articulated cores.
c) The relative merits of PVC tape and Dacron tape.
d) The effect to extension properties from changing the core solidity.

Additionally, one hexagonal pack core tether (P1-1) was specified with material (EPDM 70 Shore A) from the same supplier as the P-0 prototype. This original supplier (Polymax) could not supply other hardness values and consequently was not used generally for the P1 prototypes.

The full range of the P1 series planned for this work is described in Table 5.4.

Table 5.4 Planned P1 series prototypes

Identifyer	Core structure	Core material	Helical tape
P1-1	7 x Ø 25mm profiles	EPDM - 70A	Helically wound
	(86% original volumetric solidity)	(Polymax)	PVC adhesive tape
P1-2	7 x Ø 25mm profiles	EPDM - 50A	Helically wound
	(86% original volumetric solidity)	(Ley)	PVC adhesive tape
P1-3	7 x Ø 25mm profiles	EPDM - 60A	Helically wound
	(86% original volumetric solidity)	(Ley)	PVC adhesive tape
P1-4	7 x Ø 25mm profiles	EPDM - 70A	Helically wound
	(86% original volumetric solidity)	(Ley)	PVC adhesive tape
P1-5	7 x Ø 25mm profiles	EPDM - 80A	Helically wound
	(86% original volumetric solidity)	(Ley)	PVC adhesive tape
P1-6	7 x Ø 25mm profiles	EPDM - 90A	Helically wound
	(86% original volumetric solidity)	(Ley)	PVC adhesive tape
P1-7	6 x Ø 25mm profiles +	EPDM - 70A	Helically wound
	1 x EPDM foam Ø 25mm	(Polymax)	PVC adhesive tape
	(80% original volumetric solidity)		
P1-8	7 x Ø 25mm profiles	EPDM - 70A	Helically wound
	(86% original volumetric solidity)	(Polymax)	Dacron sailcloth tape
P1-9	Articulated	EPDM - 70A	Helically wound
	(83% original volumetric solidity)	(Harboro)	PVC adhesive tape
P1-10	Articulated	EPDM - 70A	Helically wound
	(78% original volumetric solidity)	(Harboro)	PVC adhesive tape
P1-11	Articulated	EPDM - 90A	Helically wound
	(78% original volumetric solidity)	(Harboro)	PVC adhesive tape
P1-12	Articulated	EPDM - 70A	Helically wound
	(83% original volumetric solidity)	(Harboro)	Dacron sailcloth tape

5.6 Manufacture of the P1 Prototypes

5.6.1 The Cores

Ley Rubber Ltd of Liverpool was selected as the supplier of 25 mm diameter extruded rubber cord. The company confirmed their capability to formulate EPDM rubber at Shore A hardness values of 50, 60, 70, 80 and 90 with a tolerance of +/- 5 Shore A.

Polymax Ltd of Bordon was tasked with supplying 25 mm diameter extruded EPDM rubber cord at 70 Shore A hardness as supplied for the P0 prototype and EPDM foam rubber cord (P1-7).

The Harboro Rubber Company Ltd of Harborough was selected as the tool provider and moulders of the articulated core parts. These parts were ordered in EPDM rubber at 70 Shore hardness only, due to financial pressures. This precluded the manufacture of P1-11.

PVC tape as previously specified and manufactured by Advance Tapes International Ltd was sourced.

Dacron sailcloth tape as previously specified was sourced from Penrose Sailmakers Ltd of Falmouth.

Tethers P1-1, P1-2, P1-3, P1-4, P1-5, P1-6, P1-8, P1-9 and P1-12 were assembled according to Table 5.4.

Tether P1-7 was assembled with the central strand of the hexagonal pack being of foam EPDM rubber and then completed in line with Table 5.4.

It had been intended that P1-10 would have reduced cross sectional solidity via a changeover core in the mould tool producing a larger diameter axial hole. This was not possible due to the significantly increased tooling costs and additional set up charges during production. Therefore P1-10 was assembled having a reduced axial solidity by cutting away part of the male hemispheres. This was achieved with sufficient accuracy using a wooden fixture and a hand saw. The engineering drawing for the Male double hemisphere (cropped) is provided as Appendix F. P1-10 was completed according to the specification given in Table 5.4.

5.6.2 The Hollow Rope

The core assemblies were shipped to the Lankhorst facility in Maia, Portugal where sufficient 4.5 mm diameter polyester strand had been manufactured in advance.

The allocated machine was set to the specifications provided in 5.2.1. Strand tension for the braiding operation is controlled by the selection of the springs fitted to each strand carrier. Three moderately rated springs were fitted initially which Lankhorst advised to be a typical strand tension for this diameter rope.

Rope making commenced without introducing a core and this rope was examined. The outside diameter of the rope measured approximately 60 mm

which is considerably less than required. The feed rate of the braiding manufacture is controlled by pulling the finished rope at a rate that corresponds to the required pitch length. This was set to achieve a 202.5 mm pitch. With the pitch length as required but the diameter too small, the solidity of the hollow rope was correspondingly increased making a very tight braid.

A single Female Double hemisphere moulding was then introduced into the throat of the braiding operation. Predictably, the diameter of the rope increased to accommodate the core piece and in so doing the solidity of the hollow rope decreased. Figure 5.7 shows the 60 mm diameter rope and the swollen section containing the core piece.

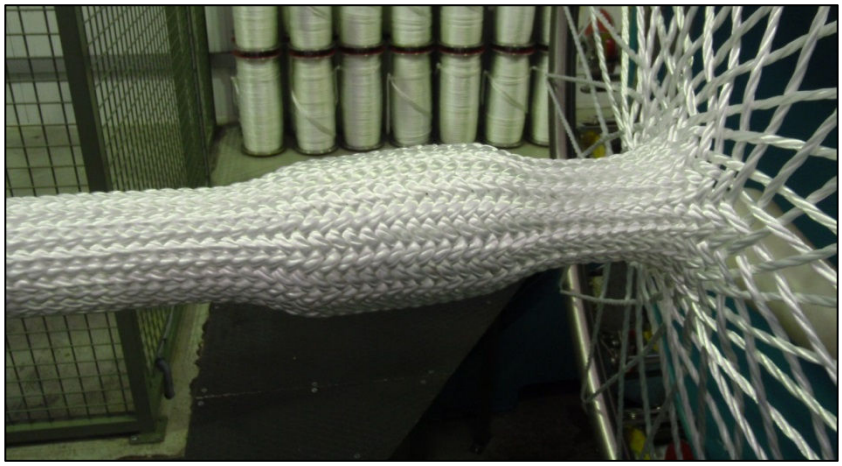

Figure 5.7 The empty hollow rope with a moulded core piece introduced.

The section of rope covering the moulded core piece was examined. The outside diameter measured 85 mm. Inspection of the axial through hole showed no significant compression of the part which indicated that the inside diameter of the rope was being controlled by the core piece and hence would be according to specification.

P1-1 was the first tether to be manufactured, using the following technique:

- Two metres of empty hollow rope was produced.
- The core assembly was fed into the back of the braiding machine by hand. When the core entered the throat of the hollow rope, the core feed rate was controlled by and matched to, the rope feed rate.

- When the full length of the core had been over-braided, a further 2 metres of empty hollow rope was produced.

Inspection of the P1-1 tether immediately after manufacture revealed that the outer diameter was slightly reduced and the braiding was overly tight. Consequently one spring was removed from each carrier to reduce the strand tension during braiding. The remaining tethers were manufactured in numerical order. Figure 5.8 shows the manufacture of tether P1-12.

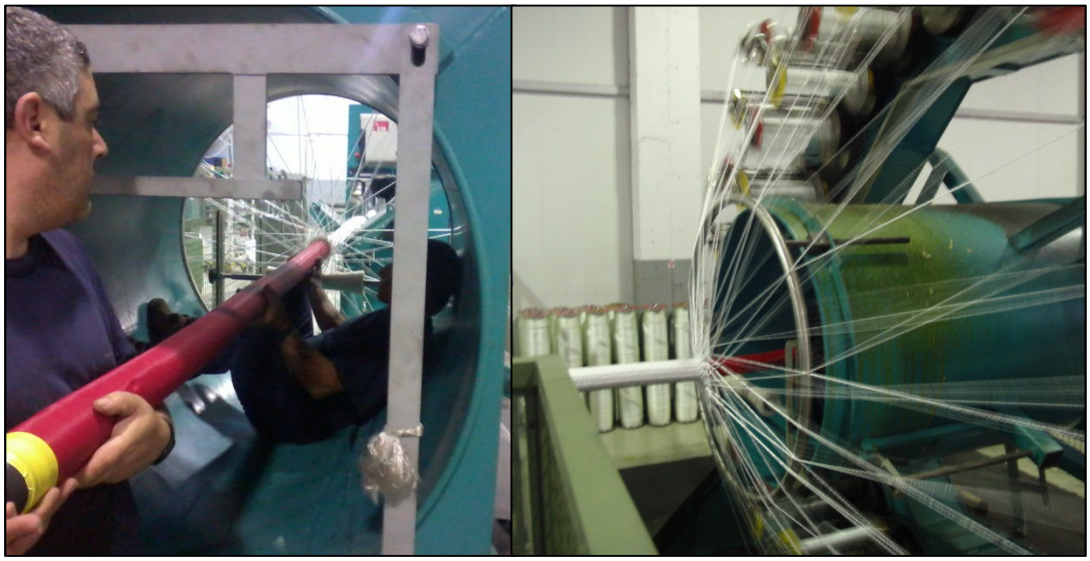

Figure 5.8 P1-12 core being fed into the back of the machine (LH) and P1-12 tether emerging from the machine (RH).

5.6.3 The Rope Terminations

Soft eye splice terminations were specified at both ends of the tether (Figure 5.6). A soft eye splice is one that does not use a rigid thimble to form the eye. McKenna et al. (2004) list three methods for eye splicing hollow single braid ropes:

1. “Tucking the rope through itself”
2. “Burying the rope in the hollow centre”
3. “Tuck splice”

The tuck splice is a complex splice which routes individual rope strands back through the parent rope in an ordered manner. For 12 strand hollow braids the

strands are paired up (McKenna et al., 2004). This type of splice is not viable when dealing with 48 strands. Neither is it possible to bury the rope back in its hollow centre because in this case the space is occupied by the polymer core. Therefore it was decided to trial method (1), tucking the hollow rope through itself, P1-1 was the trial tether.

Figure 5.9 shows this tucking through technique applied to a 12 strand hollow rope (McKenna et al., 2004).

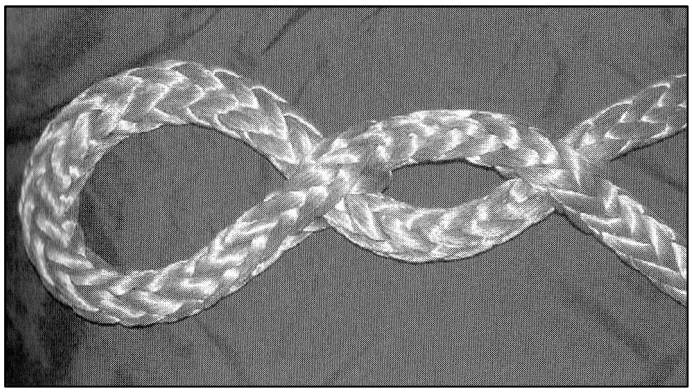

Figure 5.9 Tuck through splice in 12 strand hollow braid.

(McKenna et al., 2004)

Attempts to create the tuck through splice were not successful. The 48 strand hollow rope proved to be too tight in construction to open a sufficiently large aperture for the rope to pass through. In a final attempt to achieve this splice, a cut was made through many of the strands to enlarge the aperture. Even with this extreme measure, the tuck through splice was not achieved. Tether P1-1 was then terminated using a simple fold back and bind technique which would not provide sufficient strength for the test work.

A more robust and complex method was discussed; the hollow rope ends could be unravelled and remade by hand as a 3 or 4 strand laid rope. This rope could then be spliced easily using a tuck splice. A similar alternative is to unravel the hollow rope and hand twist the 48 strands to form two 3 strand laid ropes. These two ropes can then be spliced into one another to form the eye. This method was employed and is fully described:

1. The 2 metre length of hollow rope at the end of the tether was unravelled into 48 strands up to a point 150 mm from the start of the core.

2. Working around the circumference of the rope, adjacent strands were gathered into 6 bundles each of 8 strands.

3. Each bundle of 8 strands was twisted to form a single sub-rope, making 6 sub-ropes.

4. Two adjacent sub-ropes were twisted together and then a third sub-rope from that side of the tether was twisted in to form a 3 strand laid rope. This was repeated for the remaining three sub-ropes to produce two 3 strand laid ropes emanating from opposite sides of the tether as shown in Figure 5.10.

5. A tube of aramid cloth was scrunched up onto one of the 3 strand ropes. This would be stretched back out to cover the full length of the eye splice when completed.

6. The two ropes were spliced to each other in the way that a conventional ‘short splice’ is made. Such a splice is shown for clarity in Figure 5.11.

7. The spliced eye was then bound helically with Gaffer tape before extending the aramid sleeve over the full length. Additional whipping was added to the root of the eye splice to stabilise this area.

A finished tether eye splice is shown in Figure 5.12.

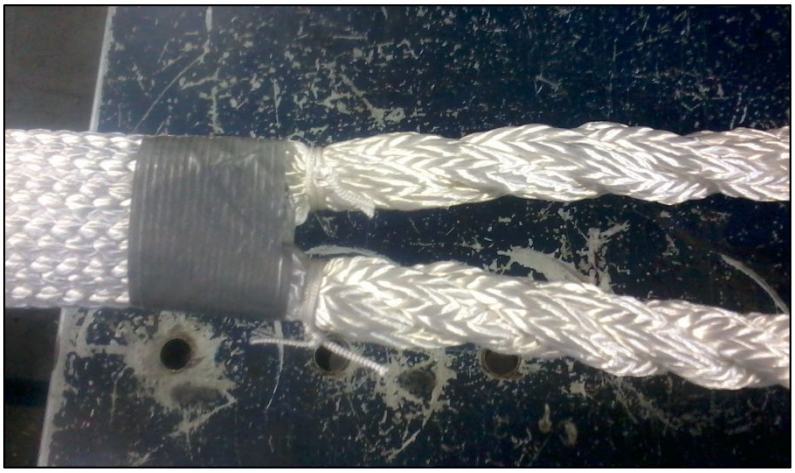

Figure 5.10 Unravelled strands re-made into two 3 strand laid ropes.

Figure 5.11 An example of a 'short splice' (LH) and applied to the tether with the aramid sleeve in place (RH).

Figure 5.12 The completed tether eye splice.

Chapter 6 The Proof of Concept Test Work

The P1 series prototype test work and outcomes are presented within this chapter. This includes a description of the DMaC test facility, adaptations made to DMaC for this work and the DMaC calibration process used. Also explained in this chapter are considerations that determined the specific formats of the tether test work.

6.1 The DMaC Test Facility

The DMaC test facility is a large horizontal test machine that has a linear hydraulic actuator, termed the tailstock, and a two DOF (degrees of freedom) hydraulic headstock. It is designed to reproduce ocean dynamics and loads in a controlled laboratory environment. The major specifications are listed as follows (UoE, 2011):

- Maximum tailstock static force +/- 441 kN
- Maximum tailstock dynamic force +/- 294 kN
- Tailstock stroke 1000 mm
- Maximum frequency at 1000 mm stroke 0.1 Hz
- Maximum frequency at 100 mm stroke 1 Hz
- Maximum frequency at 10 mm stroke 10 Hz
- Maximum specimen length 6 m
- Maximum headstock moment 10 kNm
- Headstock x and y displacement +/- 30°
- Maximum frequency at full displacement 0.25 Hz

The tailstock can be programmed to follow a prescribed time series for either displacement or force. The headstock can be programmed to follow a time series for displacement or moment in each independent axis. In all cases DMaC has full feedback control of the driving parameter.

DMaC's control and data acquisition is performed using a National Instruments LabVIEW platform. A dedicated embedded computer, branded a compact RIO, hosts the programme and interfaces with both the DMaC machine and a standard desktop PC which presents the control panel to the operator. The control data is sampled at 120 kHz (UoE, 2011) and the output data can be accessed at a frequency below this which is selected by the operator.

Test scripts that define the control time series are loaded as csv files. These files can be written using software such as Excel or MATLAB. A MATLAB programme exists that writes simple test scripts according to standard requirements such as ramp, sinewave, hold, repeat etc. The MATLAB programme runs with a user interface to facilitate quick and reliable test scripting.

The DMaC test machine can be flooded with fresh water to allow fully wet test work when required. Figure 6.1 shows an image of the DMaC test machine.

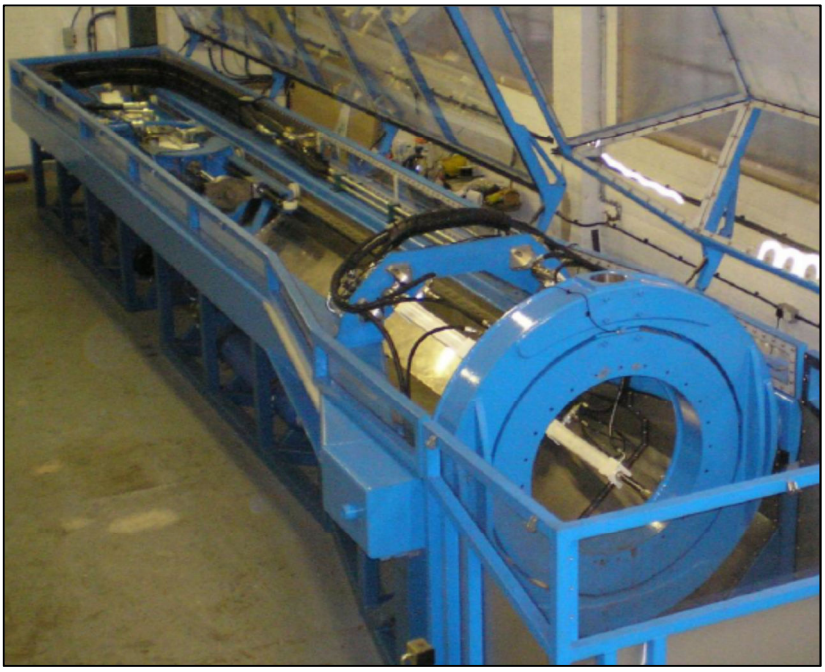

Figure 6.1 The DMaC test machine

6.1.1 Adaptations for This Work

The specifications give a maximum specimen length of 6 m. This distance between the headstock and the tailstock exists only when the tailstock is fully retracted, leaving no travel to extend the specimen. For this reason the P1 tethers were specified at 4.5 m maximum length from eye to eye. However, it was advantageous to extend the DMaC test length marginally and whilst doing this to include a manual pre-tension adjuster. The extension was achieved by designing and commissioning a replacement for the headstock platen which provides a 300 mm offset from the original plane. The pre-tension adjustment is provided by a length of high tensile steel M64 threaded bar and two high tensile

steel nuts. A M42 high tensile eye bolt is threaded into the end of the M64 threaded bar to provide the attachment point for the test piece. The pre-tension adjuster provides 800 mm of travel which allows a test specimen to be pre-tensioned without using any of the 1000 mm travel of the tailstock ram. This arrangement was designed to accept 250 kN with FEA analysis conducted using Solidworks software.

Figure 6.2 shows DMaC with a tether assembly fitted ready to test (submerged in water) and the pre-tension adjuster providing maximum pre-tension.

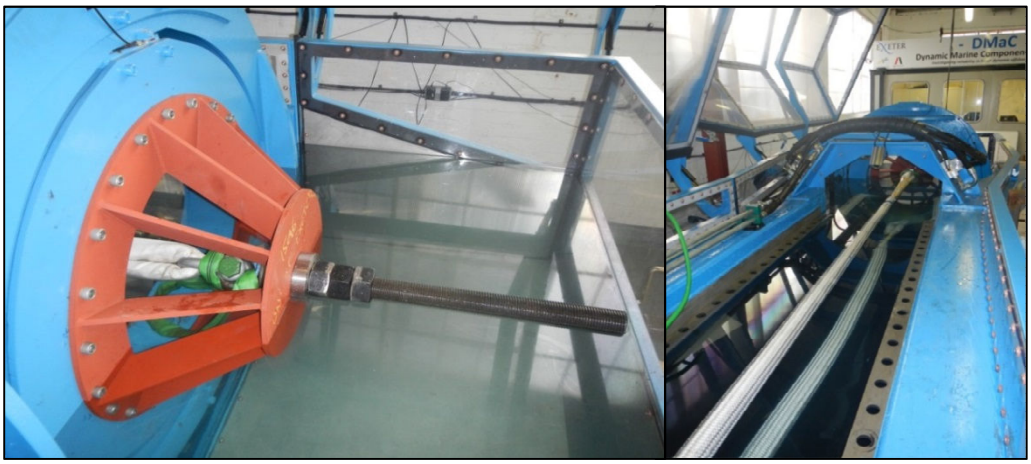

Figure 6.2 Specially designed DMaC extension and pre-tension adjuster (LH) and a tether fitted within the DMaC test bed (RH).

6.1.2 Calibration of the Tailstock Load Cell

The tailstock load cell is a model 3232, pancake type load cell supplied by Interface Force Measurements Ltd. It is capable of compression and tension load measurement and is rated to 100,000 lbf or 444 kN. When DMaC is operated using headstock motions to bend a test specimen, this load cell is afforded protection from lateral loading by re-positioning it behind the tailstock carriage. In this way the carriage's linear bearings react the lateral load rather than the load cell. The disadvantage of operating with the load cell in this protected format is that the frictional resistance of the linear bearings is included within the measured load. For the tether test work it was important to minimise any inaccuracies from the load measurement and with no lateral loads to consider, the load cell was moved in front of the carriage. Each time the load cell is moved it is necessary to re-calibrate it in order that the best possible accuracy of load measurement is achieved. Calibration was undertaken on

three occasions during the tether test work as detailed in Table 6.1. The calibration performed 28/11/2014 is typical and is described here:

Reference load links are kept at the DMaC facility, these load links having calibration status that is traceable to national standards via an accredited test house. In this case a 50 kN load link, type 5201, serial no. 87244, manufactured and calibrated by Strainstall Ltd, is used. In order that the calibration encompasses the entire data acquisition system of DMaC as well as the tailstock load cell, the reference load link is energised and read independently of DMaC.

The reference load link is mounted within DMaC using webbing slings to connect it to the tailstock and the headstock. It is energised at 10.0 VDC via a laboratory benchtop power supply. The 10.0 VDC is verified with a calibrated meter. The signal leads from the load link are connected to a calibrated laboratory voltmeter capable of resolving to 10 microvolts.

A calibration test script is loaded into DMaC's control system and run. The script is force driven and starts at a load of 2 kN. It then ramps to 3 kN, 5 kN, 10 kN, 20 kN, 30 kN, 40 kN and 50 kN, holding at each level to allow manual readings of the reference load link signal. DMaC records the load indicated by the tailstock load cell that is under examination.

Offset and gain values for the reference load link are taken from the calibration certificate to convert the signal (VDC) into force (N). This data is then plotted against itself (y = x) to obtain the 'reference force line'. On the same graph, the DMaC force results are plotted against the reference force results to display the error from the tailstock load cell. Figure 6.3 shows the initial error found during this calibration. The gradient of the DMaC force line is used to inform a correction to the gain applied to the tailstock load cell, this value being set within the DMaC control system.

Table 6.1 DMaC Z ram load cell calibrations

Date	Gain Value (N per V/V)	Offset Value (N)
10/01/2013	1.060×10^8	1300
09/04/2014	1.089×10^8	2000
28/11/2014	1.064×10^8	1700

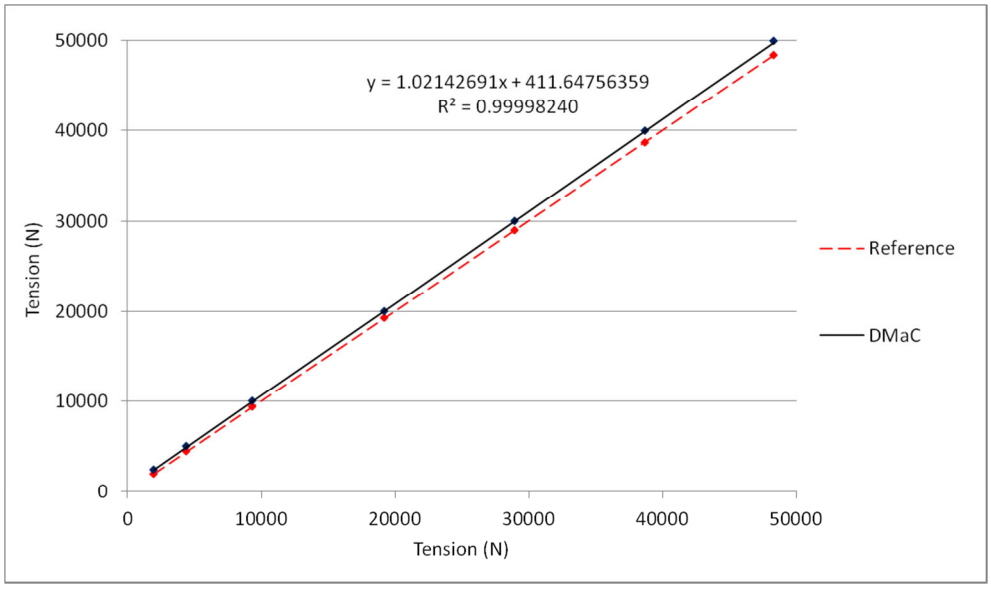

Figure 6.3 Initial calibration graph showing an error in gain, represented by the equation given.

With the gain adjusted, the calibration procedure is repeated. Figure 6.4 shows an improvement to the accuracy in terms of gain but a significant offset.

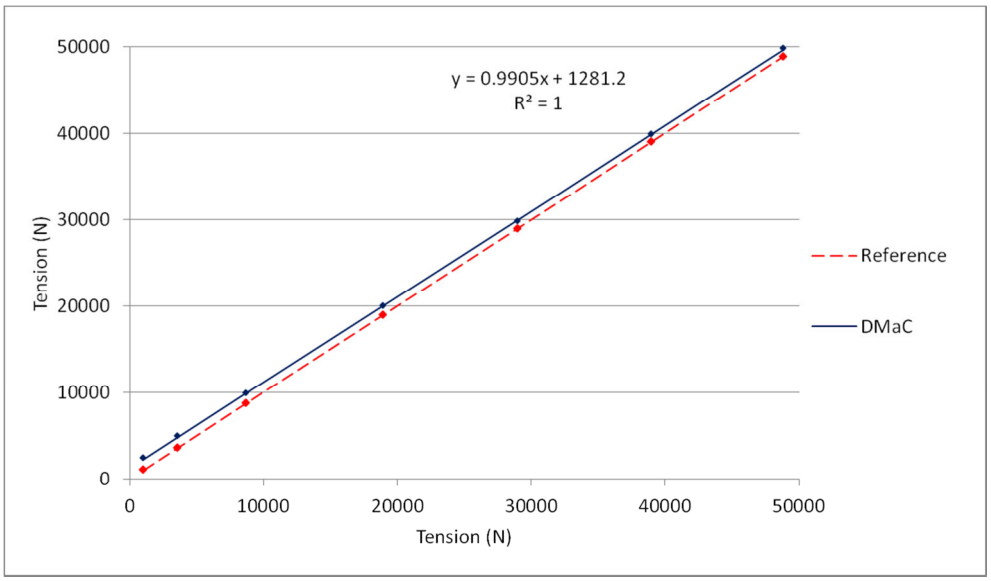

Figure 6.4 Partially corrected calibration graph with an improved calibration of gain but showing a positive offset.

The full calibration process involved four iterations to achieve a maximum calibration error of 250 N and a mean error below 100 N. The performance of the load cell at the completion of the calibration is shown in Figure 6.5.

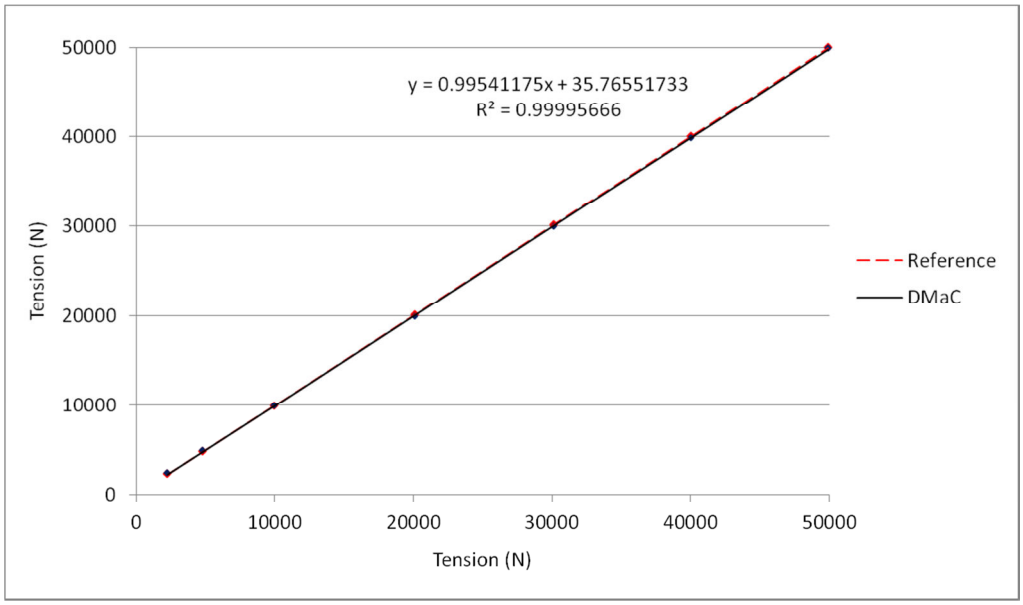

Figure 6.5 Result of the completed calibration.

6.2 Test Considerations

The following sections describe and explain some important considerations that are taken into account within the test work.

6.2.1 The Mullins Effect

The Mullins effect, alternatively termed stress softening, occurs in most thermoplastic elastomers (Mark et al., 2013). The effect is characterised by the

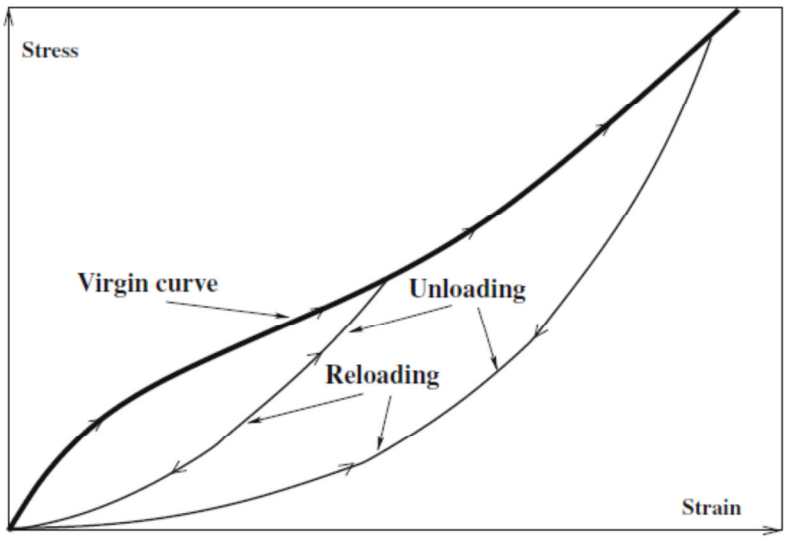

Figure 6.6 The idealised Mullins mechanical behaviour (Cantournet et al., 2009)

reduction of stress values required to achieve corresponding strain values once those strain values have been exceeded on just one occasion. The effect applies to strain in both tension and compression.

Figure 6.6 shows the idealised Mullins behaviour. Virgin loading takes the stress strain plot to a maximum at the first unload point. Unloading follows a lower energy path back to the origin describing hysteretic loss from the cycle. The second and subsequent loading paths will follow the unloading line until it reaches the virgin loading line (Cantournet et al., 2009). The effect will reoccur each time the virgin loading curve is elevated to a new high point as shown in Figure 6.7.

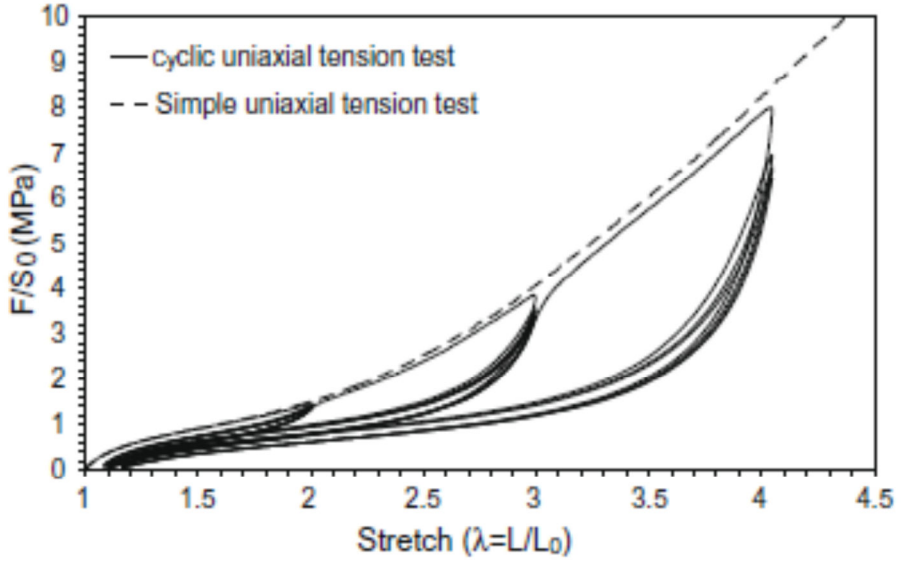

Figure 6.7 An example of uniaxial cyclic response with an increase of maximum strain every 5 cycles.

(Diani et al., 2009)

Cantournet et al. (2009) state that the actual behaviour of these materials depart from the idealised case. Whilst the major change occurs during virgin loading, significant change also occurs during the 2nd loading. However, stability is soon reached with only negligible change being observed after 5 – 10 cycles.

Steps were taken in the test work and the subsequent processing to ensure that stress softening of the core materials had concluded before critical results were recorded; these steps are as follows:

- A series of conditioning tests were performed on each tether prior to the primary data tests. These conditioning tests applied loads and extensions ≥ those of the primary data tests.
- The primary data tests applied 5 cycles to the tethers, the critical data being taken from the fifth cycle.

6.2.2 Lubrication and Cooling

Although DMaC is floodable with fresh water it is more convenient and hence quicker to operate when dry. Additionally, engaging in an extended wet test programme involves having DMaC full of water for some considerable time which has consequences in terms of maintenance actions and costs. There was a clear preference to test in the fully wet (submerged) condition to best replicate the lubrication and cooling provided by seawater. However it was necessary to justify this decision in terms of the discernible effect on tether behaviour.

Tether P1-1 was used to explore the effect of wetting on the tether behaviour. This tether was the first that was manufactured and differed from the others in two respects; braiding tension during manufacture and the eye splice termination. For this reason P1-1 would not be part of the main study and would serve well for any exploratory tests required to inform the test programme.

Test script ETT_01 was written as a force driven test imposing 5 equal tension cycles peaking at 15 kN. The cycles of this test are sinusoidal with a period of 50 seconds. P1-1 was mounted in DMaC in the dry condition and pre-tensioned to 1kN. Test ETT_01 was performed three times with the pre-tension being adjusted to take up slack between tests 1 & 2 and 2 & 3. The 3rd test was recorded as ETT_01_P1-01_01.

P1-1 was then wetted using a hosepipe for several minutes. The pre-tension did not need to be adjusted and test ETT_01_P1-1_02 was conducted.

Figure 6.8 shows the 5th cycles for these two tests, ‘Dry’ and ‘Wet’. It is clear that whilst the difference is small, there is a notable reduction in axial stiffness (gradient) for the lubricated test. It was therefore concluded that all tether testing would be performed in the fully wet (submerged) condition.

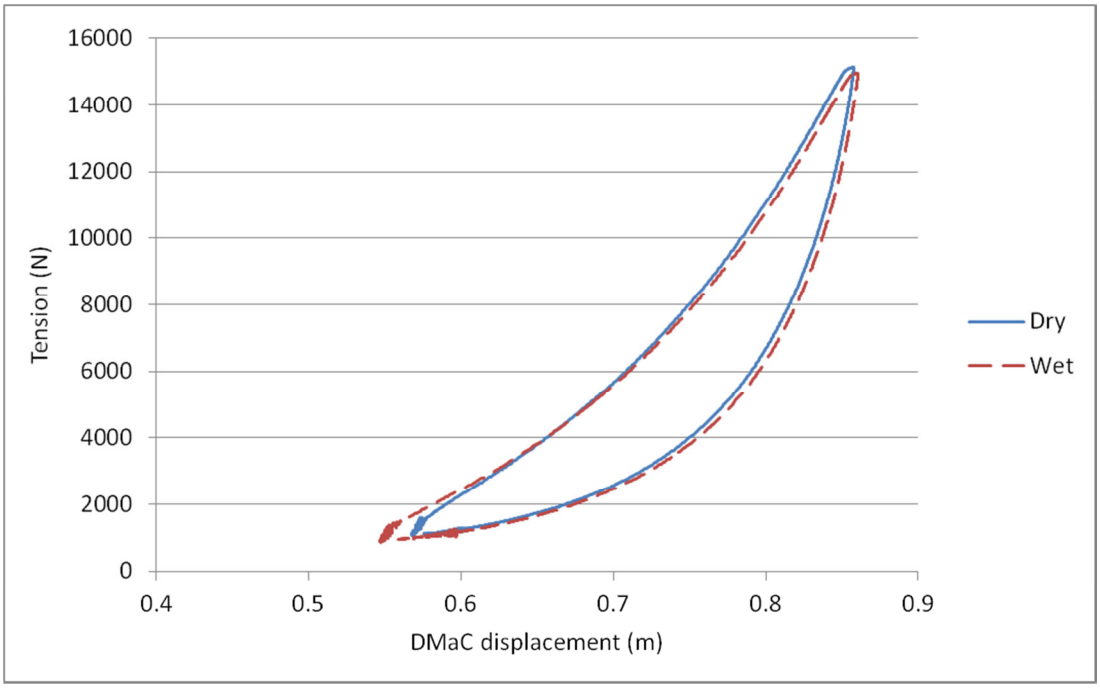

Figure 6.8 5th cycle loops for P1-1 in the dry and wet conditions.

6.2.3 Test Cycles

As described in 6.2.1, tests need to be performed as a short batch of tension cycles. There are some parallels between the tether testing within this work and conventional fibre rope testing, however there are notable differences as follows:

1. Conventional fibre ropes require several cycles to achieve stability during a test. McKenna et al. (2004) recommend 10 cycles during a test but acknowledge that individual test plans may differ.

The P1 tether rope has a less complex construction than conventional fibre rope and will therefore achieve stability more readily. This is confirmed by exploratory testing of P1-1 and might be aided by the water lubrication provided during testing as described earlier. Figure 6.9 shows the 4th and 5th cycles of test ETT_01_P1-1_02. Although creep is still ongoing at this stage, the two loops show very close parallelism which demonstrates stability in respect of axial stiffness. This is not the case between loops 2 and 3 where a change in stiffness is still evident. Whilst it would be preferential to eliminate creep from the data, this would require many more cycles. In seeking to balance the need

to achieve stability with concerns over the unknown durability of the P1 tethers, 5 cycles is considered to be the optimum at this stage.

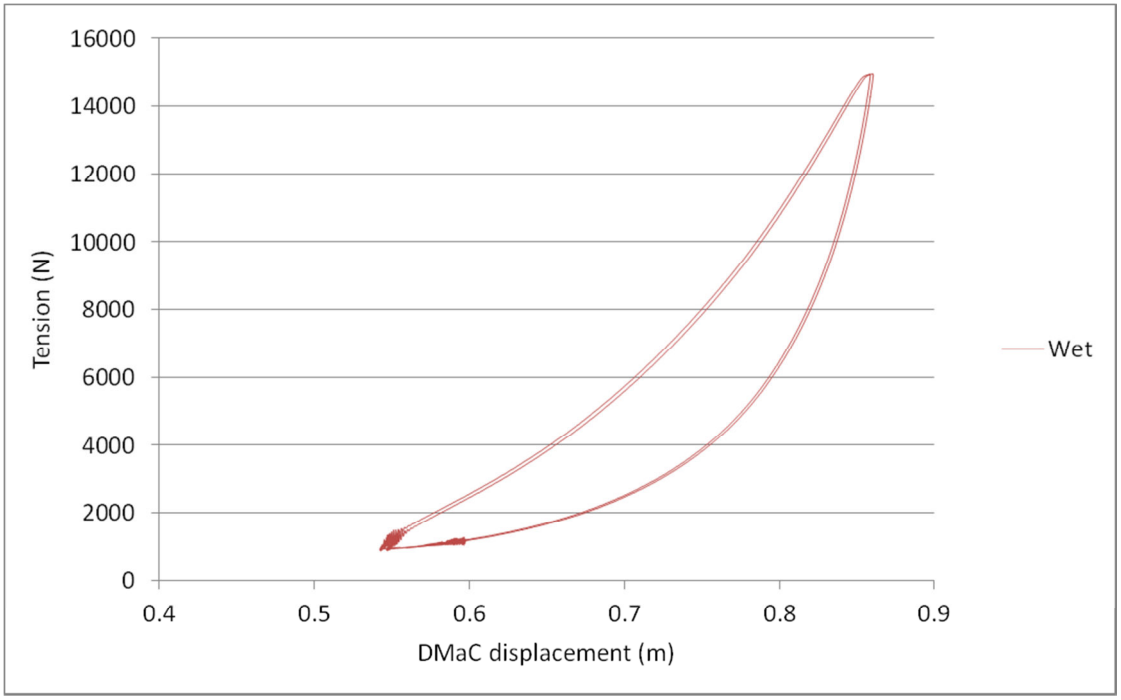

Figure 6.9 4th and 5th cycle loops for P1-1 in the wet condition

2. The rate of loading is an important consideration for conventional fibre rope testing. The Cordage Institute of Pennsylvania, in their standard CI 1500, specify that the test rope should be loaded to 20% of its estimated strength in not less than 20 seconds and no more than 200 seconds (McKenna et al., 2004).

This specification seeks to avoid two opposing issues; rapid extension of an unworked rope is liable to cause damage to some individual yarns and excessive heat generation within the structure, whilst overly slow loading will allow creep to affect the results.

In the case of the tether, the relatively simple open structure and the fully submerged testing reduce concerns regarding damage and heat, allowing tests to be carried out at higher frequencies.

3. Large rope testing plant, applying cycles at a slow rate, might employ a linear ramp up and ramp down as the test load profile.

Working at a higher cycle frequency, DMaC is best suited to applying test cycles in a sinusoidal form. This provides a smooth change of direction at each end of the tailstock travel and will have less impact on the longevity of the test machine.

A further consideration in determining the format of the test cycles for this work is the aim defined in 1.3, Q4. The stated aim is to assess the ability of the P1 tether to reduce the load generated within a highly dynamic body's mooring system. In order that this question can be answered, the tethers must be tested at a realistic cycle rate. In this case the SWMTF buoy is to represent a highly dynamic MEC for numerical modelling. Therefore a cyclic test format is selected accordingly as follows:

- Force driven and displacement driven tests follow a sinusoidal form.
- Cycle frequency is 0.125 Hz i.e. period equals 8 seconds.
- No. of cycles within a primary data test equals 5.

6.3 Test Methods

The tether test work comprised the following stages conducted at DMaC:

1. Performance tests referenced to a tension load datum.
2. Eye splice extension tests.
3. Breaking load test.
4. Testing the effect of load cycle frequency upon the tether properties.
5. Performance tests referenced to a displacement datum.

These five stages of test work were conducted in the sequence shown and are described fully in the following sections. Also described in this section are the material properties tests which form part of the results and subsequent discussions.

The sequence of results reporting (section 6.4) differs from the sequence of test methods to allow outcomes to feed into subsequent data processing as necessary.

6.3.1 Performance Tests Referenced to a Tension Load Datum

A tension load datum might refer to the static pre-tension of a mooring line when the floating body is at calm and the tide height is at a minimum.

A series of conditioning tests were run in 'force mode' (the tension load time series drives the linear actuator) to bed in the tether and its attachment to DMaC. These conditioning tests are summarised in Table 6.2.

Table 6.2 Force mode conditioning test descriptions

Test i.d.	Pre-tension (kN)	Peak tension (kN)	Sine wave period (s)	No. cycles
ETT_03	1	10	8	10
ETT_04	2	20	8	10
ETT_05	2	40	8	5
ETT_06	2	60	8	5

Following completion of the conditioning tests the pre-tension was set to 1550 N and the tether was left at this tension for a prolonged period (overnight) to stabilise. At the end of this stabilisation period the pre-tension was reset to 1550 N if any drift had occurred. A 'displacement mode' test (the displacement time series drives the linear actuator) was then conducted according to test script ETT_08. The drive data for this test is given in graphical form as Figure 6.10.

These tests were performed on all of the P1 series tethers except P1-1 and P1-10.

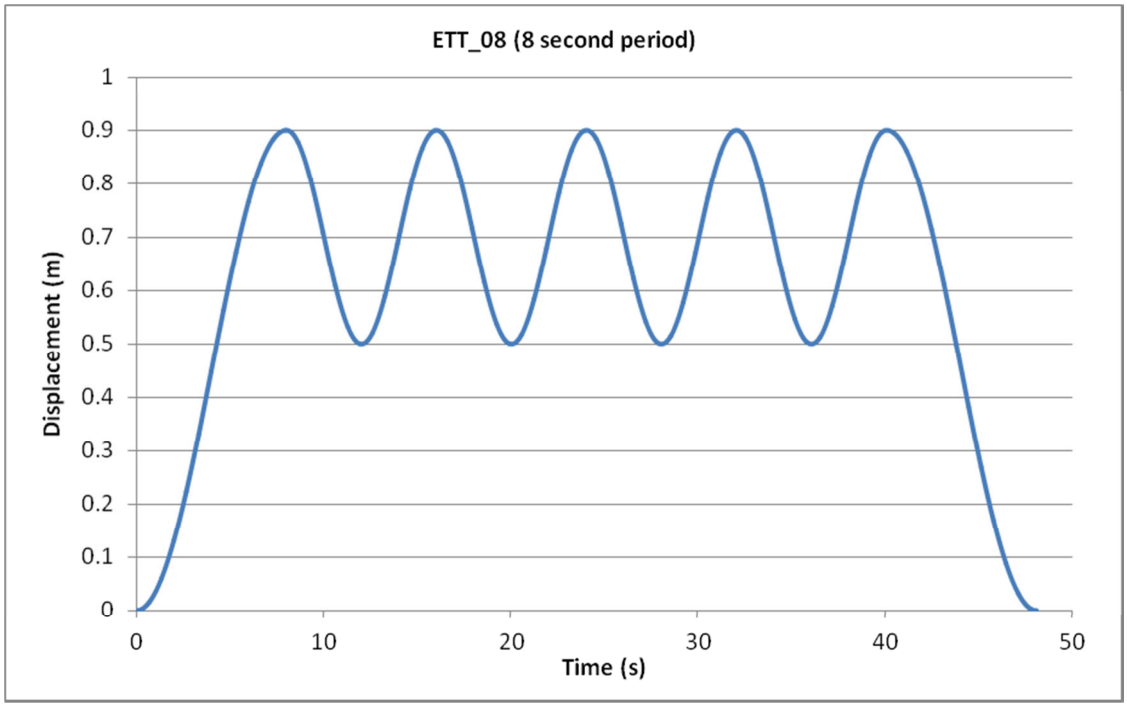

Figure 6.10 The displacement drive data for test ETT_08.

6.3.2 Eye Splice Extension Tests

The extension data output by DMaC relates to the extension of the entire tether rather than the working length. It is therefore necessary to quantify the axial stiffness of the eye splice terminations so that the eye splice extension can be subtracted from the total extension data to reveal the extension experienced by the working portion of the tether.

Tests were performed on tethers P1-3 and P1-6 to characterise the P1 series eye splices. Test script ETT_08 was used for these tests after bedding in as described in 6.3.1. A draw wire linear transducer was used to measure the extension between the connection shackle and the closest end of the core. These tests were performed without submersion to eliminate the risk of water ingress and damage to the transducer (see Figure 6.11).

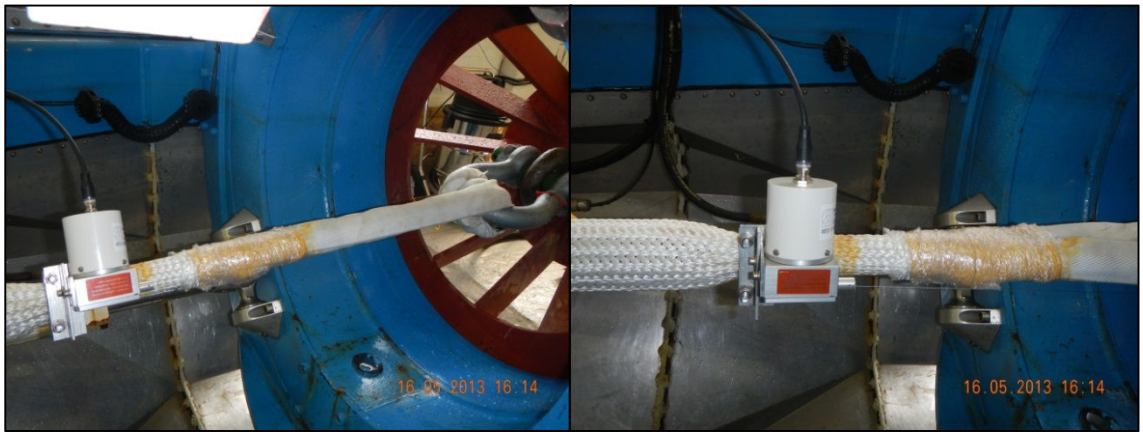

Figure 6.11 Linear transducer recording eye splice extension.

6.3.3 Breaking Load Test

It was important to quantify the breaking strength of the P1 tethers to allow the extension performance of the tethers to be normalised against breaking strength (MBL). Due to the compliance of the P1 series tethers, the maximum tension load that could be realised using all of the pre-tension and the full hydraulic stroke length of DMaC fell well short of parting a tether. It was necessary to modify P1-4 to reduce its working length to 2.0 m and to remake the eye splice. The new tether is identified as P1-17.

Force mode test ETT_06 was conducted twice to bed in the terminations before using displacement mode test ETT_08 to break the tether. All three tests were conducted without submerging the tether but using a hose to thoroughly wet the assembly.

6.3.4 Testing the Effect of Load Cycle Frequency

The elastomer core exhibits viscous behaviour in addition to its elastic behaviour. The result is that the elastic response properties of the tether are, to a degree, time dependant. To assess this time dependency a single tether (P1-8), having mid-range shore hardness, was cycled at varying frequencies. All of the tests employed for this were displacement driven and of the same general form as ETT_08 shown in Figure 6.10. The tests were conducted one after the other at 2.5 minute intervals according to the sequence shown in Table 6.3. The irregular sequence aids the discrimination between viscous effects and bedding in of the tether.

Table 6.3 The sequence and description of the load cycle frequency tests.

Test sequence no.	Test i.d.	Sine wave period (s)
1	ETT_08	8
2	ETT_11	6
3	ETT_12	10
4	ETT_13	12
5	ETT_14	14
6	ETT_14	14
7	ETT_13	12
8	ETT_12	10
9	ETT_11	6
10	ETT_08	8

6.3.5 Performance Tests Referenced to a Displacement Datum

Referencing to a displacement datum allows for easier comparisons between the P1 tethers and conventional rope.

Test ETT_19 was scripted to replace the displacement mode test ETT_08 detailed earlier. ETT_19 also operates in displacement mode but extends the tether over the fullest range possible on DMaC during each cycle (0 – 0.99 m).

Figure 6.12 shows a tether fitted into the test bed, submerged under water.

Figure 6.12 A submerged tether awaiting testing.

The tethers that were subjected to this test stage are P1-2, P1-5, P1-6, P1-7 and P1-9. Those not included had been subjected to earlier destructive tests or had been assigned to durability testing at sea which is not reported within this work.

For each tether, test ETT_19 was conducted four times. Incremental increases in the test pre-tension were made up to a maximum possible pre-tension resulting from the full uptake of the M64 thread. This incremental approach was adopted in order that the highest possible load range was achieved ultimately, whilst guaranteeing cyclic data in the event of a failure at high load. Performance of the tether is not assessed in relation to the pre-tension value. At each pre-tension setting, the working length of the tether (core length) was measured. A waterproof linear transducer was fitted as described in 6.3.2 before the execution of the 4^{th} and final test for each tether. All tests were conducted in the submerged condition.

6.3.6 Durometer Hardness Tests

The hexagonal pack core elastomer material was supplied as extruded round section lengths of 25 mm diameter having specified durometer hardness values of 50, 60, 70, 80 and 90 Shore A. A sample of 18 mm in length was cut from the middle part of each extrusion. The test end of each sample piece was polished using a wet 240 grit micro-section polishing wheel to produce a uniform flat surface. A Mitutoyo Hardmatic HH-331(A) durometer was used to take three readings for each test piece. Care was taken to distribute the three tests around the face of each test piece so as to avoid misrepresentation caused by slow material recovery after penetration of the indenter. Test indentations were made approximately 8 mm from the edge of the test face.

6.3.7 Poisson's Ratio and Young's Modulus Tests

The hexagonal pack cores are extended with the tether when it is extended. Therefore the elastomer material experiences negative transverse strain in a proportion to its longitudinal strain according to the material's Poisson's ratio. Tests were made to determine Poisson's ratio for the 50A, 60A, 70A, 80A and 90A EPDM cords. Load measurement during the tests also allows a determination of Young's modulus.

An overhead gantry crane was used to extend each test piece which was secured to a ground anchor of lead blocks. A 200 kg in-line load cell was fitted between the ground anchor and the test piece, the load cell streaming data to a laptop computer via a dedicated data acquisition module. A 1000 mm gauge length was marked onto each test piece using white PVC tape. Figure 6.13 shows the test apparatus in a schematic diagram.

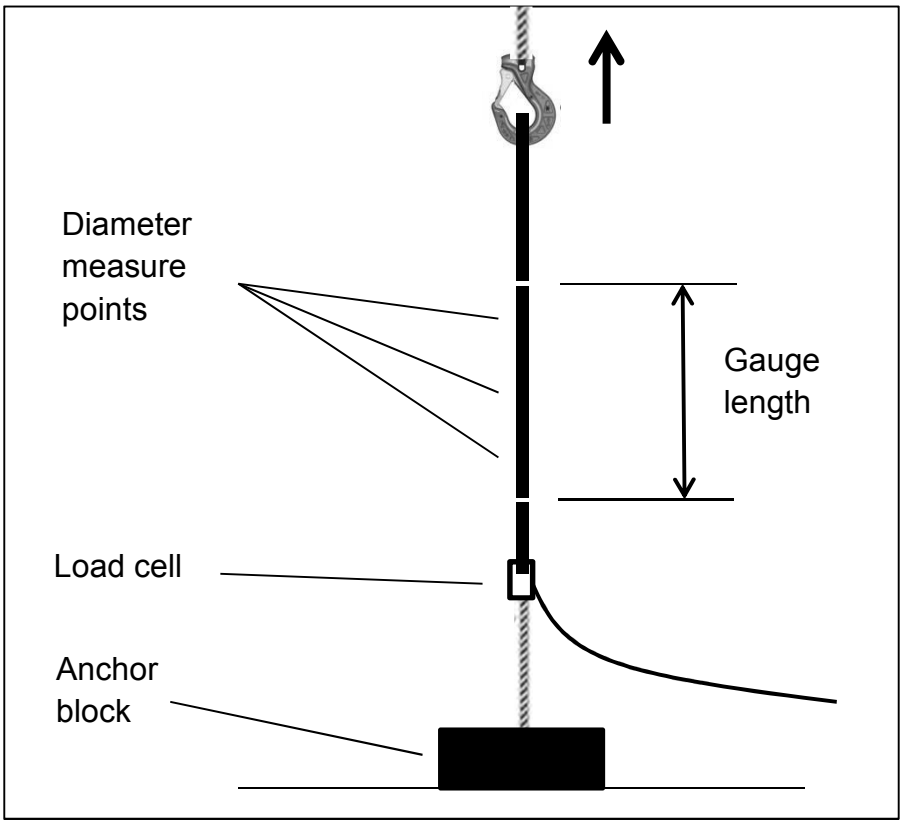

Figure 6.13 Schematic diagram of the Poisson's ratio / Young's modulus test equipment.

Each test piece was subjected to four conditioning cycles, each taking the sample from 0 - 60% strain at approximately 100 mm / second. This conditioning work being to nullify the Mullins effect.

During the test, each test cord was extended in approximately 100 mm increments. At each increment of extension, the gauge length was measured and the diameter of the cord was measured at three positions axially along the gauge length. At each axial position, four measurements of diameter were made around the cord in 45° increments, using a Vernier calliper gauge.

6.4 Test Results

Results are given here for the performance and material tests. The sequence of test reporting allows the results to inform the subsequent test reporting.

6.4.1 Durometer Hardness Tests

Durometer hardness readings and mean results are given in Table 6.4.

Table 6.4 Durometer hardness test results

Target Tether I.D.	Specified hardness	Hardness readings			Mean hardness
P1-2	50	54	54	54	54.0
P1-3	60	59	59	59	59.0
P1-4	70	70	71	71	70.7
P1-5	80	70	70	70	70.0
P1-6	90	81	80	81	80.7

From the results detailed above, it is clear that the EPDM used for both P1-5 and P1-6 was not as specified; P1-5 has been manufactured with 70A and P1-6 with 80A.

6.4.2 Eye Splice Extension Tests

Figure 6.14 shows the extension of a P1-3 eye splice recorded by the linear transducer over the five cycles of the ETT_08 test. The final sine wave is identified in the data set and from this cycle the load up data (increasing load) is extracted and plotted (Figure 6.15). Microsoft Excel software is used to perform a linear regression according to the least squares method. The regression completes with a coefficient of determination, r^2, value of 0.999. This demonstrates that the eye splice extends under tension in a manner that very closely approximates to linear behaviour.

This data analysis was repeated for P1-6 and the results are given in Table 6.5.

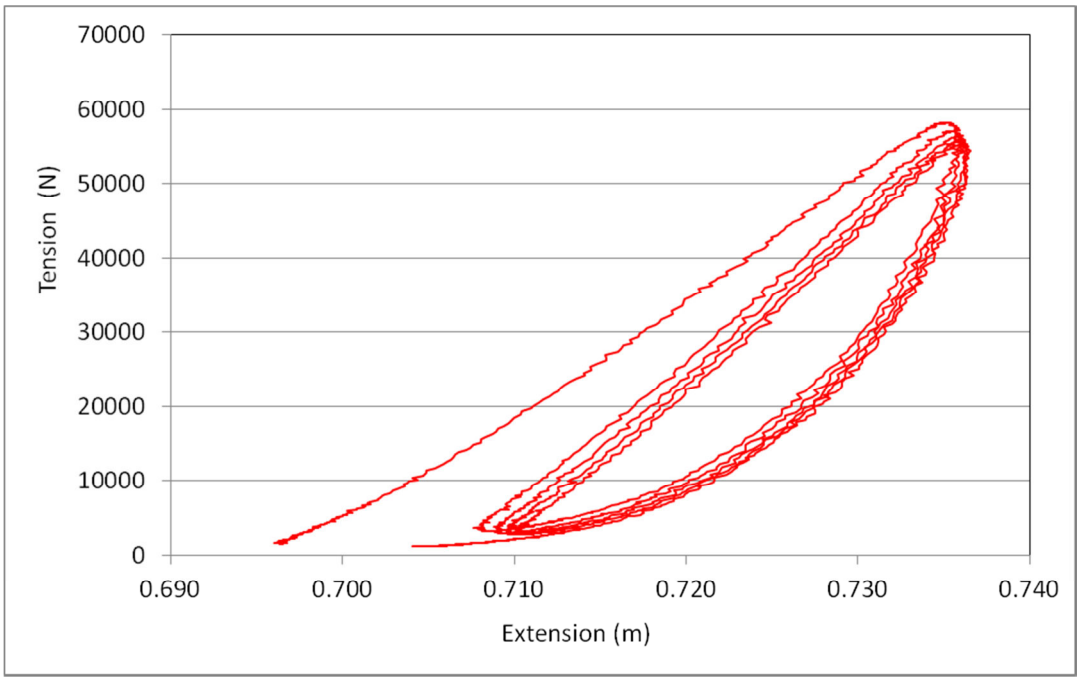

Figure 6.14 P1-3 eye splice extension during test ETT_08

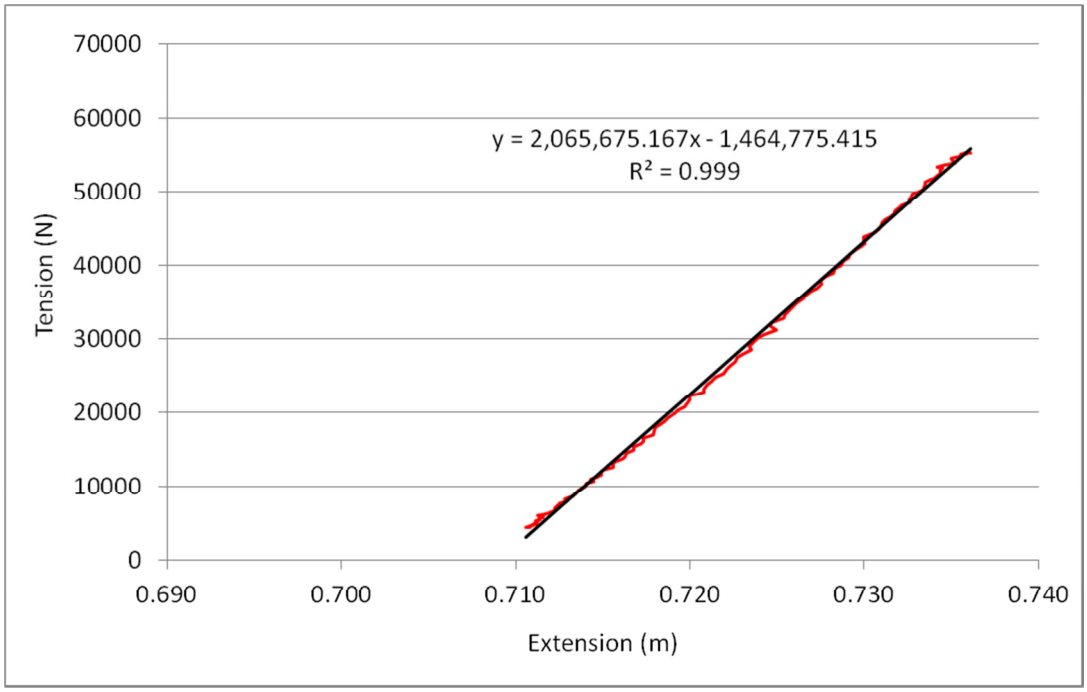

Figure 6.15 The final cycle load up data and best fit straight line.

Table 6.5 Results of the eye splice extension tests.

Tether id.	Straight line gradient (N/m)	r^2 value
P1-3 (single end)	2065675	0.999
P1-6 (single end)	1866182	0.999
Mean value (single end)	1965928.5	-

The mean value of 1965928.5 N/m is inverted as 5.087×10^{-7} m/N and then doubled to 1.017×10^{-6} m/N to represent the total eye splice extension of a typical P1 series tether under load up conditions.

6.4.3 Breaking Load Test

Figure 6.16 shows the tension vs displacement curve obtained from the breaking load test performed on tether P1-17. The maximum load recorded was 222 kN.

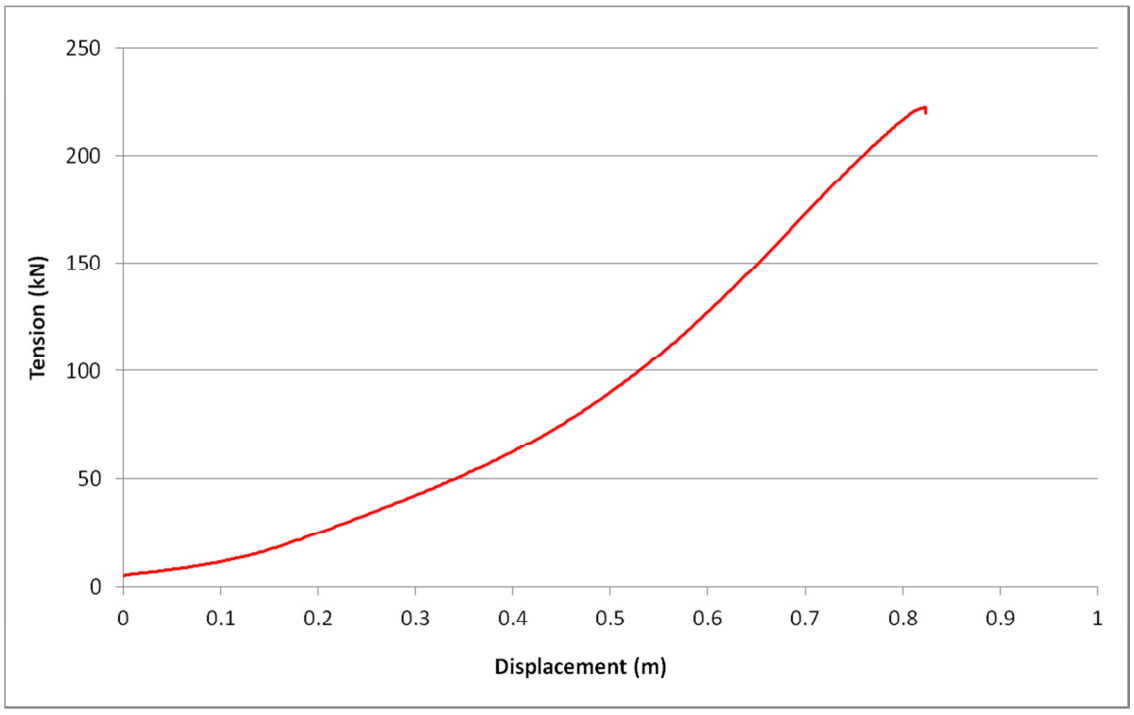

Figure 6.16 Tension vs displacement plot showing failure at 222 kN.

Failure occurred where the braided hollow rope is converted into two sub-ropes which then enter into the eye splice (Figure 6.17).

Figure 6.17 Images showing the failure of tether P1-17.

6.4.4 Performance Tests Referenced to a Tension Load Datum

The final cycle load up data is identified as described in 6.4.2. For each data time step, the incremental increase in tension is used to calculate the extension of the eye splices by applying the value 1.017×10^{-6} m/N derived in 6.4.2. The eye splice extension is then subtracted from each displacement value recorded by DMaC to provide data corresponding to the extension of the working part of the tether. The extension is normalised against the original working length and expressed as a percentage. The tension load is normalised against the MBL of 222 kN (6.4.3) and expressed as a percentage. Figure 6.18 shows the outcome of these tests in graphical form.

The divergence of the nine plot lines demonstrates the differences in axial stiffness through the range of tethers. It is clear that in all cases the tether exhibits a close to linear relationship between load and extension beyond a certain tension load. Figure 6.19 shows further analysis of this behaviour. The final 20 data points have been clipped from each data set to remove the 'curved tails' that are apparent in Figure 6.18. These tails result from the viscous (time dependant) properties of the elastomers as the displacement sine wave causes the stroke velocity to tend towards zero.

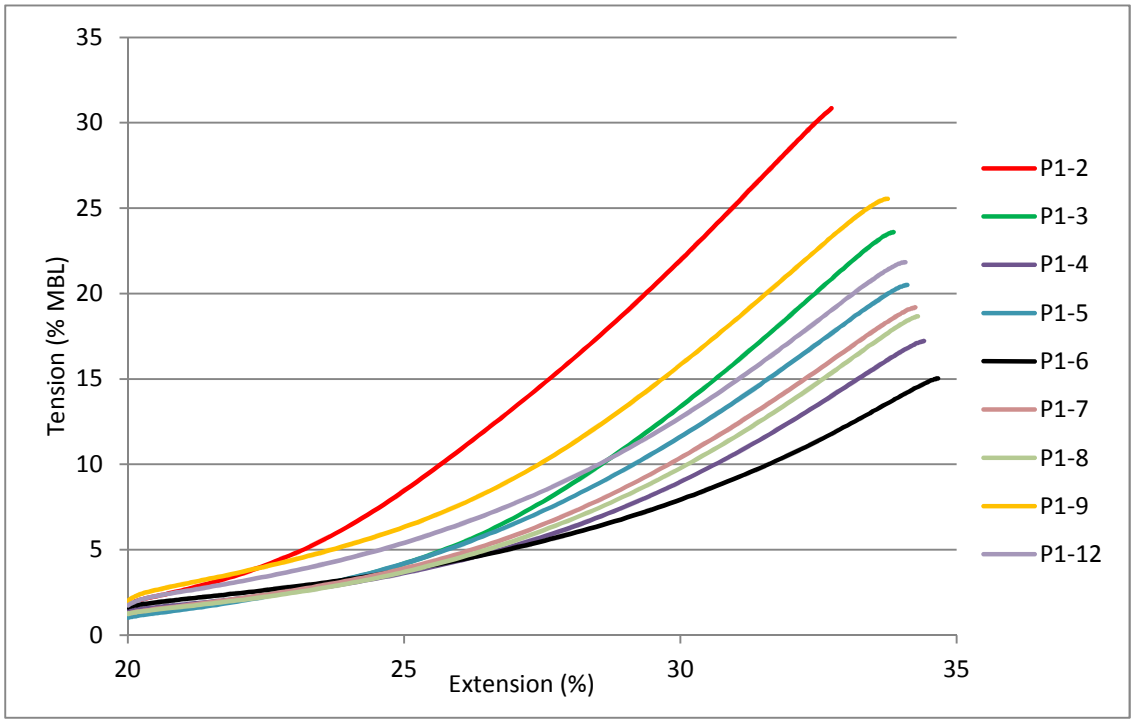

Figure 6.18 P1 series tether extension properties at > 20% extension.

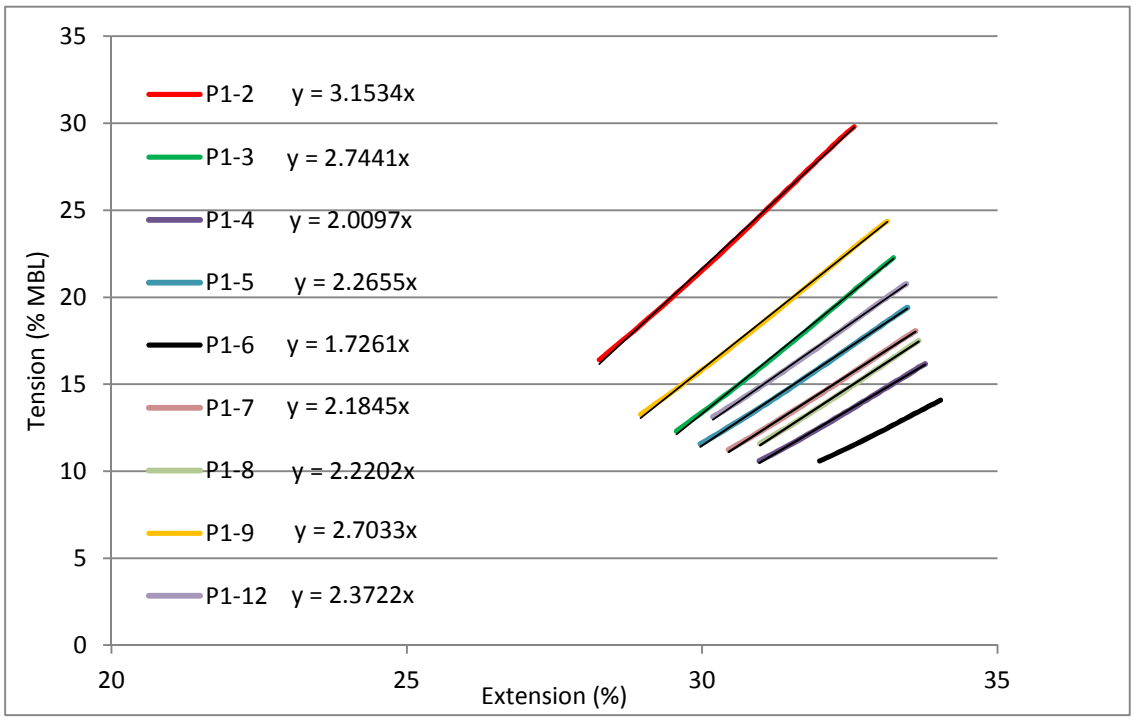

Figure 6.19 Data from Figure 6.18 clipped to achieve r2 = 0.9995 linear regressions.

To establish the equation for the best fit straight line representing the near linear behaviour, a least squares linear regression analysis is performed. Starting at the origin end of each data set, data points are removed until the linear regression achieves a r^2 value of 0.9995. The equation for this line is then detailed; the crucial value being the gradient, as this represents the tether axial stiffness. The gradient of the best fit straight line is shown on the graph and these values are repeated in Table 6.6.

Tethers P1-2 through to P1-6 have identical constructions other than a progressive change in the Shore hardness of the elastomer core. These tethers are ranked according to their gradient and it is apparent that there is a relationship between the measured hardness of the elastomer (6.4.1) and the gradient. It is also evident that changes to the hardness of the core are more significant than changes to the construction of the tether. It should be noted that the stiffest tether is achieved with the softest core material and the most compliant tether, with the hardest core material. This is counter intuitive and is discussed in Chapter 8.

Table 6.6 Tabulated results of the linear regressions shown in Figure 6.19.

Hardness (Shore A)	Tether	Gradient	Stiffness ranking
54 (measured)	P1-2	3.15	1
59 (measured)	P1-3	2.74	2
70 (measured)	P1-5	2.27	3
71 (measured)	P1-4	2.01	4
81 (measured)	P1-6	1.73	5
n/a (1 foam cord)	P1-7	2.18	-
70 (specified)	P1-8	2.22	-
70 (specified)	P1-9	2.70	-
70 (specified)	P1-12	2.37	-

6.4.5 The Effect of Load Cycle Frequency

The final cycle load up data is identified for each of the ten tests. This data is plotted for the first five tests in Figure 6.20 and for the reverse sequence tests in Figure 6.21.

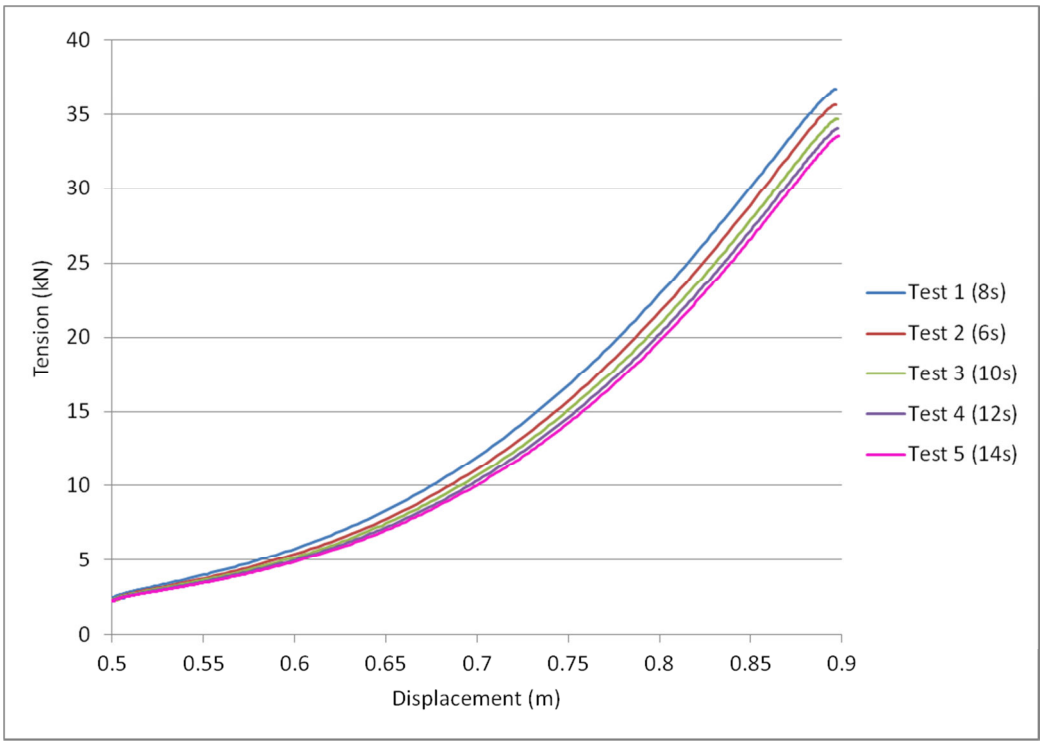

Figure 6.20 Tension vs displacement plots for tests 1 - 5

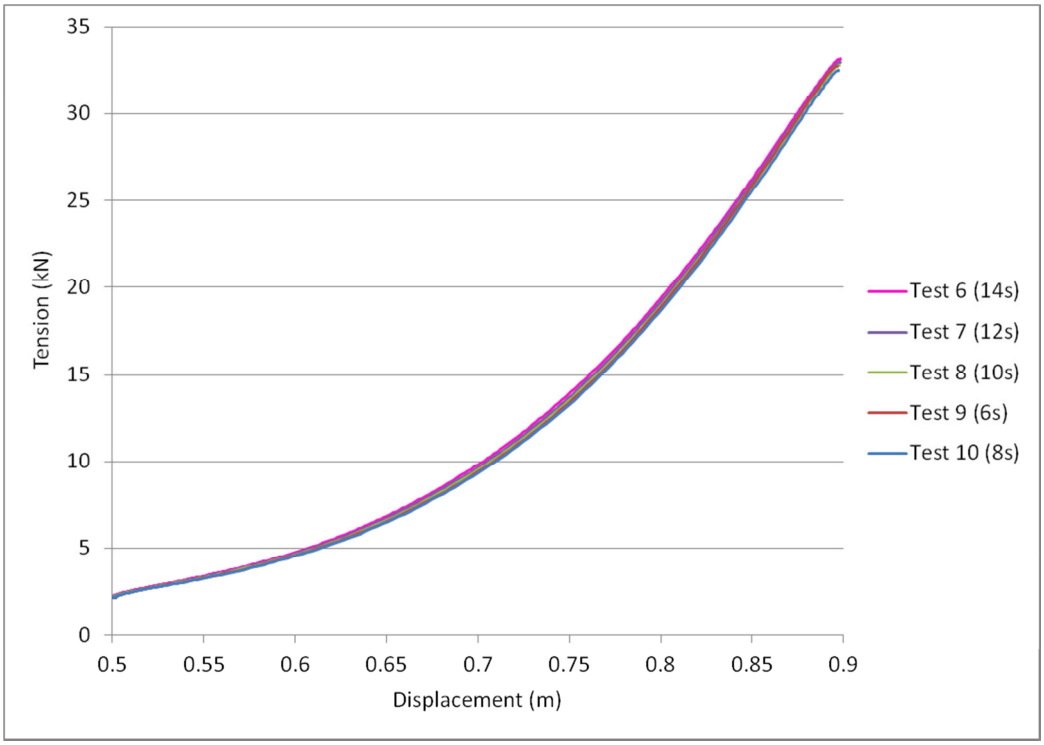

Figure 6.21 Tension vs displacement plots for tests 6 – 10 (reverse sequence).

Figure 6.20 shows a progressive 'axial softening' of the tether through the sequence of tests. Because the sequence of tests does not follow a

progression in frequency (8, 6, 10, 12, 14), it is likely that the progressive softening is due to bedding in of the tether / terminations rather than changes to the cycle frequency. This is supported by the closer alignment for tests 3, 4, 5 than for tests 1, 2, 3.

Figure 6.21 shows a close alignment for tests 6, 7, 8, 9, 10. There does not appear to be any significant sign of a change in axial extension properties resulting from changes to the cycle frequency (within the frequency range tested).

6.4.6 Performance Tests Referenced to a Displacement Datum

Figure 6.22 demonstrates that the behaviour of the tether under initial loading (upper line) is not representative of its cyclic performance and therefore nor is the original length at zero load. It is important to obtain a realistic value for the 'zero load length' during cycling so that extension (strain) can be accurately assessed for comparison with other ropes and for dynamic modelling. McKenna et al. (2004) recommend that a reference tension and a gauge length be established before a conventional rope test. When the test is complete, the reference tension is set and the gauge length re-measured.

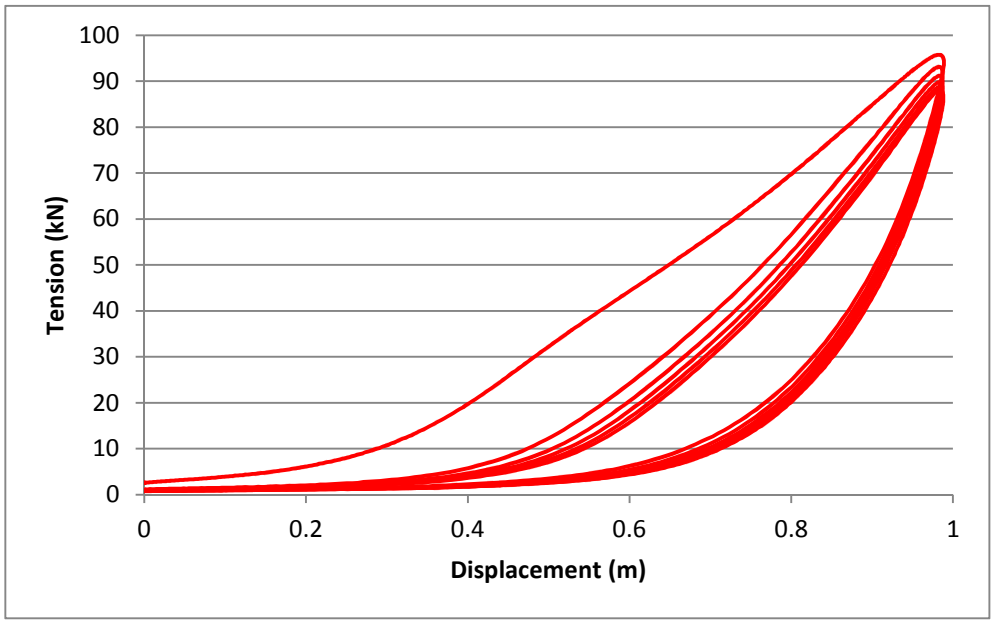

Figure 6.22 Full ETT_19 test data for P1-2

The 'zero load length' of the tether changes significantly under cyclic operation and yet it recovers quickly. It is not possible to return to a reference tension

immediately after a test because the tether recovers too quickly to identify any steady tension value. This makes the standard procedure described above unsuitable for this work and an alternative technique is employed.

A result derived from the data that represents the 'dynamic zero load length' of each tether is used to assess extension in these results. The spring rate of the tether at low loads is found from the pre-tension and working length (W/L) measurements taken before each ETT_19 test (6.3.5); an example is given for P1-2 (Figure 6.23).

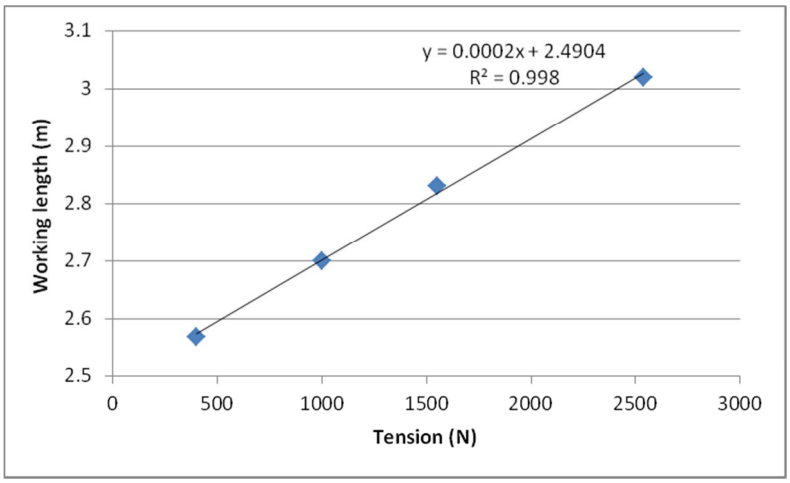

Pre tension (N)	W/L (m)
400	2.57
1000	2.7
1550	2.83
2540	3.02

Figure 6.23 Pre-tension data used to obtain the 'dynamic zero load' length.

The gradient obtained from the linear regression of this quasi-static analysis is applied to the tension value of the first data point in the final cycle load up data. This provides a value for the working length of the tether at zero load at the start of the final cycle.

The eye splice extension is subtracted from the DMaC displacement data as described in 6.4.4. In this case however, the eye splice extension data taken for each final ETT_19 test is used rather than the characteristic result used in 6.4.4.

Figure 6.24 shows the extension properties for the tethers together with a reference rope. The tether tension load is normalised against the MBL (222 kN) to allow comparison with the reference rope. Data for the reference rope has been obtained by digitising a graph provided by Lankhorst UK Ltd. The reference rope is a double braid construction of polyester, the same material as the tethers.

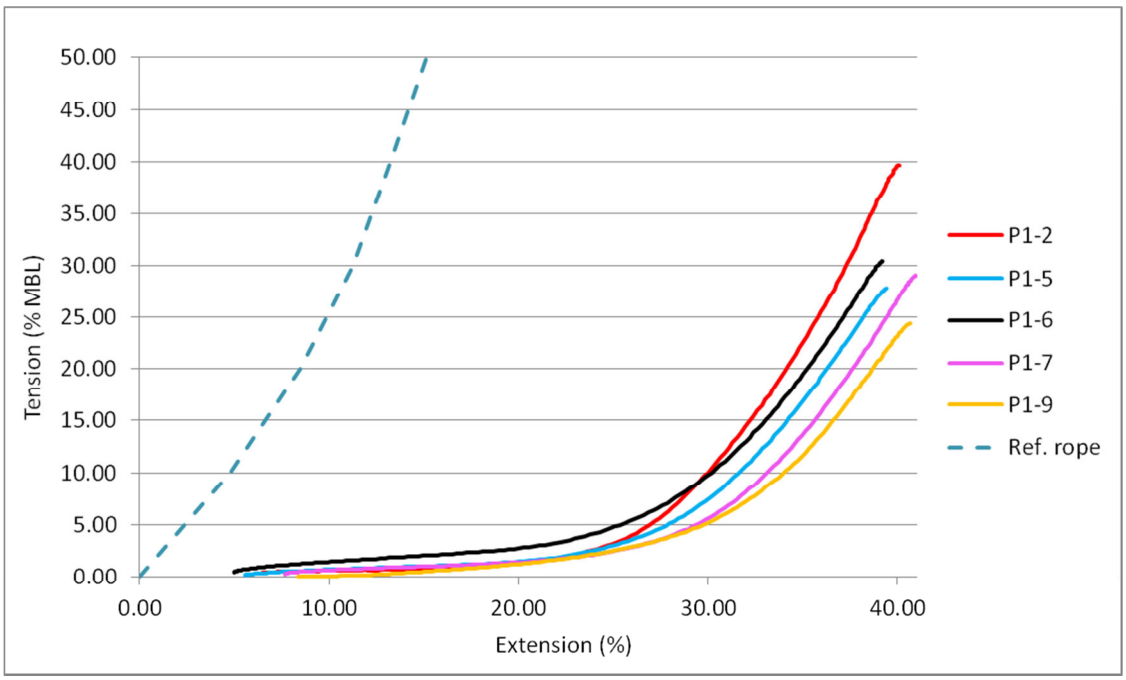

Figure 6.24 Comparison of tether extension properties with a double braid polyester reference rope.

Figure 6.25 shows only P1-2 and P1-6 for clarity. These two tethers have the softest and hardest elastomer core material. Also included is a second reference rope, a Superline (parallel Lay) rope of Nylon. This represents the most compliant fibre rope recommended for WECs by Ridge et al. (2010).

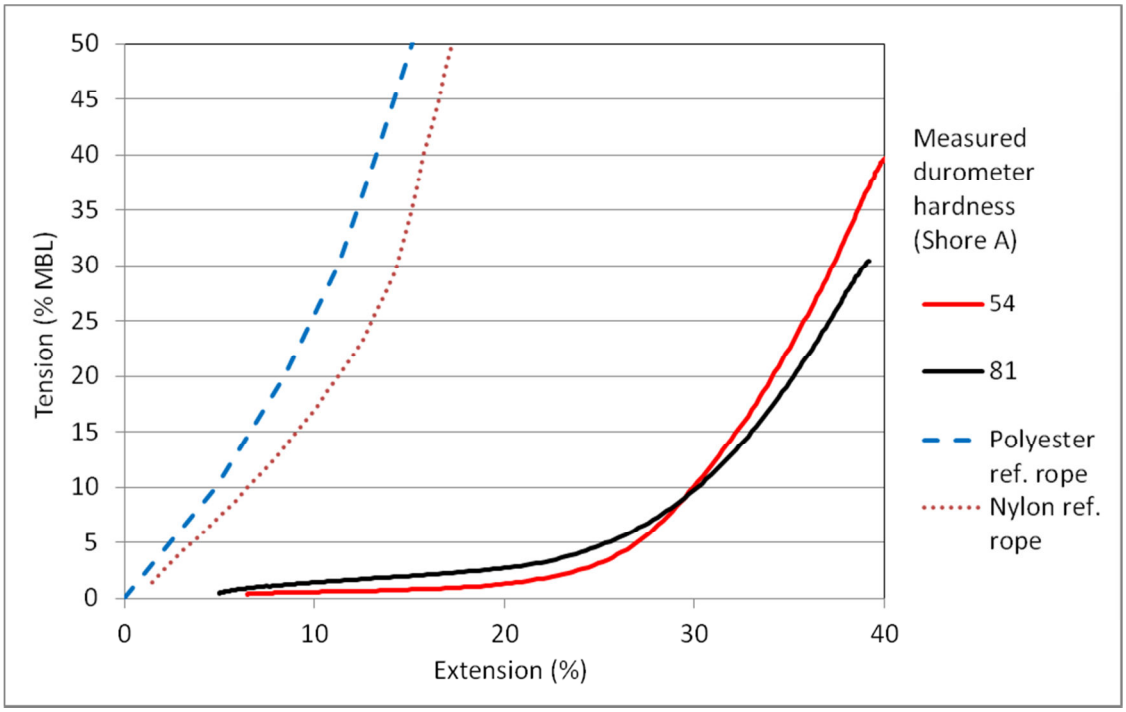

Figure 6.25 Further comparison of tether extension properties with conventional highly compliant fibre rope.

It is clear that the P1 series prototypes exhibit two phases of extension with an intermediate transition phase. The initial phase is one that provides soft extension properties up to a load limit of around 5% of MBL. The second phase of extension displays a markedly stiffer behaviour.

Table 6.7 provides a numerical comparison of these outcomes in terms axial stiffness represented by a secant line taken between the origin and 30% MBL. For clarity, the normalised tension is reverted to tension assuming an MBL of 222 kN. Therefore the axial stiffness is defined as load divided by strain and given in units of kN. It is clear that the soft first phase acts to reduce the secant modulus for the working load range of the tether very considerably.

Table 6.7 Comparison of axial stiffness outcomes by secant method.

Line type	Axial stiffness (kN)
Polyester reference rope	590
Nylon reference rope	463
54 Shore A hardness tether (P1-2)	74
81 Shore A hardness tether (P1-6)	72

6.4.7 Poisson's Ratio and Young's Modulus Tests

Poisson's ratio defines the extent to which a uniform section of a material changes size laterally when deformed axially. The extension or compression is termed as the strain. Young's Modulus, often termed the modulus of elasticity defines the stiffness of an elastic material.

For each level of axial extension applied to a test cord, the mean diameter is calculated from the 12 measurements taken. The diametral strain is then calculated as:

$$\text{diametral strain} = \text{change in diameter} / \text{original diameter}$$

The axial strain is calculated as:

$$\text{axial strain} = \text{change in length} / \text{original length}$$

The Poisson's ratio is calculated as:

$$\text{Poisson's ratio} = -\text{diametral strain} / \text{axial strain}$$

Figure 6.26 shows the results obtained for Poisson's ratio at increasing levels of axial strain.

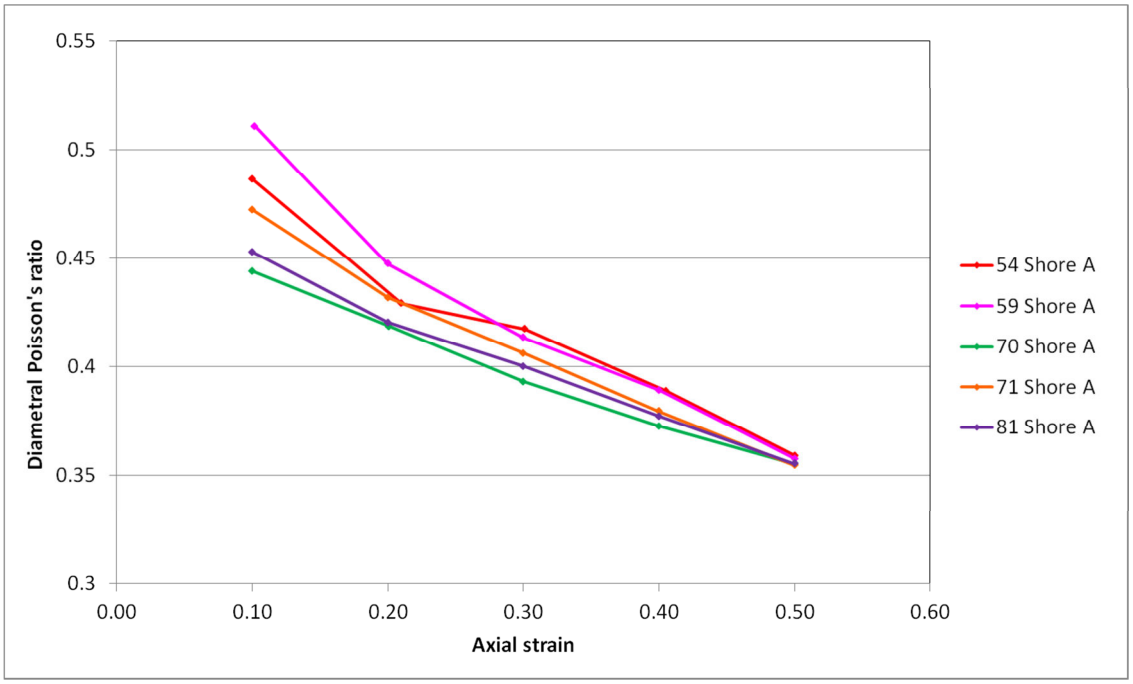

Figure 6.26 Poisson's ratio of the EPDM cord materials.

For each level of axial extension applied to a test cord, the axial stress is calculated as:

$$\text{stress} = \text{tension (N)} / \text{original cross section area (mm}^2\text{)}$$

The Young's modulus is calculated as:

$$\text{Young's modulus} = \text{stress} / \text{strain}$$

Figure 6.27 shows the results obtained for Young's modulus at increasing levels of strain.

Due to the non-linear behaviour of viscoelastic rubbers, Young's modulus is not a constant for these materials. Alternative moduli such as the 100% modulus and the 300% modulus are often used to more precisely describe behaviour at defined extensions. In Figures 6.26 and 6.27 the non-linear behaviour is evident in both Poisson's ratio and Young's modulus. The mean values for Poisson's ratio and Young's modulus are calculated for extensions of between 30% and 40% and are given in Table 6.8. This level of extension represents the second phase of tether extension shown in Figure 6.25. The rankings given

for Poisson's ratio and Young's modulus sequence from 1 to 5 with 1 representing the condition that is expected to provide the most compliant tether.

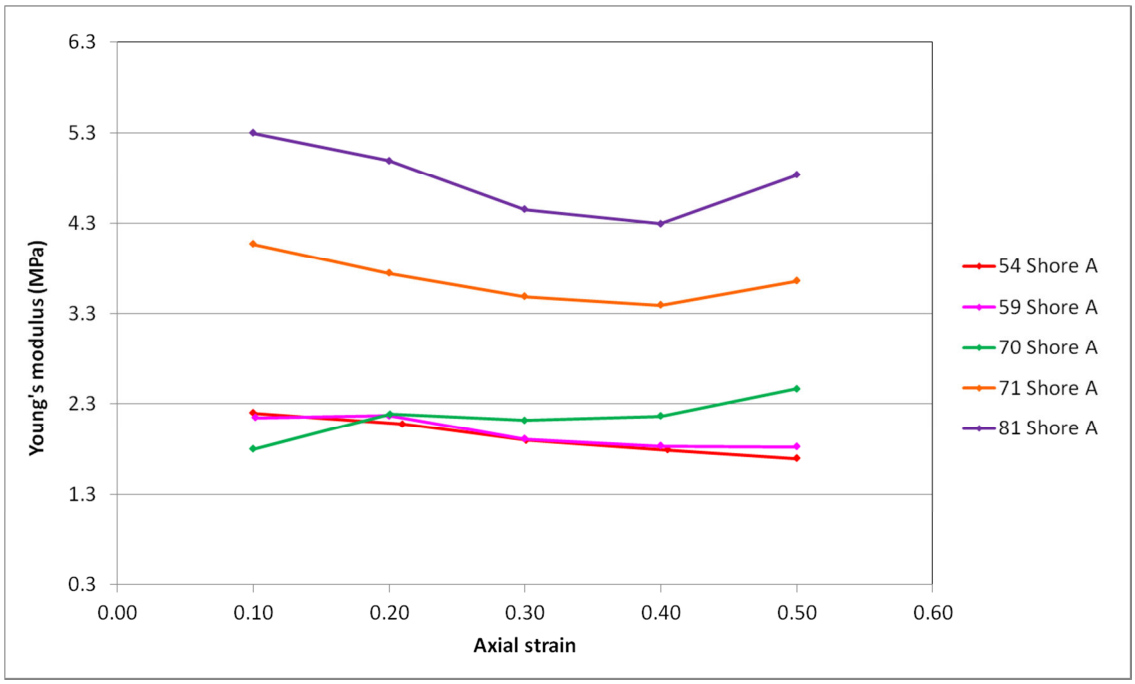

Figure 6.27 Young's modulus of the EPDM cord materials.

Table 6.8 Poisson's ratio and Young's modulus of the EPDM cords measured between 30% and 40% extension.

EPDM Shore A (tether)	Mean Poisson's ratio (30% - 40% strain)	Poisson's ratio ranking	Mean Young's modulus (MPa) (30% - 40% strain)	Young's modulus ranking
54 (P1-2)	0.403	1	1.84	1
59 (P1-3)	0.401	2	1.87	2
70 (P1-4)	0.383	5	2.14	3
71 (P1-5)	0.393	3	3.44	4
81 (P1-6)	0.389	4	4.37	5

The Young's modulus (E) is used to assess the contribution towards axial load carrying that is made by the hexagonal pack cores. For this calculation a 25% MBL axial tether load is assumed, i.e. 55.5 kN, applied to tethers P1-2 and P1-6. The tether strain at 55.5 kN is taken from the test data displayed in Figure 6.24. The mean original rubber cord diameter is taken from the data recorded

during the Poisson's ratio tests. The calculation is made for each tether as follows:

$$E = \frac{\sigma}{\varepsilon}$$

$where\ E = Young's\ modulus,\ \sigma = stress,\ \varepsilon = strain$

Therefore the tension force (F) within the rubber core bundle is given by:

$$F = \varepsilon \times E \times A$$

$where\ A\ is\ the\ cross\ section\ area\ of\ the\ core\ bundle$

The calculation results are given in Table 6.9.

Table 6.9 The calculation of tension load carried by the hexagonal pack core bundles.

Tether	Mean cord Ø (mm)	Section area (mm^2)	Strain at 55.5 kN	Core load (kN)	Contribution to tether load (%)
P1-2	25.13	3472	0.36	2230	4.0%
P1-6	24.81	3384	0.37	5472	9.9%

6.4.8 Hysteretic Damping

The viscoelastic and mechanical behaviour of both the hollow rope and the elastomeric core result in significant hysteresis within an extension cycle, as is evident in Figure 6.22. The hysteresis is revealed by the reduced tension during the unloading of the tethers compared to the tension during loading.

With one joule of energy being equivalent to the work done when one newton acts over a displacement of one metre, the area beneath the loading curve represents the energy input to achieve the extension. If the unload curve returns at a lower path, the area beneath it is reduced and hence the energy returned from the system is reduced. The balance of energy, that lost, is termed the hysteretic loss and is accounted for as heat generated within the system. Such hysteretic loss can be deemed to be advantageous where a

spring like response is undesirable. In such cases the hysteresis is referred to as hysteretic damping.

The 5th cycle, load vs displacement loops, from tests ETT_08 are shown in Figure 6.28 (hexagonal pack core tethers) and Figure 6.29 (articulated core tethers).

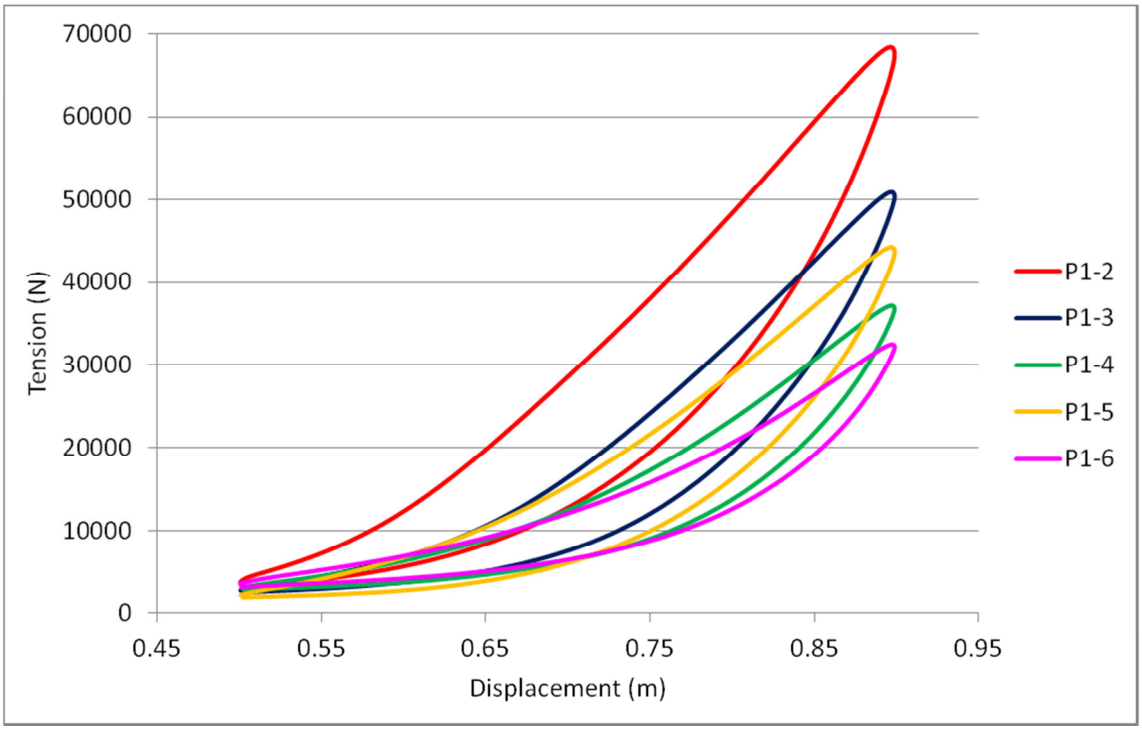

Figure 6.28 Hysteresis loops for the hexagonal pack core tethers.

Values are obtained for the hysteretic losses using DIAdem data analysis software by National Instruments. The software cannot evaluate the area within the hysteresis loop in a single step and therefore the data is split into the load-up and unload curves as shown in Figure 6.30 for tether P1-2. It is then possible to integrate each curve individually. The DIAdem integration applies the trapezoidal rule to approximate the area under the curve, bounded by the minimum and maximum extents of the displacement. The determination of the hysteretic energy loss, E, is represented by:

$$E = \int_b^a f(x)dx - \int_b^a f'(x)dx$$

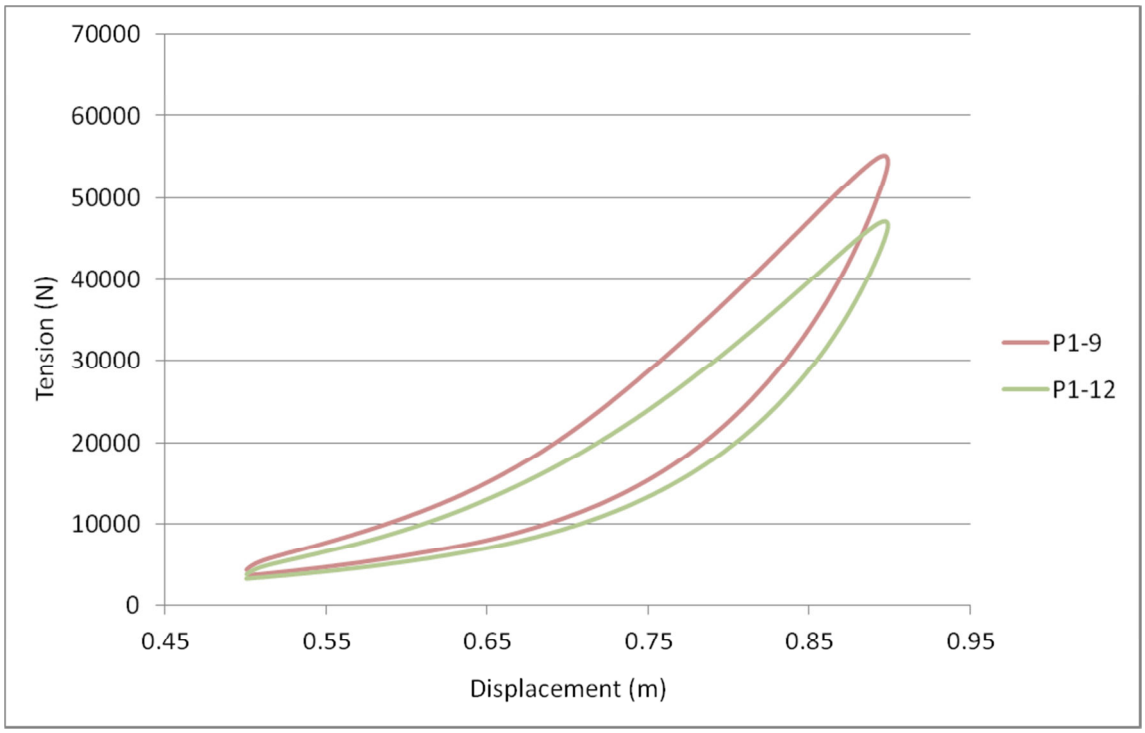

Figure 6.29 Hysteresis loops for the articulated core tethers.

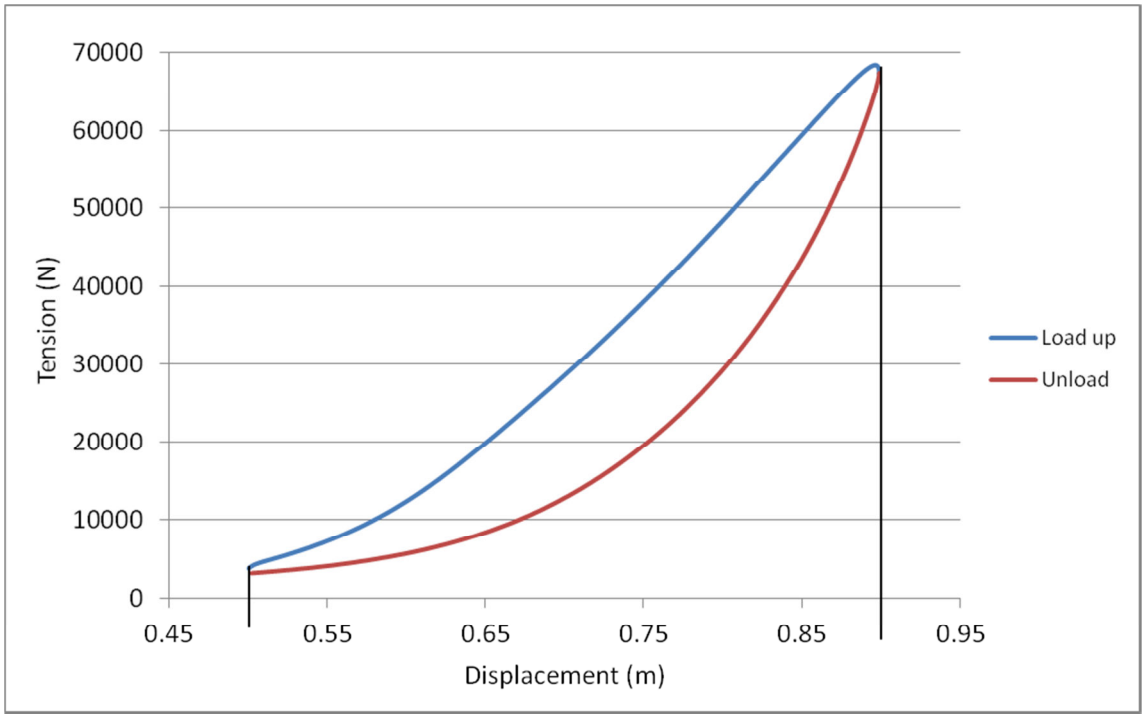

Figure 6.30 The hysteresis loop split into load up and unload components for integration (P1-2).

where $f(x)$ is the function describing the increasing load and $f'(x)$ is the function describing the decreasing load. Limits a and b are set according to the intersections of the two curves which are marked on Figure 6.30 at 0.5 m and 0.9 m.

The energy input and returned from tethers during the 5th cycle of ETT_08 is given in Table 6.10. Also provided is the difference in these values which represents the hysteretic loss during this cycle. The final column addresses the energy dissipation in terms of mean power through the cycle; the hysteretic loss is divided by 8 seconds, the period of the cycle, giving the hysteretic loss in joules per second.

Table 6.10 Hysteretic losses during ETT_08 5th cycle.

Tether id.	Energy input (J)	Energy returned (J)	Hysteretic loss (J)	Hysteretic loss (%)	Mean dissipation power (W)
P1-2	12428	7710	4718	38	590
P1-3	8182	5234	2948	36	368
P1-4	6139	3974	2165	35	271
P1-5	7339	4351	2988	41	373
P1-6	5684	3762	1922	34	240
P1-9	9844	6335	3509	36	439
P1-12	8321	5463	2858	34	357

Chapter 7 Modelling the Tether in Operation

This chapter presents the processes and results of a numerical study conducted to predict the potential outcomes resulting from deployment of the tether. The work utilises the SWMTF as a case study which offers real data representing loads and displacements of an appropriate scale to the P1 series prototypes. Numerical modelling is performed using Orcaflex 9.8 software by Orcina Ltd. The chapter includes descriptions of the SWMTF, the real data utilised within the modelling work and Orcaflex software.

7.1 Methodology for the Numerical Study

The study brings three elements together to predict the effect that the tether will have upon the peak mooring loads and corresponding station keeping of the SWMTF buoy, these are:

- Measured data from the SWMTF comprising wave, wind, current, mooring loads and station keeping.
- Numerical modelling and dynamic simulation of the SWMTF.
- Tether extension properties derived from the test work described in chapter 6.

The stages of the work are:

1. Measured data from the SWMTF is searched so as to identify a time period when exceptional mooring loads were recorded.
2. Numerical models of the SWMTF are configured and simulations are performed in Orcaflex. Environmental conditions within the models are set to reproduce those recorded at SWMTF. Waves are specified by measured time series data for surface elevation recorded by the ADCP.
3. Validation of the models is conducted against the real SWMTF load data.
4. The tether properties are substituted in place of the existing Nylon ropes within the models and the simulations are repeated. The axial stiffness profile loaded into the models represents tethers of an equivalent MBL to the existing Nylon ropes.
5. The reduced peak loads output by Orcaflex are adopted as the new ‘load case’ for the SWMTF allowing the tethers in the model to be substituted by tethers of a lower MBL and axial stiffness. Simulations are re-run.

6. A downward iteration of load case, stiffness and mass is performed which includes reversion to 19 mm chain and constitutes a reversal of the upward spiral discussed in 1.2.
7. A final revised mooring design is achieved and the peak loads and station keeping are compared to the original case.

7.2 The SWMTF

The SWMTF comprises a highly instrumented autonomous data buoy, three limbed catenary mooring system and a seabed mounted ADCP (acoustic Doppler current profiler). The facility is owned and operated by the University of Exeter and is provided to advance the research of mooring systems and mooring components for highly dynamic floating bodies. Figure 7.1 provides an image of the SWMTF buoy in calm conditions together with a map showing its position in Falmouth Bay, off the south coast of Cornwall.

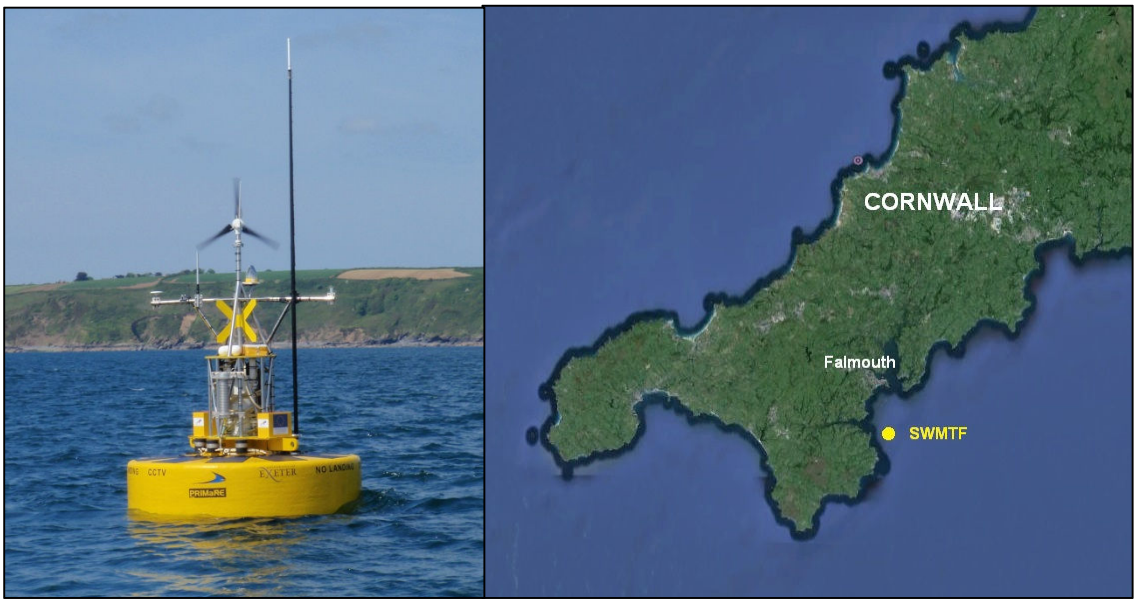

Figure 7.1 The SWMTF buoy in calm water (LH) and its position in Falmouth Bay (RH).

7.2.1 The SWMTF Mooring System

The SWMTF buoy is moored in 28 metres water depth (chart datum) with approximately 2 metres slope across the 100 metre moorings footprint. The tidal height range at the site is 5.9 metres and the seabed is predominantly fine sand having a particle size that borders on that of mud. Anchoring is by means of three drag embedment anchors each weighing 1.0 – 1.1 tonnes in air.

Figure 7.2 is a plan view diagram of the SWMTF mooring spread and the ADCP position.

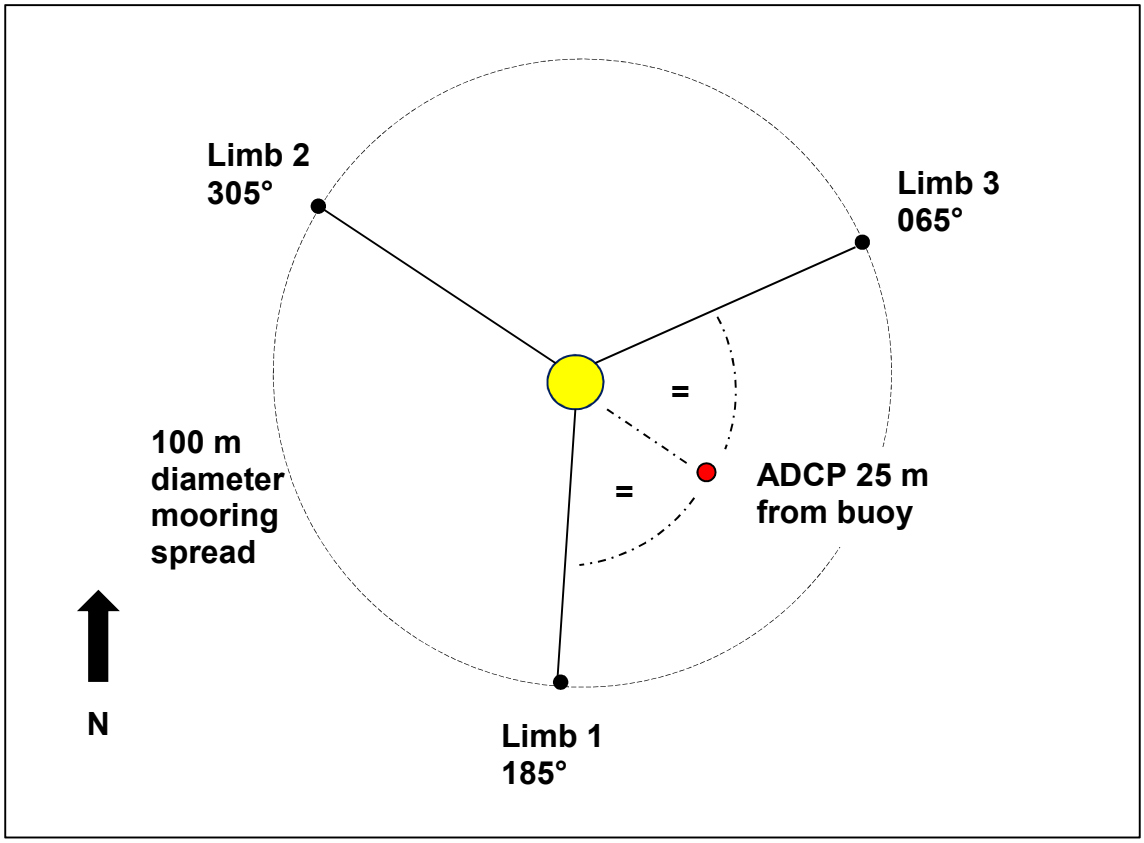

Figure 7.2 Plan view diagram of the SWMTF mooring spread and ADCP position.

The composition of the mooring limbs is occasionally changed in accordance with the requirements of particular research projects. However, the system of relevance here is the original mooring limb design which is described from the buoy down in Table 7.1.

Table 7.1 The component parts and effective length of the mooring limbs.

Item no.	Description	Effective length (m)
1	Pitch, roll and yaw swivel arm	0.3
2	Fed. spec. D shackle, 9.5 tonne	0.09
3	Bespoke axial load cell	0.257
4	Fed. spec. D shackle, 9.5 tonne	0.09
5	10 tonne axial swivel	0.275
6	Fed. spec. D shackle, 9.5 tonne	0.09

7	Fed. spec. D shackle, 25 tonne	0.149
8	44mm Nylon Bridon Superline rope	20.0
9	Fed. spec. D shackle, 25 tonne	0.149
10	Fed. spec. D shackle, 9.5 tonne	0.09
11	10 tonne axial swivel	0.275
12	Fed. spec. D shackle, 9.5 tonne	0.09
13	DN 24 open link chain	36.0
14	Fed. spec. D shackle, 9.5 tonne	0.09
15	DN 32 stud link chain, forerunner assembly	5.0
16	1.0 / 1.1 tonne drag embedment anchor	n/a
Total effective length		62.945

The mooring system described above results from the iterative design process discussed in 1.2. The process returned a peak load case of 69 kN to which a FOS of 3 was applied to components in the 'as new' condition. For steel components the FOS was applied to the yield strength rather than the ultimate tensile strength. The FOS of 3 reflects the uncertainties inherent within the derivation of the load case as well as material and component variations. The uncertainties include those of wave climate modelling, dynamic modelling and anchor positioning. The Nylon rope was further safeguarded to account for strength loss due to the eye splices, water absorption, general degradation and accidental damage.

7.2.2 The SWMTF Instrumentation and SCADA Unit

The data recorded at the SWMTF falls into three categories:

- Environment - wave, wind, current
- Dynamics – pitch, roll, yaw, surge, sway, heave, position, heading
- Mooring loads – vector, axial magnitude

Wave and current data is acquired via the seabed mounted ADCP, the remaining data is acquired by the buoy's on-board SCADA (system control and data acquisition) system. The two data acquisition systems are independently set to UTC, the buoy's timing being set by the GPS time stamp and the ADCP being set to UTC via an on-line atomic clock during instrument set up.

Table 7.2 summarises the instrumentation, measurement frequency and sensor location for the primary SWMTF data.

Table 7.2 A summary of the primary SWMTF instrumentation.

Parameter(s)	Frequency	Sensor	Location
Wave conditions	2 Hz	RDI Workhorse Sentinel 600 kHz ADCP	Seabed
Water current	2 Hz	RDI Workhorse Sentinel 600 kHz ADCP	Seabed
Wind conditions	4 Hz	Gill Instruments Windsonic ultrasonic anemometer	Buoy superstructure
Kinematics	20 Hz	Systron Donner Inertial, MotionPak, inertial sensor	Buoy SCADA module
Position	10 Hz	Trimble 57001-51-46 DGPS RTK rover station	Buoy SCADA module
Heading	20 Hz	Tilt compensated flux-gate compass	Buoy SCADA module
Mooring load vectors	20 Hz	Bespoke tri-axial load cells, rated to 69 kN	Underside of buoy
Axial mooring loads	20 Hz	Bespoke axial load cells, rated to 69 kN	Top end of mooring limb

The Workhorse Sentinel ADCP is set to record continuous wave measurement. The instrument operates in 'burst mode' for waves and to achieve continuity it is set to burst for 17.07 minutes every 17.07 minutes, providing 2048 data points in each burst. Current measurement is made in 'ensembles', each being of 10 minutes duration, these too being triggered back to back for continuity. Current measurement is made in cells through the water column to achieve the depth profile. In this case cells are 0.5 metres in height are used to a maximum height of 38 metres above the transducer head. The raw data recovered from the ADCP after each deployment is post processed using RDI software 'WavesMon'. The post processing software offers a variety of processing options according to the data output required. For the SWMTF, the log 9 option

is used to provide wave parameters, directional / frequency spectra and surface elevation time series.

The DGPS rover station receives a dedicated error correction via 458 MHz radio from the SWMTF DGPS base station. The base station is located at the SWMTF shore station within Nare Point NCI station, 2300 metres distant from the buoy. The buoy GPS antenna is mounted on the superstructure at a distance of 1.2 metres from the vertical axis of the buoy. In this mode of operation the manufacturers claim position accuracy (of the antenna) to within 0.1 m.

The SCADA unit is housed in a bespoke sealed vessel manufactured from acetal polymer and designed to withstand submersion in water to 10m. The system is based around the National Instruments Labview platform and utilises a Compact Rio embedded computer. Data is written to a 32 GB solid state hard drive in 10 minute zip files. Each zip file contains 7 data files which divide the data into groups according to frequency, format etc. The data is transmitted to the shore station via a dedicated 5.4 GHz Wi-Fi bridge or can be retrieved by Wi-Fi access within 200 metres using a laptop computer or a hard wire connection to the SCADA module. The SCADA housing is nested into the central framework of the superstructure providing a high level of mechanical protection.

7.2.3 The SWMTF Buoy

The SWMTF buoy is constructed around a galvanised, welded steel column assembly to which a PU foam collar, stainless steel superstructure and galvanised steel ballast is added. The steel column assembly is of S355 structural steel having a yield strength of not less than 355 MPa. The steel tube that provides the main structure of the column assembly has an outside diameter of 355 mm and wall section of 16 mm. Figure 7.3 shows an isometric drawing view of the column assembly. The column assembly weighs 804 kg and steel ballast totalling 684 kg is bolted in place above the bottom plate.

The mooring limb connections to the floating structure are made via the tri-axial load cells. These are bolted to the underside of the bottom plate on a PCD (pitch circle diameter) of 700 mm.

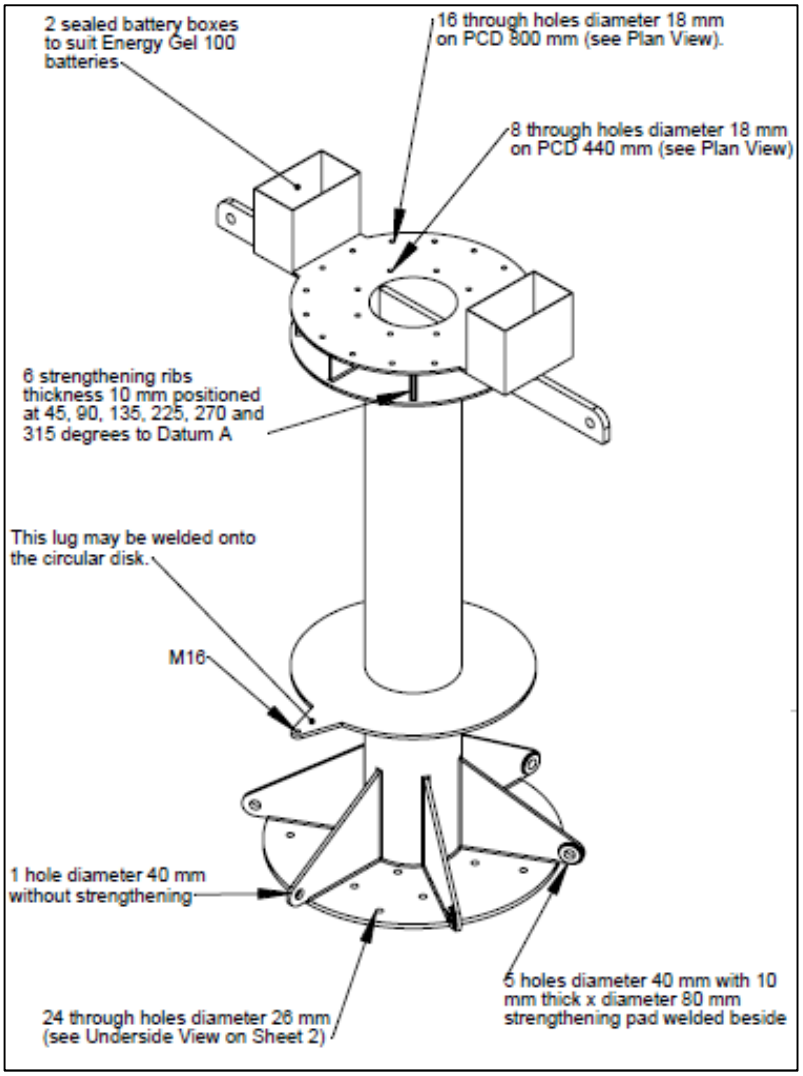

Figure 7.3 The welded steel column assembly that provides the SWMTF buoy structure.

The polyurethane float is trapped between the upper flange plate and the lower clamp plate of the column assembly during manufacture. The float has an outside diameter of 2.9 metres and has 1.0 metre of cylindrical length plus tapers at both ends. Figure 7.4 shows the outline dimensions together with the design draft of 1908 mm when the buoy is subjected to mooring pre-tension at mid tide.

The mass properties of the buoy are given in Table 7.3.

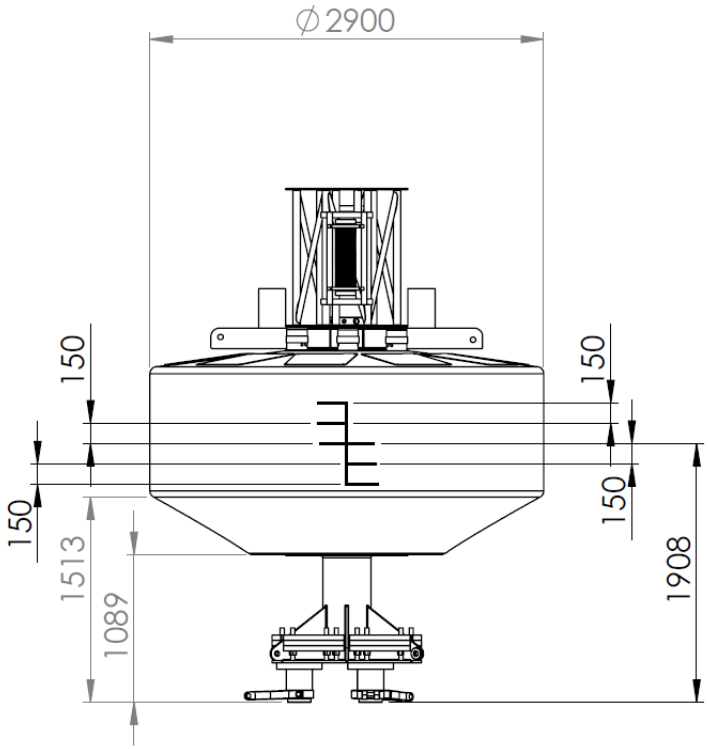

Figure 7.4 Outline dimensions of the float including the buoy draft at mid tide (upper structure omitted).

Table 7.3 Mass properties of the SWMTF buoy

Mass property	Value	Unit
Weight in air	3243	kg
Centre of gravity (below mean sea level)	499	mm
Moment of inertia (pitch / roll)	4250	kg m^2
Moment of inertia (yaw)	1179	kg m^2

7.3 Measured Data from the SWMTF

Referring back to 1.3 Q4, it is the peak mooring loads that are of interest in this study. The SWMTF was fully commissioned in September 2010 and the first deployment ended during September 2011. During this period, recorded mooring line loads peaked at between 50 and 55 kN on four occasions, three of these peak loads arising on limb 3 and the forth on limb 1.

Limb 3 dominates the load bearing during easterly sea conditions which provide the most ordered waves at the site. There is a long fetch of approximately 400 km from this direction and lower wind strength is required to achieve the peak mooring loads. This being the case there is less uncertainty in modelling these conditions whereas the higher energy events from the south add some problems regarding wave crest breaking and severe wind gusts. Figure 7.5 shows the SWMTF buoy in rough breaking seas during a southerly gale.

Figure 7.5 The SWMTF buoy during a southerly gale.

Harnois (2014), demonstrates a drift in the limb 3 axial load cell output commencing late in 2010. By selecting the earliest peak event the effect of this drift is avoided. The earliest of the three peak load events for limb 3, occurring at 09.32 on 9th October 2010, is therefore selected for the modelling.

7.3.1 Wave Data

Whereas the wave parameters and spectra are derived from all four ADCP beams, the time series for surface elevation is given individually for each beam. The beams of the Workhorse Sentinel ADCP are divergent from the vertical axis by 20°. In the mean water depth during the event of interest (31m) this gives each beam a horizontal displacement from the instrument of 11.3 metres at the mean water surface. Therefore with the ADCP being 25 metres from the nominal buoy position, the elevation data has a horizontal offset to the buoy, of between 13.7 (25 – 11.3) and 36.3 (25 + 11.3) metres +/- the buoy excursion. Assuming a maximum excursion for the buoy of 6 metres and an easterly sea,

the maximum offsets between any of the beams and the buoy during the event of interest are 38 metres aligned with the wave direction and 32 metres along the crest, as shown in Figure 7.6.

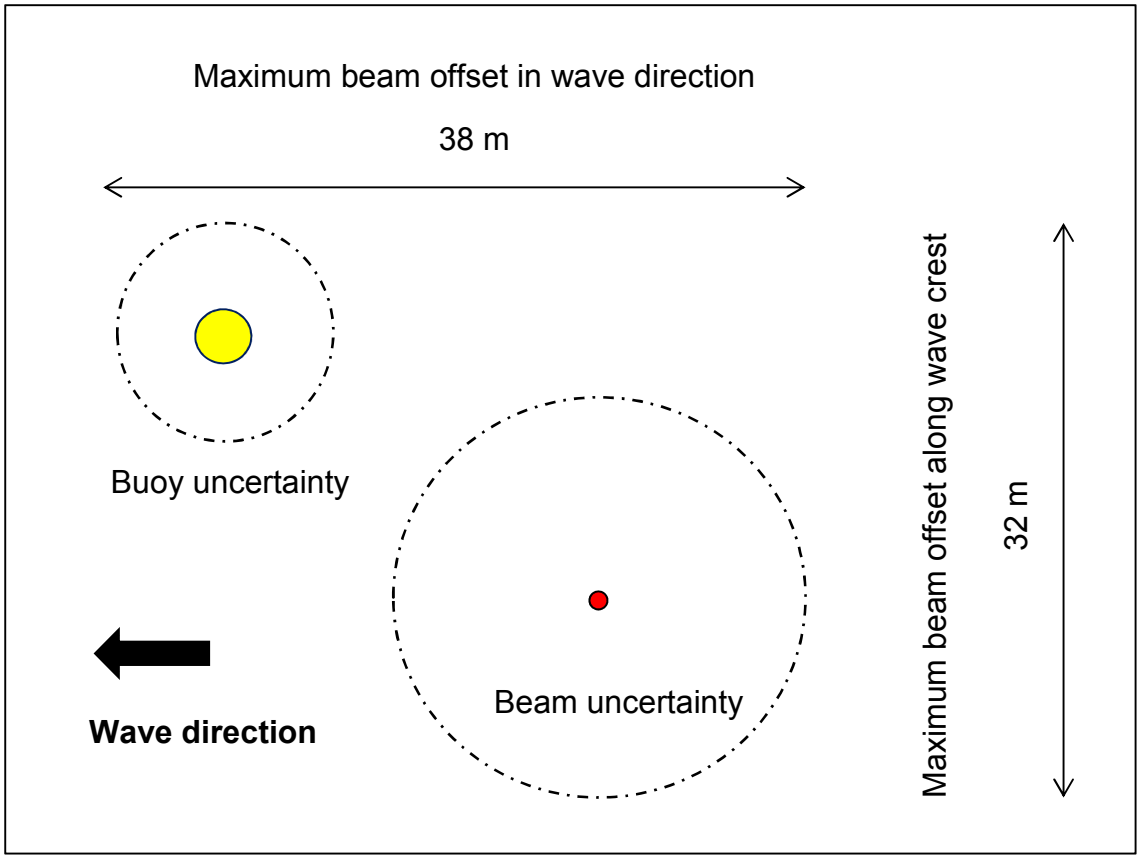

Figure 7.6 The maximum offsets between an ADCP beam and the instantaneous buoy position

Figure 7.7 shows the directional spectrum output by WavesMon for the wave burst of interest. This plot displays a distinctly unimodal sea, that is a sea with one strongly dominant wave direction.

The non-directional wave parameters output by WaveView for the 17.07 minute burst are given in Table 7.4.

Table 7.4 Non-directional wave parameters 09.18 – 09.35 09/10/2010

Parameter	Value
H_s (significant wave height)	2.51 m
T_p (peak wave period)	6.70 s
H_{max} (maximum wave height)	4.4 m

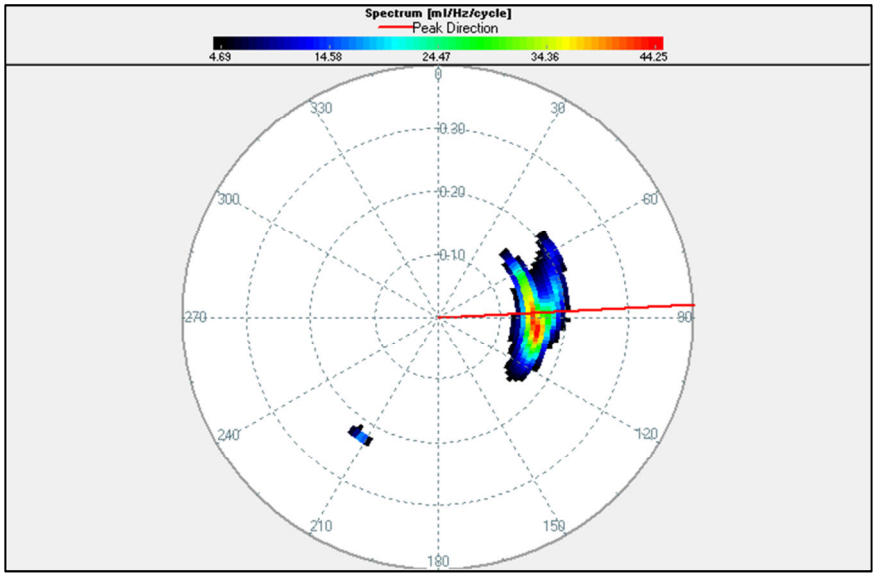

Figure 7.7 Directional spectrum output from WaveView for the 17.07 minute peak load wave burst.

In order that time series surface elevation data can be used within Orcaflex, it is necessary to identify a sub-set of the full 17.07 minute wave burst data. A time window defined by two relative lulls in wave energy is identified so that the impact of the ADCP offset from the buoy is minimised. The wavelength corresponding to T_P for this data is 40 metres and therefore the maximum offset described in Figure 7.6 equates to around 6.5 seconds. A time series data set of 240 seconds duration that includes the peak event and commences and completes with a 20 second relative lull is selected. Figure 7.8 shows plots of surface elevation (metres) against time (seconds) for the 4 beams during the selected time window.

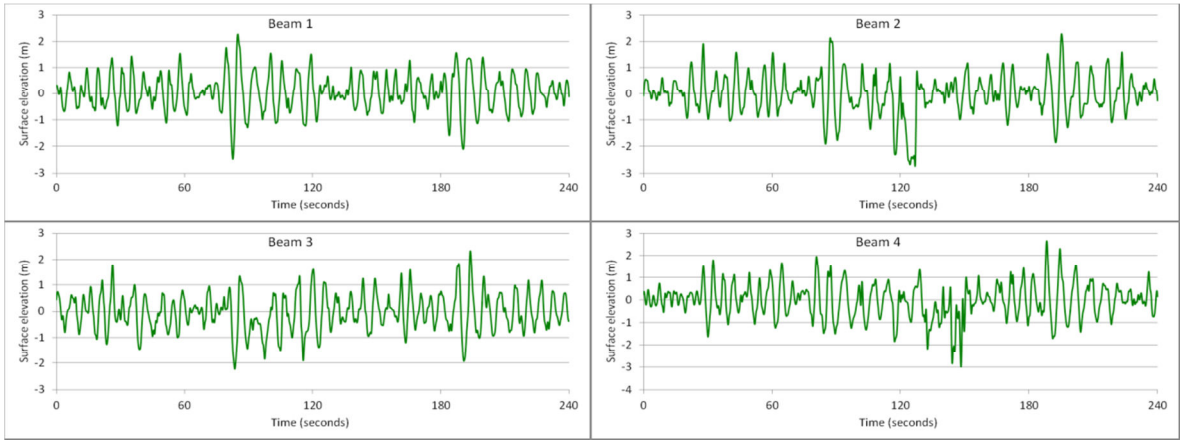

Figure 7.8 Time series plots (s) of surface elevation (m) for beam 1 (top left), beam 2 (top right), beam 3 (bottom left) and beam 4 (bottom right) – given for comparison.

7.3.2 Mooring Line Tension and Buoy Excursion

The corresponding 240 seconds of time series data is identified within the buoy data. Figure 7.9 shows the peak load of 55 kN on limb 3 and the peak excursion towards the west of 6 metres both occurring at T = 188 seconds within this isolated data.

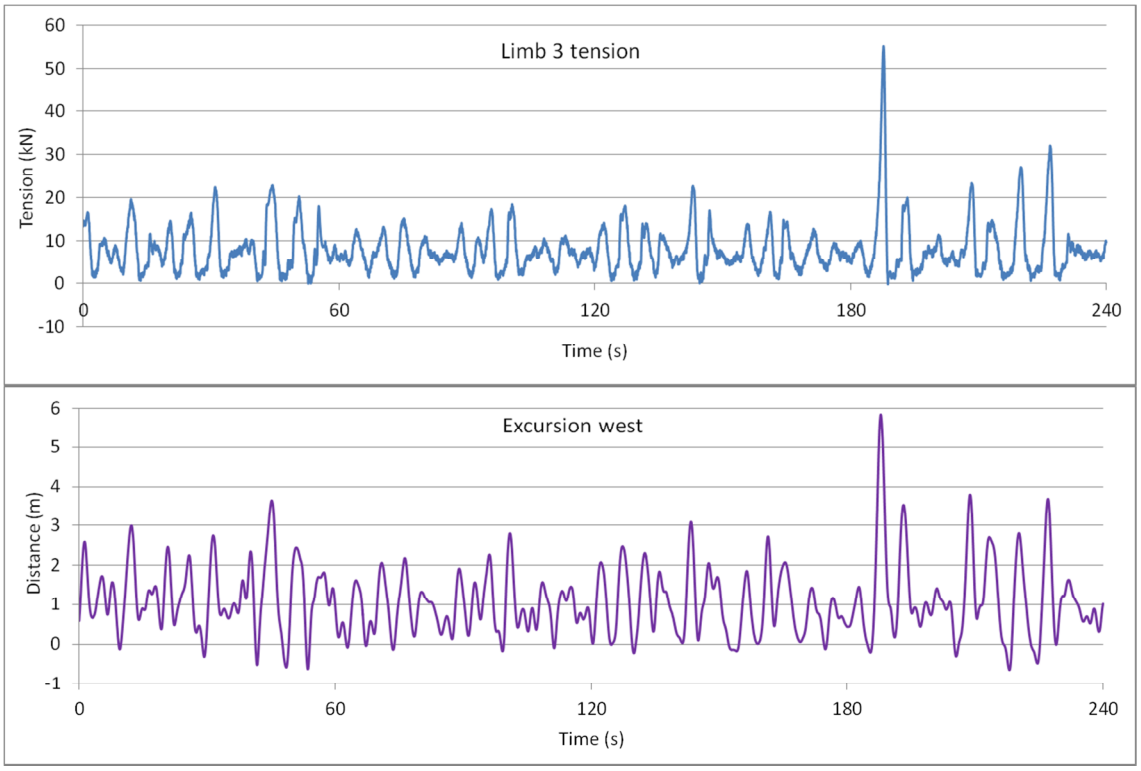

Figure 7.9 Limb 3 tension (upper) and buoy excursion to the west (lower) time series plots for the 240 second data.

Observing the two time series shown in Figure 7.9, it is evident that there is a strong interdependency between limb 3 tension and excursion to the west, which is an intuitive result.

7.3.3 Wind Data

The wind parameters recorded by the buoy during the corresponding time window are given in Table 7.5.

Table 7.5 Wind parameters recorded by the SWMTF buoy during the time window under consideration.

Parameter	Value
Mean wind speed	12.4 m/s
Maximum wind speed	19.5 m/s
Minimum wind speed	6.5 m/s
Mean direction (emanating from)	089°

7.3.4 Current Data

Current profile data is plotted from the 10 minute ensemble commencing 09.30 09/10/2010 and is given in Figure 7.10.

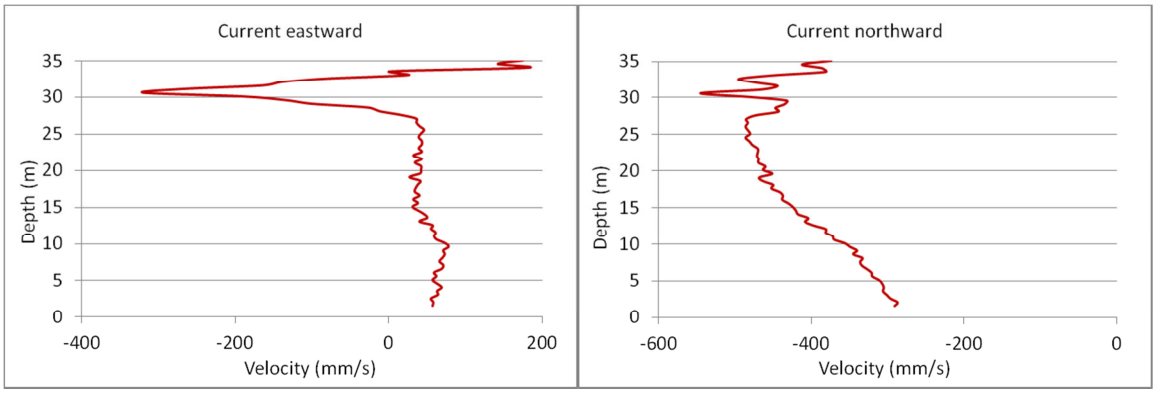

Figure 7.10 Current profiles eastward (LH) and northward (RH) during the peak event.

The mean water level depth at this time is 31 metres. It is clear that the tidal current at the surface is running in a southerly direction at approximately 0.5 m/s with a velocity component to the east of approximately 0.05 m/s. This resolves to a tidal current at the surface of 0.5 m/s (1 dp) flowing towards a bearing of 174°.

At the surface there is considerable current attributable to the wind and wave action that is superimposed on the tidal current. The ADCP bins within the wave elevation zone (31m +/- wave amplitude) return a maximum mean current of 0.32 m/s to the west and 0.55 m/s to the south. The resultant of these components is a surface current of 0.64 m/s towards a bearing of 210°.

7.4 Orcaflex

Orcaflex is a commercial marine dynamics software package used to conduct static and dynamic analysis of many different types of offshore systems. It is a 3D, non-linear, finite element program operating in the time domain and being capable of dealing with large magnitude deflections (Orcina, 2014). Orcaflex can model the coupled behaviour of a surface vessel and its mooring system. In what is often referred to as a discretised cable model, Orcaflex employs an idealised system of mass components (nodes) and visco-elastic elements (segments) to represent cables and mooring lines (Masciola et al., 2011).

Some of the important options selected within Orcaflex for this work are described in the following sections.

7.4.1 6D Buoys

Floating bodies fall into two main categories in Orcaflex; vessels and buoys. A 6D buoy represents the fullest modelling available in terms of imparted loads and kinematics. They have mass, moments of inertia, added mass, damping and drag. 6D buoys are subject to wave slam forces, connection loads, fluid flow effects, applied loads and contact forces (Orcina, 2014).

Three subsets exist for 6D buoys; these are lumped buoys, spar buoys and towed fish. Spar buoys are intended for modelling axi-symetric buoys having a vertical axis. Hydrodynamic loads are calculated according to Morison's equation implying that the buoy in question is small in relation to the wavelength (Orcina, 2014).

7.4.2 Waves

Orcaflex allows one or more wave trains to be defined. Orcina (2014) suggest that a single wave train is normally sufficient in all but complex cases such as a crossing sea.

Each wave train can be specified by a regular wave theory such as Airy, a particular type of spectrum for random waves such as JONSWAP, or by a time history input file (Orcina, 2014).

When a time history input file is used to define the wave environment, Orcaflex performs a FFT (fast Fourier transform) on the time series for surface elevation.

The programme then assigns a single Airy wave to each of the frequency components that result from the transform. These Airy waves are then used in combination to recreate the waveform described by the input file (Orcina, 2014).

Importantly with this method, the input time series must be appropriate for the FFT. "The FFT requires the number of samples it uses from the time history file, N say, to be a power of 2, and it produces N/2 components. Because of this, the time history file must contain a sequence of N samples that covers the period of the simulation, where N is a power of 2 that is at least twice the specified minimum number of components" (Orcina, 2014). To achieve this, a time series that is greater in duration than the simulation is input to Orcaflex and the wave origin and duration is set to define the time window of the simulation. Orcaflex will then use a longer duration of the time series for the FFT.

7.4.3 Lines

Orcaflex provides for three main types of line:

- 'Homogenous pipe' which is used to represent pipes where the properties can be defined by material properties such as Young's modulus.
- 'Equivalent line' which represents multiple pipes either arranged concentrically or adjacently.
- 'General' which is used in all other cases. In this category the functional properties of the line such as axial stiffness, bending stiffness and linear density are input directly. This category of line is therefore appropriate for ropes, chains, umbilicals etc.

Geometry and mass can be defined by the user from which the programme will derive buoyancy. Bending stiffness and torsional stiffness can be defined or deemed to be negligible. Axial stiffness can be defined as a profile of tension (kN) against extension (%). Where appropriate generic values for these parameters can be used via Orcaflex's line wizard (Orcina, 2014).

7.4.4 Integration Methods

Orcaflex provides two integration methods, explicit and implicit. The explicit integration is described as robust and reliably accurate but computation time can be much higher than implicit integration (Orcina, 2014). By contrast the

implicit integration is much quicker but the accuracy of results can be sensitive to the time step selected for use. Orcina recommend that results from implicit integration simulations are compared to results from explicit simulations if possible (Orcina, 2014).

7.5 The SWMTF Model and Model Validation

Several Orcaflex models of the SWMTF have been created since 2008 including those created by this author during the design stages. The most recent SWMTF model is constructed and reported by Herduin (2015) and shows good validation against real SWMTF data. This Orcaflex model is described in the following section and is utilised in specifically modified formats throughout the simulation studies.

7.5.1 The SWMTF Model

The Model uses a 6D spar buoy to represent the SWMTF buoy. The mass properties are set as described in Table 7.3. The modelled buoy has five cylinders to approximate the geometry of the SWMTF buoy as shown in Figure 7.11 and detailed in Table 7.6 (Herduin, 2015).

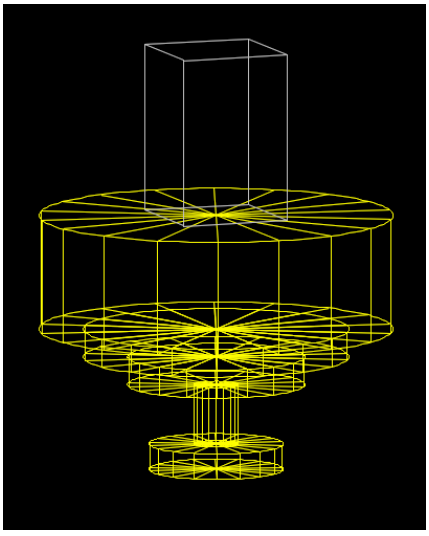

Figure 7.11 The modelled SWMTF buoy

Table 7.6 Modelled buoy dimensions (Herduin, 2015)

Cylinder no.	Length (m)	Diameter (m)
1 (upper)	0.940	2.900
2	0.230	2.175
3	0.230	1.450
4	0.490	0.360
5 (lower)	0.210	1.100

The buoy model has a wing feature which is represented by the square prism above the buoy cylinders. The wing which is specified as 1.37 m high x 0.9 m wide, adds wind forces to the buoy model according to the wind environment specified.

Herduin (2015) assigns hydrodynamic properties to the modelled buoy as shown in Table 7.7.

Table 7.7 Hydrodynamic coefficients assigned to the modelled buoy (Herduin, 2015).

Property	Condition	Formula	Coefficient	Basis / reference
Drag forces	Normal area (m^2)	Ø x L	1.0	Irregular wave, KC>10 (Sumer and Fredsoe, 2006).
	Axial area (m^2)	(π x $Ø^2$)/4	1.0	
Drag moments	Normal area moments (m^5)	(L x $Ø^4$)/32	1.0	(Orcina, 2014)
	Axial area moments (m^5)	$Ø^5$/60	1.0	
Added mass	Normal	-	(Ca) 1.0	(Sumer and Fredsoe, 2006)
	Axial	-	(Ca) 0.64	
Inertia	Normal	-	(Cm) 2.0	Cm = Ca + 1 (Orcina, 2014)
	Axial	-	(Cm) 1.64	

The three mooring limbs are represented as lines with the structure being as described in Table 7.1. The 44 mm diameter Nylon Bridon Superline rope is assigned axial stiffness properties by importing a digitised stiffness curve (Bridon, 2007) for the rope with 466 kN MBL in the worked condition. Figure 7.12 shows the Bridon curve and the digitised version imported to the model. The rope's geometry and weight in water are known from Bridon (2007) and are entered accordingly. The Orcaflex Line Wizard is used to enter properties for the chains.

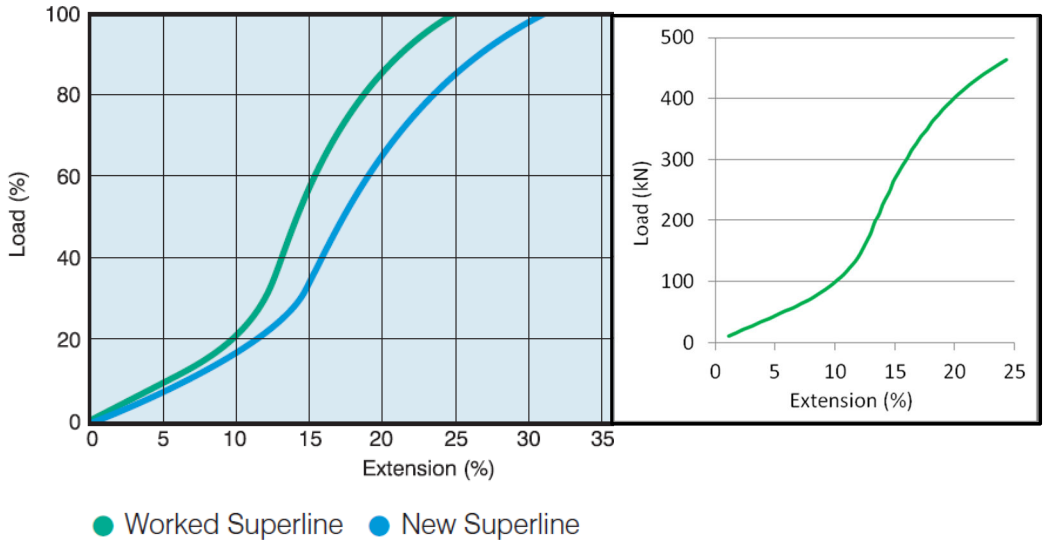

Figure 7.12 The Bridon stiffness curves for Nylon Superline rope (LH) (Bridon, 2007) and the digitised version imported to the model (RH).

7.5.2 Model Validation

Herduin (2015) performed three simulations to validate the model against real SWMTF data. These were conducted in three simulated environments corresponding to real data gathered at SWMTF. These simulations are summarised in Table 7.8.

Table 7.8 Environmental inputs and peak load results for the validation simulations (Herduin, 2015).

Parameter	Simulation A	Simulation B	Simulation C
Significant wave height H_s (m)	2.47	2.39	2.62
Period T_P (s)	5.90	6.90	7.70
Mean water depth (m)	28.5	31.0	31.9
Wave direction (bearing from)	122°	177°	172°
Current direction (as above)	196°	225°	030°
Current velocity (m/s)	0.30	0.15	0.15
Peak load – real data (kN)	37	20	60
Peak load – simulation (kN)	30	23	60

Further validations and amendments to the model are conducted by this author and are described hereafter. Validation is performed using real SWMTF data from 9th October 2010 as described in 7.3. Four simulations, beam 1, beam 2, beam 3 and beam 4 are prepared according to the following:

- Explicit integration (default time step settings)
- 240 second duration with 10 second build up
- Time history input of surface elevation for beam 1, 2, 3, or 4
- Wave direction 090° (emanating from)
- Wind velocity 12.4 m/s, bearing 089° (emanating from)
- Current velocity 0.5 m/s, bearing 174° (direction of flow)
- Water depth 31 m

Simulations covering 240 seconds are sufficient in duration to replicate the dynamics of the SWMTF buoy during an energetic wave set, whilst not being too time consuming in processing. The time series surface elevation data input to the simulation is 1200 seconds in duration with the 240 second window of interest being central within this series. Orcaflex conducts the FFT on the specified 240 second window spanning enough data points equally on both sides of the window to achieve the FFT as described in 7.4.2. Figure 7.13 shows the full 1200 second time series for beam 1 with the 240 second simulation window identified in the middle.

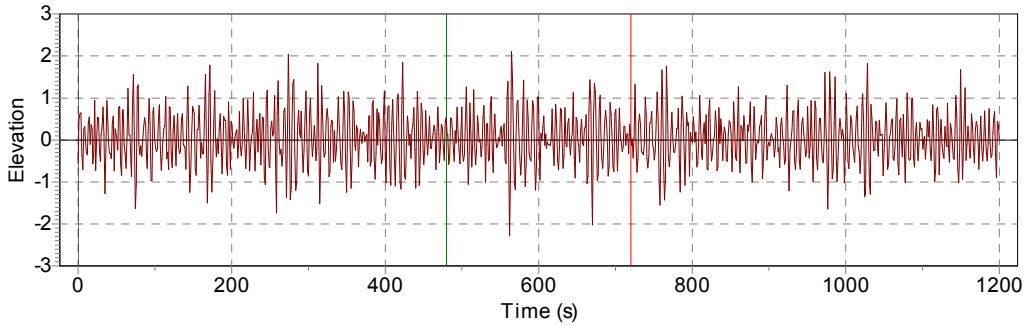

Figure 7.13 The full 1200 second surface elevation time series from beam 1 with the 240 second simulation period identified.

Orcaflex allows the frequency spectrum generated by the FFT to be viewed as a spectral density plot. The spectral density plots for beams 1 – 4 are given in Figure 7.14. It is apparent that the plots for beams 2, 3 and 4 display low frequency signals that may include erroneous data.

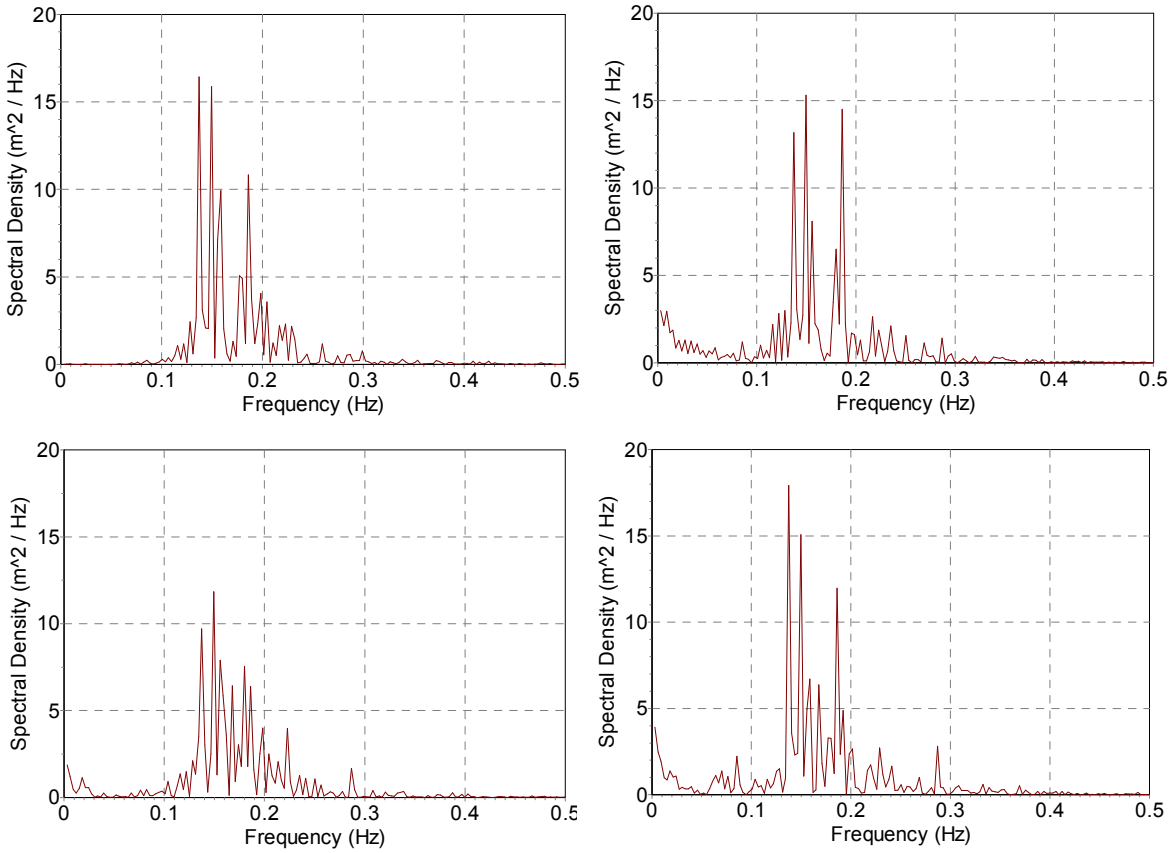

Figure 7.14 Spectral density plots for each ADCP beam time series computed by Orcaflex. Beam 1 top left, beam 2 top right, beam 3 bottom left, beam 4 bottom right.

The simulation outputs for tension in limb 3 are compared to the real SWMTF data. The time series for limb 3 tension given in Figure 7.9 is reproduced in each of the four plots given in Figure 7.15. Each plot has a simulated tension time series overlaid for comparison.

The beam 1 results display the best agreement between real and modelled tension. The real peak load of 55 kN that occurs at T = 188 seconds is reproduced closely by the model with a peak of 48 kN at T = 187 seconds.

The beam 4 simulation results display the best agreement in terms of tension magnitude with a peak of 55 kN but this occurs at T = 82 seconds. The time offset of nearly 100 seconds is too much to be accounted for by the maximum beam position offset from the buoy described in Figure 7.6.

The results of these validation simulations are summarised in Table 7.9.

Figure 7.15 Simulation outcomes for limb 3 tension, beams 1 – 4, overlaid onto the real data for comparison.

Table 7.9 Summary of the validation simulations using time history wave data.

Source	Limb 3 peak tension (kN)	Peak tension at T = (s)	Mean tension (kN)	Standard deviation
Real data	55	188	7.8	5.6
Beam 1 simulation	48	187	7.0	7.2
Beam 2 simulation	34	30	5.4	4.6
Beam 3 simulation	39	115	5.9	5.1
Beam 4 simulation	55	82	6.5	6.9

The good agreement of the beam 1 simulation outputs with the real data in terms of peak load magnitude, peak load occurrence and mean load, dictates that beam 1 time series data is used in all subsequent simulations.

7.6 The Tether Performance Simulations

The tether performance simulation studies have three strings of simulations and design iterations as described in 7.1, these are:

1. Explicit integration simulations mirroring the simulations presented in 7.5.2.
2. Implicit integration simulations whereby the only change from (1) is the integration type.
3. Implicit integration simulations with an increased surface current as described in 7.3.4.

The design iterations in each of the three simulation series are conditional upon the simulation outcomes obtained within that series. The stages and outcomes of each series leading towards and then past the optimal condition (lowest peak load) are given in table form for each series (Tables 7.10, 7.12 and 7.14). These results are also shown graphically in Figure 7.24 with the optimal solutions and the advantage gained being summarised in Table 7.15.

7.6.1 Explicit Integration Simulations

The explicit simulation using the beam 1 time series is repeated with the P1-6 tether substituted for the 20 metre Nylon Superline rope on all three limbs. The axial stiffness curve presented for P1-6 in Figure 6.25 (81 Shore A) is assigned

a MBL of 466 kN matching that of the Superline rope. The geometry and weight are taken from an approximate guide to tether scaling that is based on Table 5.1 and is given as Appendix G.

Figure 7.16 shows the simulated time series for tension on limb 3 for the Superline rope together with that of the P1-6 tether. The tether time series shows a peak tension of 15 kN occurring at T = 188 seconds. This corresponds to a 69% reduction to the magnitude of the peak load from the original value of 48 kN. The mean load during the simulation is 5 kN compared to 7 kN in the Superline rope simulation.

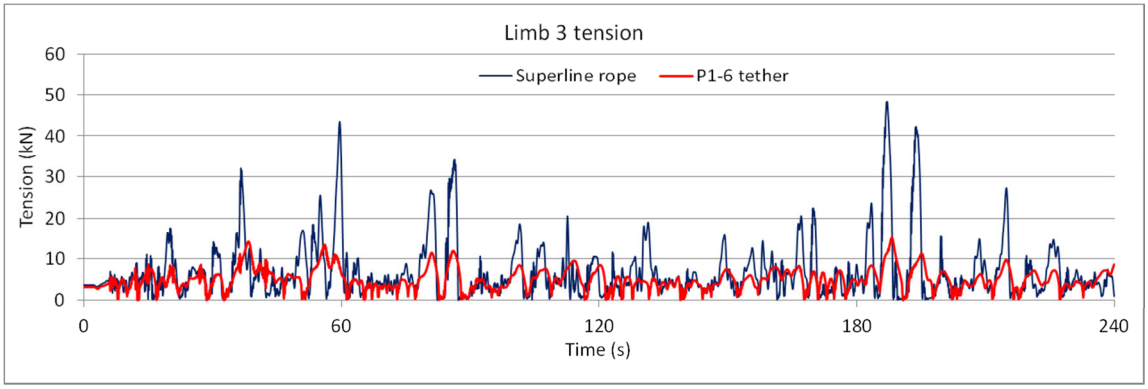

Figure 7.16 Simulated limb 3 tension for Superline rope and the P1-6 tether.

The buoy excursion is expected to increase with the lower axial stiffness of the P1-6 tether. Figure 7.17 gives the magnitude of excursion for the Superline rope simulation and the P1-6 tether simulation. The buoy's excursion increases from 8.3 metres to 10.2 metres during the peak load at T = 188 seconds. The mean excursion increases from 3.5 metres to 4.2 metres.

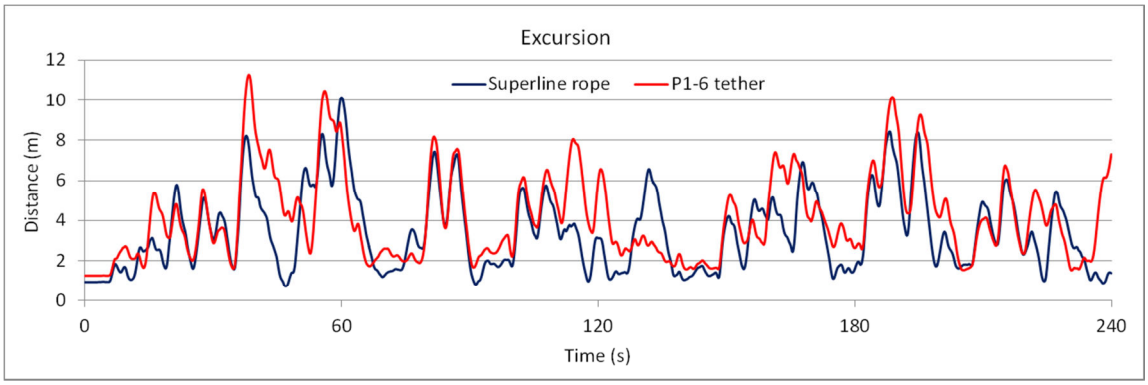

Figure 7.17 Simulated buoy excursion for Superline rope and the P1-6 tether.

7.6.1.1 Reduced MBL Tether

The reduction in peak load achieved with the P1-6 tether allows the assigned MBL of the tether to be reduced whilst maintaining the same FOS. By applying a lower MBL to the axial stiffness curve, the axial stiffness is reduced. The revised MBL is determined as follows:

$$MBL_{\ revised} = MBL \times \frac{15\ kN}{48\ kN}$$

$$MBL_{revised} = 466\ kN \times \frac{15\ kN}{48\ kN}$$

therefore

$$MBL_{revised} = 146\ kN$$

The simulation is repeated with the revised MBL applied to the tether. This results in a further reduction of the peak tension from 15 kN to 12 kN occurring at T = 187 seconds. The mean value also decreases from 5.0 kN to 3.8 kN. Figure 7.18 shows the simulated time series for tension on limb 3 for the Superline rope together with that of the P1-6 146 kN MBL tether.

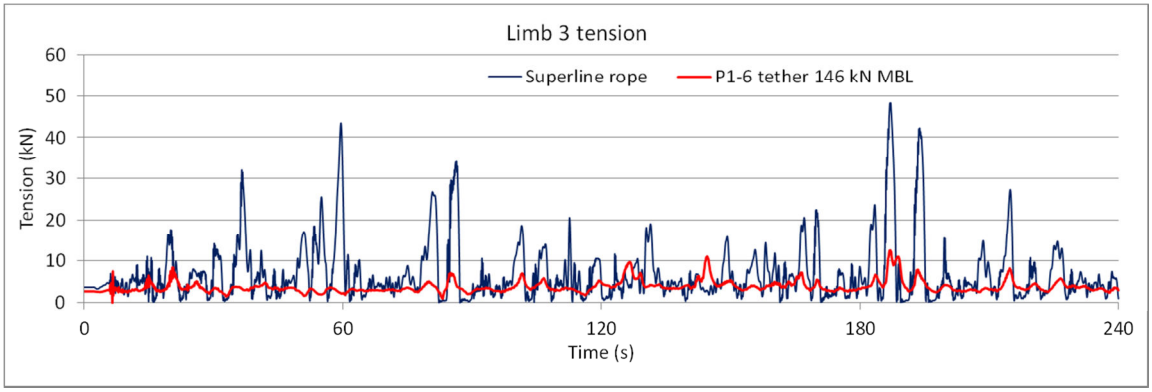

Figure 7.18 Simulated limb 3 tension for Superline rope and the P1-6 146 kN MBL tether.

The excursion associated with the peak tension increases slightly from 10.2 m to 10.8 m with the reduced stiffness tether.

7.6.1.2 Reduced Chain Mass

The reduction in peak load achieved with the P1-6 tether allows the 24 mm open link chain to be replaced with 19 mm chain without compromising the

original FOS. The properties for 19 mm open link chain are entered and the simulation is re-run.

The result of this change is an increase in peak tension rather than a further reduction. The load spike generated by the Superline rope simulation at T = 60 seconds is reproduced by the P1-6 / 19 mm chain simulation at T = 61 seconds. The simulated time series for limb 3 tension is given as Figure 7.19.

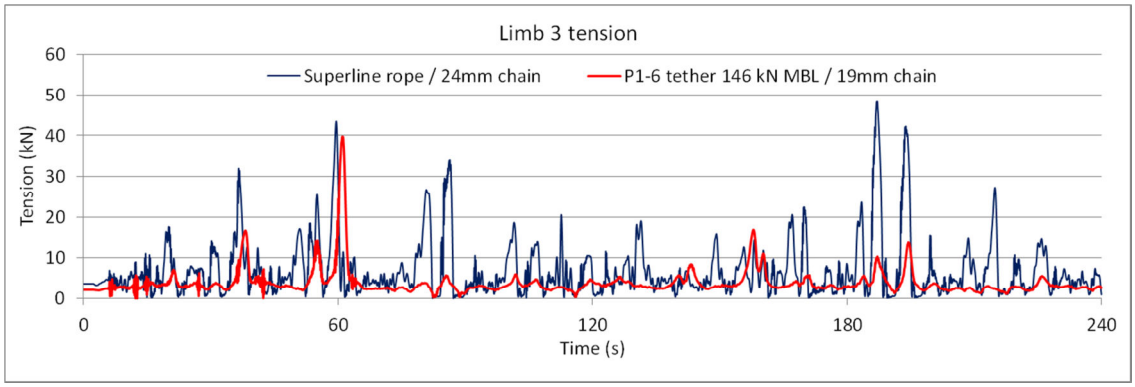

Figure 7.19 Simulated limb 3 tension for Superline rope (24mm chain) and the P1-6 146 kN MBL tether (19mm chain).

The full results of the explicit simulations of tether performance including details of the design iterations are summarised in Table 7.10.

Table 7.10 A summary of the iteration steps and simulated outcomes from the explicit integration simulations.

Iteration step		Peak tension (kN)	Mean tension (kN)	Standard deviation (kN)	Peak excursion (m)	Mean Excursion (m)	Standard deviation (m)
-	Base case Superline rope	48	7.0	7.2	10.1	3.5	2.0
0	P1-6 466 kN MBL	15	5.0	2.6	11.3	4.2	2.2
1	P1-6 146 kN MBL	13	3.8	1.5	10.8	5.2	1.6
2	P1-6 146 kN MBL 19 mm chain	40	3.9	3.4	15.4	6.0	2.2

7.6.2 Implicit Integration Simulations

This series of simulations and iterations follows the process described in 7.6.1. The integration method is implicit rather than explicit and the axial stiffness increments are changed in accordance with findings. The design iterations progress further before a negative effect is encountered.

The implicit integration time step is set to 0.05 second and the time history wave data is sampled at 0.2 second intervals. These settings are critical in achieving simulation stability for the implicit integration.

The implicit simulation for the base case, Superline rope, shows reasonable agreement with the explicit simulation in terms of tension and excursion magnitudes. Whilst generally reproducing a similar timing of peak loads and excursions, there is not an exact match between the simulations in this respect. Figure 7.20 shows the comparison of the tension time series for the two simulations of the base case and Figure 7.21 does so for the excursion. Table 7.11 summarises the comparison between outputs of the explicit and implicit simulations for the Superline rope.

The results of the implicit simulations of tether performance including details of the design iterations are given in Table 7.12.

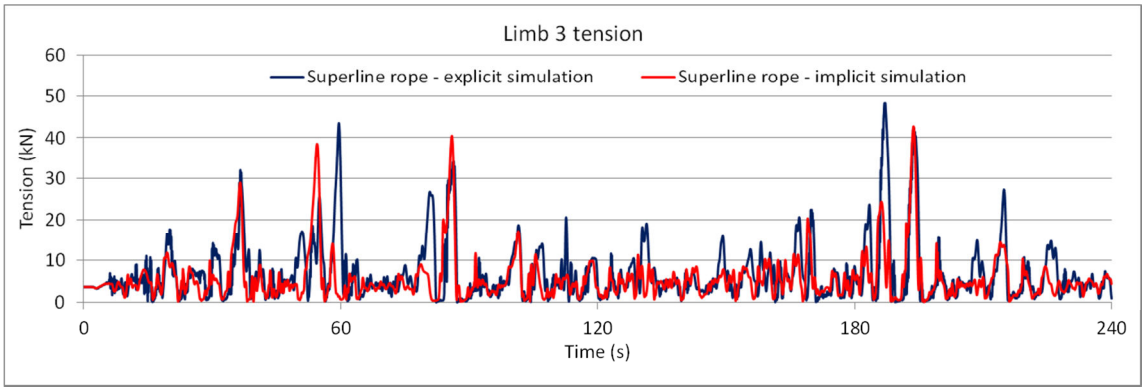

Figure 7.20 Simulated limb 3 tension for Superline rope by explicit and implicit integration simulations.

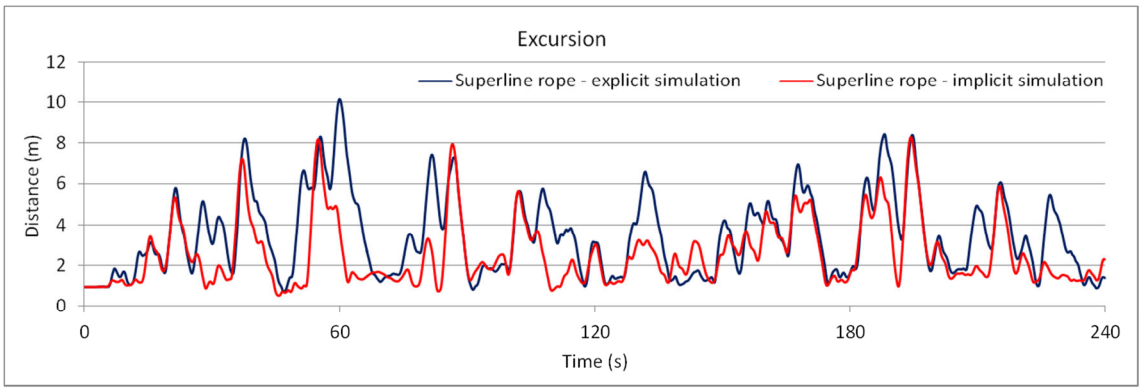

Figure 7.21 Simulated buoy excursion for Superline rope by explicit and implicit integration simulations.

Table 7.11 Simulated outcomes for comparison of explicit and implicit integration.

Simulation type	Peak tension (kN)	Mean tension (kN)	Standard deviation (kN)	Peak excursion (m)	Mean Excursion (m)	Standard deviation (m)
Superline rope explicit simulation	48	7.0	7.2	10.1	3.5	2.0
Superline rope implicit simulation	43	5.7	5.7	8.3	2.6	1.6

Table 7.12 A summary of the iteration steps and simulated outcomes from the implicit integration simulations.

Iteration step		Peak tension (kN)	Mean tension (kN)	Standard deviation (kN)	Peak excursion (m)	Mean Excursion (m)	Standard deviation (m)
-	Base case Superline rope	43	5.7	5.7	8.3	2.6	1.6
0	P1-6 466 kN MBL	19	6.0	2.3	10.3	3.5	1.8
1	P1-6 206 kN MBL	17	5.3	1.5	10.5	4.3	1.8
2	P1-6 206 kN MBL 19 mm chain	13	4.6	1.1	10.2	4.3	1.6
3	P1-6 152 kN MBL 19 mm chain	14	4.5	1.2	11.4	4.8	1.7
4	P1-6 152 kN MBL 16 mm chain	17	3.8	1.5	11.2	5.4	1.7

7.6.3 Implicit Simulations with Increased Surface Current

The base case, Superline rope, simulation in this series mirrors that of 7.6.2 other than the current velocity which is set to represent the wave and wind driven surface current described in 7.3.4.

Figure 7.22 shows that the simulated tension time series has less agreement with the real data than the previous Superline rope simulations. Whilst the load spike at T = 187 seconds is present in the output, it is of reduced magnitude. A peak tension of 48 kN is now indicated at T = 86 seconds, this spike not featuring in the real data.

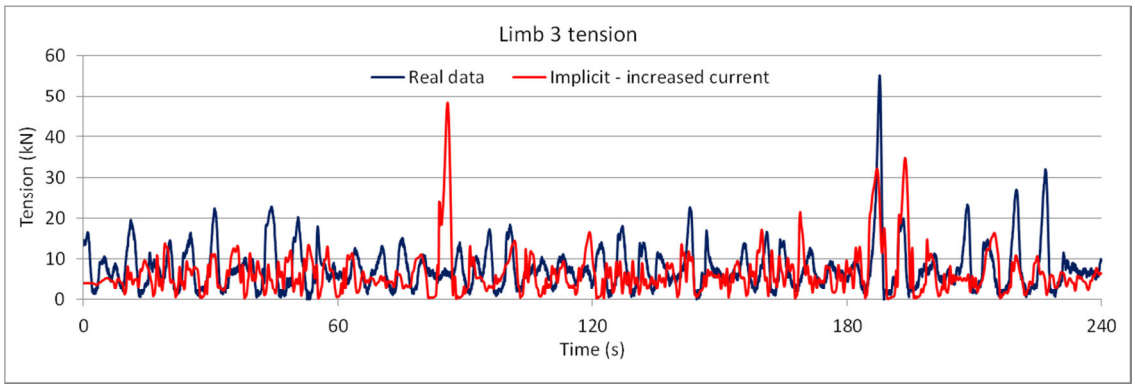

Figure 7.22 Simulated outcome for limb 3 tension with increased current, overlaid onto the real data for comparison.

Figure 7.23 shows a comparison of the simulated excursion for the base case rope from the first implicit series and that of increased current velocity. It is notable that the peak excursions do not increase in magnitude but the mean excursion does. Table 7.13 summarises the outputs of these two base case simulations for comparison.

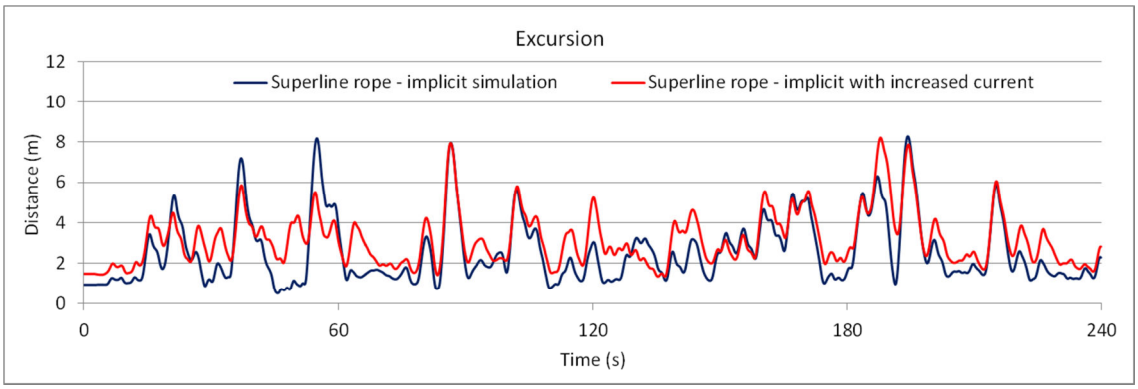

Figure 7.23 Simulated excursion time series for the first implicit simulation base case and that of increased current velocity.

Table 7.13 Simulated outcomes for comparison of the first implicit integration simulation and that of increased current velocity.

Simulation type	Peak tension (kN)	Mean tension (kN)	Standard deviation (kN)	Peak excursion (m)	Mean Excursion (m)	Standard deviation (m)
Superline rope implicit simulation	43	5.7	5.7	8.3	2.6	1.6
Superline rope implicit simulation with increased current	48	6.5	5.5	8.2	3.2	1.3

The sequence of design iterations that successfully provides incremental reductions in peak tension is different in this case. The reduction in chain mass is required before the reduction in P1-6 tether MBL. Table 7.14 summarises the iteration steps and the simulated outcomes.

Table 7.14 A summary of the iteration steps and simulated outcomes from the implicit integration simulations with increased current velocity.

Iteration step		Peak tension (kN)	Mean tension (kN)	Standard deviation (kN)	Peak excursion (m)	Mean Excursion (m)	Standard deviation (m)
-	Base case Superline rope	48	6.5	5.5	8.2	3.2	1.3
0	P1-6 466 kN MBL	23	7.2	2.4	10.5	4.8	1.6
1	P1-6 466 kN MBL 19 mm chain	22	6.3	2.3	10.8	5.1	1.5
2	P1-6 223 kN MBL 19 mm chain	22	5.8	1.8	11.6	6.1	1.4
3	P1-6 223 kN MBL 16 mm chain	31	5.4	2.6	14.0	6.8	1.5

7.6.4 Summary of Simulation Outcomes

The explicit integration simulation gives the best agreement with the real SWMTF data for limb 3 tension. This series of simulations also provides the greatest decrease in peak tension through utilising the P1-6 tether and iterating the mooring limb design. Table 7.15 summarises the outcomes from the three series of simulations and limb design iterations.

Table 7.15 Summary of the outcomes of the simulations and mooring limb design iterations.

Simulation type	Original Peak tension (kN)	Revised peak tension (kN)	Reduction of peak tension	Original peak excursion (m)	Revised peak excursion (m)	Increase of peak excursion
Explicit series	48	13	73%	10.1	10.8	7%
Implicit series	43	13	70%	8.3	10.2	23%
Implicit series 2 with increased current	48	22	54%	8.2	10.8	32%

In all three series of simulations and iterations, the peak tension decreased significantly with the introduction of the tether and the initial design iterations. In all cases the peak tension then increased with further reductions of catenary mass and axial stiffness. Figure 7.24 shows the peak tension through the iteration stages for the three series of simulations.

The reduction in peak tension is accompanied by an increase in the buoy excursion. However, the mean peak excursion increase is just 21% whilst the mean peak tension reduction is 66%.

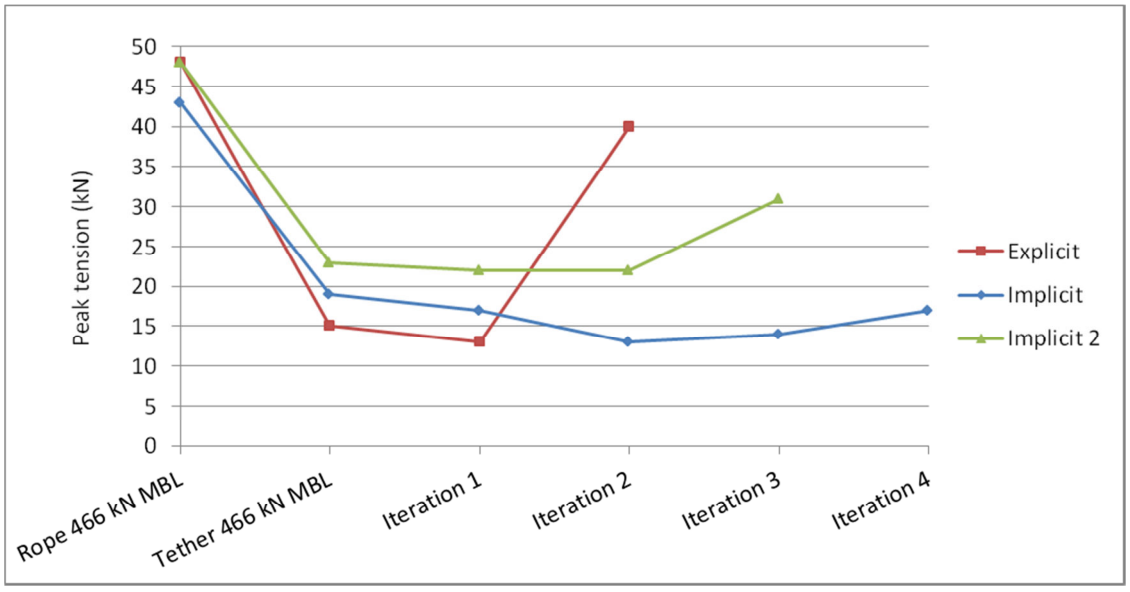

Figure 7.24 Limb 3 peak tensions through the three series of simulations and limb design iterations.

7.7 Mooring System Stiffness

A quazi-static analysis of the mooring system stiffness is performed for each of the mooring designs described in 7.6, using Orcaflex software. Analysing the system stiffness follows the methodology utilised by Pecher et al. (2014), Fitzgerald and Bergdahl (2007) and others. The existing models are modified to eliminate all wave, wind and current inputs. These forces are replaced by an 'applied global load' acting on the buoy. This applied load ramps up slowly from zero to 50 kN linearly over 500 seconds and acts horizontally in a direction directly away from anchor 2 which conveniently aligns with the model's x axis. An implicit simulation is performed over a corresponding 500 seconds for each of the mooring designs. The very slow excursion of the buoy, according to the 500 second ramp, minimises the drag effects experienced by the mooring lines as the catenary straightens.

Results are taken for the buoy excursion and the mooring line tension at the top of limb 2. The quasi-static mooring system stiffness curves are given for the implicit simulation mooring system designs in Figure 7.25. Three of these curves; the base case, the equivalent MBL tether and the optimised case, are reproduced in Figure 7.26. Horizontal lines are added to represent the peak tension that was indicated by the dynamic simulation for each of these cases.

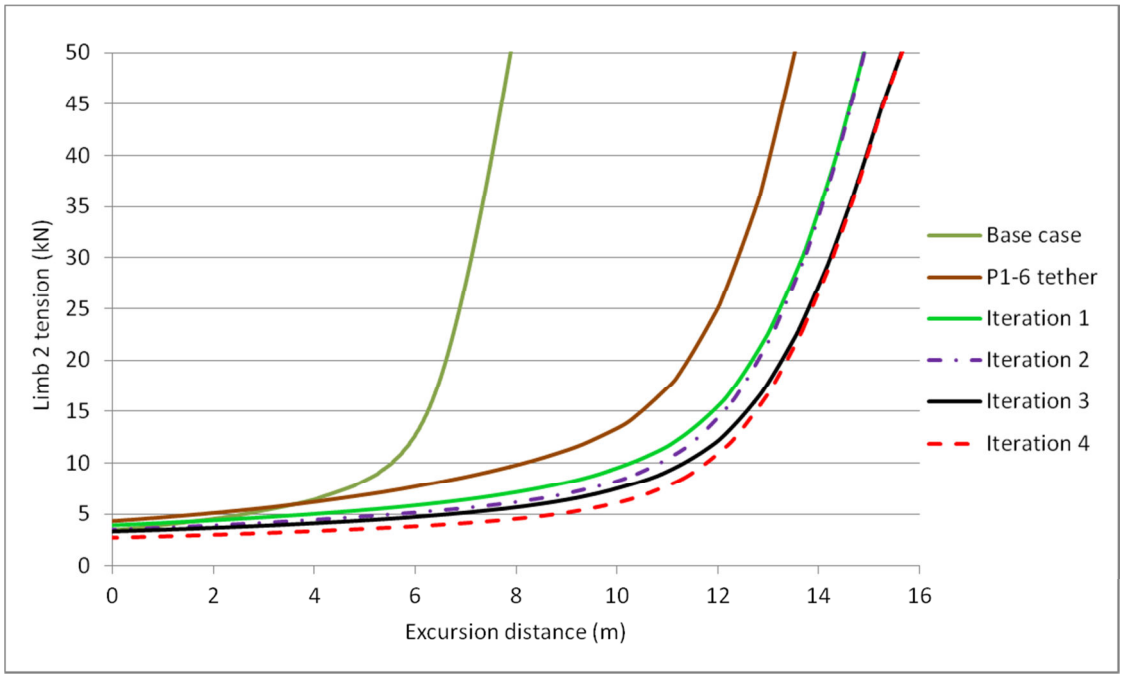

Figure 7.25 Quazi-static mooring system stiffness curves for the implicit simulation series mooring designs.

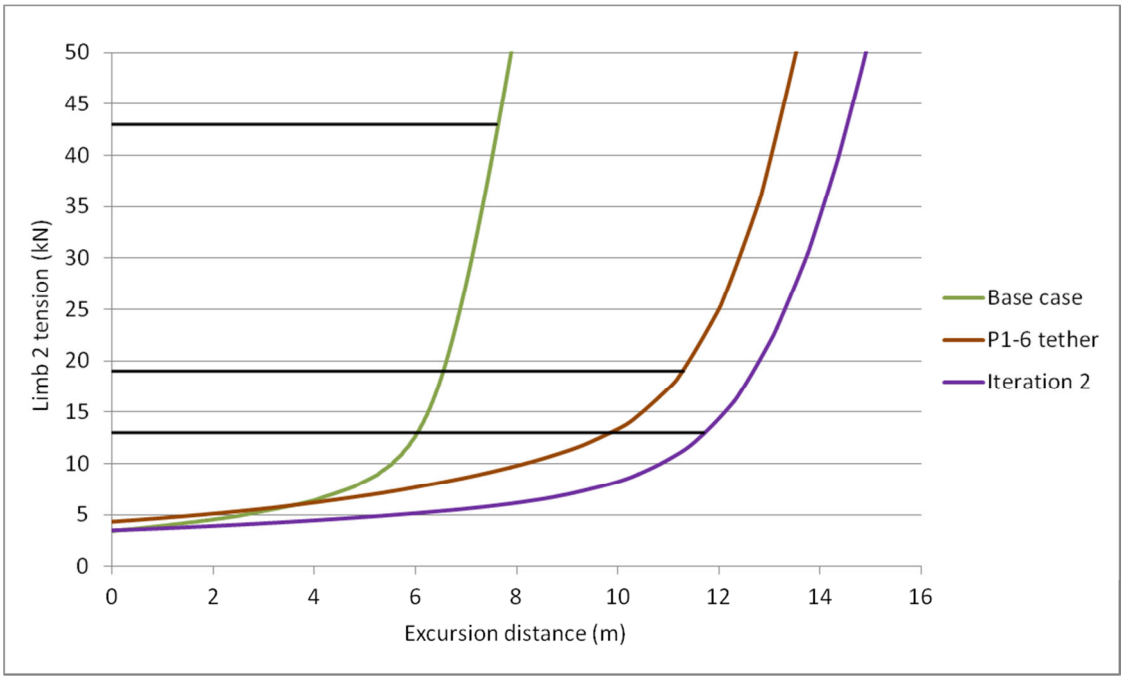

Figure 7.26 Mooring system stiffness curves reproduced from Figure 7.25 shown with corresponding peak tension from the dynamic simulation.

The gradient of the stiffness curve at any point can be described as the tangent modulus. The tangent modulus of the mooring stiffness curve is determined at the tension corresponding to the peak tension for all 15 dynamic simulation

cases described in 7.6; the results are given in Table 7.16 and displayed in graphical form in Figure 7.27.

Table 7.16 Mooring stiffness tangent moduli at dynamic simulation peak tensions.

Dynamic simulation case	Simulated peak tension (kN)	Tangent modulus at peak tension (kN/m)
explicit base case	48	25.2
explicit iteration 0	15	4.5
explicit iteration 1	13	7.5
explicit iteration 2	40	15.3
implicit base case	43	24.6
implicit iteration 0	19	7.6
implicit iteration 1	17	6.5
implicit iteration 2	13	4.7
implicit iteration 3	14	5.3
implicit iteration 4	17	8.3
implicit 2 base case	48	25.2
implicit 2 iteration 0	23	8.5
implicit 2 iteration 1	22	9.2
implicit 2 iteration 2	22	9.7
implicit 2 iteration 3	31	13.7

A best fit straight line is applied to this data in Figure 7.27 using the least squares regression method and achieves an r^2 value of 0.94. This regression analysis is then repeated for the three individual groups of simulations and this result is shown in Figure 7.28. For the separated data regressions, r^2 values of 0.99 (implicit series), 0.99 (implicit 2 series) and 0.90 (explicit series) are achieved. The close agreement of the individual regression outcomes to each other and to the mixed data regression gives an indication that there is a fundamental relationship displayed here.

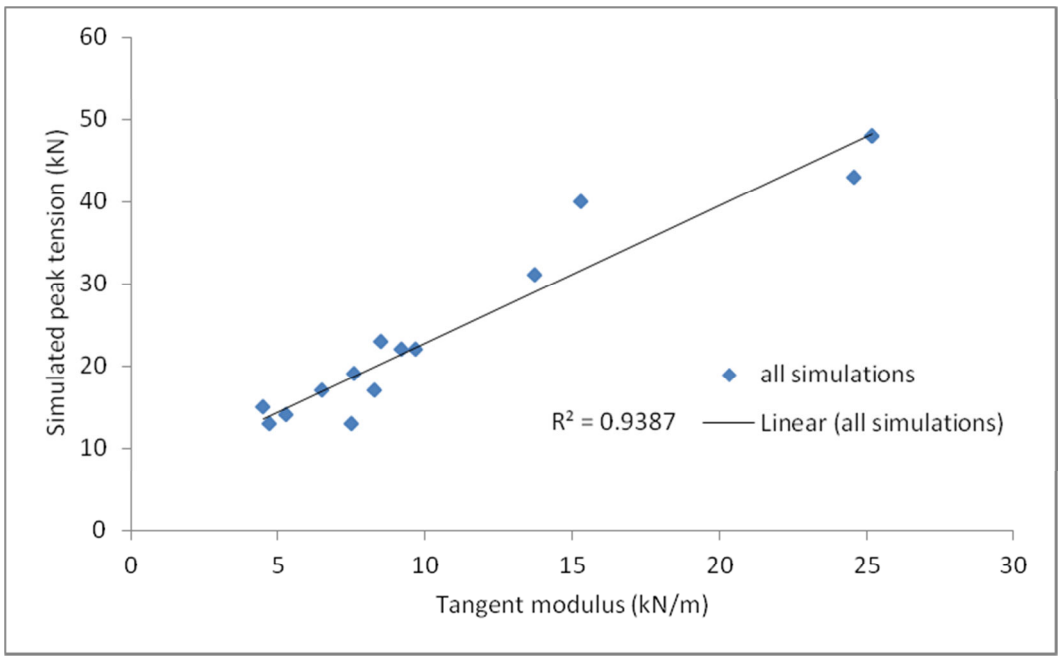

Figure 7.27 Mooring stiffness tangent modulus vs simulated dynamic peak tension (all simulations).

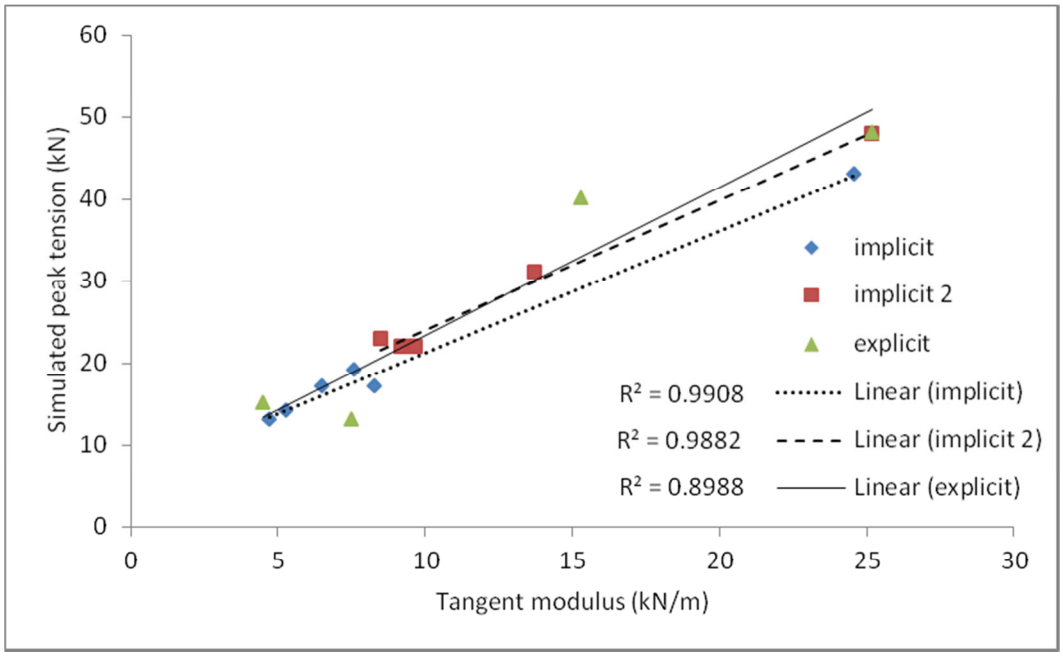

Figure 7.28 Mooring stiffness tangent modulus vs simulated dynamic peak tension by simulation series.

7.8 Limitations and Assumptions

The study using Orcaflex software takes no account of the hysteretic damping provided by the tether. Orcaflex does not readily allow the line properties to be changed between the loading up and unloading parts of the load cycle. The assumption in the results presented within Table 7.15, is that the hysteresis provided to the mooring system by the tether (Table 6.10) will not significantly affect the dynamics of the buoy.

The above assumption is somewhat validated by the real SWMTF data which displays very considerable mooring system hysteresis without the tether. Figure 7.29 shows the SWMTF data for limb 3 tension plotted against excursion away from anchor 3, during the 240 seconds of interest. The peak hysteresis loop is identified and a gap in the unload line is bridged with a straight line as shown in Figure 7.30. The hysteretic loss is quantified at 81% using the method described in 6.4.8. With such a high hysteretic loss occurring in the original mooring system, the proportionate increase in hysteresis that results from substituting the tether for the Nylon rope is minimised.

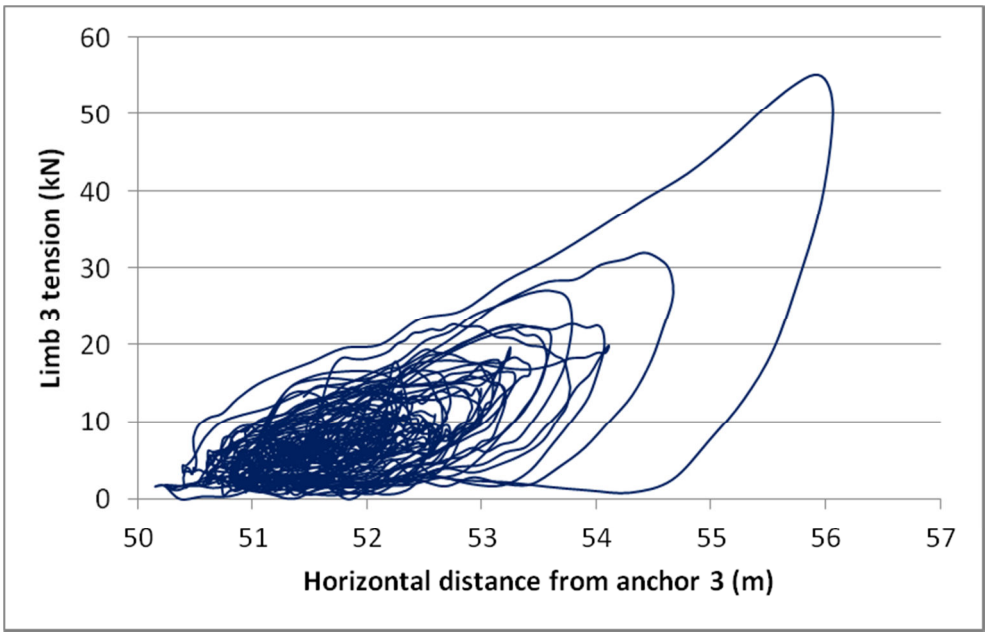

Figure 7.29 Hysteresis loops evident in the SWMTF peak load data.

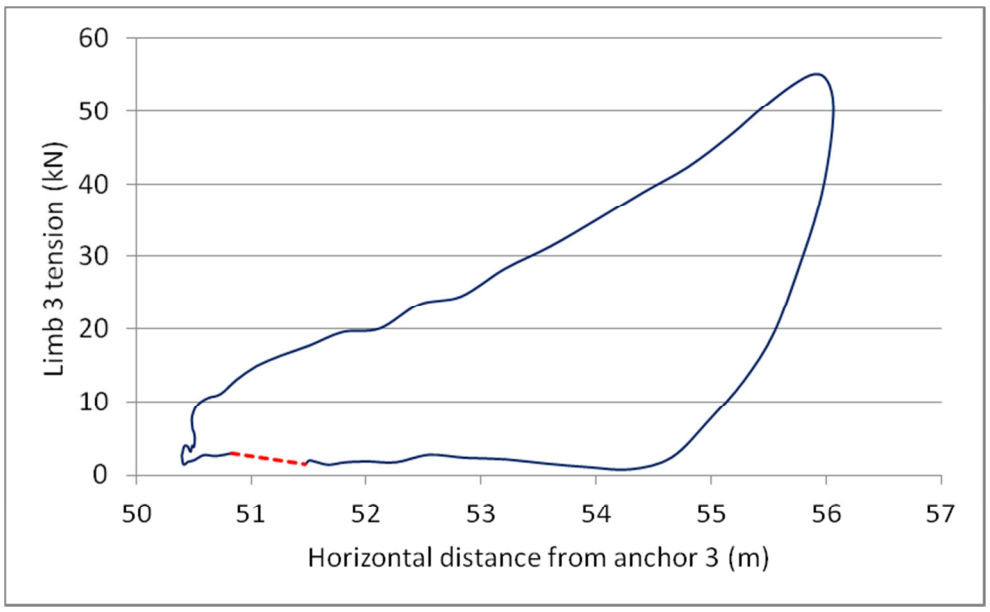

Figure 7.30 The peak hysteresis loop showing the straight line bridge used to close the gap.

A second assumption is implied by this work regarding the sea conditions that provoke peak loading. This work assumes that the same sea state will remain responsible for the peak loadings in the revised mooring system and therefore the ratios for peak tension reduction are valid.

7.9 Summary of Operational Tether Modelling and Outcomes

Real data from the SWMTF has been used to validate a base numerical model of the SWMTF using Orcaflex software. The real data included wave measurements presented as a surface elevation time series, water currents, buoy excursion and mooring loads, again in time series formats. The data used corresponds to a particular high energy weather event that occurred 9th October 2010, resulting in extreme mooring loads.

The validated numerical model was then modified to replace the existing Nylon Superline ropes with P1-6 tethers of the same breaking strength (MBL). Simulations were performed in three variant series; explicit integration, implicit integration and implicit integration with increased surface current. For each series, a design iteration process reduced the breaking strength of the tether (and correspondingly the axial stiffness) or reduced the catenary chain mass,

according to the outcome of the previous simulation. The design iteration progressed until an optimal condition of reduced magnitude peak load was achieved and departed from.

In each of the three series the peak load reduced considerably with the substitution of P1-6 for the Nylon rope and reduced further with iteration as described in 7.6.4.

The modelled mooring system was assessed in terms of system stiffness, producing mooring stiffness curves for horizontal displacement of the buoy. These were then examined in relation to the corresponding peak load case established through the modelling.

The results of the modelling and simulation studies clearly indicate that a significant decrease in the magnitude of peak loads is achieved by exchanging the Nylon ropes for the novel tether. A mean reduction of 66% is achieved with a mean increase of just 21% for excursion of the buoy. These outcomes are more fully discussed in Chapter 8.

Chapter 8 Discussions

This chapter presents discussions relating to the tether design and its mechanisms, test work methodologies, test findings and implications for mooring system design.

8.1 The Tether Design and Mechanisms

8.1.1 The Hollow Rope

The functionality of the tether relies on the hollow rope having the ability to extend freely whilst contracting diametrally. This ability is dependent upon the hollow rope construction having a high initial braid angle and a relatively loose construction. These two conditions act together to allow the braid angle to decrease significantly from its initial specification. The simplistic and logical approach to the hollow rope design that is described in 5.2 is shown to be a satisfactory method which allowed successful scaling from the P-0 to the P1 prototypes. This method specifies the cross sectional solidity of the annulus defined by the inside and outside diameters of the hollow rope. It is found that a cross sectional solidity of 53% is suitable at an initial braid angle of 52.5°. The work has not sought to define the optimum initial braid angle and solidity but the specifications set for the P1 prototypes are considered to be close to optimal. Neither has the work defined the limits of solidity that are appropriate for a given braid angle. If the solidity is too low, the linear density of the rope will be correspondingly low as will the strength of the rope. Additionally, a low cross sectional solidity will result in an open structure to the braid which will encourage the elastomer core material to bulge through under high loading. If the solidity is too high, the extension of the tether will be blocked when the braid angle reaches a lower limit, due to the rope strands becoming fully compacted.

The annulus solidity design method discussed above is also used to determine the linear density of the hollow rope and from this, the rope's strength. The method is validated by the test results which showed failure of the P1 tether at 222 kN (6.4.3) with a predicted breaking strength of 236 kN (5.2.1). This test result is within 6% of the predicted outcome although it is noted that the prediction is conditional on the assumed values for the strength conversion factors. It is also noted that with a sample size of one, the result for the MBL of

the P1 series tethers must be treated with caution. A further consideration in the determination of rope strength is the braid angle at failure. Applying the initial linear density to determine the strength assumes a 'like for like' final braid angle across rope designs. Differences in final braid angles can be catered for by the strength conversion factor that is applied.

8.1.2 The Eye Splice

The eye splices performed well during the test work and caused no concerns. The short splice is a well developed solution for joining two laid ropes together and Lankhorst's novel application of this to achieve an eye splice appears to be a sound concept. Intuitively there is a weakness where the individual strands of the hollow rope are formed into two laid ropes and this is where the single test sample failed. Referring to Figure 5.10, there is a lack of symmetry across the root of each laid rope. These ropes gather their strands from around the circumference of the hollow rope and whilst this is performed with care there will inevitably be some disparity in load path and strand tension. These disparities will translate to uneven distribution of load and this will initiate earlier failure than for a perfectly balanced construction. It is likely that this accounts for the difference between the predicted strength of the P1 tether and that found by experimentation. It can therefore be argued that the strength conversion factor for the tether, which was assumed as 70% to reflect the load path, should be reduced further to a value of 66%. Characterising the strength of the P1 series tethers according to the terminations would seem to be a necessity at this stage, pending the development of improved termination designs. This allows for representative comparisons with conventional fibre ropes which have breaking strengths that are independent of well made terminations.

The alternative method to form an eye splice that is described in 5.6.3 might result in a more balanced construction. This format would see all of the hollow rope strands being brought together to form a single laid rope which would then be conventionally spliced to form an eye. Forming a single laid rope from the hollow rope will result in less asymmetry at its root and hence less disparity in strand load path and tension.

8.1.3 The Core Architecture

The hexagonal pack cores and the articulated cores both performed well during the tests. Figure 6.24 shows that the articulated core tether, P1-9, displayed a longer 1st phase of extension during test ETT_19 than the four hexagonal pack tethers also tested. This is due to an axial separation of the moulded parts as the tether extends. The axial spaces represent portions of hollow rope that are able to contract diametrally without resistance from the core. In effect, the volume created between the core components adds to the volume created by the cross sectional free area. It is also evident from Figure 6.24 that the 1st phase axial stiffness is relatively low for P1-9 in comparison to the test group. This is an inevitable outcome with the 'free' extension provided by the opening of the axial spaces.

From Table 6.6 it is clear that the articulated core tethers, P1-9 and P1-12, are amongst the stiffer tethers during the 2nd phase of extension. Tether P1-9 is the 3rd stiffest and P1-12, the 4th stiffest within the full test group. This change of behaviour from the soft 1st phase, relative to the hexagonal pack tethers, is most probably explained by the lesser Poisson's diminution of these core components. By contrast, the hexagonal pack cores, being full length continuous cords are subjected to full tether elongation and thus sustain a greater Poisson's diminution. This aspect of tether behaviour is more fully discussed in 8.1.6.

Whilst a financial analysis of the tether is outside of the scope of this work, it is clear that extruded elastomer cord is a more cost effective product than moulded elastomer parts. Therefore there will need to be a decisive advantage to the properties of the articulated core tethers if this solution is to be adopted. From the results of the test work, no such clear advantage is apparent in terms of extension properties.

One advantage that should be noted is that of bending stiffness. Whilst no quantitative assessment of this has been made, it is noted that the articulated core tethers have a significantly lower bending stiffness than the hexagonal pack tethers. This would provide an advantage in terms of handling, allowing these tethers to be coiled onto smaller spools than their hexagonal pack

counterparts. Figure 8.1 shows the articulated core tether P1-12 curved into a tight arc.

Figure 8.1 An articulated core tether demonstrating advantageous bending stiffness.

8.1.4 The Core Material

The EPDM rubber performed well throughout the test work. Whilst the visco-elastic nature of the material was observed, this didn't adversely affect the tether performance. Significant changes in the materials response are evident at the extremities of the load vs extension loops, where velocities tend towards zero. These changes are indicated by smooth radii at the ends of the loops as seen in Figure 6.28 for instance. Importantly though, these time related changes to load response, do not arise within the predicted range of cycle frequency for mooring systems. The results presented in 6.4.5 show a repeatable outcome for sinewave periods of between 6 and 14 seconds. This will allow the axial stiffness of tethers to be specified by a single curve, avoiding the undesirable complexity of time related, conditional specifications.

The intention to carry a maximum of 5% of the tether load within the hexagonal pack cores is only satisfied by the softest (54 Shore A) EPDM material. The stiffest EPDM material used (81 Shore A) carried 10% of the axial load but this

exceedance of the target is not viewed as problematic in terms of tether performance. There is however a failure mode that might be promoted by excessive tension in the core. With the considerable diametral reduction of the tether under high load, it is not possible to anchor the core to the hollow rope at its ends. The hexagonal pack tethers rely on the tight grip of the hollow rope on the core bundle to prevent the rope from gradually slipping off the ends of the core bundle. This is aided by the braided rope imprinting itself into the compliant surface of the core bundle which enhances the axial grip. For the hardest EPDM materials, not only is the axial tension higher, the axial grip of the rope is lower due to less pronounced imprinting of the rope into the harder surface.

8.1.5 1st Phase Tether Extension

The tether achieves a low axial stiffness during a distinct 1st phase of extension as intended. The mechanism for this soft phase relies on the deformation of the core to eliminate the free cross sectional free area as described in 5.3.2. The effect is exaggerated by the mechanical advantage that the braid angle affords to the rope in compressing the core during early stage extension. Figure 8.2 shows tether P1-2 at zero extension (LH) and 30% extension (RH) to demonstrate this point. At zero extension the tether has a rounded hexagon form giving a mean diameter of 77 mm, whereas at 30% extension it has a round form of 66 mm diameter.

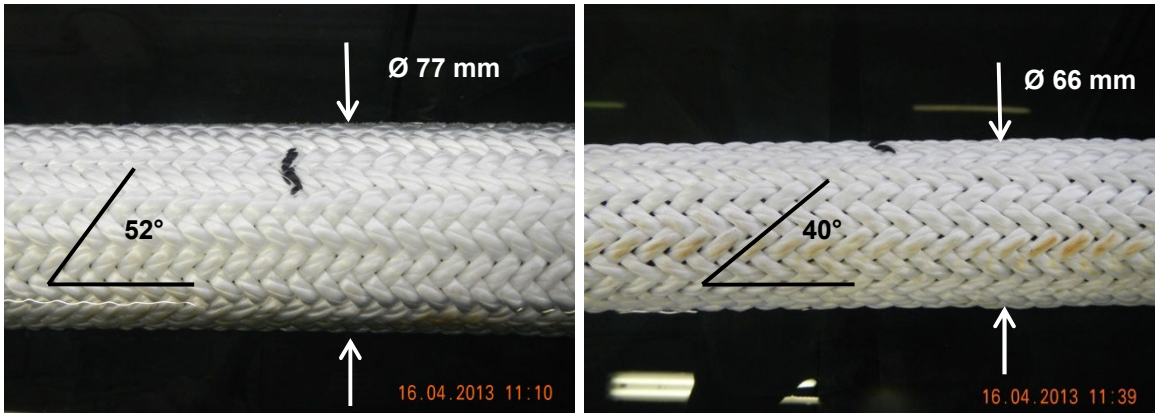

Figure 8.2 Tether P1-2 at zero extension having a rounded hexagon form (LH) and at 30% extension with a fully round form (RH) (Gordelier et al., 2015).

The tether design assumes therefore, that this 1st phase stiffness can be controlled by selecting the core components so as to produce a particular

resistance to radial deformation. In this work these adjustments are made by varying the hardness of the elastomer core material. This form of adjustment will vary the stiffness of the 1st phase without changing the extent of extension over which the 1st phase acts. This mechanism is validated by the 1st phase extension behaviour of P1-2 (54 Shore A) and P1-6 (81 Shore A) which is shown in Figure 6.25. These tethers have the softest and hardest core materials and their 1st phase stiffness are accordingly softest and hardest.

A second means by which the stiffness of the 1st phase might be adjusted lies with the braid angle. A hollow rope with a reduced initial braid angle will have less mechanical advantage in deforming the core and will therefore provide a stiffer 1st phase response. However, this means of controlling the 1st phase stiffness will also act to reduce the extent of the 1st phase and the full extension capability of the tether.

The extent of the 1st phase extension can be controlled by varying the cross sectional solidity of the core; this control action will not impact upon the full extension of the tether. This mechanism is demonstrated by the later transition to 2nd phase extension shown by tethers P1-7 and P1-9 in Figure 6.24. P1-7 has a central core strand of EPDM foam giving a core solidity of 80% rather than the standard 86%. P1-9 is an articulated core tether which develops additional free space as discussed in 8.1.3.

8.1.6 2nd Phase Tether Extension

At the end of the 1st phase of extension there is a smooth transition to a markedly stiffer 2nd phase. During this 2nd phase the core has a solid cross section having been fully deformed during the 1st phase and the transition. During test work, it is noted that the hexagonal pack tethers take a round form during the transition stage confirming the completion of deformation (Figure 8.2).

The ranking of hexagonal pack tethers according to 2nd phase stiffness produced a counter intuitive outcome which is given in Table 6.6. The tether with the softest core displays the stiffest 2nd phase and all five tethers rank sequentially according to this counter intuitive result.

During the 2nd phase of extension, the hexagonal pack core is extending as a solid round section of rubber. If the hollow rope had infinite axial stiffness and no penetration of the rope strands into the core was possible, then the high bulk modulus of rubber would prevent any tether extension. In reality the hollow rope yields axially and embeds into the core surface. Both of these actions allow a degree of tether extension and as the tether extends, the core diameter reduces according to the materials Poisson's ratio. This Poisson's diminution acts as a positive feedback to extension, perpetuating the extension as the load is increased.

The results for the Poisson's ratio tests given in Table 6.8 do not offer any explanation for the counter intuitive results for 2nd phase stiffness. Any trend evident in the Poisson's ratio acts counter to the stiffness results. Currently, the only plausible theory to account for the stiffness ranking is associated with the penetration of the rope strands into the surface of the core. Strand penetration will be greatest for the softest core material with a logical and sequential reduction in penetration for the other materials. As the tether extends, the rope strands must shift across the surface of the core with the changing braid angle. If the rope strands are penetrating into the surface of the core, they will be somewhat confined and the change in braid angle will meet with resistance. The deeper that the rope strands embed into the core surface, the greater this resistance is likely to be. Hence a softer core might produce a stiffer axial response according to this theory.

8.1.7 Radial Core Pressure

It is important to have an understanding of the pressures acting on the core and to validate the methodology for determining these pressures. Numerical modelling of the tether operation is not within the scope of this work but will be necessary to facilitate the design of bespoke tethers in the future. The work to determine the radial pressure numerically and to validate this experimentally has confirmed that the tether acts with a predictable and rational mechanism.

8.2 The Tether Test Work

8.2.1 Wet Testing

It is important that all of the tether performance tests are conducted in the submerged condition. This is to ensure that the tether is properly lubricated by water throughout the core structure which is difficult to achieve with a sprinkler type system. The results shown in Table 6.10 demonstrate that considerable heat is generated within the tethers. Without adequate water cooling, the tether components will absorb this heat and the visco-elastic behaviour might be affected.

A potential further benefit of submerged testing is that the weight of the tether is greatly reduced in water. By minimising the catenary mass of the tether at low axial tension, the quality of the data at low tension can be improved. Conversely however, as the catenary straightens underwater, the tether experiences hydrodynamic drag which degrades the quality of the axial tension data.

8.2.2 Tension Data Accuracy

The load cell that is fitted to the DMaC linear ram is rated to 100,000 lbf or 444 kN. The manufacturer's specification states the accuracy to be within a static error band of +/- 0.06% of full scale. This represents a potential error band of +/- 266 N throughout the load cell's measurement range. This error band is applied to the processed data for test ETT_19 performed on tether P1-6 and is shown graphically in Figure 8.3.

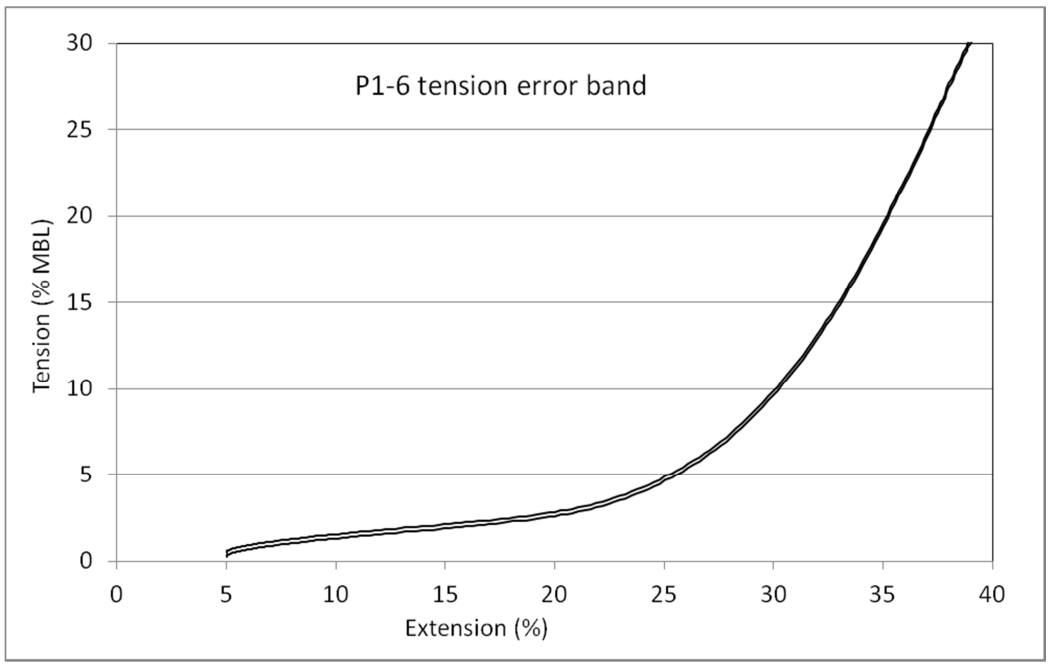

Figure 8.3 The tension error band limits applied to P1-6 performance data.

8.2.3 Extension Data Accuracy

The extension data provided by the instrumentation is of high accuracy. DMaC is fitted with a linear encoder with a specified accuracy of +/- 20 microns per metre. The draw wire sensor used to measure the eye splice extension achieves a displacement accuracy of 0.1%. When these two components of accuracy are combined according to the worst cases, the error remains negligible in respect of the results presented.

The greater potential for inaccuracy in the extension data might arise from the assumption that both eye splice terminations extend equally. This assumption is made in the test work because only a single transducer was available to record the eye splice extension. This assumption might produce inaccuracy via two mechanisms:

1. The making of the two laid ropes by hand and their subsequent short splicing might be performed with differing tensions which can affect the axial stiffness of the termination.
2. The eye splices at each end of a single tether might be of marginally different lengths and will therefore extend differently whilst having equal axial stiffness.

The maximum variation of termination length is 0.050 m which is 5% of the nominal termination length. With the near linear behaviour of the terminations (Figure 6.15), a 5% difference in termination length will produce a 5% difference in extension for equal axial stiffness. If a 5% variation in axial stiffness is assumed and the worst case errors are combined to give a 10% error on the un-measured termination, the total eye splice extension of a tether has a possible error of +/- 5%.

The extension error band is applied together with the tension error band to give the worst case for tether P1-6 and the outcome is shown graphically in Figure 8.4. The resulting combined potential error does not significantly affect the outcome for axial stiffness. In particular, the combined error is minor for 1st phase extension which is key to the major outcomes of the modelling work that are presented in 7.6 and 7.7.

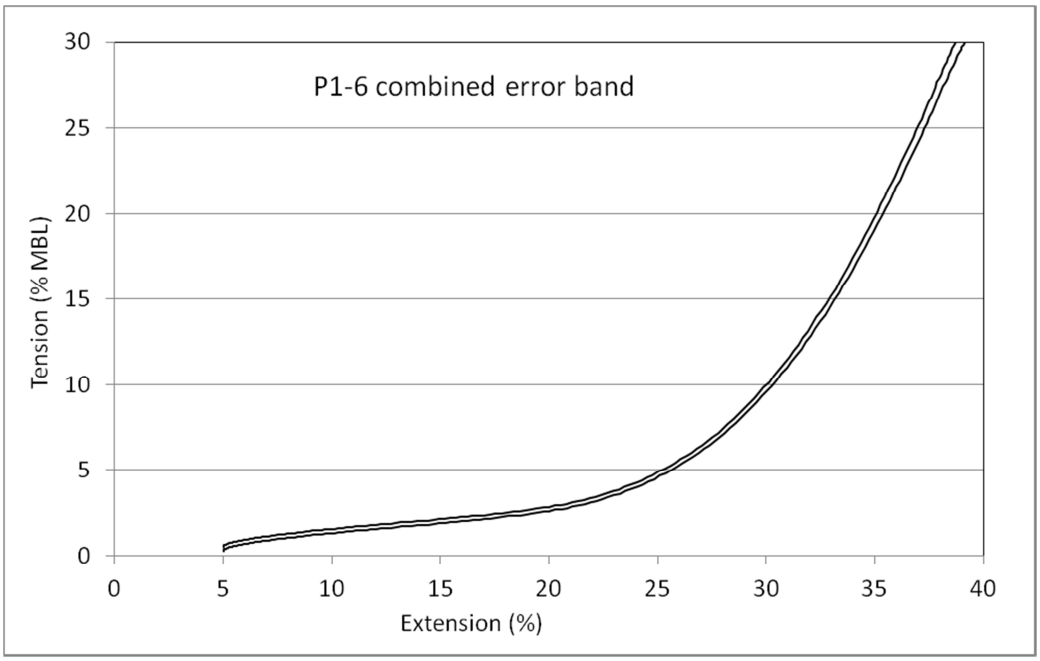

Figure 8.4 The combined extension and tension error band applied to P1-6 performance data.

8.2.4 Dynamic Zero Load Length

The visco-elastic properties of the tether are much more pronounced than for conventional fibre ropes. If the axial stiffness curves derived from the test work

are to be used accurately within modelling work, the zero load datum must be valid for the cyclic loading that is being modelled.

The method used to define a dynamic length datum is explained in 6.4.6. The method is imperfect, using the quasi-static linear spring constant to extrapolate down from the first data point of the dynamic load cycle. Despite some remaining concerns over the methodology, the resulting datum length is far more representative than the conventional datum.

As a result of the extreme visco-elastic behaviour and the adoption of a dynamic length datum, there is an offset between the dynamic zero load length and the fully recovered, or as new, static free length. This has implications for the design of tethers to meet specific dynamic requirements and this issue is raised as further work in 9.2.

8.3 The Modelling Outcomes and Interpretation

In the absence of real sea trials data comparing the tether's performance to that of conventional fibre ropes, the modelling and simulation studies performed within this work represent the best assessment of the tether's performance. By validating the base case model against real sea trials data for the same case, a large part of the uncertainty attributed to numerical modelling is removed. Changes to the models incorporating the tethers in exchange for the Nylon ropes are limited to the line properties. All other mass properties, hydrodynamic properties, geometry and environmental inputs remain unchanged. Therefore the resulting reduction to the axial line loads can be assumed to be a realistic representation of the advantage gained.

The peak load reductions reported in Table 7.15 are broadly in line with the magnitudes of load reduction suggested in the literature relating to elastomeric mooring tethers, discussed in 2.4 and 2.5. Some predictions of greater decreases are made in the literature but these relate to a change from a simple catenary mooring to an elastomeric mooring. In this work the base case is the SWMTF buoy which already has a Nylon rope element for compliance. It is of note that the explicit simulation studies, described by Orcina as the most accurately solved method (7.4.4), returned the greatest load reduction of 73%.

In all three simulation series the upward load case spiral described in 1.2 was reversed for two or three iterations of reduced mooring stiffness. However, it then showed an upward turn as the mooring stiffness was reduced further (Figure 7.24). This leads to the intuitive conclusion that for a given size and mass of floater, an optimal mooring stiffness curve will provide the lowest load case for a given permitted excursion; this aligns with the results presented by Pecher et al. (2014), discussed in 2.2.2. The difference between the upward iteration described in 1.2 and the reverse iteration presented in 7.6, is that the latter case excluded changes to the size and mass of the floater. If the size and mass of the floater remain constant, then the energy imparted to the floater and mooring system will be unchanged for a given wave cycle and permitted excursion. Therefore the optimal mooring system will be that which most effectively absorbs the energy during the excursion, to the point of zero kinetic energy at the permitted excursion. If the rate of energy absorption into the mooring system is too low during the majority of the excursion, then the rate will be high at the end of the excursion. A higher rate of energy transfer into the mooring system will result in higher forces; this is demonstrated in Figure 7.26 and further supported by the relationship shown in Figure 7.27. A lower tangent modulus at the limit of excursion represents a lower rate of energy exchange and hence a lower force.

A simplistic analogy might be drawn with a train hitting the buffers at the end of the line; the buffers define the maximum permitted excursion of the train. At a given distance from the buffers, the brakes are applied progressively creating an increasing retarding force. Insufficient braking will result in a high rate of energy exchange at the buffers. Too much braking will stop the train earlier than necessary and hence the peak retarding force will be higher than necessary. The optimal solution will be a rate of braking such that the train's motion is gently arrested by the buffers. A potential weakness in this analogy is that hydrodynamic forces resulting from slam and drag might still be acting when the floating body is stationary at its point of maximum excursion.

8.4 Hydrodynamic Line Damping

Whilst the hydrodynamic damping properties of mooring lines is not within the scope of this work, some discussion is warranted here.

The hysteretic loss of 81% for the SWMTF mooring system shown in Figure 7.30 is very significant. Ridge et al. (2010) do not quantify the hysteretic loss for Nylon rope witnessed in their work but Figure 2.9 shows that it does not approach the level of 81%. Therefore the assumption here is that the majority of the 81% hysteretic loss can be attributed to hydrodynamic drag as the catenary straightens. The associated assumption is therefore that the hydrodynamic drag contributes significantly to the retarding force acting upon the moving floater. In this case the form of the catenary and the diameter or drag properties of the mooring line are significant parameters affecting the design outcomes.

8.5 An Alternative View of MEC Moorings Design

The iterative moorings design methodology described for the SWMTF in 1.2 has also been applied to MEC mooring systems such as Fred Olsen's BOLT 2 WEC (Harnois, 2014). In this process, the mooring limb design is iterated through several stages of dynamic simulation to achieve the lowest load case. Having selected the mooring limb composition to achieve compliance, the axial and hydrodynamic properties of the limb are driven by the strength requirements of the previous iteration outcome. The maximum excursion is then an outcome from the process rather than a design input.

For MEC array moorings it is envisaged that a design process that drives the outcomes more strongly will be required. The tether might aid such a process by virtue of its selectable two stage extension properties and 1st stage extent.

With reference to the train and buffer analogy used above, the mooring system might be visualised by approximating it with a mass spring damper system as shown in Figure 8.5.

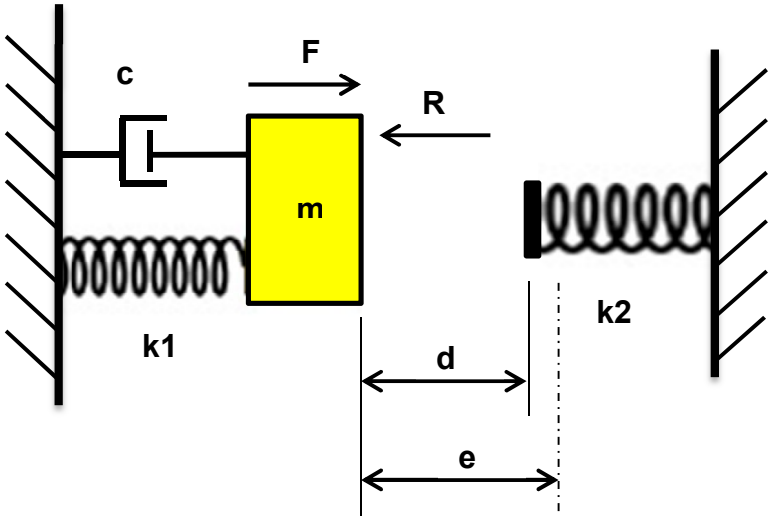

Figure 8.5 Schematic representation of the train and buffer analogy as a mass, spring, damper system.

The floating body has mass m and is subjected to environmental force F, the 1st phase stiffness is given by the spring rate k1 and has an extent d, the 2nd phase stiffness by k2 and the hydrodynamic line damping by c. For an array of MEC devices within a given consented area, distance e (the maximum excursion) will be an input to the mooring design. The retarding force is represented by R which will initially comprise components of damping force and 1st phase spring force. The retarding force will rise more steeply when the 2nd phase spring force is added to the 1st phase spring force at which point the damping force will tend towards zero. The peak retarding force will be experienced at the maximum displacement.

Therefore to minimise the peak retarding force an optimal balance must be achieved between k1 and c to accept a certain fraction of the energy into the mooring at distance d, say 70% for example. Rate k2 must be set so that the mooring system absorbs the remaining 30% energy whilst the floater moves on to distance e.

For MECs that use surge for energy conversion, the energy being taken up by the PTO will need to be considered, although the PTO is likely to be disabled in storm conditions. Tension mooring systems will have a lesser component for hydrodynamic line damping and therefore k1 will dominate the 1st phase.

Chapter 9 Conclusions and Further Work

In this chapter conclusions are drawn relating to the research questions posed in 1.3 and the additional findings. These conclusions are referenced to the current development status of the tether and a summary of necessary further work is presented.

9.1 Research Questions

The research questions are repeated for convenience:

Q1. Is it possible to develop a novel, fibre rope mooring tether whereby the axial stiffness is decoupled from the MBL of the rope?

Q2. Can the novel tether provide more favourable axial extension properties for MEC mooring lines than conventional fibre ropes?

Q3. Can the novel tether facilitate the selection of axial stiffness, for a given MBL, at the tether design stage?

Q4. Does the novel tether have the capability to significantly reduce peak mooring loads for highly dynamic MEC devices?

Addressing these in turn:

Q1. This work has demonstrated that by introducing an elastomeric core mechanism into a fibre rope, the relationship between axial stiffness and the MBL can certainly be altered very significantly. The work has also shown than by adjustment to the composition of the elastomer core, the axial stiffness of the tether can be changed without changing the MBL. Therefore it is concluded that the axial stiffness can be decoupled from the MBL within certain limits. These limits will be defined by the limitations of variability that are achievable in the core properties and the hollow rope design.

Q2. The simple answer to this is yes. It is clear from the test outcomes that the axial stiffness of the tether is much reduced from that of conventional fibre ropes of corresponding strength. This is evident from the data presented in Figure 6.25 which contrasts the axial stiffness of the tether with polyester double braid rope and Nylon Superline rope. The Nylon

Superline rope represents the most compliant fibre rope that has adequate fatigue properties for WEC mooring systems (Ridge et al., 2010). Assuming a FOS of 3 and therefore observing the extension at 33% MBL; the tethers achieve more than 3 times the extension of the polyester rope and more than 2.5 times that of the Nylon rope.

Q3. This is partly addressed above in relation to question no. 1. The results of the test work demonstrate a range of 1st phase and 2nd phase axial stiffness according to the core composition. It will be possible to increase the breadth of this range by changes to the geometry and solidity of the core and perhaps by increasing the hardness range of the elastomers. It will also be possible to adjust the extension limit of 1st phase axial stiffness as discussed in 8.1.5. The limits of these extension properties must be defined by further work which is discussed in 9.2.

Q4. The modelling and simulation work shows that this is certainly the case. The mean peak tension is reduced by a factor of three in the simulation studies. Much of this advantage is achieved by simply exchanging an existing Nylon Superline rope for an equivalent strength tether but the full advantage is gained from iterating to the optimal mooring stiffness.

A further question is raised at this stage regarding the relevance of the MBL to the design of such tethers. Clearly it is always necessary to have a thorough understanding of the strength and fatigue properties for a structural element. However, the elastomeric tether solution changes the emphasis of design. Designing a mooring system with the tether should focus on the system stiffness that is required to achieve the necessary energy absorption during the specified maximum excursion. The required mooring system stiffness will then drive the detailed mooring limb design incorporating the required axial stiffness phases of the tether. In turn, this will dictate the geometry and sizing of the tether and it is likely that the resulting MBL will be significantly higher than is required by the FOS. Put simply, the tether FOS and MBL will become factors that are checked during the mooring design process rather than factors that drive the design process.

In summary, the tether having two phases of extension, selectable axial stiffness within limits for both phases and selectable 1st phase extent, presents a new methodology for moorings design and provides a greatly reduced load case. The tether achieves these advantages whilst maintaining the load path within a fibre rope with proven terminations and couplings. The simplicity and maturity of the load carriers brings an inherent reliability and predictability to the tether, introducing little or no added risk to the mooring system.

9.2 Further Work

Further work is required to finalise the understanding of the tether mechanisms, its operational capabilities and how its properties can best be selected during the moorings design process in order that the optimal solution is identified. These points are broken down as follows:

1. Work is required to determine the optimum solidity of the hollow rope in relation to initial and final braid angles. Whilst an optimum case might exist, it is also important to define the limits of solidity that are appropriate so that the linear density of the rope can be adjusted for any defined axial stiffness regime. This will allow increases and decreases in the tether's MBL to achieve suitable strength without excessive material use.

2. The scalability of the tether must be defined and the maximum limit for MBL must be identified for tethers using polyester rope. This work will be conditional upon (1).

3. Further investigation of the counter intuitive result for 2nd phase axial stiffness that is reported in Table 6.6 and discussed in 8.1.6, must be undertaken. The mechanism responsible for this effect must be determined and characterised.

4. The minimum and maximum axial stiffness of phase 1 and phase 2 need to be further defined. As these two phases are largely governed by the tether construction, the interdependency of these phase properties must also be mapped. This work will integrate with work in (1), (5) and (6).

5. Tests must be performed to determine the maximum extent that is achievable for the 1st phase. This will be determined by progressively reducing the cross sectional solidity of the core and by invoking the greatest possible initial braid angle.

6. A more detailed analysis of suitable elastomer materials is warranted. This work should integrate with the work to define the axial stiffness limits and the work to assess the durability of the tether.

7. Alongside (6), the offset between the dynamic zero load length and the 'as new' free length needs to be defined for each material.

8. A numerical model of the tether mechanisms must be created. This model will bring all of the above points into a single predictive tool that will allow the functional properties of any tether to be predicted according to a set of design parameters. Conversely the tool must provide a design capability whereby the functional requirements of 1st and 2nd phase axial stiffness and extent are input and the design parameters are given as the outcome. This model will need to take into account the offset between dynamic zero load length and the 'as new' free length.

9. The durability of the tether must be fully assessed. This study will include fatigue strength, resistance to marine growth, internal abrasion, changes to material properties and all other known failure and degradation factors. Real sea trials are required alongside laboratory tests to fully characterise the operational lifetime of the tether.

10. The benefits attributed to the tether via modelling and simulation must be substantiated using real sea trials. This will best be performed by replacing elements in an existing mooring system where adequate data has been gathered. Parallel modelling and simulation work should be conducted for maximum learning and validation.

11. The moorings design approach discussed in 8.5 should be progressed. A goal might be to evolve design algorithms that will specify 1st phase axial stiffness, 1st phase extent and 2nd phase axial stiffness for a mooring system to achieve an optimal solution for a given maximum excursion. These algorithms would need to recognise the boundary envelopes that define the capability of the integrated systems at work.

Appendices

Appendix A – UK Patent Application GB 2467345 A

(12) UK Patent Application (19) GB (11) 2467345 (13) A

(43) Date of A Publication 04.08.2010

(21) Application No: 0901529.8

(22) Date of Filing: 30.01.2009

(71) Applicant(s):
The University of Exeter
(Incorporated in the United Kingdom)
The Innovation Centre, Rennes Drive, EXETER, Devon, EX4 4RN, United Kingdom

(72) Inventor(s):
David Parish

(74) Agent and/or Address for Service:
Handsome I.P. Ltd
Innovation Centre, Carpenter House, Broad Quay, BATH, Somerset, BA1 1UD, United Kingdom

(51) INT CL:
B63B 21/00 (2006.01)

(56) Documents Cited:
GB 2175945 A **GB 2152183 A**
WO 2001/051345 A1 **US 4493282 A**

(58) Field of Search:
UK CL (Edition X) **B7V**
INT CL **B63B**
Other: **EPODOC, WPI, TXTE**

(54) Title of the Invention: **Mooring limb**
Abstract Title: **Mooring limb**

(57) A mooring limb for use in a fluid comprises at least one substantially impervious sleeve 150 defining at least one chamber. The shape of the at least one chamber is variable and the device includes at least one orifice 80 for allowing a fluid into and/or out of the at least one chamber. The mooring limb may act as a pump and/or as a damping device. Also disclosed is a method of mooring a floating object (20, Fig 1) comprising attaching one end of the limb to the floating object and the other end to a fixed object (30, Fig 1). A method of damping the movement of a floating object is also disclosed in which the mooring limb is connected between the floating object and a fixed object and the flow of fluid in and out of the limb is controlled, to damp the change in the length of the limb due to the movement of the floating object with respect to the fixed object.

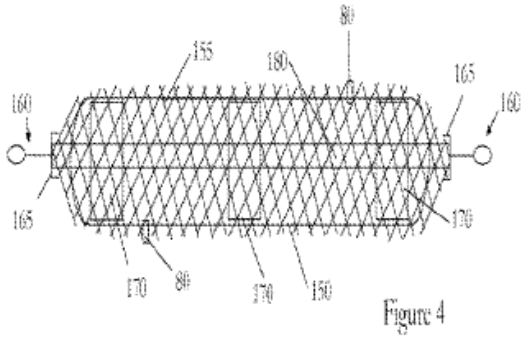

Figure 4

Hydraulic core tether patent application (Parish, 2010).

Appendix B – UK Patent Application GB 2476986 A

(12) UK Patent Application (19) GB (11) 2476986 (13) A

(43) Date of A Publication 20.07.2011

(21) Application No: 1000800.1

(22) Date of Filing: 19.01.2010

(71) Applicant(s):
The University of Exeter
The Queen's Drive, EXETER, EX4 4QJ,
United Kingdom

(72) Inventor(s):
David Parish

(74) Agent and/or Address for Service:
Handsome I.P. Ltd
Innovation Centre, Carpenter House, Broad Quay,
BATH, Somerset, BA1 1UD, United Kingdom

(51) INT CL:
B63B 21/00 (2006.01) ***B63B 21/20*** (2006.01)
B63B 21/50 (2006.01)

(56) Documents Cited:
JP 590195486 A **US 5483911 A**
US 20020053277 A1

(58) Field of Search:
UK CL (Edition X) **B7V**
INT CL **B63B**
Other: **EPODOC, WPI**

(54) Title of the Invention: **Mooring limb**
Abstract Title: **A resilient mooring limb**

(57) A mooring limb 110 for damping the oscillations of a moored object (20, Fig 1) comprises an axially extensible outer sheath 50, and an inner radially compressible core 180, the core being compressible radially by the sheath as the axial length of the limb increases. The limb is also axially contractible as a result of a force provided by the core acting radially outward onto the sheath. The sheath may be attached to the core in at least one place 120, or the sheath and the core may be unattached to one another. The limb may have more than one core. A method of mooring an object with the mooring limb and a method of making the mooring limb are also disclosed.

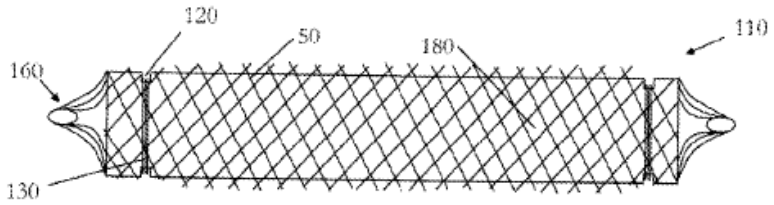

Figure 5

Solid core tether patent application (Parish, 2011).

Appendix C – FMEA Guidance

(Generic) Design FMEA Severity Evaluation Criteria

Effect	Criteria: Severity of Effect on Product (Customer Effect)	Rank
Failure to Meet Safety and/or Regulatory Requirements	Potential failure mode affects safe vehicle operation and/or involves noncompliance with government regulations without warning.	10
	Potential failure mode affects safe vehicle operation and/or involves noncompliance with government regulations with warning.	9
Loss or Degradation of Primary Function	Loss of primary function (vehicle inoperable, does not affect safe vehicle operation).	8
	Degradation of primary function (vehicle operable, but at reduced level of performance).	7
Loss or Degradation of Secondary Function	Loss of primary function (vehicle inoperable, but comfort/convenience functions inoperable).	6
	Degradation of primary function (vehicle inoperable, but comfort/convenience functions at reduced level of performance).	5
Annoyance	Appearance or Audible Noise, vehicle operable, item does not conform and noticed by most customers (>75%).	4
	Appearance or Audible Noise, vehicle operable, item does not conform and noticed by many customers (50%).	3
	Appearance or Audible Noise, vehicle operable, item does not conform and noticed by discriminating customers (<25%).	2
No effect	No discernible effect.	1

(Generic) Design FMEA Occurrence Evaluation Criteria

Likelihood of Failure	Criteria: Occurrence of Causes – DFMEA (Design life/reliability of item/vehicle)	Incidents per item/vehicle	Rank
Very High	New technology/new design with no history.	≥100 per thousand ≥1 in 10	10
High	Failure is inevitable with new design, new application, or change in duty cycle/operating conditions.	50 per thousand 1 in 20	9
	Failure is likely with new design, new application, or change in duty cycle/operating conditions.	20 per thousand 1 in 50	8
	Failure is uncertain with new design, new application, or change in duty cycle/operating conditions.	10 per thousand 1 in 100	7
Moderate	Frequent failures associated with similar designs or in design simulation and testing.	2 per thousand 1 in 500	6
	Occasional failures associated with similar designs or in design simulation and testing.	0.5 per thousand 1 in 2,000	5
	Isolated failures associated with similar designs or in design simulation and testing.	0.1 per thousand 1 in 10,000	4
Low	Only isolated failures associated with almost identical design or in design simulation and testing.	0.01 per thousand 1 in 100,000	3
	No observed failures associated with almost identical design or in design simulation and testing.	≤0.001 per thousand 1 in 1,000,000	2
Very Low	Failure is eliminated through preventive control	Failure is eliminated through preventive control.	1

Source: Reprinted from Potential Failure Mode and Effects Analysis, (FMEA 4th edition, 2008 Manual) with permission of DaimlerChrysler, Ford and GM Supplier Quality Requirements Task Force.

Design FMEA severity and occurrence evaluation criteria (McDermott et al., 2009)

(Generic) Design FMEA Prevention/Detection Evaluation Criteria

Opportunity for Detection	Criteria: Likelihood of Detection by Design Control	Rank	Likelihood of Detection
No detection opportunity	No current design control; Cannot detect or is not analyzed.	10	Almost Impossible
Not likely to detect at any stage	Design analysis/detection controls have a weak detection capability; Virtual Analysis (e.g., CAE, FEA, etc.) is **not correlated** to expected actual operating conditions.	9	Very Remote
Post Design Freeze and prior to launch	Product verification/validation after design freeze and prior to launch with **pass/fail** testing (Subsystem or system testing with acceptance criteria such as ride and handling, shipping evaluation, etc.).	8	Remote
	Product verification/validation after design freeze and prior to launch with **test to failure** testing (Subsystem or system testing until failure occurs, testing of system interactions, etc.).	7	Very Low
	Product verification/validation after design freeze and prior to launch with **degradation** testing (Subsystem or system testing after durability test, e.g., function check).	6	Low
Prior to Design Freeze	Product validation (reliability testing, development or validation tests) prior to design freeze using **pass/fail** testing (e.g., acceptance criteria for performance, function checks, etc.).	5	Moderate
	Product validation (reliability testing, development or validation tests) prior to design freeze using **test to failure** (e.g., until leaks, yields, cracks, etc.).	4	Moderately High
	Product validation (reliability testing, development or validation tests) prior to design freeze using **degradation** testing (e.g., data trends, before/after values, etc.).	3	High
Virtual Analysis – Correlated	Design analysis/detection controls have a strong detection capability; Virtual Analysis (e.g., CAE, FEA, etc.) **is highly correlated** with actual or expected operating conditions prior to design freeze.	2	Very High
Detection not applicable; Failure Prevention	Failure cause or failure mode cannot occur because it is fully prevented through design solutions (e.g., proven design standard, best practice or common material, etc.).	1	Almost Certain

Source: Reprinted from Potential Failure Mode and Effects Analysis, (FMEA 4th edition, 2008 Manual) with permission of DaimlerChrysler, Ford and GM Supplier Quality Requirements Task Force.

Design FMEA prevention / detection evaluation criteria (McDermott et al., 2009)

Appendix D – Male double hemisphere drawing

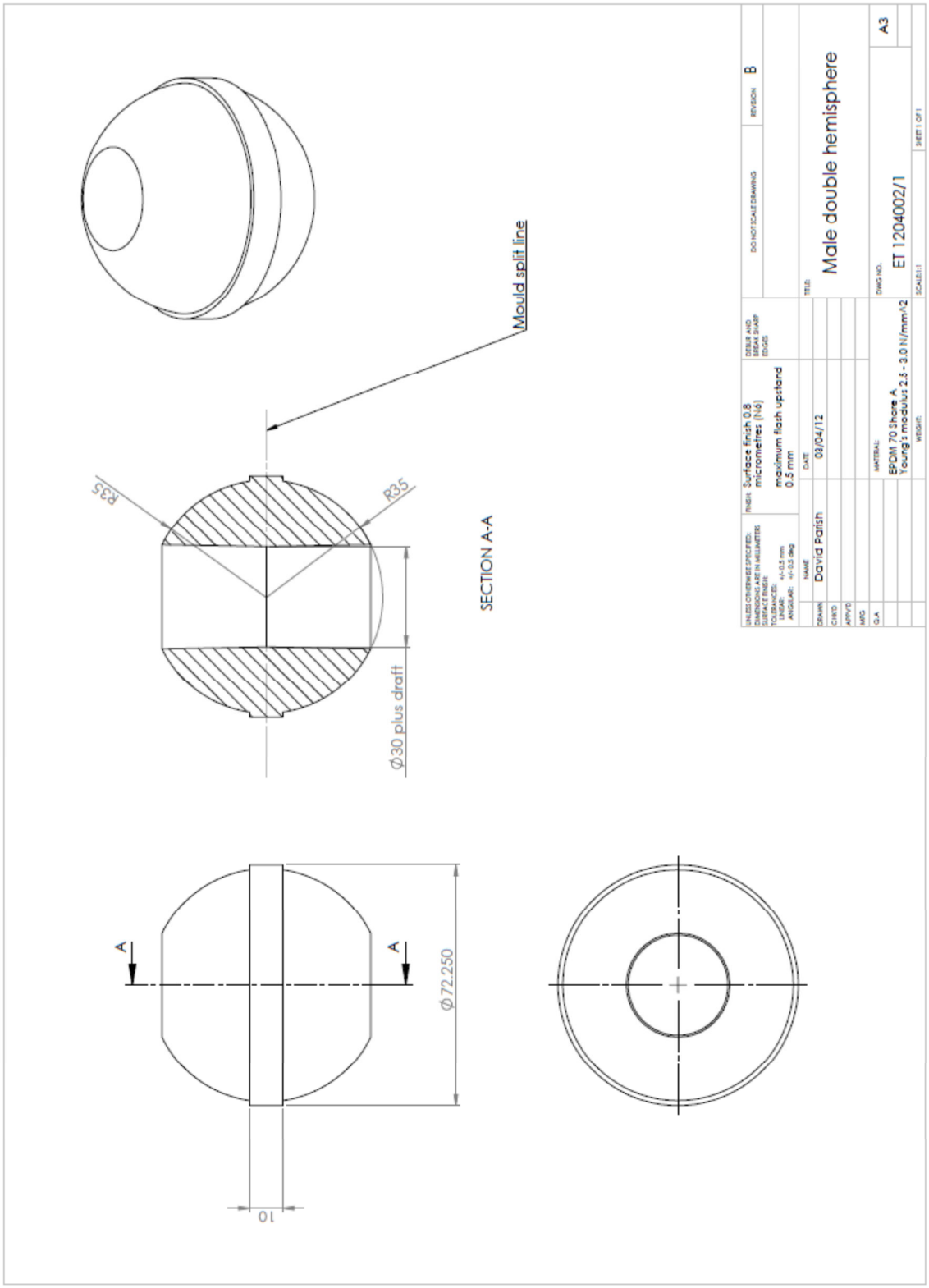

Appendix E – Female double hemisphere drawing

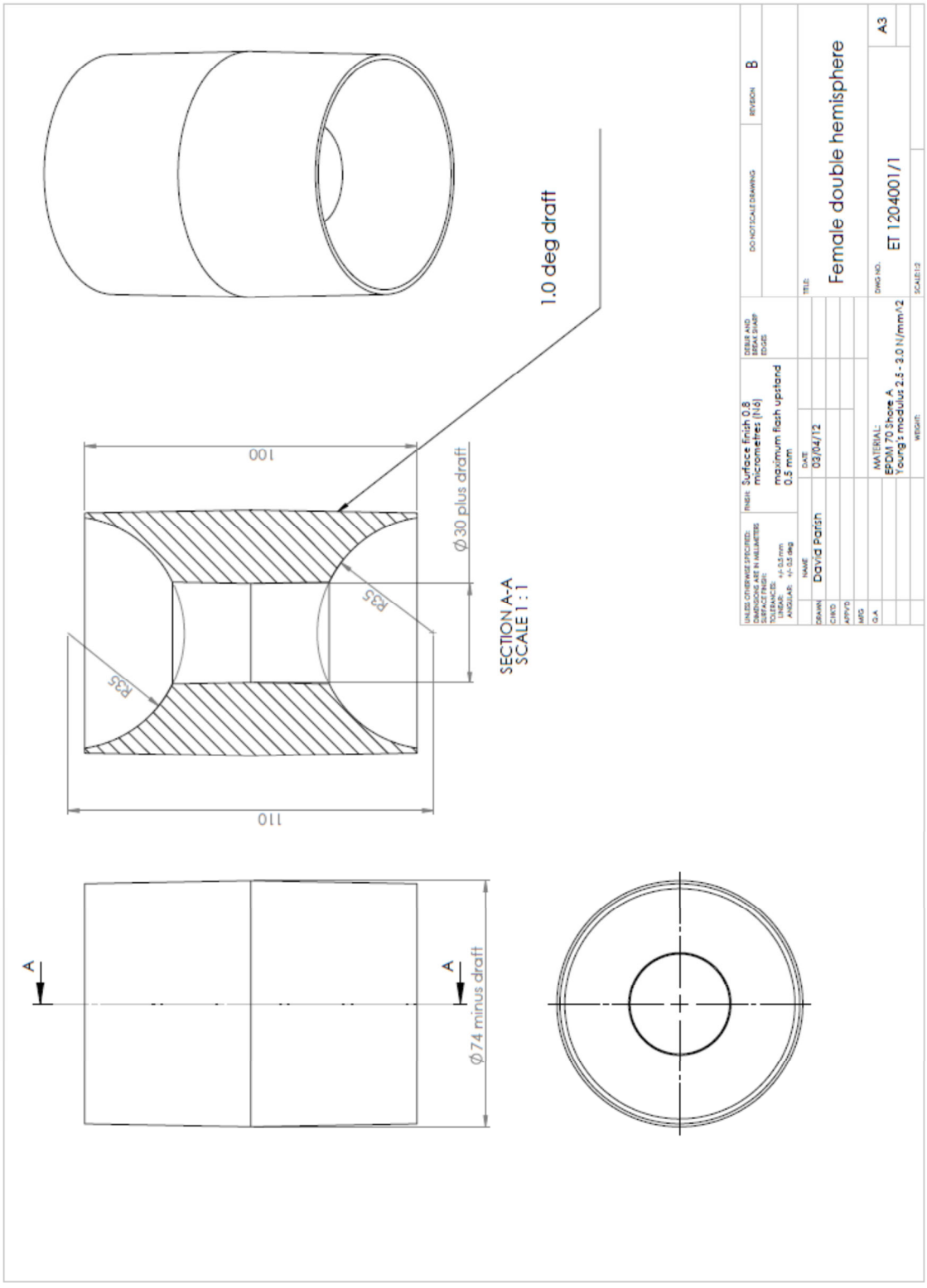

Appendix F – Male double hemisphere (cropped) drawing

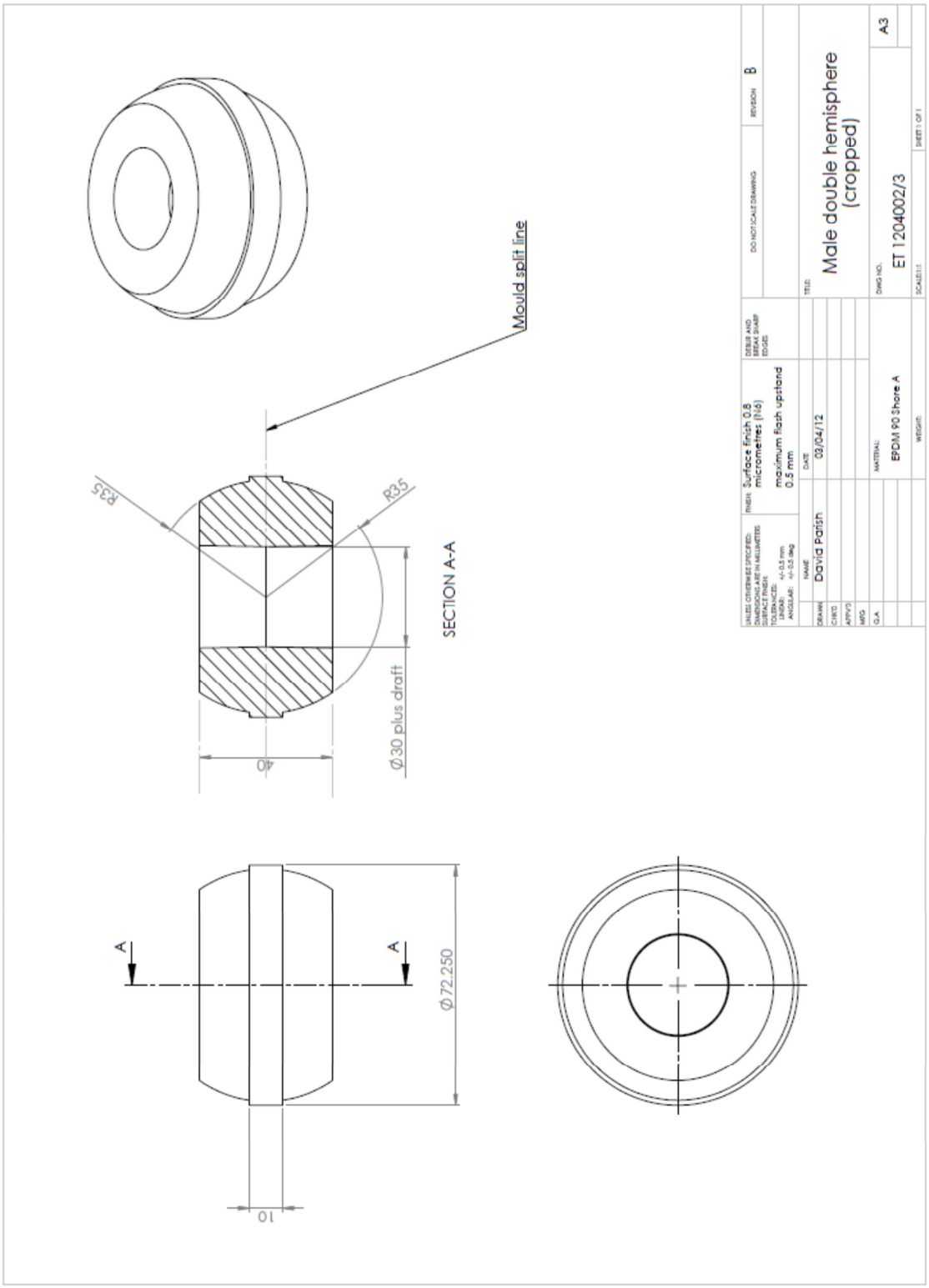

Appendix G – Tether Scaling Guide

Realistic outside diameter (mm)	**45**	**51**	**57**	**62**	**68**	**74**	**79**	**85**	**91**	**96**	**102**	**108**	**113**	**119**	**125**	**130**	**136**
Tether weight in air (kg/m)	**1.8**	**2.2**	**2.8**	**3.3**	**4.0**	**4.7**	**5.4**	**6.2**	**7.0**	**8.0**	**8.9**	**9.9**	**11.0**	**12.1**	**13.3**	**14.6**	**15.9**
Core linear density (kg/m)	1.5	1.9	2.3	2.8	3.3	3.9	4.5	5.2	5.9	6.6	7.4	8.3	9.2	10.1	11.1	12.1	13.2
Cross section area of cord (mm^2)	139.6	176.7	218.2	264.0	314.2	368.7	427.6	490.9	558.5	630.5	706.9	787.6	872.7	962.1	1055.9	1154.1	1256.6
EPDM cord diameter (mm)	13.3	15.0	16.7	18.3	20.0	21.7	23.3	25.0	26.7	28.3	30.0	31.7	33.3	35.0	36.7	38.3	40.0
Rope linear density (kg/m)	0.30	0.37	0.46	0.56	0.67	0.78	0.91	1.04	1.18	1.34	1.50	1.67	1.85	2.04	2.24	2.45	2.66
MBL (kN)	**63**	**80**	**99**	**119**	**142**	**167**	**193**	**222**	**253**	**285**	**320**	**356**	**395**	**435**	**478**	**522**	**568**
Linear density scale factor	2.8	3.5	4.3	5.3	6.3	7.3	8.5	9.8	11.1	12.5	14.1	15.7	17.4	19.1	21.0	23.0	25.0
Solidity (%)	53	53	53	53	53	53	53	53	53	53	53	53	53	53	53	53	53
Rope strand area (mm^2)	357	451	557	674	803	942	1092	1254	1427	1611	1806	2012	2229	2458	2698	2948	3210
Strand elipse area (mm^2)	7.4	9.4	11.6	14.0	16.7	19.6	22.8	26.1	29.7	33.6	37.6	41.9	46.4	51.2	56.2	61.4	66.9
Annulus area (mm^2)	676	855	1056	1277	1520	1784	2069	2375	2702	3051	3420	3811	4222	4655	5109	5584	6080
Outside diameter without strand flattening (mm)	49.6	55.8	62.0	68.2	74.4	80.6	86.8	93.0	99.2	105.4	111.6	117.8	124.0	130.2	136.4	142.6	148.8
No. strands	48	48	48	48	48	48	48	48	48	48	48	48	48	48	48	48	48
Braid angle (°)	52.5	52.5	52.5	52.5	52.5	52.5	52.5	52.5	52.5	52.5	52.5	52.5	52.5	52.5	52.5	52.5	52.5
Strand diameter (mm)	2.4	2.7	3	3.3	3.6	3.9	4.2	4.5	4.8	5.1	5.4	5.7	6.0	6.3	6.6	6.9	7.2
Inside diameter (mm)	40	45	50	55	60	65	70	75	80	85	90	95	100	105	110	115	120

Note: Density of EPDM = 1500 kg / m^3 (Polymax, 2015)

References

API (2005) *API RP 2SK: Recommended Practise for Design and Analysis of Station Keeping Systems for Floating Structures*, 3rd Edition: American Petroleum Institute.

BARLTROP, N. D. P. (1998) *Floating Structures: a guide for design and analysis,* Ledbury: Oilfield Publications Ltd.

BENGTSSON, N. & EKSTRÖM, V. (no date) *Seaflex: the Mooring Buoy System,* [online], Available: http://buoymooring.com/data/archive/White-Paper-SEAFLEX-Buoy-Mooring.pdf [accessed 21/05/15].

BOUD, R. (2012) *Carbon Trust Report: UK Wave Energy Resource,* [online], Available: https://www.carbontrust.com/media/202649/ctc816-uk-wave-energy-resource.pdf [accessed 16/05/15].

BOWIE, A. E. D. (2012) *Flexible Moorings for Tidal Current Turbines,* Master of Science thesis. University of Strathclyde, [Online], Available: http://www.esru.strath.ac.uk/Documents/MSc_2012/Bowie.pdf [accessed 15/08/15].

BRIDON (2007) *Fibre Rope Catalogue: Specialist fibre rope solutions*, [Online], Available: http://www.bridon.com/china/x/downloads/fibre/Fibre.pdf [accessed 18/01/15].

BUDAL, K. & FALNES, J. (1980) *Interacting point absorbers with controlled motion: Power from sea waves,* (B. Count, ed.), London: Academic Press.

BV (2007) *Guidance Note NI 432 DTO R01E: Certification of Fibre Ropes for Deepwater Offshore Services*, Bureau Veritas.

CANTOURNET, S., DESMORAT, R. & BESSON, J. (2009) 'Mullins effect and cyclic stress softening of filled elastomers by internal sliding and friction thermodynamics model', *International Journal of Solids and Structures,* vol. 46**,** pp. 2255-2264.

CASAUBIEILH, P., THIEBAUT, F., BOSMA, B., RETZLER, C., SHAW, M., LETERTRE, Y. & SHENG, W. (2014) 'Performance improvements of mooring systems for wave energy converters', *RENEW - Conference Proceedings*, 1st International Conference on Renewable Energies Offshore, Lisbon, Portugal.

CHAKRABARTI, S. K. (2005) *Handbook of Offshore Engineering,* Oxford, UK: Elsevier.

DARUVALA, J. (2009) *SW Wave Hub: Metocean Design Basis,* [Online], Available: http://www.wavehub.co.uk/downloads/Resource_Info/Metocean_design_basis_Metoc_JP_Kenny_Report_2009.pdf [accessed 13/06/15].

DATAWELL (2015) *Datawell Rubber Cords,* [online], Available: http://www.datawell.nl/Portals/0/Documents/Brochures/datawell_brochure_rubbercords_b-21-02.pdf [accessed 19/05/15].

DAVIES, P., WELLER, S., JOHANNING, L. & BANFIELD, S. J. (2014) 'A review of synthetic fiber moorings for marine energy applications', *ICOE – Conference Proceedings*, 5th International Conference on Ocean Energy, 4th-6th November 2014, Halifax, Canada.

DECC (2014) *DUKES: Digest of United Kingdom Energy Statistics 2014,* London: TSO.

DIANI, J., FAYOLLE, B. & GILORMINI, P. (2009) 'A review on the Mullins effect', *European Polymer Journal,* vol. 45**,** pp. 601-612.

DNV (2013a) *DNV-OS-E301: Offshore Standard Position Mooring*: Det Norske Veritas AS.

DNV (2013b) *DNV-OS-E303: Offshore standard Offshore Fibre Ropes*: Det Norske Veritas AS.

DREW, B., PLUMMER, A. & SAHINKAYA, M. A. (2009) 'A review of wave energy converter technology', *Part A: Journal of Power and Energy,* vol. 233 (8)**,** pp. 887-902.

DULMISON (2016) *Anchor scope,* [Online], Available: http://www.dulhunty.com/dmp3.htm [accessed 12/03/16].

FALTINSEN, O. M. (1990) *Sea Loads on Ships and Offshore Structures,* Cambridge: Cambridge University Press.

FITZGERALD, J. & BERGDAHL, L. (2007) 'Considering Mooring Cables for Offshore Wave Energy Converters', *EWTEC – Conference Proceedings*, 7th European Wave and Tidal Energy Conference, 11-14 September 2007, Porto, Portugal.

FLORY, J. F. (2000) 'The Revised OCIMF Hawser Guidelines', *OCEANS 2000 – Conference Proceedings,* Conference of the Marine Technology Society and Ocean Engineering Society, 11 -14 Sep 2000, pp. 1399 – 1402, Providence, USA.

FUJIFILM (2007) *Prescale,* [online], Available: http://www.fujifilm.eu/fileadmin/products/prescale/media/Prescale_Film_Brochure_klein_e.pdf [accessed 25/02/2015].

GORDELIER, T., PARISH, D., JOHANNING, L. & THIES, P. (2014) 'A Novel Mooring Tether for Highly Dynamic Offshore Applications; Mitigating Peak and Fatigue Loads via Selectable Axial Stiffness', *Conference Proceedings - International Conference on Offshore Renewable Energy*, 15th - 17th September 2014. Glasgow, UK.

GORDELIER, T., PARISH, D., THIES, P. R. & JOHANNING, L. (2015), 'A Novel Mooring Tether for Highly-Dynamic Offshore Applications; Mitigating Peak and Fatigue Loads via Selectable Axial Stiffness', *Journal of Marine Science and Engineering,* vol. 3**,** pp. 1287-1310.

HAMEDNI, B. (2012) *Discussion regarding Exeter Tether development,* Pers. comm. to PARISH, D. & JOHANNING, L., 7th November 2012.

HAMEDNI, B., MATHIEU, C. & FERREIRA, C. B. (2014) *Generic WEC System Breakdown: Structural Design of Wave Energy Devices,* Revision B, [Online], Available: http://www.sdwed.civil.aau.dk/digitalAssets/97/97538_d5.1.pdf [accessed 17/06/15].

HARNOIS, V. R. (2014) *Analysis of highly dynamic mooring systems: peak mooring loads in realistic sea conditions,* PHD thesis, University of Exeter, [Online], Available: https://ore.exeter.ac.uk/repository/handle/10871/17205 [accessed 28/03/16].

HARRIS, R. E., JOHANNING, L. & WOLFRAM, J. (2004) 'Mooring systems for wave energy converters: A review of design issues and choices', *MAREC – Conference Proceedings*, 3rd International Conference on Marine Renewable Energy, 1st July 2004, Blythe, UK.

HERDUIN, M. (2015) *MRCF: Testing, Qualification and Commercialisation of Advanced Mooring Systems for Wave & Tidal Arrays Milestone 2 Orcaflex report (WP 3.3)*. Penryn: University of Exeter.

HUANG, Y. P. (2005) *Flexible anchoring rope,* US Patent US6899050 B1.

IRISH, J. D. & KERY, S. (1996) 'Elastic tether technology for shallow water moorings in harsh environments: results from Georges Bank', *OCEANS 96 – Conference Proceedings,* Conference of the Marine Technology Society and Ocean Engineering Society, 23-26 September 1996, pp. 635-639 vol.2.

JOHANNING, L. (2015) *Discussions regarding IEC standard,* Pers. Comm. to PARISH, D. 14/05/15.

JOHANNING, L. & SMITH, G. H. (2008) 'Station Keeping Study for WEC Devices Including Compliant Chain, Compliant Hybrid and Taut Arrangement', *OMAE – Conference Proceedings,* 27th International Conference on Offshore Mechanics and Arctic Engineering. Estoril, Portugal.

JOHANNING, L., SMITH, G. H. & WOLFRAM, J. (2007) 'Measurements of static and dynamic mooring line damping and their importance for floating WEC devices', *Ocean Engineering,* vol. 34**,** pp. 1918-1934.

JOHANNING, L., SPARGO, A. & PARISH, D. (2008) 'Large scale mooring test facility: A technical note', *ICOE – Conference Proceedings*, 2nd International Conference on Ocean Energy, 15th – 17th October 2008, Brest, France.

KARIMIRAD, M., KOUSHAN, K., WELLER, S., HARDWICK, J. & JOHANNING, L. (2014) 'Applicability of offshore mooring and foundation technologies for marine renewable energy (MRE) device arrays', *RENEW – Conference Proceedings*, 1st International Conference on Renewable Energies Offshore, Lisbon, Portugal.

LCICG (2012) *Technology Innovation Needs Assessment (TINA) - Marine Energy Summary Report*: Low Carbon Innovation Coordination Group.

MA, K., DUGGAL, A., SMEDLEY, P., L'HOSTIS, D. & SHU, H. (2013) 'A Historical Review on Integrity Issues of Permanant Mooring Systems', *Offshore Technology Conference – Conference Proceedings*, 6th - 9th May 2013. Houston, Texas.

MACGILLIVRAY, A., JEFFREY, H., HANMER, C., MAGAGNA, D., RAVENTOS, A. & BADCOCK-BROE, A. (2013) *Ocean Energy Technology: Gaps and Barriers*: S I Ocean, [Online], Available: http://www.si-ocean.eu/en/upload/docs/WP3/Gaps%20and%20Barriers%20Report%20FV.pdf [accessed 23/01/15].

MARK, J. E., ERMAN, B. & ROLAND, C. M. (2013) *The Science and Technology of Rubber,* Oxford, UK, Elsevier.

MASCIOLA, M., ROBERTSON, A., JONKMAN, J. & DRISCOLL, F. (2011) 'Investigation of a FAST-OrcaFlex Coupling Module for Integrating Turbine and Mooring Dynamics of Offshore Floating Wind Turbines', *Conference Proceedings - International Conference on Offshore Wind Energy and Ocean Energy.* Beijing, China.

MC EVOY, P. (2012) 'Combined Elastomeric & Thermoplastic Mooring Tethers', *ICOE – Conference Proceedings*, 4th International Conference on Ocean Energy (ICOE). Dublin, Ireland.

MCDERMOTT, R. E., MIKULAK, R. J. & BEAUREGARD, M. R. (2009) *The Basics of FMEA,* New York, USA: Taylor & Francis Group LLC.

MCKENNA, H. A., HEARLE, J. W. S. & O'HEAR, N. (2004) *Handbook of fibre rope technology,* Cambridge, England: Woodhead Publishing Ltd.

ORCINA, L. (2014). *Orcaflex Manual 9.8a*. Orcina Ltd.

PACHAURI, R. K. & MEYER, L. A. (2014) *Climate Change 2014: Synthesis Report. Contribution of Working Groups I, II and III to the Fifth Assessment Report of the Intergovernmental Panel on Climate Change,* Geneva, Switzerland: IPCC.

PAREDES, G. M., BERGDAHL, L., PALM, J., ESKILSSON, C. & PINTO, F. T. (2013) 'Station keeping design for floating wave energy devices compared to floating offshore oil and gas platforms', *EWTEC – Conference Proceedings*, 10th European Wave and Tidal Energy Conference, 2-5 September 2013. Aalborg, Denmark.

PARISH, D. (2010) *Mooring Limb*, UK patent application GB 2467345 A.

PARISH, D. (2011) *Mooring Limb,* UK patent application GB 2476986 A.

PAUL, W., CHAFFEY, M., HAMILTON, A. & BODUCH, S. (2005) 'The use of snubbers as strain limiters in ocean moorings', *OCEANS – Conference Proceedings*, Conference of the Marine Technology Society and Ocean Engineering Society, 18-23 September 2005. pp. 2722-2729 Vol. 3, Washington, USA.

PECHER, A., FOGLIA, A. & KOFOED, J. (2014) 'Comparison and Sensitivity Investigations of a CALM and SALM Type Mooring System for Wave Energy Converters', *Journal of Marine Science and Engineering,* vol. 2**,** pp. 93-122.

POLYMAX (2015) *Polymax EPDM Cord,* [online], Available: https://www.polymax.co.uk/media/documents/Datasheet/Cord_EPDM.pdf [accessed 21/08/15].

RIDGE, I. M. L., BANFIELD, S. J. & MACKAY, J. (2010) 'Nylon fibre rope moorings for wave energy converters', *OCEANS – Conference Proceedings,* Conference of the Marine Technology Society and Ocean Engineering Society, 20-23 September 2010, pp. 1-10, Seattle, USA.

RINNBAUER, M. (2007) *Technical Elastomers: The basis of high-tech sealing and vibration control technology solutions,* Munich, Germany: SV Corporate Media GmbH.

SEGERLJUNG, M. (2013) *Fastening device for an elastic element in a resilient unit included in an anchoring system*. International patent application WO 2013/141773 A1.

SMITH, B. (1988) *Design Your Own Yacht,* London: Adlard Coles.

SUMER, B. M. & FREDSOE, J. (2006) *Hydrodynamics around cylindrical structures,* Singapore: World Scientific Publishing Co. Pte. Ltd.

SUPFLEX (2014) *Superflex mooring test result,* [online], Available: http://supflex.com/home4.html [accessed 21/05/15].

SUPFLEX. (2015) *Offshore,* [online], Available: http://supflex.com/Mooring1.html [accessed 26/05/2015].

THIES, P. R., JOHANNING, L. & MCEVOY, P. (2014) 'A novel mooring tether for peak load mitigation: Initial performance and service simulation testing', *International Journal of Marine Energy,* vol. 7**,** pp. 43-56.

UOE (2011) *DMaC Specification Sheet,* [online], Available: http://emps.exeter.ac.uk/media/universityofexeter/emps/renewable/research/DMaC_-_Spec_A2_11022011.pdf [accessed 24/03/2015].

VAN NIEUWKOOP, J. C. C., SMITH, H. C. M., SMITH, G. H. & JOHANNING, L. (2013) 'Wave resource assessment along the Cornish coast (UK) from a 23-year hindcast dataset validated against buoy measurements', *Renewable Energy,* vol. 58**,** pp. 1-14.

WANG, W., YOU, Y., HUANG, S., YE, Y. & WANG, Z. (in review) 'Research and Application of Optimum Design of Multi-component Mooring line of offshore Wave energy converters Mooring system under storm surge'

WELLER, S., DAVIES, P., VICKERS, A. & JOHANNING, L. (2015a) 'Synthetic rope responses in the context of load history: Operational performance', *Ocean Engineering,* vol. 96**,** pp. 192-204.

WELLER, S. D., JOHANNING, L., DAVIES, P. & BANFIELD, S. J. (2015b) 'Synthetic mooring ropes for marine renewable energy applications', *Renewable Energy*, vol. 83, pp. 1268-1278.